
The University Of Sheffield.

# Development of Anthracene-Based Conjugated Polymers for Solar Cell Applications

**By:**

Sulaiman Ali Sulaiman Al-Isaee

A thesis submitted in partial fulfilment of the requirements for the degree of Doctor of Philosophy

The University of Sheffield

Department of Chemistry

**October 2016**

# Declaration

I hereby declare that the work presented herein is a result of my research project conducted in the Department of Chemistry at University of Sheffield from October 2012 to October 2016 for the degree of doctorate of philosophy (PhD). The research findings thereof are original unless otherwise stated. This thesis has not been submitted either in part or in its entirety to any other university or institution for my academic qualification.

_____

**Sulaiman A. S. Al-Isaee**

October 2016

# Abstract:

In this thesis, a series of organic conjugated polymers were designed, synthesised and characterized for their use in BHJ organic photovoltaic devises. The development of organic conjugated materials with alternating donor and acceptor units provides polymers with medium optical band gaps and suitable energy levels for OPV applications. Conjugated polymers with donor units such as anthracene, and acceptor units such as benzothiadiazole (BT) or thieno[3,4-*c*]pyrrole-4,6-dione (TPD) units, with a variety of side chains, have shown a good efficacy in manipulating both the band gaps of these materials as well as their energy levels.

Polymers **PATA(D)TBT**, **PATA(BO)TBT** and **PAA(PU)TBT** display limited solubilities in common organic solvents at ambient temperature; due to the lack of solubilising groups on the **BT** units. The prepared polymers show multiple absorption bands in both solutions and thin films with optical band gaps in the range of 1.75–1.85 eV. In order to overcome the low solubility of these three polymers, octyloxy substitutents were attached to the **BT** unit to obtain another series of polymers **PATA(D)TBT-8**, **PATA(BO)TBT-8** and **PAA(PU)TBT-8**. However, substituting the **BT** units with octyloxy groups has led to a rise of the LUMO energy levels of these polymers in comparison to the corresponding polymers without the octyloxy groups. The 3$^{rd}$ series of polymers was prepared by introducing of bithiophene spacers between the anthracene units and benzothiadiazole units to improve the optical properties of the resulting polymers in comparison to the polymers with single thiophene spacers. However, these polymers displayed shallower HOMO energy levels when compared to counterpart polymers with single thiophene spacers owing to the enhanced intramolecular charge transfer along the polymer backbone. The photovoltaic performance of all the polymer devices (**PATA(D)TBT**, **PATA(D)TBT-8**, **PATA(BO)TBT-8**, **PATA(D)T2BT-8**, **PATA(BO)T2BT-8** and **PAA(PU)T2BT-8**) were quite modest in the range of 0.76% to 1.80%, due to the low $J_{sc}$ and *FF* values obtained.

The last series of alternating copolymers comprising 9,10-functionalised anthracene flanked by thienyl donor units and TPD acceptor units were prepared using direct arylation reactions. Polymers with ethynyl side chains at the 9,10 positions of the anthracene units (**PATA(BO)TPD-8**, **PATA(BO)TPD-DMO**, **PAA(PU)TPD-8** and **PAA(PU)TPD-DMO**) show medium optical band gaps. However, when ethynyl substituents on the 9,10-positions of anthracene units are replaced with alkene substituents which leads to polymers (**PAV(PU)TPD-8** and **PAV(PU)TPD-DMO**) with higher optical band gaps. The HOMO levels of the polymers **PAV(PU)TPD-8** and **PAV(PU)TPD-DMO** were deeper than those of the corresponding polymers with ethynyl-substituents.

# Acknowledgements

First of all, I would like to express my gratitude and deep appreciation to my supervisor, Dr Ahmed Iraqi, for his guidance, assistance and supervision.

Special thanks are extended to the support staff at the Department of Chemistry, in particular, Sue Bradshaw for NMR measurements, Simon Thorpe for mass spectroscopy, Rob Hanson for his help in GPC and TGA analysis, Jennifer Louth for her help in elemental analysis, Heather Grievson, Nick, Peter, Sharon and everyone at the chemistry department at the University of Sheffield who has assisted me.

I also owe a great amount of thanks to Ary Murad, Hunan Yi, Ahmed Al-Azawee, Omar and Luke Cartwright for providing me with a lot of help and support.

Special thanks to the Ministry of Higher Education in the Sultanate of Oman for having given me leave of absence from the College of Applied Sciences to further my studies at the University of Sheffield.

Finally, I would like to gratefully thank my parents, my lovely wife and my children for their support, patience and encouragement.

## Contents

# List of Figures

# List of Schemes:

## List of Tables

# List of Abbreviations

| | |
|---|---|
| AcOH | Acetic acid |
| AM 1.5 | Air Mass |
| a.u. | Arbitrary Units |
| A | Acceptor |
| BHJ | Bulk Heterojunciton |
| BLA | Bond length alternation |
| br | Broad peak (NMR) |
| CB | Chlorobenzene |
| CV | Cyclic Voltammetry |
| CuI | Copper(I) iodide |
| d | Doublet (NMR) |
| dd | Double doublet (NMR) |
| D-A | Donor-Acceptor |
| DCM | Dichloromethane |
| DMF | N,N-Dimethylformamide |
| DP | Degree of polymeristion |
| $E_g$ (opt) | Optical Bandgap |
| $E_g$ (elec) | Electrochemical Bandgap |
| eV | Electron Volt |
| EI | Electron impact |

| | |
|---|---|
| $Et_3N$ | Triethylamine |
| $E_{vac}$ | Vacuum level energy |
| EtOH | Ethanol |
| FF | Fill Factor |
| GPC | Gel Permeation Chromotography |
| HOMO | Highest Occupied Molecular Orbital |
| Hz | Hertz |
| ICT | Intramolecular Charge Transfer |
| ITO | Indium Tin Oxide |
| IR | Infrared spectroscopy |
| $I_{sc}$ | Short circuit current |
| $J_{sc}$ | Short Circuit Current |
| J-V | Current-Voltage |
| LED | Light-Emitting Diode |
| LUMO | Lowest Unoccupied Molecular Orbital |
| $\lambda_{max}$ | Maximum Absorption Wavelength |
| m | Multiplet (NMR) |
| $M_n$ | Number-Average Molecular Weight |
| $M_w$ | Weight-Average Molecular Weight |
| MeOH | Methanol |
| NMR | Nuclear Magnetic Resonance |
| NBS | N-Bromosuccinimide |

| | |
|---|---|
| *n*-BuLi | *N*-Butyllithium |
| OFETs | Organic field-effect transistors |
| OLED | Organic light emitting diode |
| OLETs | Organic light-emitting transistors |
| OSC | Organic Solar Cell |
| OPV | Organic Photovoltaic |
| (*o*-tolyl)$_3$P | Tri(o-tolyl) phosphine |
| PA | Polyacetylene |
| Pd | Palladium |
| PPV | Poly(*para*-phenylenevinylene) |
| PSC | Polymer Solar Cell |
| PV | Photovoltaic |
| $PC_{70}BM$ | Phenyl-$C_{70}$-Butyric Acid Methyl Ester |
| PCE | Power Conversion Efficiency |
| PDI | Polydispersity Index |
| $Pd_2(dba)_3$ | Tris(dibenzylidene acetone) palladium (0) |
| $Pd(OAc)_2$ | Palladium(II) acetate |
| $P_{in}$ | Incident light power |
| ppm | part per million |
| R.T | Room temperature |
| s | Singlet (NMR) |
| t | Triplet (NMR) |

| | |
|---|---|
| Td | Decomposition temperature |
| TGA | Thermogravimetric Analysis |
| THF | Tetrahydrofuran |
| TMS | Tetramethylsilane |
| UV-vis | Ultraviolet-Visible Spectroscopy |
| $V_{oc}$ | Open Circuit Voltage |
| $V_{mpp}$ | Voltage at maximum power point |

# Chapter 1

## 1.1 The Need for New Sources of Energy

Energy resources have helped to establish the recent civilisation and have powered the sweeping economic changes that have transformed the world over the last 250 years. Beside conventional fossil fuels, new technologies have been developed over time to harness energy, expanding the menu of energy resources that could be utilised. However, the continued increase in power consumption has resulted in the annual world power usage to increase to 16.5 TW in 2012.[1] This is expected to increase to around 24 TW by 2030. The current resources of energy that are available are not enough to meet this growth in energy consumption.

The majority of the global energy demands are provided by fossil fuels. However, in order to reduce the dependence on fossil fuels and their environmental damaging effects, other energy sources have been investigated. Renewable energy resources are essential in providing environmentally friendly alternatives to dwindling fossil fuels. Solar energy will definitely play an important role in future energy production as one of these resources. Therefore, converting energy from sunlight into electrical energy using photovoltaic (PV) technology is being used as a fundamental factor of the future global renewable energy production [2].

In 1839 a French physicist, Edmond Becquerel, discovered what is called the photovoltaic (PV) effect which is the conversion of absorbed light into electrical energy [3]. A century later, exactly in 1954, Bell Laboratories attempted to commercialise PV technology by developing the first crystalline silicon p-n junction solar cell with an efficiency up to 6% [4]. Recently, solar cells based on crystalline silicon have dominated PV technology with efficiencies reaching up to 25% [5]. Despite their high efficiency and the efforts in reducing the price of the raw materials, this technology only contributes less than 0.1% of the total world energy production.

Along with crystalline silicon solar cells, active investigations and research efforts have taken place to develop the second generation of photovoltaics for further reduction of the costs to produce electricity. Examples of inorganic semiconductor materials used

with the second generation of solar cells, include cadmium sulphide (CdS), cadmium telluride (CdTe), copper indium diselenide (CIS) or copper indium gallium selenide (CIGS), amorphous and nanocrystalline silicon. These materials absorb more light than crystalline silicon. Moreover, they can be processed into large area substrates using different techniques like physical vapour deposition, sputtering, and plasma-enhanced chemical vapour deposition. However, despite their low cost of fabrication and the reasonable power conversion efficiencies (10-19%) they produce, control of their manufacturing remains a challenge and their commercialisation are not widespread so far [5].

A new emerging photovoltaic technology based on organometal halides has gained a considerable attention nowadays called Perovskite solar cells. Perovskite solar cells can be consider as a branch from dye-sensitized solar cells. The technology was first discovered in 2009 when the adsorption of methylammonium lead halide perovskite on a nanocrystalline $TiO_2$ surface gives a photocurrent with a PCE around 3–4%. Two years later, the PCE was doubled by improving the perovskite coating conditions. In 2012, A more stable and high efficient perovskite solar cell (~10%) was made by replacing the solid hole conductor with a liquid electrolyte. Efficiencies have quickly risen to over 20% in the last 4 years which make perovskite solar cells are a promising photovoltaic technology [6].

Among the PV technologies investigated by researchers, polymer-based organic photovoltaics (OPVs) have recently gained a significant attention due to their advantages compared to the silicon-based devices such as their low-cost of production, device flexibility, light weight and solution processability [7]. In addition, the organic materials being investigated for OPV are abundant, have tuneable properties and high molar absorptivities [8]. However, OPV technology is still a long way from commercialisation due to the low stability and low efficiency of devices which are still problems to be solved. As a result, the development of OPVs and their efficiencies has become quite a popular and promising topic for scientific research. In fact, over the last ten years the PCEs achieved by organic polymer solar cells have increased noticeably from 2.5 to 11 % [9]. Design of materials by tuning their energy levels and band gaps has

played a curial role in developing new organic conjugated polymers for efficient organic solar cells (OSCs).

## 1.2 Background to Conjugated Polymers

The first discovery of electrical conductivity in organic compounds by Shirakawa, MacDiarmid and Heeger opened-up a new attractive field in the semiconducting properties of conjugated polymers [10]. They were awarded the Nobel prize in chemistry in the year 2000 for their pioneering work on conjugated polymers, where they found that the conductivity of *trans*-polyacetylene increased greatly, by exposing it to vapours of iodine, bromine and chlorine [11]. These organic conjugated polymers along with other organic photoconductors have triggered the first applications of organic materials as conductive coatings or photoreceptors in electrophotography [12, 13]. *Cis*- and *trans*-polyacetylene were the first generation of semiconducting polymers, however the *trans* form is more stable compared to the *cis* form which can be converted thermally to the *trans* form (**Figure 1-1**).[14]

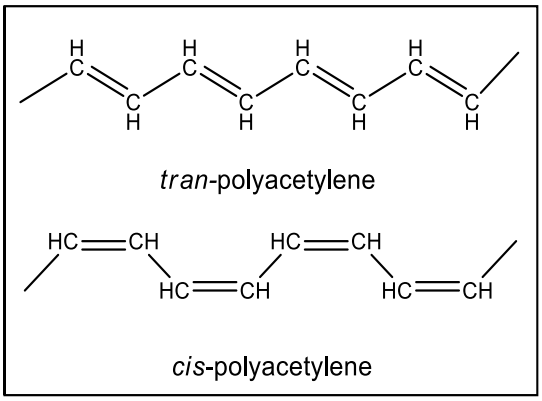


**Figure 1-1:** *Trans*- and *cis*- structure of polyacetylene.

Since 1990, organic conjugated polymers have emerged as potentially useful electronic materials, including uses in photovoltaics and light emitting diodes. Some examples of conjugated polymers are shown in **Figure 1-2**.

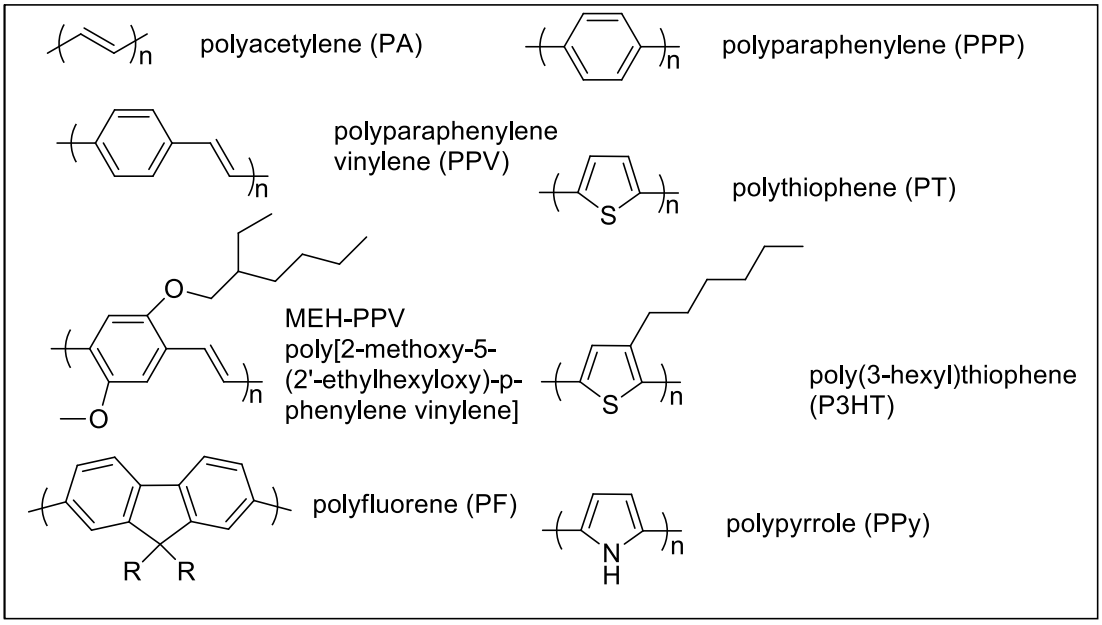


**Figure 1-2:** Structure of some common conjugated polymers

Organic semiconducting materials can be classified into two main groups: polymers and low molecular weight compounds. The main feature of these two groups is their electronic conjugation with alternation of single and double bonds between the carbon atoms in their main backbone providing the mechanism for electrons delocalisation [15].

In *trans*-polyacetylene, there is a large number of C=C double bonds, and as this number increases, there will be more degenerate levels which form because of the large number of π bonds formed. **Figure 1-3** shows the molecular structure of ethene, 1,3-butadiene, and 1,3,5-hexatriene and their π molecular orbitals. In the case of 1,3,5-hexatriene there are 2 electrons within each π bond and 3 π bonds, so the numbers of electrons in the π orbitals are 6 electrons. The three ground state π orbitals are fully occupied by the electrons, which can be referred as bonding orbitals. The $\pi_3$ orbital is known as the Highest Occupied Molecular Orbital (HOMO). The anti-bonding $\pi_1^*$ orbitals is known as the Lowest Unoccupied Molecular Orbital (LUMO). As conjugated chains grow, more and more C=C double bonds are added in backbone, as a result π and $\pi^*$ orbitals are added to give the familiar full valence band and the empty conduction band of the semiconductor, separated by a band gap much similar to that in inorganic semiconductors. A typical band gap separation of the HOMO-LUMO orbitals in semiconducting conjugated polymers occurs in the range of 1 to 3 eV [16, 17].

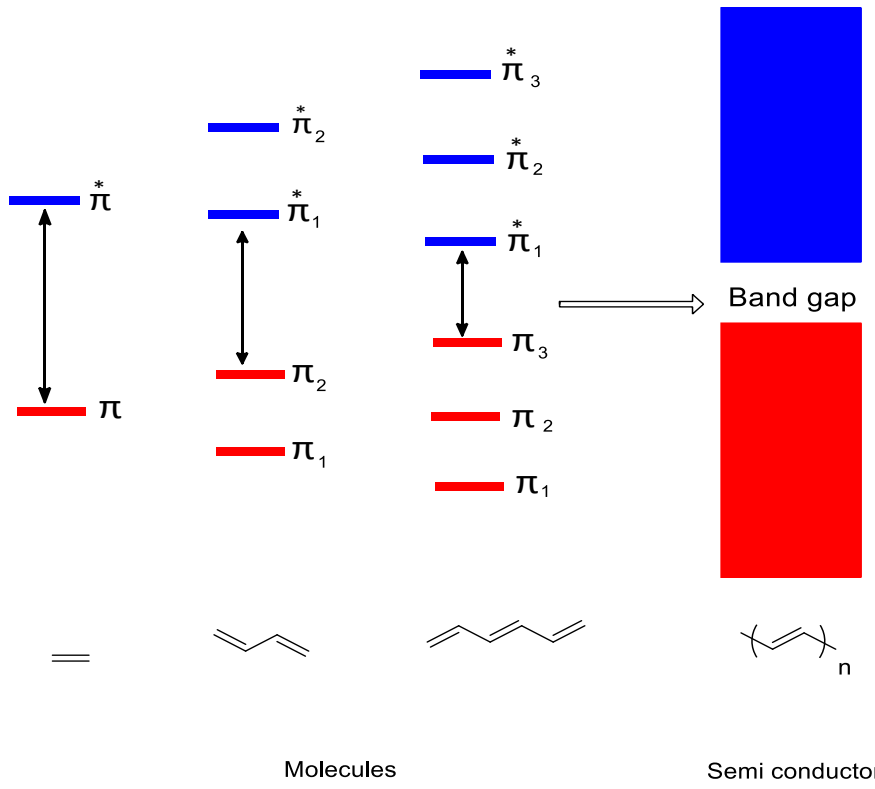


**Figure 1-3:** Development of the band gap structure of polyacetylene from energy levels of corresponding monomer during polymerisation. (adapted from Chochos *et el.*)[18]

In the basic energy band structure of organic semiconductors, the absorption of light leads to the excitation of electrons from the π-band to the π*-band resulting in mobile electrons and holes, as shown in **Figure 1-4**. As a result, it is expected to observe photoconductivity in response to an applied electric field [19].

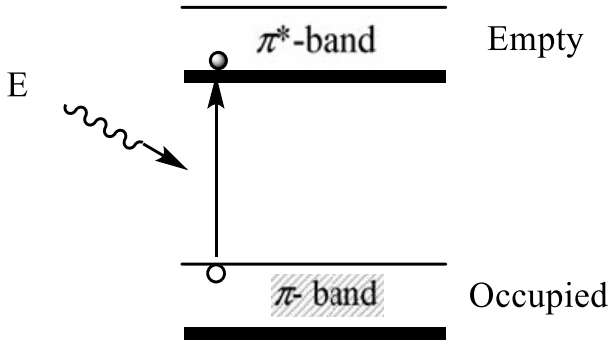


**Figure 1-4:** π– π * interband transition with associated generation of a mobile electron in the π*-band and a mobile hole in the π-band. (Adapted from Heeger *et al.*) [19].

The generated electrons and holes through the interband optical absorption transition rapidly relax toward the respective band edges and subsequently form neutral intrachain excitons. When the resulting charge carriers are on separate chains, the carriers will be self-localised to form polarons. Singlet and triplet excitons are stable excitations as well in semiconducting polymers [19].

## 1.3 Electronic Properties of Conjugated Polymers

The charged species in organic semiconductors are not simply free electrons and holes like in inorganic semiconductors [20]. According to the ground state structure of the conducting polymers, they can be divided into two types: nondegenerate and degenerate structures. Aromatic polymers, such as polythiophene, belong to the nondegenerate form where the polarons and bipolarons are thought to be formed on doping with charge storage in bipolarons [21]. In contrast, the degenerate structure is a main feature in *trans*-polyacetylene where solitons and polarons are believed to be the intrinsic excitations which have charge and/or spin and structural deformation associated with them [22].

The model, polaron-bipolaron has been used in order to explain the electrochemical and optical properties of conjugated polymers. Actually, these two states are related to the intermediate energy levels developed in the polymer within the band gap region caused by oxidation or reduction [23]. As quasi-one-dimensional materials, the structure of organic conjugated polymers can easily be distorted because of electron lattice interactions. As a result, upon doping, charge injection, or photoexcitation a local distortion in geometry can occur due to the localising the charge, which costs the polymer some of its energy. On the other hand, the formation of this local geometry increases the electron affinity of the polymer making it more able to accommodate the newly formed charges. In addition, it reduces the ionization energy of the polymer chain. The energy of the polymer according to this method is less than it would if the charge was delocalised and takes place in preference of charge delocalisation. This combination of an excitation and distortion lead to the formation of the polaron and bipolaron [23]. However, the existence of the bipolaron is more favorable compared to the formation of two polarons as it was suggested by Brédas *et al.* [24, 25].

Organic conjugated polymers with large band gaps do not conduct to a significant extent until charge carriers are formed within the conjugated backbone. Oxidising or reducing the polymer will create either positive or negative charge carries respectively, accompanied with structural changes limited to a couple of rings in case of aromatic polymers leading to new electronic states within the band gap.

**Figure 1-5** gives an example for the oxidative doping process of polypyrrole [26]. First, a free radical and a spinless positive charge are produced by removing an electron from the π-system of the backbone. These free radical and positive charge are coupled to each other *via* local resonance which takes the form of quinoid-like rings arrangement (**Figure 1-5 a-b**). The distortion produced by this is of higher energy than the remaining portion of the polymer chain. A considerable amount of energy will be lost due to the creation and separation of these defects. As a consequence, the number of quinoid-like rings will be limited to 4 rings in case of polypyrrole [27]. This combination of a charge site and a radical is called a polaron which could be either a radical cation (chemical oxidation) or radical anion (chemical reduction). Further oxidation to the polymer chain will remove another electron leading to a new spinless defect called a bipolaron which is energetically favorable as compared to the formation of two polarons [27].

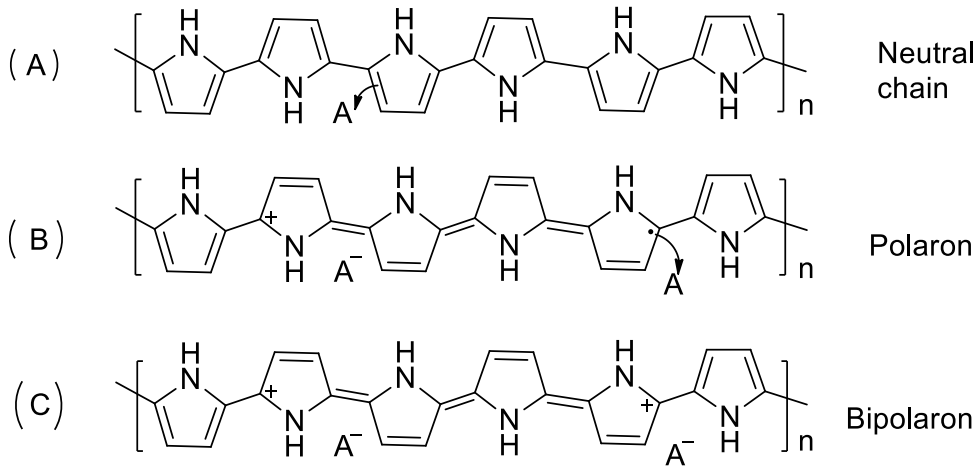


**Figure 1-5:** Oxidation of polypyrrole and creation of polaron and bipolaron states.

As the doping level increases, bands will form due to the overlapping between the polaron and bipolaron states which will, with time, merge with valance and conduction

bands. The evolution of the polypyrrole band structure upon doping is shown in **Figure 1-6**.

Oxidative doping results in the formation of energy levels between the conduction and valance bands, that help in narrowing the band gap. As a result, conductivity of the polymer increases and its absorption is shifted to longer wavelengths. As the doping of the polymer increases, overlap between these energy levels with the valance and conduction bands can occur, leading to quasi-metallic behavior. In general, as the conjugation length of the polymer increases, the conduction and valance bands will be broader which lead to a smaller band gap, and consequentially better conductivities and absorptivities [28, 29].

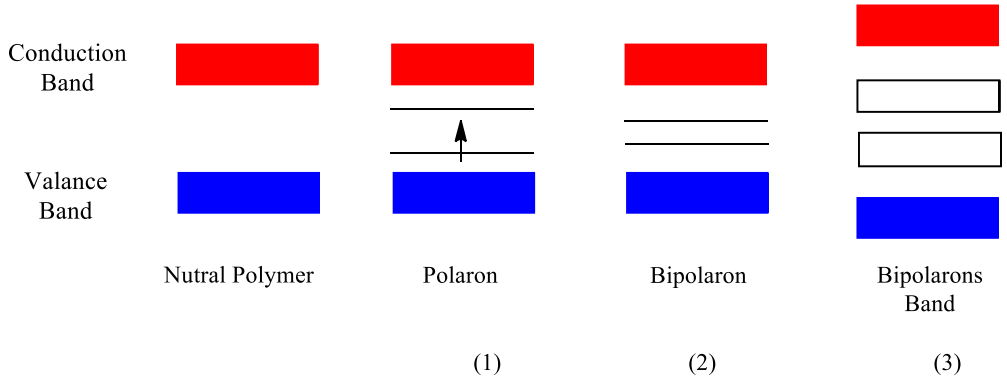


**Figure 1-6**: Evolution of the polypyrrole band structure upon doping: 1) low doping level; 2) moderate doping level; 3) high doping level. (Adapted from Brédas *et al*) [25].

The essential electronic excitations which exist in the case of *trans*-polyacetylene are called solitons where two patterns of alternating double and single bonds exist. When these two patterns co-exist on the polymer chain, a domain wall will exist and separates the two phases as shown in **Figure 1-7** [25]. Due to the existence of this domain wall or what can be called 'soliton', a non-bonding state will occur within the energy gap (at mid-gap attributable to the symmetry of the structure). This soliton or the domain wall will form by adding charge or removing charge form the polymer backbone. Conjugated polymers with nondegenerate ground states does not have solitons [25].

As the doping level increases the population of polarons, bipolarons, and/or solitons will increase. The localised polarons, bipolarons or solitons near to individual dopant ions could overlap at high doping levels which will lead to new energy bands between

and even overlapping the valence and conduction bands, through which electrons can flow. The bulk conductivity of conducting polymers should consist of contributions from intra-chain, inter-chain and inter-domain electron transportations [30].

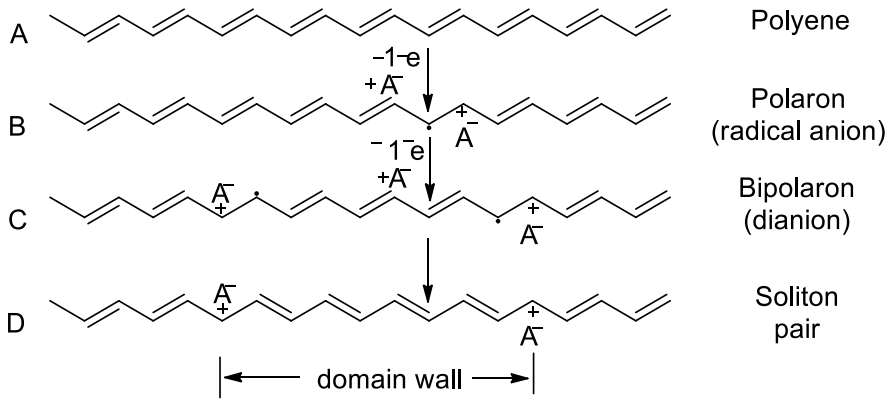


**Figure 1-7:** Formation of two solitons upon oxidative doping of polyacetylene.

## 1.4 Band Gap Engineering of Organic Conjugated Materials

Because of the important role played by conjugated polymers in emerging electronic, photovoltaics and display technologies, narrowing their band gap and fine-tuning their energy levels have been main tasks for polymer chemists for a long time. As a result, a rapid development in this research area has taken place due to the need of a variety of different polymers with different properties such as: emission or absorption, hole or electron affinities, and conductivities.

Conjugated polymers show intrinsic band gaps due to the presence of the so-called bond length alternation (BLA) between double and single bonds along their backbones. Hypothetically, the band gap would be zero in the case of a conjugated polymer and should show a complete electron delocalisation. But because of Peierls instability, such a system is unstable leading to electron localisation on carbon-carbon double bonds and subsequently bond length alternation [31]. To improve the optical and electronic properties of a polymer, its band gap can be optimized though molecular design by simple manipulation of the chemical nature of its building blocks and the way they are connected. In fact, the band gap can be controlled by manipulating several parameters including: bond-length alternation, planarity, resonance energy, interchain coupling in

the solid state and inductive effects of the substituents [7, 32]. Two main methods towards engineering the band gap in conjugated polymers will be discussed here.

The first method involves alternating the repeating units of the conjugated polymer upon incorporating electron-rich and electron-deficient units along the polymer backbone in the so-called donor acceptor (D-A) or push-pull approach. This concept of push-pull engineering was first suggested in 1993 [33], where π electrons on the electron-rich donor are drawn toward the neighbouring electron-poor unit, thus increasing electron delocalisation and enhancing the existence of quinoid mesomeric structures ($D{-}A \leftrightarrow D^{+}{=}A^{-}$) [34]. In addition, these types of polymers are prone to what is known as internal charge transfer (ICT), in which electronic charge is transferred between the donor and the acceptor. This leads to stronger double bond characteristics between the two components of the polymer. As a result, the conjugated backbone adopts a more planar conformation to accommodate for the extra π-electron delocalisation present which lead to a low band gap due to increased conjugation [35].

The other advantage of the D-A approach is the ability to tune the energy levels of the conjugated polymers by altering the strength of the donor and acceptor moieties as well as being able to tune the band gap. This is because the LUMO level is thought to be localised on the acceptor unit and so can be changed by making modifications to this part of the polymer. The HOMO level is more delocalised along the polymer backbone despite that there is some evidence for it being localised on the donor unit (**Figure 1-8**) [35-37]. On the other hand, this approach typically have molar absorption coefficients up to an order of magnitude lower than their corresponding homopolymers [38]. This disadvantage is attributed to the poor spatial overlap between the HOMO and LUMO levels because of their localisation on different aromatic moieties.

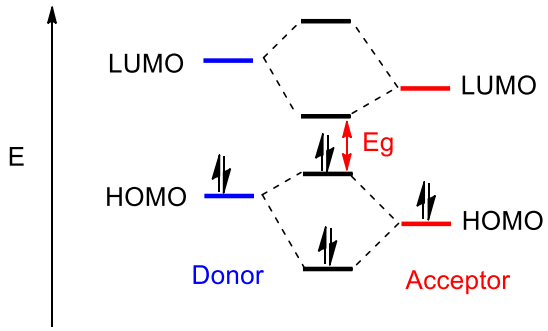


**Figure 1-8**: A schematic representation of band gap lowering by donor-acceptor interaction [37].

The second approach for lowering (BLA) and band gap is to stabilise the quinoid resonance structure, where aromatic building units are designed to have intrinsic quinoidal character. Thus, two molecular resonance structures will be created leading to more overall electron delocalisation along a conjugated polymer backbone [8]. However, energetically the quinoid structure is less stable compared to the aromatic form due to the aromaticity destruction and hence this loss in the stabilization energy is required for quinoid formation [37]. So to tackle this drawback, Wudl *et al*, suggested that the quinoid structure can be stabilised by fusing another aromatic ring to the polymer chain [39], such as isothianaphthene, thienothiophene and thienopyrazine.

The reduction of the band gap energy in the polymer induced by quinoidal effect can be justified with molecular orbital theory (**Figure 1-9**). In this case, the molecular band gap of aromatic materials can be lowered by the quinoidal effect through destabilizing the HOMO-LUMO levels of the material, because polymers with considerable quinoidal character have less aromatic forms and hence low aromatic stabilisation energy. The main disadvantage of this approach lies in their relatively high lying HOMO levels, so further engineering these quinoid monomers by introducing substituents on their backbone can help in lowering the HOMO levels [35].

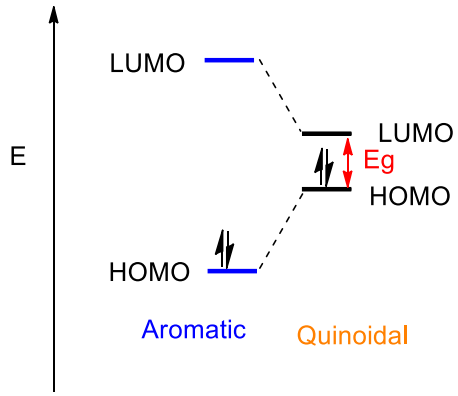


**Figure 1-9:** A schematic representation of band gap lowering by quinoidal effect.

## 1.5 Applications of Organic Conjugated Polymers

A number of potential applications of organic conducting polymers have been investigated since 1961. These include organic photovoltaic cells (OPV), organic light emitting diodes (OLED) [40, 41], organic semiconductor lasers [42], organic field-effect transistors[43, 44] and biosensors [45]. In some applications, conducting polymers were suitable replacements for metals. One of the advantages of organic polymers is their flexibility if they are compared to inorganic materials. In fact, they can be chemically modified and shaped in accordance with the requirements of a certain device. Organic polymers are used for electronic devices due to their versatility and compatibility as well as the ease of fabrication and light weight. The potential applications of these conjugated polymers came from their conducting or neutral forms.[46] This work focuses on organic photovoltaic applications of semiconducting polymers, so it will be discussed in some details in the coming sections.

## 1.6 Organic Photovoltaics (OPVs)

Organic polymer solar cells are attracting a great deal of interest. These systems have potential technological value due to their ease of fabrication and their relatively low production costs compare to silicon-based solar cells, ease of processing and mechanical flexibility. Although researches on organic solar cells started in the 1980s, N.S. Sariciftci *et all*, provided the first example of polymer solar cells with a convenient physical and chemical explanation. The power conversion efficiency (PCE) was 0.04% which was obtained by using monochromatic light [47, 48]. Later, donor–acceptor bilayer planar heterojunction cells were introduced by Tang *et al.* and afforded

organic photovoltaic (OPV) cells, achieving around 1% of power conversion efficiency [8]. However, the efficiency of bilayer heterojunction devices is largely limited by the reduced area of charge generating interface between the acceptor and donor. The bulk heterojunction (BHJ) cell has been introduced as an alternative to the former techniques to improve the PCEs of the polymer solar cells due to the formation of a donor-acceptor bicontinuous inter-penetrated network. As a result, a large interfacial area is created between the polymers and electron acceptors (e.g. fullerene derivatives), therefore this leads to efficient photo-induced charge separation in devices [49]. The development of OPVs and their efficiencies has become quite a popular and promising topic for scientific research, and is likely to continue to maintain this encouraging rate of progression. Recently, polymer solar cells (PSCs) technology have achieved a dramatic progress with its key parameter, power conversion efficiencies (PCE) reaching a new world record 11.7% [50, 51]. However, improving the PCE still is the most important goal to researchers as well as increasing the lifetime of these polymer solar cells. Essentially, Konarka Technology has achieved the best stability for the PSCs, which was more than a year [52].

## 1.7 Development of OPV Active Layer Architecture

A short overview will be given here about the most successful approaches towards improvements in the efficiency of organic solar cells to-date.

### 1.7.1 Single Layer Organic Solar Cells

Single layer solar cells could be considered as the first OPV device which had the simplest structure of the organic solar cells. Basically in this device, an organic photoactive layer is comprised between two electrodes of different working functions, an indium tin oxide (ITO) and Al electrode [53] as shown in **Figure 1-10**. The difference of work function between the two conductors sets up an electric field in the organic layer. Absorbing light by the organic layer will lead to the excitation of electrons to the LUMO level leaving holes in the HOMO level and hence excitons will be formed. The separation of the exciton pairs will take place when the potential created by the different work functions, pulling electrons to the positive electrode and holes to the negative electrode.

The proper clarification for the behavior of this device can be illustrated by the MIM-model or by the formation of a Schottky barrier between the metal with the lower work function and the *p*-type organic layer as stated by Harald Hoppe *et al* [54].

Single layer cells suffered low efficiencies below 0.5 % because of poor charge carrier generation and an unbalanced charge transfer. There are other problems which also arise at the surface interface with electron-hole binding and recombination of electrons [55].

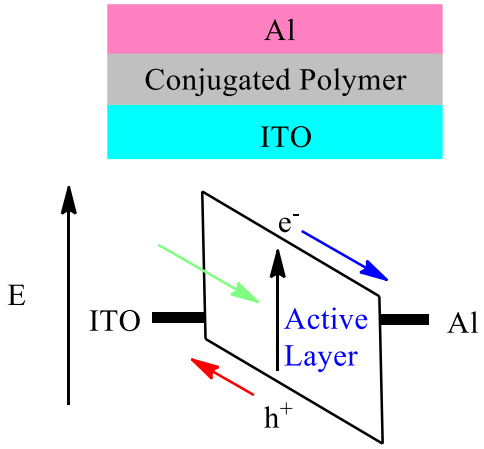


**Figure 1-10:** A schematic diagram single layer organic solar cell (Adapted from L. Wang *et al*) [56].

### 1.7.2 Bilayer Organic Solar Cells

A new approach has been introduced by Tang in 1986 called bilayer organic solar cells to overcome the low power conversion efficiency of the first generation of solar cells. The new system has been fabricated from copper phthalocyanine and a perylene tetracarboxylic derivative introducing the concept of donor–acceptor heterojunction. What distinguishes the new system is that it is consisting of two layers of materials which have different electron affinity and ionisation energy that help the emergence of electrostatic forces at the interface between these two layers. This enables the break-up of excitons much more efficiently than single layer systems do. The two materials are selected carefully so as to assist the development of strong local electric fields between them. The layer with lower electron affinity and ionisation potential is the electron donor, and the other layer is the electron acceptor [57].

In bilayer organic solar cells (**Figure 1-11**), once the excitons are photogenerated in the photoactive materials, they have to reach the (D-A) interface by diffusion where charge transfer can occur, where electrons will transfer to LUMO levels of the acceptors and the holes to the HOMO levels of donors. The diffusion process should be fast enough before the excitation energy of the excitons is lost *via* either radiative and non-radiative decay processes to the ground state. In fact, this issue is one of the drawbacks affecting the performance of bilayer devices, because the excitons diffusion length in the D-A phases typically is limited to 5-15 nm [58]. Only light that is absorbed within a very thin region around the interfacial area contributes to the photovoltaic effect, hence such a thin layer cannot absorb all the incident light [59]. The other limitation which reduces the efficiency of bilayer organic solar cells is the low donor-acceptor interfacial area where the excitons can dissociate into separated charges. So the excitons formed far from this interfacial area will recombine to the ground state.

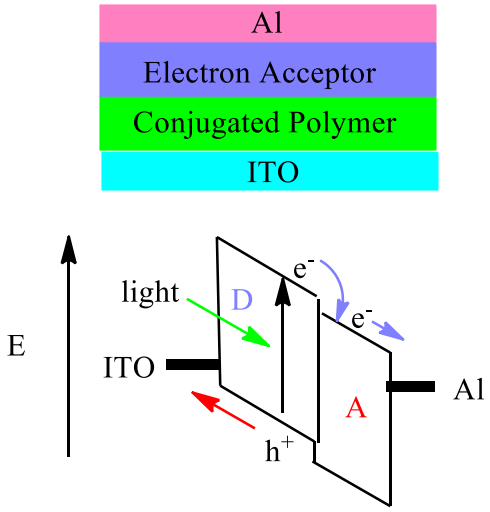


**Figure 1-11**: A schematic diagram of bilayer organic solar cell (Adapted from L. Wang *et al*)[56].

### 1.7.3 Bulk Heterojunction Devices (BHJ)

To overcome the disadvantages faced by bilayer devices described above, in terms of both the short lifetime and low mobility distance of excitons, blending donor and acceptor constituents with different electron affinities has shown rapid excitons dissociation [60]. Anywhere in the active layer of the organic solar cell, the distance to the interface should be on the order of the exciton diffusion length. This problem was solved by introducing bulk heterojunction devices where *p* and *n*-type materials are

mixed together and hence junctions are created in the interfacial area between the two materials. This junctions will ensure that each photogenerated exciton leads to charge transfer, irrespective of the thickness of the layer [61, 62]. **Figure 1-12** showed BHJ solar cells and the materials used in the active layer.

In 1995, the first organic bulk heterojunction organic solar cell was fabricated by Yu *et al*, based on a mixture of soluble poly-*p*-phenylene-vinylene (PPV) derivative with a fullerene acceptor. They found that this arrangement enhanced the incident photon to electron conversion by 10 fold compared to bilayer systems [63].

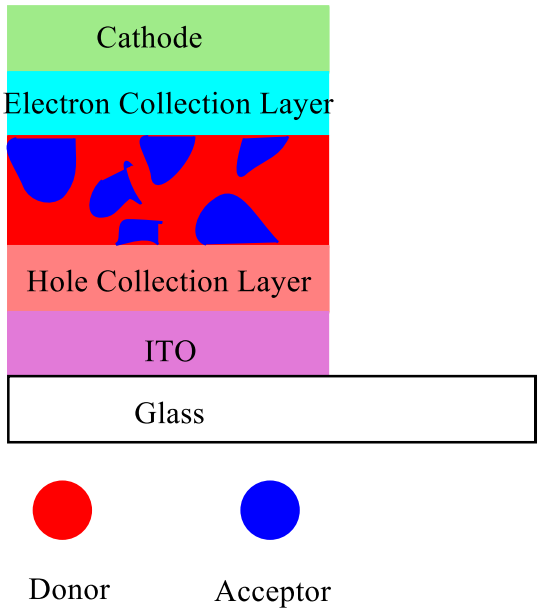


**Figure 1-12:** Schematic diagram of BHJ solar cell (Adapted from *Organic Solar Cells; Materials and Device Physics*) [64].

Compared to bilayer devices, BHJ morphology offers two distinct performance advantages. The first one is that, maximising the donor–acceptor interfacial area through the interpenetrating network, and hence minimising the distance needed for the excitons to travel to the interface before they decay to the ground state. Secondly, this blending of donor-acceptor network offers better charge transport pathways to enable the charges to be collected at the electrodes [61].

Controlling the morphology is crucial for efficient BHJ solar cells, so to reach the best performance, simple methods of optimization have been achieved in the last few years. For example, choosing the solvent to deposit films from, and annealing the processed

donor-acceptor films of the active layer resulted in favorable inner structure for the dissociation of the excitons and the subsequent charge transfer [61, 62].

## 1.8 Elementary Processes in Organic Solar Cells

As represented in **Figure 1-13**, when an organic solar cell is subjected to light, photons will be absorb by the photoactive layer resulting in the formation of neutral excitons (localised electron-hole pairs) instead of free charged carries [65]. The formed excitons have to migrate towards the interfacial area between donor-acceptor (D-A) within their lifetimes of femtoseconds [66, 67] with diffusion length of a few tens of nanometers [68, 69] where they dissociate *via* an electron transfer process. Excitons formed away from the interfacial area of (D-A) will recombine by decaying by thermalisation or emitting photons [70, 71].

In the (D-A) interface, the excitons will dissociate where electrons transfer from the LUMO of the donor to the LUMO of the acceptor and hence charge separation take place. In parallel with the previous electron transfer, hole transfer occurs between the HOMO of PCBM and the HOMO of the donor at the D-A interface. The driving force needed for exciton dissociation is the difference between the energy level of LUMO of the excited donor and LUMO of the acceptor material to overcome the binding energy of the excitons [70]. Scharber *et al*, estimated the difference between these two levels to be at least 0.3 eV [60].

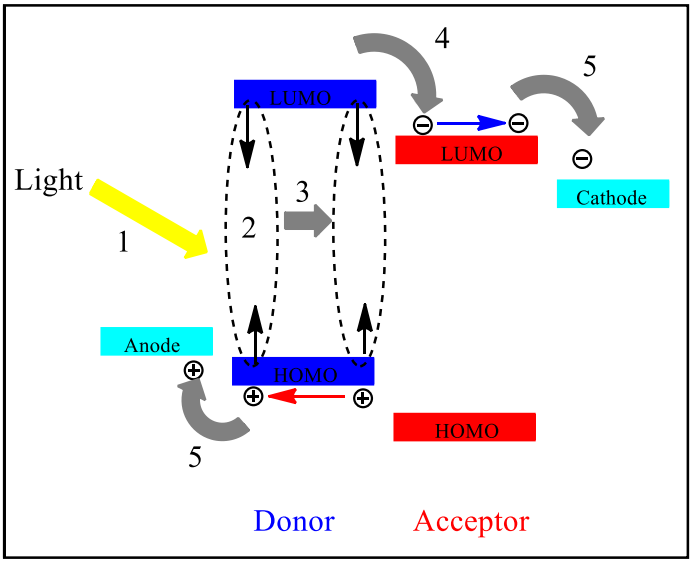


**Figure 1-13:** The basic processes occurring in organic solar cells. These include; 1. light absorbance; 2. photo-generation of excitons; 3. excitons diffusion; 4. exciton dissociation into separated charges; 5. transport of the separated charges to the electrodes. (Adapted from reference Li *et al*) [72].

In fact, after exciton dissociation, positive and negative polarons are formed in the donor and acceptor phase respectively. These charged polarons are still coulombically bound polaron pairs. The polaron pairs are broken up due to the internal electric field set up by the work function difference of the electrodes where positive polarons drift to the anode and negative polarons go to the cathode. Efficiency of charge transport rely on the charge mobilities (mobility of the negative polaron in the acceptor and positive polaron in the donor), but because of the weak electron-vibration coupling in organic systems, the charge mobilities are very low compared to those in inorganic systems [36]. Polaron hopping between the adjacent chains is the way for hole transportation in the conjugated organic systems. Because of that, these mobilities are greatly dependant on solar cells morphology. As a result, amorphous films have shown low hole mobilities compared to their crystalline counterparts [36]. At the end, the polarons have to be collected from the bulk-heterojunction. To do the collection sufficiently, ohmic contacts between the two electrodes and the active layer are curial where the anode has to match the HOMO level of the donor and cathode has to match the LUMO level of the acceptor [61, 73].

## 1.9 Ideal Polymer Required for OPV

The challenge in developing an ideal donor material is to design and synthesise an organic semiconductor polymer that simultaneously shows good film-forming properties, strong light harvesting, high hole mobility, and suitable HOMO-LUMO energy levels. A good understanding of molecular design and versatile polymer synthetic methods help us for an effective manipulation of the properties of conjugated polymers to meet the requirements of the desired purpose and address the required application needs [7].

As it was discussed in section 1.4, the band gap and the HOMO–LUMO energy positions are the most important criteria to determine the optical and electrical properties of a certain organic semiconducting material due to their ability to control its ultimate photovoltaic performance. In fact, the first step in the photovoltaic mechanism involves the absorption of sunlight by the photoactive organic semiconducting materials which should cover the most important part of the spectrum of solar radiance. Organic semiconducting materials with optical band gaps ranging from 1–2 eV are preferred to increase the efficiency of organic solar cells. It's also crucial when you begin to design and synthesise organic semiconducting materials to take into account their optical band gaps which should be narrow to provide a wider absorption of sunlight. High overall extinction coefficients of the polymers are also of critical importance to efficiently absorb light, so it should not be sacrificed as the optical band gaps become smaller. Lowering the band gap can be attained by either raising the HOMO or lowering the LUMO level of the polymer or by compressing the two levels closer together simultaneously [7].

Also, designing and synthesising a conjugated polymer to work as an ideal donor-polymer in polymer-based BHJ solar cells obtaining high PCE need to meet these coming requirements represented by the power conversion efficiency equation[58]:

$$PEC = \frac{Voc \times Jsc \times FF}{Pin}$$

where $V_{oc}$ is open-circuit voltage, $J_{sc}$ is short-circuit current, *FF* is the fill factor, and $P_{in}$ is incident light power density.

Achieving high $V_{oc}$ and high $J_{sc}$ is very important as well as high fill factor to enhance organic solar cell efficiency toward its theoretical maximum. The band gap of the organic photoactive material and the positions of the HOMO and LUMO levels are thought to have influence on $V_{oc}$ and high $J_{sc}$ with respect to PCBM acceptor used in the OPV device [58].

When two terminals of a device are disconnected from a circuit, the resulting difference in electrical potential is known as the open circuit voltage ($V_{oc}$). The maximum open circuit voltage ($V_{oc}$) is correlated to the difference between the PCBM's LUMO energy level and the donor's HOMO energy level based on experimental evidence. As a result, to have an OPV device with high $V_{oc}$, a conjugated polymer with a reasonable low lying HOMO level should be used. However, the LUMO energy level of the donor should be located above the LUMO level of the acceptor (PCBM) by a range of 0.2-0.3 eV to make sure that efficient electron transfer occurs from the polymer donor to the PCBM acceptor in the BHJ blend[74]. Therefore, the HOMO level of the donor polymer cannot go too low. It worth to mention that, the HOMO level of a material, which describes the accessibility of the material molecule to be oxidised, reflects the air stability of the material. The oxidation threshold of air is between -5.2 eV and around -5.3 eV against vacuum level. Therefore, the HOMO level shouldn't ideally exceed this value to preserve the air stability to the polymer. According to these factors the ideal HOMO level of a polymer should be in the range of -5.2 eV to -5.8 eV against vacuum level due to the compromise of stability and band gap as illustrated in **Figure 1-14**. It should also be noted the bulkiness of side chains, interchain distances, and morphology of active layers have also been demonstrated to have a noticeable effect on $V_{oc}$ [7, 37, 60, 75].

The short circuit current ($J_{sc}$) is known as the maximum current between the terminals of an OPV device when connected as part of complete circuit. Most of the solar flux is distributed within 380-900 nm; so a polymer with a band gap near to 1.5 eV should be used to be compatible with the solar spectrum to increase the excitons generation. In fact, the number of excitons generated during sunlight exposure determines the theoretical upper limit of $J_{sc}$, so it is important that the active layer absorb as much of

the sunlight as possible. Using narrow band gap polymers could help in absorbing more of the solar flux lifting the $J_{sc}$ value. However, continuing to reduce the band gap of the donor would increase the HOMO level and hence reducing the $V_{oc}$. The real short circuit current obtained in a polymer solar cell is lower than that estimated because of different loss mechanisms including recombination during transport and extraction [74, 76].

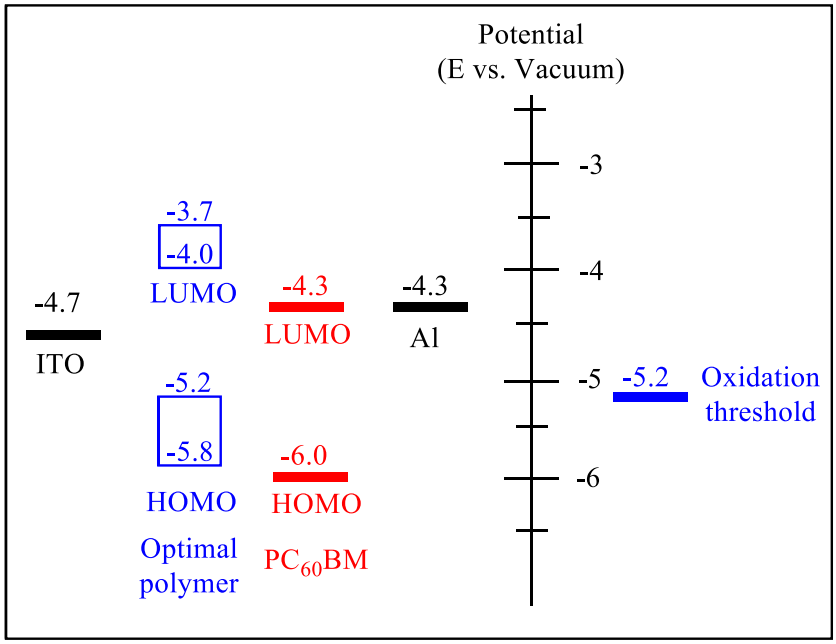


**Figure 1-14:** Optimal HOMO/LUMO energy level of optical polymer used in BHJ solar cell with $PC_{60}BM$ as acceptor. (Adapted from Blouin *et el.*)[75].

## 1.10 Synthetic Routes to Conjugated Polymers

During the last few decades, a significant progress has been achieved in the synthesis of conjugated organic materials. The most important part in the synthesis of conjugated polymers lies in the formation of new C–C single bond between two unsaturated monomers [7]. Along with chemical oxidative and electrochemical polymerisation, metal catalysed cross coupling reactions have been introduced as a powerful method for the preparation of new C$sp$– C$sp^2$ and C$sp^2$– C$sp^2$ bonds [7]. Cross coupling polymerisations using transition metal catalysts are usually used in the preparation of conjugated polymers including the Negishi [77], Heck [71,78], Suzuki [79] and Stille [73,80] coupling reactions.

### 1.10.1 Chemical Oxidative Coupling Polymerisation

Oxidative coupling polymerisation was used extensively in the early stages of conjugated polymer investigations. Compounds like thiophene, aniline and fluorene which have electron-rich sites around their ring system can react with oxidative reagents (ammonium persulfate, $FeCl_3$, etc.) leading to the conjugated polymers [81-83]. The first attempt to synthesis soluble and processable conjugated polymers was established by Yoshino *et al* [84] when he reacted 9,9-dihexylfluorene with $FeCl_3$ as the oxidant to produce the conjugated polymer as shown in **Figure 1-15**. However, one of the disadvantages of this reaction is the poor regioselectivity which leads to defects in the desired 2,7-linkage positions. The other disadvantage associated with this polymerisation is that, the resulting polymers are obtained in their oxidised (doped) state which could cause problems in certain applications if the polymers are required in their neutral state.

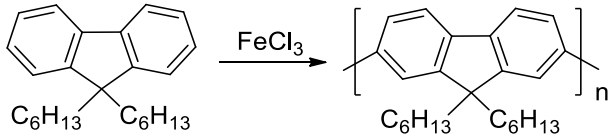


**Figure 1-15**: Oxidative preparation route to poly(9,9-dihexylfluorene).

### 1.10.2 Electrochemical Oxidative Polymerisation

The electrochemical polymerisation method has been employed for the synthesis of some conjugated polymers like polythiophenes and polypyrrole. It shows several advantages that makes it a unique method for electrochemical studies of conjugated polymers. One of its advantages is that, it requires small amount of monomer to yield both electrode-supported and free standing films. Also, the polymers prepared by this tool are prepared as thin films directly [85]. Electrodes used for this method should be inert electrodes, such as gold, platinum or ITO coated glass slide. The electrodes are then polarized positively in an electrolytic solution containing the monomer. The applied potential induces oxidation of monomers to polymers. Essentially, electrochemical polymerisation involves electrogenerated radical cations as the reactive species. Polymer synthesis will take place through a series of radical coupling reactions and electrochemical reoxidation following the general $E(CE)_n$ mechanism [86]. The

suggested mechanism for the electropolymerisation of heterocyclic monomers by anodic coupling is shown in **Figure 1-16** [87]. The first step (E) involves oxidation of the monomer to give a radical cation. Since the migration of the monomer from the bulk solution is slower than the electron-transfer reaction, so a high concentration of radicals is continuously maintained near the electrode surface [86].

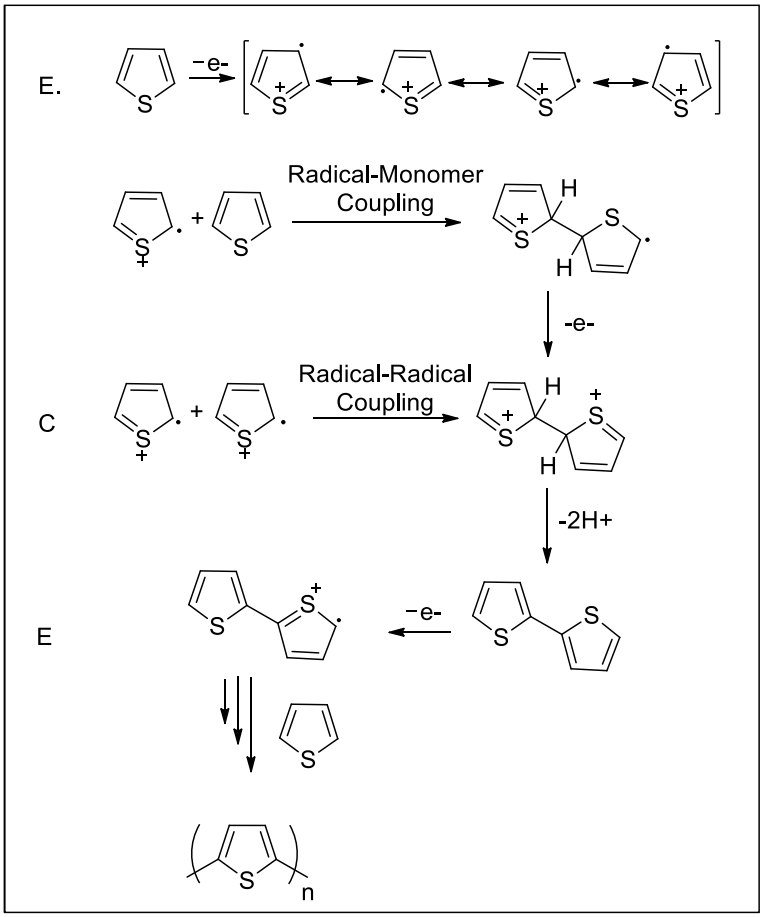


**Figure 1-16**: The mechanism of electrochemical polymerisation of heterocyclic polymers.

The next step (C) involves the coupling reactions which takes place either by the combination of two radical cations to give a dication or by the radical cation coupling with a molecule to give a radical cation dimer which in turn loses one more electron to form dication. This dication easily loses two protons to give a neutral dimer. Reproducing the aromaticity is the driving force for this chemical step (C). Oxidation of the resulting dimer is easier when compared to the starting materials and hence it occurs in its radical form and undergoes a further coupling with a monomeric radical

due to the applied potential. The formation of a long polymer chain will be led by subsequent electrochemical and chemical reactions follow the general E(CE) pathway [86].

### 1.10.3 Cross-Coupling Reactions

Organic conjugated polymers without any substituents are generally unprocessable due to aggregation issues. For this reason, the synthesis of organic conjugated compounds is often conducted with monomers with suitable alkyl or alkoxy solubilising groups using transition metal–catalyzed reactions [88]. Cross-coupling reactions are considered as important methods in the field of organic synthesis for creating new C–C bonds between two unsaturated molecules in the presence of a transition metal catalyst [89].

Groups 8–10 transition metals have the ability to activate a variety of organic compounds and so can catalyze the creation of new bonds. Palladium and nickel are the metals widely used for catalytic organic transformations due to their Pd(II)/Pd(0) and Ni(II)/Ni(0) ease of redox exchange which is needed to complete catalytic cycles [89-91]. However, due to its low sensitivity to oxygen and low toxicity, palladium catalysts are more preferable for cross coupling reactions. In addition, Pd catalysts are reacted without intervention of radical intermediates, that can give rise to side products like those from homocoupling [89]. $Pd^0$ can be used directly in the reaction mixture or can be generated from Pd(II) complex sources. As an examples of zero-valent Pd complexes which can be used as a source for $Pd^0$ are $Pd(PPh_3)_4$ and $Pd_2(dba)_3$. While $Pd(PPh_3)_4$ can be used as a catalyst for a number of cross-coupling reactions, $Pd_2(dba)_3$ is treated with suitable ligands to form the desired catalyst [92]. One of the reasons why Pd(II) pre-catalysts are used to generate catalytically active Pd species *in situ* is the instability of $Pd^0$ complexes. $Pd(OAc)_2$ and $Pd(PPh_3)_2Cl_2$ are examples of extensively used catalyst precursors, which can be reduced to $Pd^0$ by phosphine ligands [93].

The suggested catalytic cycle scheme of the transition metal–catalyzed cross coupling reactions is shown in **Figure 1-17**, where the reaction occurs in three main steps which include oxidative addition, transmetalation and reductive elimination [90]. In the oxidative addition, the metal such as palladium can complex to more molecules leading to the increase in the oxidation state of the Pd(0) by two units.

In the second stage of the coupling, a transmetallation process take place where another organometallic complex reacts with the palladium complex to remove the halide and transfer organic group R from the metal (M1) to the Pd one. The new organometallic compound M1–R will react with the generated transition metal complex formed in the oxidative addition. The R group will be transferred to the transition metal *via* exchange of the halide with organic group. The differences in the electronegativity between the two metals is the main driving force for transmetalation, where the transition metal must be more electronegative than the main group metal (M1) [89, 94].

Finally, reductive elimination will occur which is the reverse of oxidative addition. In this step, a new compound (R–R) will form resulting from the formation of a new covalent bond between the two organic groups which is resulted from the cleavage of two ligands around the transition metal center. This process reproduces the palladium complex to the original form to be used again in the cross-coupling reaction cycle [94].

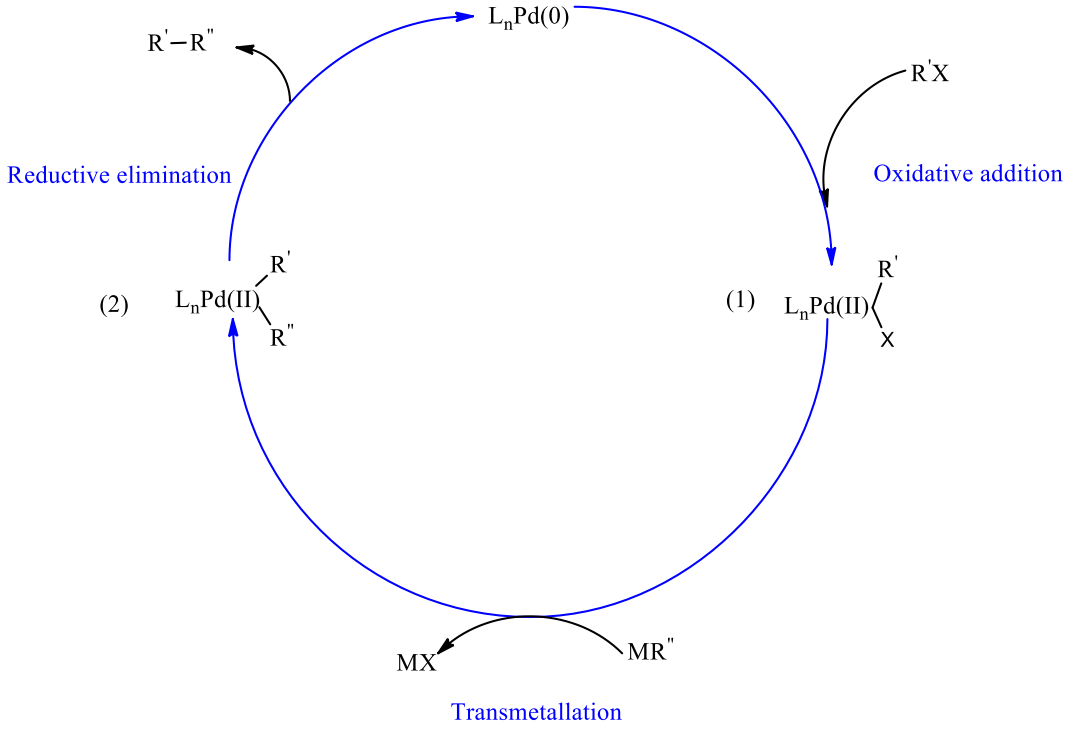


**Figure 1-17:** The proposed cross-coupling reaction mechanism, where L is ligand, R'-R" are organic moieties, X is halide, M is metal, and n is number of ligand.(adopted from Pretze *et al.*)[95]

In this work, palladium cross coupling polycondensations have been employed to prepare the conjugated donor materials including, Stille, Sonogashira and direct arylation polymerisation.

### 1.10.3.1 Sonogashira Coupling Reaction

The Sonogashira coupling reaction is able to couple terminal carbon from alkynes with aryl or vinyl halides for the synthesis of arylalkynes, conjugated enynes and diaryl-substituted acetylenes as illustrated in **Scheme 1-1**. The importance of the reaction comes from being a valuable tool for producing liquid crystals and conjugated materials with a certain electronic and optical properties. The reaction generally proceeds easily at room temperature using a Pd catalyst, combined with a catalytic amount of CuI in an amine as a solvent. According to Sonogashira, the addition of CuI significantly enhances the reaction, and improved the yield of the product. As a result, this makes this reaction as the preferred method for the alkynylation of aryl or alkenyl halides [93, 96]. However, using Cu(I) salts in Sonogashira coupling has some drawbacks which are still widespread today. In addition to including a reagent in the reaction mixture that is difficult to recover and environmentally unfriendly. Exposing the copper co-catalyst to air will lead to homocoupling between the generated copper acetylides along with the desired cross–coupling with aryl or vinyl halide compounds [97].

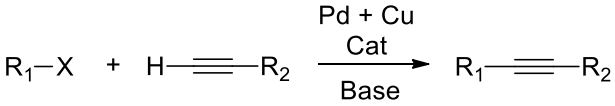


**Scheme 1-1**: The Sonogashira coupling reaction.

The exact mechanism for the Sonogashira coupling reaction is not fully understood because of the difficulty facing the isolation and analysis of the organometallic compound which are present as intermediates in this reaction [93, 98]. However, the hypothesised mechanism of Sonogashira coupling reaction is as shown in **Figure 1-18**.

**Figure 1-18**The suggested mechanism of the reaction is thought to occur through two independent catalytic cycles, Pd catalytic cycle as well as Cu catalytic cycle. The Pd catalytic cycle is the classical mechanism representation of cross-coupling reaction. The cycle starts in the catalytically active species $Pd(0)L_n$ including the base and/or

solvent molecules, and once the activated Pd(0) complex is formed the reaction starts with the oxidative addition of R–X (R1 = aryl or vinyl, X = halide) to a palladium complex $Pd(0)L_n$. This step is considered to be rate limiting step of the reaction. After that, the Pd-cycle will connect with the co-catalyst Cu-cycle which is still poorly understood. However it is thought that, the amine base assists the formation of copper acetylide with the help of a π-alkyne copper complex which would make the alkyne terminal proton more acidic. Then, the copper acetylide produced in the Cu cycle reacts with the palladium complex in the transmetalation step of the Pd cycle. The formed complex after transmetalation will be subject to *trans/cis*- isomerisation. Finally, in the reductive elimination step the desired product of the Sonogashira coupling will form and the Pd(0) is regenerated to be used in the reaction [93, 98].

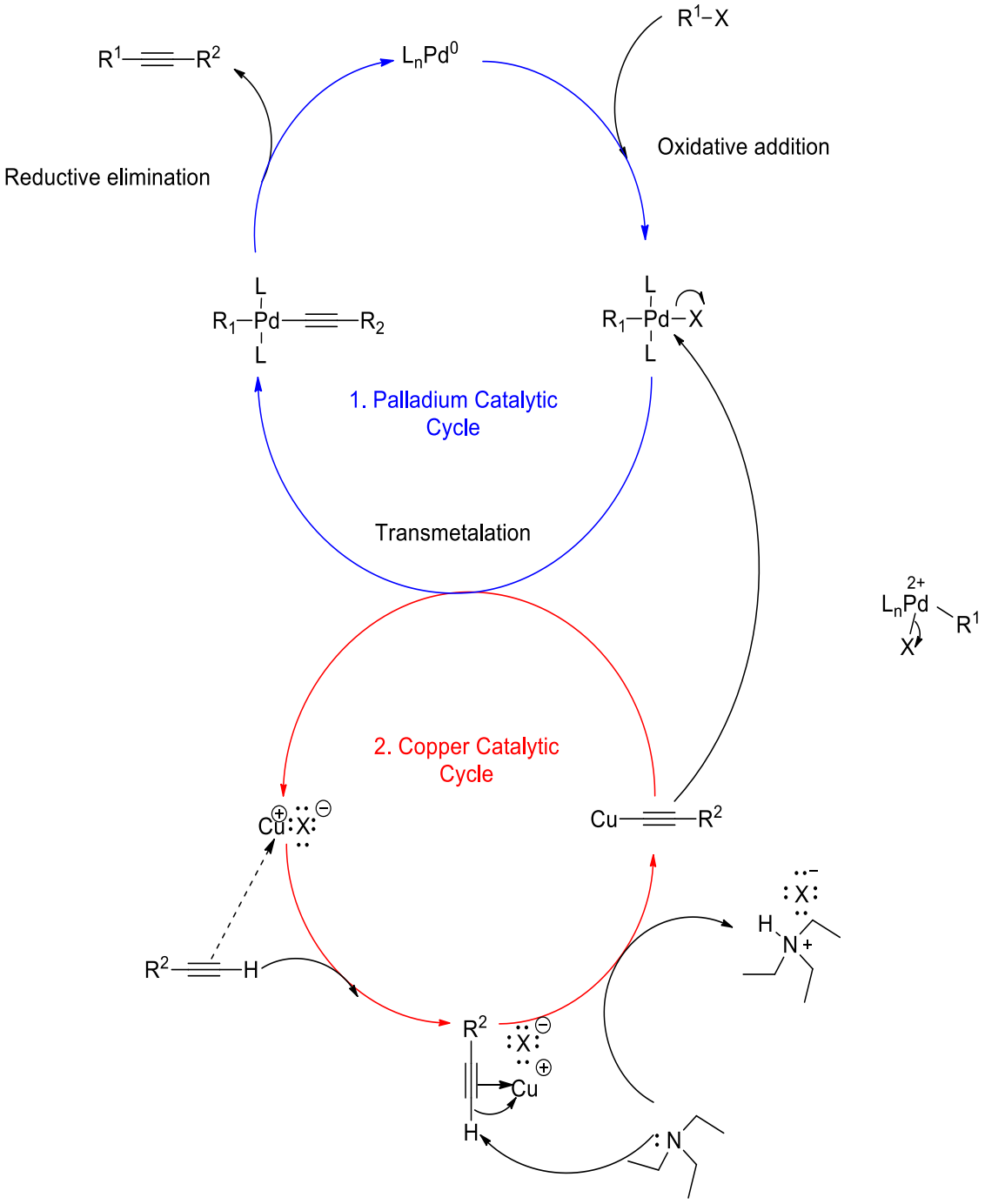


**Figure 1-18**: The mechanism of the Sonogashira coupling reaction (adopted from Chinchilla *et al.*) [93].

### 1.10.3.2 Stille Coupling Reaction

The Stille reaction (**Scheme 1-2**) couples organo-electrophiles such as aryl, alkyl or vinyl halide with organostannanes in the presence of palladium catalyst which is one of the useful and utilized method for C–C bond formation [80]. The reaction was first reported in 1978 by Stille *et al.* dealing with a ketone preparation using organotin compounds [80].

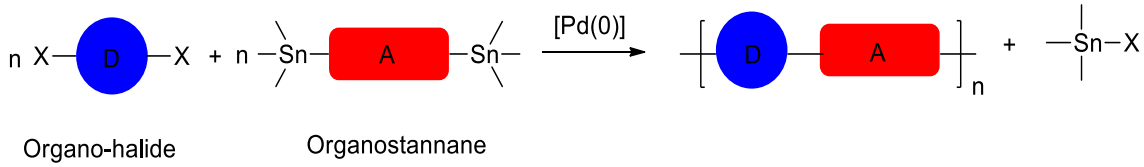


**Scheme 1-2:** The Stille coupling reaction.

One of the advantages of the reaction, is its ability to provide polymers in high yields and with high molar masses [88]. In addition, the highly covalent character of the Sn–C bond in contrast to other organometallic reagents make these reagents less nucleophillic and more stable. Also, the absence of base in the Stille coupling reaction makes it exceptionally tolerant for a large variety of functional groups. Therefore, Stille coupling remains one of the preferred synthetic methods at the small laboratory scale. However, due to the involvement of organostannanes and the poor atom economy of the tin reagents, this reaction generates a lot of toxic waste [99]. So it is difficult to use stannanes in large scale due to the safety requirements. As a result, other coupling reactions such as Suzuki coupling are industrially more favorable. Moreover, tin by-products are another problem which emerges from this method, so most often the Stille coupling requires chromatographic purification in order to get rid of unwanted tin derivatives in the final products [100, 101].

The most accepted mechanism for the Stille coupling is shown in **Figure 1-19**. The palladium catalyst used in the reaction can be used either as the active $Pd^0$ or as generated $Pd^0$ form Pd(II) precursor [102]. The active Pd(0) complex reacts with the organic halide R–X to give Pd complex 1. In the next step, the transmetallation is

thought to form complex 2. In fact, this complex was the only species that could be observed in the catalytic cycle, which indicated that the transmetallation reaction with the organictin was the slowest step in the reaction. A *trans* to *cis* isomerisation occurs to give complex 3, which then undergoes a reductive elimination to give the final coupled product and regenerates the palladium(0) catalyst [103, 104]. For more details on the Stille reaction, please refer to these reviews [104, 105]

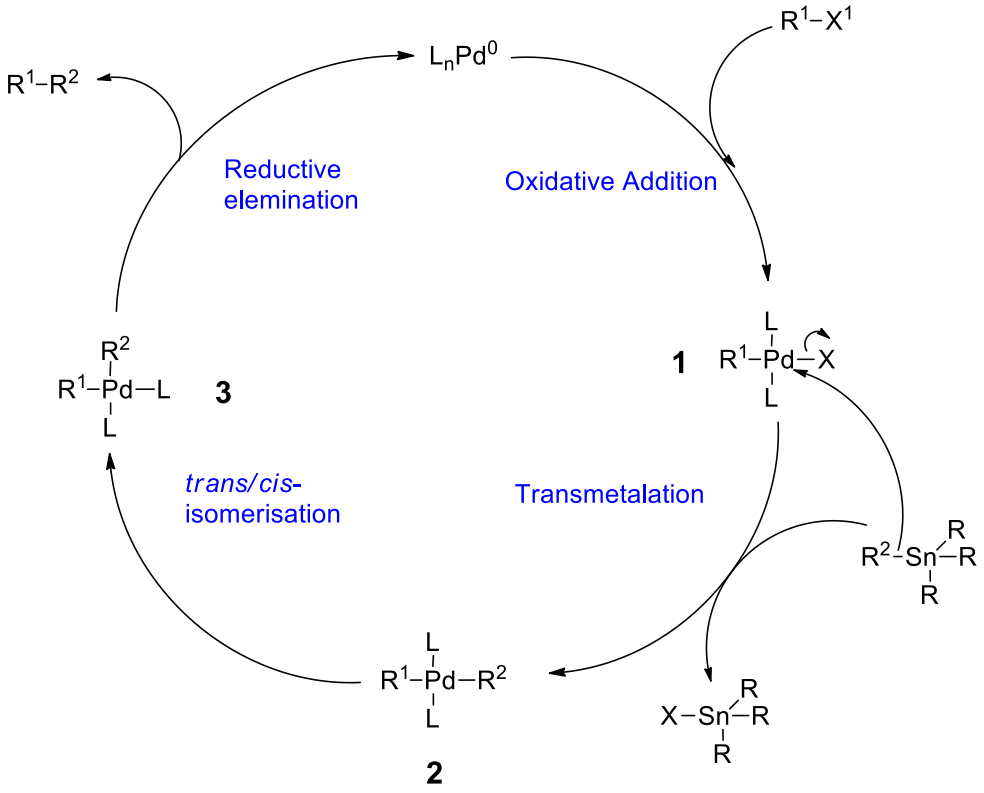


**Figure 1-19:** The mechanism of the Stille coupling reaction (adopted from Milstein *et al.*) [80].

### 1.10.3.3 Direct Arylation Reactions

As an alternative and promising methodology to the available coupling procedures to produce C–C bonds (Stille, Sonogashira, Suzuki, etc.), direct (hetero) arylation reactions are appealing due to the fewer reaction steps they require, low cost, only acidic by-product and ease of purification of products [106, 107]. This new reaction couples a (hetero)aryl halide and (hetero) arene forming a new C–C bond (**Scheme 1-3**). Direct

arylation reactions do not require any organometallic intermediates, therefore they require less synthetic steps. What also makes this reaction as an interesting reaction is its dependent on the energy required to deprotonate the (hetero)arene, that can be overcome through the activation of the C–H bonds either by directing groups or catalytic systems. However, the drawback of this reaction is its poor selectivity especially when the monomers used in the polymerisation have different aromatic C–H bonds which can result in structural defects in the final polymers [106-108].

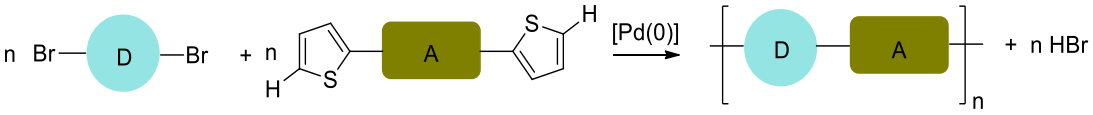


**Scheme 1-3:** (Hetero)direct arylation reaction.

The mechanisms of direct arylation is dependent on the substrate and catalytic system used, however, most of (hetero)arenes seem to follow a base-assisted concerted metalation-deprotonation. According to the previous studies, two catalytic cycles for the coupling of aryl halide and (hetero)arene are suggested. The first one depends on a carboxylate-mediated process where C–H activation takes place intermolecularly. Whereas, the other suggested catalytic cycle was designed for reactions that proceed in the absence of a carboxylate additive. However, the former catalytic cycle is not an issue for this thesis and will not be further discussed here [109].

The suggested mechanism, in the presence of carboxylate additives is shown in **Figure 1-20**. The first step of the coupling starts with oxidative addition of the C–X bond which is followed by exchange of the halide atom for the carboxylate anion leading to complex 1. In the second step, complex 1 deprotonates the arene substrate with the assistance of the carboxylate ligand while at the same time forming a M–C bond through transition state 2-TS. To reach reductive elimination step, two pathways are suggested. In pathway 1, the phosphine ligand can recoordinate to the metal center, while pathway 2 proposes that, the carboxylate will remain coordinated throughout the whole process. Finally, reductive elimination will give the final coupled product [109].

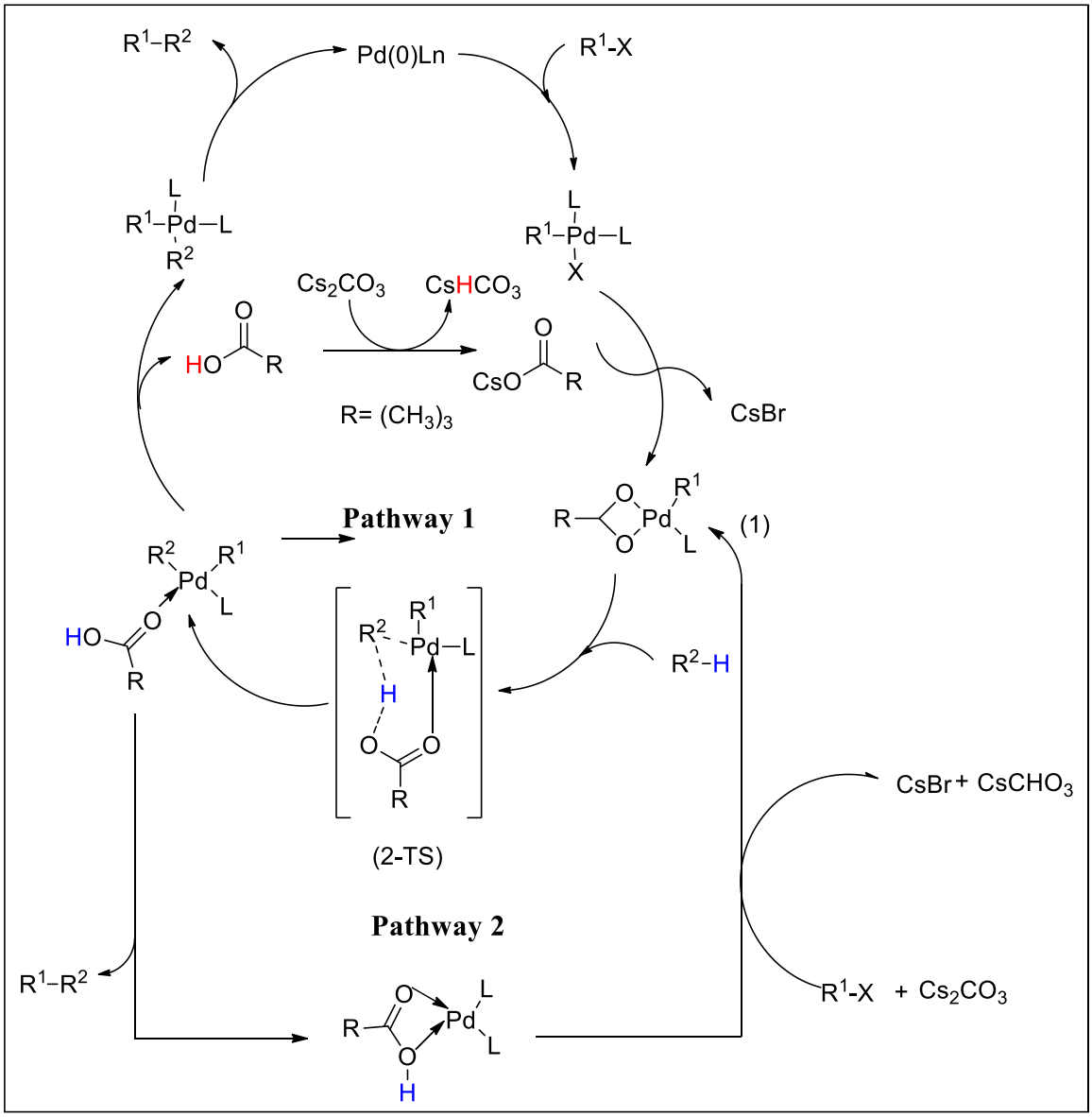


**Figure 1-20:** The mechanism of the direct arylation reaction using carboxylate additives (adopted from *Conjugated Polymer; A Practical Guide to Synthesis*) [109].

## 1.11 Aims of the Project:

Organic solar cells were investigated extensively during the last decades due to their potential to be mass-produced at low costs as well as to provide flexible organic photovoltaics devices. They also have attractive properties in terms of light incoupling and photocurrent generation.[110, 111] These organic, polymer-based photovoltaic devices will be able to introduce cheap and easy methods to produce energy from sunlight. The observed advantages of organic semiconductors are summarised as follow: [112]

- Low-cost synthesis.
- Easy production of thin film devices, either by the vacuum evaporation or solution processing as well as by printing methods.
- The thin films produced can show high absorption coefficient which is important for optoelectronic applications.
- Engineering of the electronic band gap of organic semiconductors can easily be achieved by chemical synthesis.

The design of conjugated polymers with low band gaps and suitable molecular energy levels is of crucial importance for PSC devices. Achievement of this aim is usually made by modifying the structural and electronic properties of conjugated polymers in order to tune a number of parameters [113]. Anthracene-based systems have attracted a wide interest in organic field-effect transistors due to their good hole mobilities [114, 115]. Anthracene derivatives do also play an important role in the development of organic light emitting diodes [116, 117]. Anthracene derivatives have attracted some interest as a common unit in conjugated polymers for the use in organic photovoltaic applications due to their relatively weak donating properties along with their enlarged planarity. Incorporation of anthracene units into conjugated polymers through their 9,10-positions has been reported with PCE up to 3.14 % [118]. However, the drawback of polymers based on 9,10-linked anthracene repeat units is the strong twisting out of planarity of these units in relation to adjacent units along the polymer backbone, which limits electronic conjugation severely due to the high steric hindrance.

The main objective of the work presented in this thesis is focused on the exploration and development of new synthetic approaches for the preparation of conjugated polymers based on 2,6-linked anthracene units for solar cells applications. In order to solve the issue of solubility, alkylarylethynyl and alkynyl groups will incorporated to anthracene at its 9,10-positions. Attaching these side chains *via* ethynyl groups are expected to maintain the planarity and π-π stacking of the polymer chains.

The aims of this project are to:

1. Design and synthesise a range of donor-acceptor anthracene-*alt*-benzothiadiazole copolymers (**Figure 1-21**). The study focuses on the impact of using various substituents at the 9,10-positions of the anthracene repeat units, on the solubility of the resulting polymers, their optical and electrochemical properties. Also, we want to know the effect of the spacer units between the anthracene and benzothiadiazole units along polymer chains, on the physical and optical properties of the resulting polymers.

2. Design and synthesis a series of alternating copolymers containing thieno[3,4-*c*]pyrrole-4,6-dione (TPD) with different substituents as electron deficient units and 2,6-linked anthracene derivatives as electron-rich moieties (**Figure 1-21**). We want to investigate the influences of a variety of alkyl chains on the solubility, photophysical and electrochemical properties of the resulting polymers.

Polymerisation will occur *via* the Stille coupling or direct arylation methods. In the case of the Stille coupling polymerisation, stannane groups will be added to the acceptor monomers which will be then coupled to the 2,6-dibromo-anthracene derivatives to form the desired conjugated polymers. Whereas in case of direct arylation polymerisation, unfunctionalised TPD monomers will be coupled with 2,6-dibromo anthracene derivatives resulting in the second batch of conjugated polymers. The current set of polymers are designed for use as electron donors to fullerene derivatives in BHJ cells. Initial investigations of the photovoltaic properties of the resulting polymers are also to be undertaken in this study.

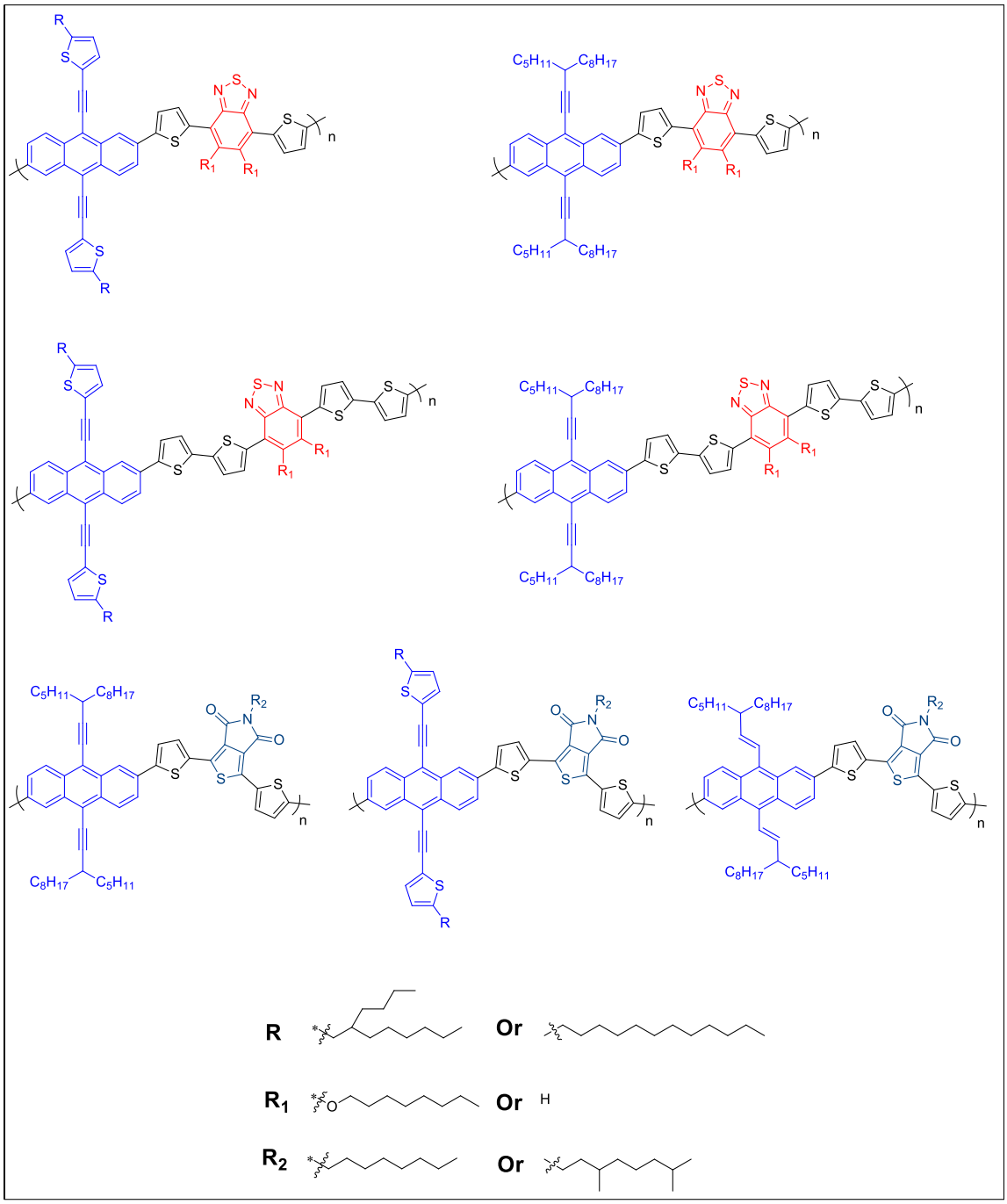


**Figure 1-21:** The general chemical structures of targeted polymers.

## 1.12 References:


1. M. Finley, *BP statistical review of world energy*, BP technical report, 2013.
2. N. S. Lewis, *science*, 2007, **315**, 798-801.
3. L. Dai, *ChemSusChem*, 2010, **3**, 797-799.
4. D. M. Chapin, C. Fuller and G. Pearson, *J. Appl. Phys.*, 1954, 676-677.
5. M. A. Green, K. Emery, Y. Hishikawa, W. Warta and E. D. Dunlop, *Prog. Photovoltaics Res. Appl.*, 2015, **23**, 1-9.
6. N.-G. Park, *Mater. Today*, 2015, **18**, 65-72.
7. Y.-J. Cheng, S.-H. Yang and C.-S. Hsu, *Chem. Rev.*, 2009, **109**, 5868-5923.
8. G. Li, R. Zhu and Y. Yang, *Nat. Photonics*, 2012, **6**, 153-161.
9. Y.-W. Su, S.-C. Lan and K.-H. Wei, *Mater. Today*, 2012, **15**, 554-562.
10. M. Pope and C. E. Swenberg, *Electronic processes in organic crystals and polymers*, Oxford University Press on Demand, 1999.
11. H. Shirakawa, E. J. Louis, A. G. MacDiarmid, C. K. Chiang and A. J. Heeger, *J. Chem. Soc., Chem.Commun.*, 1977, 578-580.
12. P. M. Borsenberger and D. S. Weiss, *Organic photoreceptors for imaging systems*, M. Dekker New York, 1993.
13. T. A. Skotheim, *Handbook of conducting polymers*, CRC press, 1997.
14. A. J. Heeger, *Chem. Soc. Rev.*, **39**, 2354-2371.
15. A. Świst and J. Sołoducho, *Chemik*, 2012, **66**, 289-296.
16. A. J. Heeger, S. Kivelson, J. Schrieffer and W.-P. Su, *Rev. Mod. Phys.*, 1988, **60**, 781.
17. U. Salzner, J. Lagowski, P. Pickup and R. Poirier, *Synth. Met.*, 1998, **96**, 177-189.
18. C. L. Chochos and S. A. Choulis, *Prog. Polym. Sci.*, 2011, **36**, 1326-1414.
19. A. J. Heeger, *Chem. Soc. Rev.*, 2010, **39**, 2354-2371.
20. M. D. Archer and R. Hill, *Clean electricity from photovoltaics (Series on Photoconversion of Solar Energy vol. 1)*, Imperial College Press, London, 2001.
21. A. J. Heeger, *Polym. J.*, 1985, **17**, 201-208.
22. Y. Furukawa, A. Sakamoto, H. Ohta and M. Tasumi, *Synth. Met.*, 1992, **49**, 335-340.
23. M. Santos, A. Brolo and E. Girotto, *Electrochim. Acta*, 2007, **52**, 6141-6145.

24. J. Bredas, R. Chance and R. Silbey, *Phys. Rev. B*, 1982, **26**, 5843.
25. J. L. Bredas and G. B. Street, *Acc. Chem. Res.*, 1985, **18**, 309-315.
26. H. S. Abdulla and A. I. Abbo, *Int J Electrochem Sci*, 2012, **7**, 10666-10678.
27. P. Colin, *Journal*, 1996.
28. E. H. Elandaloussi, P. Frère, P. Richomme, J. Orduna, J. Garin and J. Roncali, *J. Am. Chem. Soc.*, 1997, **119**, 10774-10784.
29. J. Roncali, *Annu. Rep. Sec. C. Phys. Chem.*, 1999, **95**, 47-88.
30. L. Dai, *Intelligent macromolecules for smart devices: from materials synthesis to device applications*, Springer, 2004.
31. B. P. Rand and H. Richter, *Organic Solar Cells: fundamentals, devices, and upscaling*, CRC Press, 2014.
32. J. Roncali, *Chem. Rev.*, 1997, **97**, 173-206.
33. E. Havinga, W. Ten Hoeve and H. Wynberg, *Synth. Met.*, 1993, **55**, 299-306.
34. E. Bundgaard and F. C. Krebs, *Sol. Energ. Mat. Sol. Cells*, 2007, **91**, 954-985.
35. H. Zhou, L. Yang and W. You, *Macromolecules*, 2012, **45**, 607-632.
36. J.-L. Brédas, J. E. Norton, J. Cornil and V. Coropceanu, *Acc. Chem. Res.*, 2009, **42**, 1691-1699.
37. L. Dou, Y. Liu, Z. Hong, G. Li and Y. Yang, *Chem. Rev.*, 2015, **115**, 12633-12665.
38. J. Nelson, *The physics of solar cells*, World Scientific, 2003.
39. F. Wudl, M. Kobayashi and A. Heeger, *J. Org. Chem.*, 1984, **49**, 3382-3384.
40. J. Morgado, N. Barbagallo, A. Charas, M. Matos and F. Cacialli, *J. Phys. D: App.Phys.*, 2003, **36**, 434.
41. J. Żmija and M. Małachowski, *Arch. Mater. Sci. Eng.*, 2009, **40**, 5-12.
42. Y. Wang, in *Low Threshold Organic Semiconductor Lasers*, Springer, 2014, pp. 9-32.
43. G. Horowitz, *Adv. Mater.*, 1998, **10**, 365-377.
44. J. Zaumseil and H. Sirringhaus, *Chem. Rev.*, 2007, **107**, 1296-1323.
45. M. A. Rahman, P. Kumar, D.-S. Park and Y.-B. Shim, *Sensors*, 2008, **8**, 118-141.
46. C. Craver and C. Carraher, *Applied polymer science: 21st century:*, Elsevier Science, Oxford, 2000.

47. N. Sariciftci, D. Braun, C. Zhang, V. Srdanov, A. Heeger, G. Stucky and F. Wudl, *App. Phys. Lett.*, 1993, **62**, 585-587.
48. N. Sariciftci, L. Smilowitz, A. J. Heeger and F. Wudl, *Science*, 1992, **258**, 1474-1476.
49. L. Li, W.-C. Chow, W.-Y. Wong, C.-H. Chui and R. S.-M. Wong, *J. Organomet. Chem.*, 2011, **696**, 1189-1197.
50. L. Bian, E. Zhu, J. Tang, W. Tang and F. Zhang, *Prog. Polym. Sci.*, 2012, **37**, 1292-1331.
51. J. Zhao, Y. Li, G. Yang, K. Jiang, H. Lin, H. Ade, W. Ma and H. Yan, *Nat. Energy*, 2016, **1**, 15027.
52. W. Cai, X. Gong and Y. Cao, *Sol. Energ. Mat. Sol. Cells*, 2010, **94**, 114-127.
53. V. Jain, B. K. Rajbongshi, A. T. Mallajosyula, G. Bhattacharjya, S. S. K. Iyer and G. Ramanathan, *Sol. Energ. Mat. Sol. Cells*, 2008, **92**, 1043-1046.
54. H. Hoppe and N. S. Sariciftci, *J. Mat. Res.*, 2004, **19**, 1924-1945.
55. M. Scharber and N. Sariciftci, *Prog. Polym. Sci.*, 2013, **38**, 1929-1940.
56. L. Wang, H. Liu, R. M. Konik, J. A. Misewich and S. S. Wong, *Chem. Soc. Rev.*, 2013, **42**, 8134-8156.
57. C. W. Tang, *App. Phys. Lett.*, 1986, **48**, 183-185.
58. S. Günes, H. Neugebauer and N. S. Sariciftci, *Chem. Rev.*, 2007, **107**, 1324-1338.
59. A. Haugeneder, M. Neges, C. Kallinger, W. Spirkl, U. Lemmer, J. Feldmann, U. Scherf, E. Harth, A. Gügel and K. Müllen, *Phys. Rev. B*, 1999, **59**, 15346.
60. M. C. Scharber, D. Mühlbacher, M. Koppe, P. Denk, C. Waldauf, A. J. Heeger and C. J. Brabec, *Adv. Mater.*, 2006, **18**, 789-794.
61. C. Deibel and V. Dyakonov, *Rep. Prog. Phys.*, 2010, **73**, 096401.
62. C. J. Brabec, S. Gowrisanker, J. J. Halls, D. Laird, S. Jia and S. P. Williams, *Adv. Mater.*, 2010, **22**, 3839-3856.
63. P. W. Blom, V. D. Mihailetchi, L. J. A. Koster and D. E. Markov, *Adv. Mater.*, 2007, **19**, 1551-1566.
64. W. C. Choy, *Organic Solar Cells*, Springer, 2013.
65. Y. Li, *Acc. Chem. Res.*, 2012, **45**, 723-733.
66. N. Banerji, S. Cowan, M. Leclerc, E. Vauthey and A. J. Heeger, *J. Am. Chem. Soc.*, 2010, **132**, 17459-17470.

67. X.-Y. Zhu, Q. Yang and M. Muntwiler, *Acc. Chem. Res.*, 2009, **42**, 1779-1787.
68. J. Halls, K. Pichler, R. Friend, S. Moratti and A. Holmes, *App. Phys. Lett.*, 1996, **68**, 3120-3122.
69. D. E. Markov, E. Amsterdam, P. W. Blom, A. B. Sieval and J. C. Hummelen, *J. Phys. Chem. A*, 2005, **109**, 5266-5274.
70. N. Sariciftci, L. Smilowitz, A. Heeger and F. Wudl, *Synth. Met.*, 1993, **59**, 333-352.
71. C. J. Brabec, N. S. Sariciftci and J. C. Hummelen, *Adv. Funct. Mater.*, 2001, **11**, 15-26.
72. Y. Li, Q. Guo, Z. Li, J. Pei and W. Tian, *Energ. Environ. Sci.*, 2010, **3**, 1427-1436.
73. D. Konios, G. Kakavelakis, C. Petridis, K. Savva, E. Stratakis and E. Kymakis, *J. Mater. Chem. A*, 2016.
74. L. Koster, V. Mihailetchi and P. Blom, *App. Phys. Lett.*, 2006, **88**, 052104.
75. N. Blouin, A. Michaud, D. Gendron, S. Wakim, E. Blair, R. Neagu-Plesu, M. Belletete, G. Durocher, Y. Tao and M. Leclerc, *J. Am. Chem. Soc.*, 2008, **130**, 732-742.
76. C. Winder and N. S. Sariciftci, *J. Mater. Chem.*, 2004, **14**, 1077-1086.
77. E. Negishi, A. O. King and N. Okukado, *J. Org. Chem.*, 1977, **42**, 1821-1823.
78. R. F. Heck and J. Nolley Jr, *J. Org. Chem.*, 1972, **37**, 2320-2322.
79. N. Miyaura, K. Yamada and A. Suzuki, *Tetrahedron Lett.*, 1979, **20**, 3437-3440.
80. D. Milstein and J. Stille, *J. Am. Chem. Soc.*, 1978, **100**, 3636-3638.
81. M. Leclerc, F. M. Diaz and G. Wegner, *Die Makromolekulare Chemie*, 1989, **190**, 3105-3116.
82. J.-E. Österholm, J. Laakso, P. Nyholm, H. Isotalo, H. Stubb, O. Inganäs and W. Salaneck, *Synth. Met.*, 1989, **28**, 435-444.
83. K. Yoshino, S. Nakajima, M. Onoda and R. Sugimoto, *Synth. Met.*, 1989, **28**, 349-357.
84. M. Fukuda, K. Sawada and K. Yoshino, *J. Polym. Sci. A: Polym. Chem.*, 1993, **31**, 2465-2471.
85. J. Roncali, *J. Mater. Chem.*, 1999, **9**, 1875-1893.
86. J. Roncali, *Chem. Rev.*, 1992, **92**, 711-738.

87. H. S. Nalwa, *Advanced Functional Molecules and Polymers: Electronic and Photonic Properties*, CRC Press, 2001.
88. Z. Bao, W. K. Chan and L. Yu, *J. Am. Chem. Soc.*, 1995, **117**, 12426-12435.
89. M. G. Melchor, *A Theoretical Study of Pd-Catalyzed CC Cross-Coupling Reactions*, Springer Science & Business Media, 2013.
90. S. L. Buchwald, K. Fugami, T. Hiyama, M. Kosugi, M. Miura, N. Miyaura, A. Muci, M. Nomura, E. Shirakawa and K. Tamao, *Cross-coupling reactions: a practical guide*, Springer, 2003.
91. J. Bäckvall, *Scientific Background on the Nobel Prize in Chemistry 2010*, 2010, **6**.
92. S. S. Zalesskiy and V. P. Ananikov, *Organometallics*, 2012, **31**, 2302-2309.
93. R. Chinchilla and C. Nájera, *Chem. Rev.*, 2007, **107**, 874-922.
94. J. Tsuji, *Transition metal reagents and catalysts: innovations in organic synthesis*, John Wiley & Sons, 2002.
95. M. Pretze, P. Große-Gehling and C. Mamat, *Molecules*, 2011, **16**, 1129-1165.
96. M. Bakherad, A. Keivanloo, B. Bahramian and T. A. Kamali, *J. Braz. Chem. Soc.*, 2009, **20**, 907-912.
97. A. Elangovan, Y.-H. Wang and T.-I. Ho, *Org. Lett.*, 2003, **5**, 1841-1844.
98. R. Chinchilla and C. Nájera, *Chem. Soc. Rev.*, 2011, **40**, 5084-5121.
99. I. J. Boyer, *Toxicology*, 1989, **55**, 253-298.
100. S. Caron, *Practical synthetic organic chemistry: reactions, principles, and techniques*, John Wiley & Sons, 2011.
101. Á. Molnár, *Palladium-catalyzed coupling reactions: practical aspects and future developments*, John Wiley & Sons, 2013.
102. V. Farina, *Pure App. Chem.*, 1996, **68**, 73-78.
103. N. G. J. Clayden, S. Warren and P. Wothers, *Organic Chemistry*, Oxford University Press, 1St Edn edn., 2001.
104. P. Espinet and A. M. Echavarren, *Angew. Chem. Int. Ed.*, 2004, **43**, 4704-4734.
105. C. Cordovilla, C. Bartolomé, J. s. M. Martínez-Ilarduya and P. Espinet, *ACS Catalysis*, 2015, **5**, 3040-3053.
106. P.-O. Morin, T. Bura and M. Leclerc, *Mater. Horiz.*, 2016, **3**, 11-20.
107. P.-O. Morin, T. Bura, B. Sun, S. I. Gorelsky, Y. Li and M. Leclerc, *ACS Macro Letters*, 2014, **4**, 21-24.

108. M. Lafrance, C. N. Rowley, T. K. Woo and K. Fagnou, *J. Am. Chem. Soc.*, 2006, **128**, 8754-8756.
109. K. Müllen, J. R. Reynolds and T. Masuda, *Conjugated Polymers: A Practical Guide to Synthesis*, Royal Society of Chemistry, 2014.
110. Y.-H. Chen, L.-Y. Lin, C.-W. Lu, F. Lin, Z.-Y. Huang, H.-W. Lin, P.-H. Wang, Y.-H. Liu, K.-T. Wong and J. Wen, *J. Am. Chem. Soc.*, **134**, 13616-13623.
111. C. Deibel and V. Dyakonov, *Rep. Prog. Phys.*, 2010, **73**, 096401.
112. S. Günes, H. Neugebauer and N. S. Sariciftci, *Chem. Rev.*, 2007, **107**, 1324-1338.
113. J. Hou, M.-H. Park, S. Zhang, Y. Yao, L.-M. Chen, J.-H. Li and Y. Yang, *Macromolecules*, 2008, **41**, 6012-6018.
114. S. Jo, J. A. Hur, K. H. Kim, T. W. Lee, J. Shin, K. S. Hwang, B. D. Chin and D. H. Choi, *Bull. Korea Chem. Soc.*, 2012, **33**, 3061-3070.
115. L. Jian-Feng, C. Wen-Li, T. Chun-Lan, O. Gu-Ping and Z. Fu-Jia, *Chin. Phys. Lett.*, 2008, **25**, 4476.
116. J. Huang, J.-H. Su and H. Tian, *J. Mater. Chem.*, 2012, **22**, 10977-10989.
117. P. Raghunath, M. A. Reddy, C. Gouri, K. Bhanuprakash and V. J. Rao, *J. Phys. Chem. A*, 2006, **110**, 1152-1162.
118. D. A. Egbe, S. Turk, S. Rathgeber, F. Kuhnlenz, R. Jadhav, A. Wild, E. Birckner, G. Adam, A. Pivrikas and V. Cimrova, *Macromolecules*, 2010, **43**, 1261-1269.

# Chapter 2

## *Synthesis And Characterisation of a New Series of 2,6-Linked-Anthracene–Benzothiadiazole Based Polymers and Their Applications in Solar Cells*

# Chapter 2

## 2.1 Introduction

Polymer solar cells (PSCs) with bulk heterojunction (BHJ) structures have attracted a considerable attention during the past few decades because of their advantages of low fabrication cost, light weight, easy manufacturing and flexibility [1-3]. Blending a π-conjugated polymer as an electron donor with soluble $PC_{61}BM$ or $PC_{71}BM$ electron acceptor in BHJ solar cells are one of the most successful PSCs [4, 5].

New π-conjugated polymers with low band gaps were designed and developed to exhibit good matching absorption spectra with that of the solar spectrum as well as enhanced power conversion efficiency (PCE) of PSCs [6, 7]. The push-pull architecture is used as the most effective strategy to obtain low band gap polymers and to control the polymer electronic and optical properties [8]. The donor units should have relatively weak electron donating ability to afford a conjugated polymer with a low-lying HOMO level which is favorable to produce PSCs with high $V_{oc}$. Furthermore, good charge mobilities can be achieved by using polymers having donor-acceptor blocks with good planarity, large π-conjugation and high molecular weights [9].

One of the explored building blocks in the literature, for the synthesis of low band gap polymers are the anthracene units. The anthracene moieties were used as weak electron donor units with their enlarged planarity and rigidity which lead to good charge transporting properties [3, 10]. Incorporation of anthracene into conjugated polymers through its 9,10-positions such as poly(*p*-phenylene-ethynlene)-*alt*-(poly(*p*-phenylenevinylene) (PPE-PPV) (**Figure 2-1**) has shown good results with respect to hole carrier mobilities and power conversion efficiency (up to 3.8%) [11, 12]. However, the main backbone of these type of polymers is strongly twisted out of planarity which affects the conjugation of the polymers due to the high steric hindrance [13].

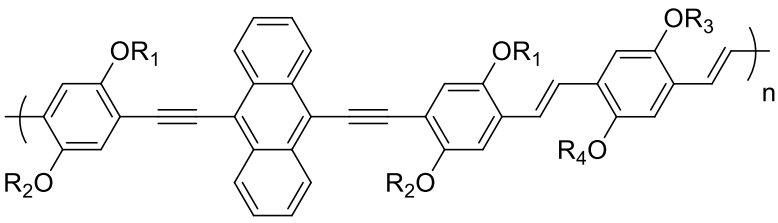


**Figure 2-1:** The chemical structure of an anthracene-containing poly(*p*-phenyleneethynylene)-alt-poly(*p*-phenylene-vinylene)s (PPE-PPV) copolymer.

To overcome this disadvantage, polymers based on 2,6-linked anthracene units have been used recently which improves electronic conjugation along the backbone of these polymers [14]. During the past few years, a number of polymers containing 2,6-linked anthracene units have been reported for organic photovoltaic applications [7, 13, 15-18] with the highest PCE recorded by Jung *et al.* (up to 8.05%) [18]. The possibility of introducing different substitutions to the 9,10-positions on the central benzene core of the anthracene units can allow for molecular design constructing two dimensional conjugated structures.

Indeed, the need for reducing the band gap of the 2,6-linked anthracene-based polymers has led to prepare a variety of copolymers incorporating various acceptor moieties. Among these acceptor units are benzothiadiazole (BT) derivatives, which have strong electron-deficient features, due to the existence of two electron withdrawing imines (C=N) along with the bridged sulphur atom [19]. By incorporating electron-deficient benzothiadiazole units into the polymer backbone, 2,6-linked anthracene-based polymers exhibit reduced LUMO levels and hence narrower bandgaps. Iraqi and co-workers developed polymers using 2,6-linked anthracene units with aryloxy groups at their 9,10-positions and benzothiadiazole alternate repeat unit **PPATBT** [15] (**Figure 2-2**). The polymer exhibited a broad absorption in the range of 400–700 nm and an optical band gap of 1.84 eV. By introducing a 2-(2-hexyldecyl)-thienyl group in the 9,10-postions of the anthracene-based polymer backbone, Jung *et al*, synthesised a polymer **PTADTBT** (**Figure 2-2**) with optical band gap of 1.78 eV and PCEs reached 6.92% [18].

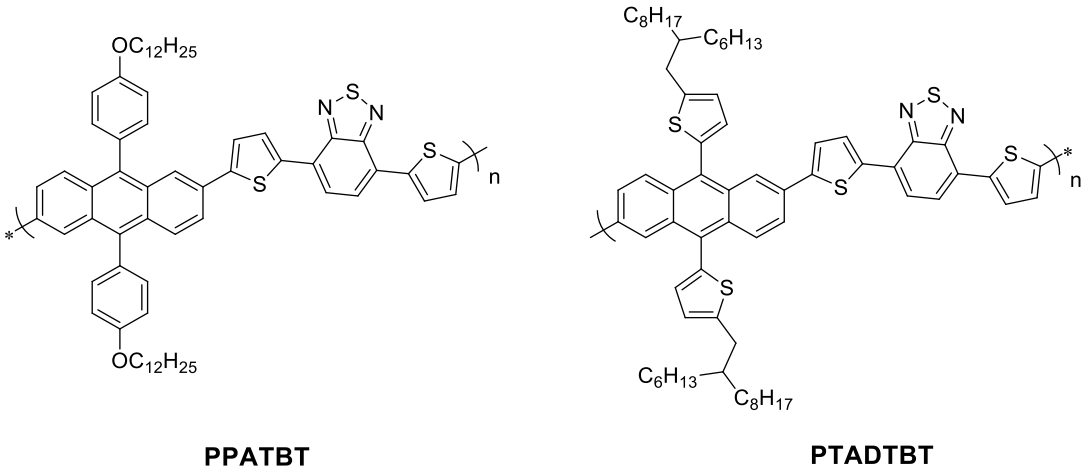


**Figure 2-2:** The Chemical structures of **PPATBT** and **PTADTBT**.

In an effort to change the molecular structure to fine-tune the $V_{oc}$ and $J_{sc}$ for BHJ solar cells, three novel conjugated polymers were designed and synthesised in this project. The polymers are substituted with 5-dodecyl-(thien-2-yl)-ethynyl, 5-(2-butyloctyl)-(thien-2-yl)-ethynyl and 3-pentylundec-1-yne side chains incorporated at the 9,10-postions of the anthracene moieties as shown in**Figure 2-3**.

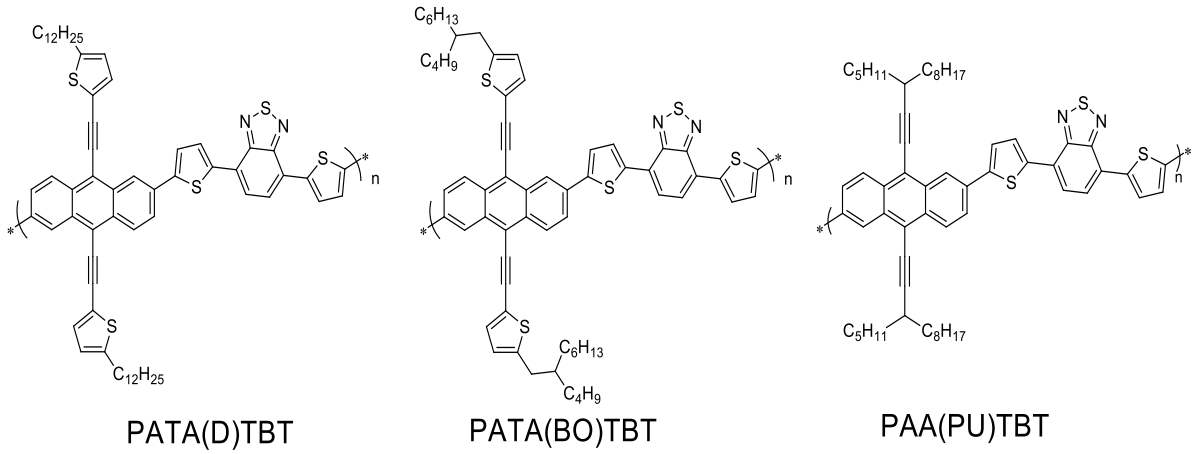


**Figure 2-3:** The Chemical structures of the target polymers, **PATA(D)TBT**, **PATA(BO)TBT**, and **PAA(PU)TBT**.

It was hoped that attaching alkylthienyl units through an acetylene spacer will extend electronic conjugation laterally as well as along the polymer chain to create a two dimensional conjugated system 2-D, which is hoped to promote planarity and light absorption resulting in a lower band gap. Furthermore, the incorporation of these substituents to the anthracene could result in enhanced charge mobility as well as good

solubility of the prepared polymers in common organic solvents given the size of the alkyl substituents used.

## 2.2 Results and Discussion

### 2.2.1 Synthesis of the Monomers

To obtain our desired alternating copolymers, we employed direct arylation coupling polymerisation using 2,6-dibromo-anthracene derivatives and 4,7-bis(thiophen-2-yl) benzo[c][1,2,5]-thiadiazole (**M4**). The synthetic routes of **M1**, **M2** and **M3** and their corresponding polymers are outlined in**Scheme 2-1**. 4,7-Bis(thiophen-2-yl) benzo[c][1,2,5]-thiadiazole (**M4**) was prepared by A. Almaliky of Iraqi group according to a procedure by Fu *et al*. (**Figure 2-4**) [20]. The purity and chemical structure of the monomers were confirmed by $^{1}$H-NMR, $^{13}$C-NMR, mass spectroscopy, elemental analysis and FT-IR. All the $^{1}$H-NMR spectra of the monomers are displayed in Chapter 7 (Figure 7-1, Figure 7-2, and Figure 7-3).

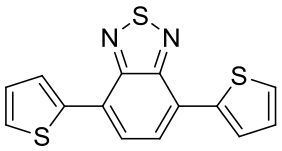


**Figure 2-4:** The chemical structure of monomer **M4**.

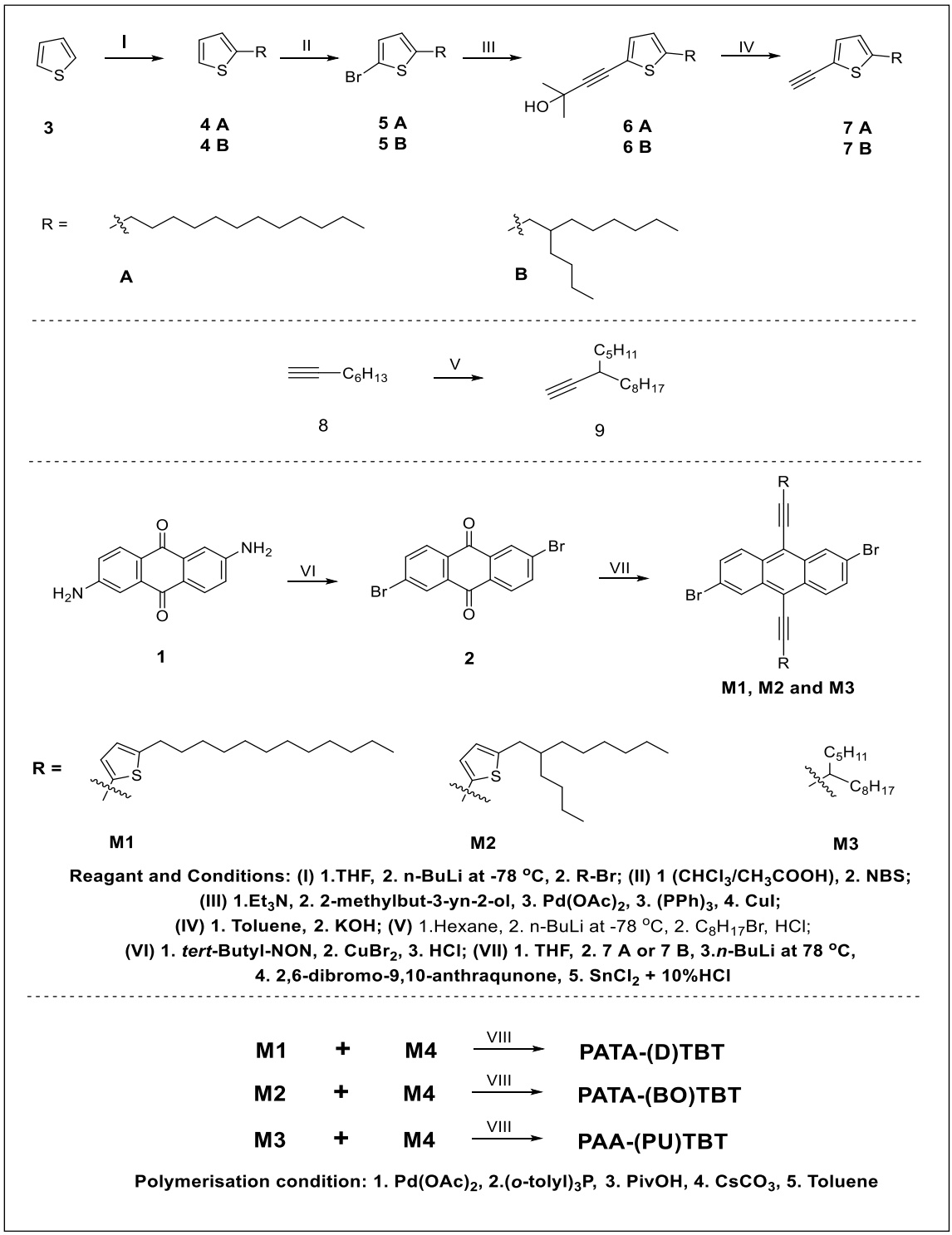


**Scheme 2-1:** The reaction pathway to the anthracene monomers and their corresponding polymers.

First, 2,6-dibromo-9,10-anthraquinone (**2**) was brominated using a modified procedure of Sandmeyer reaction developed by Doyle *et al* [21]. In this reaction, 2,6-diamino-9,10-anthraquinone (**1**) was reacted with $CuBr_2$ and *tert*-butyl nitrite to form compound (**2**). The suggested mechanism for the reaction is depicted in **Scheme 2-2**.

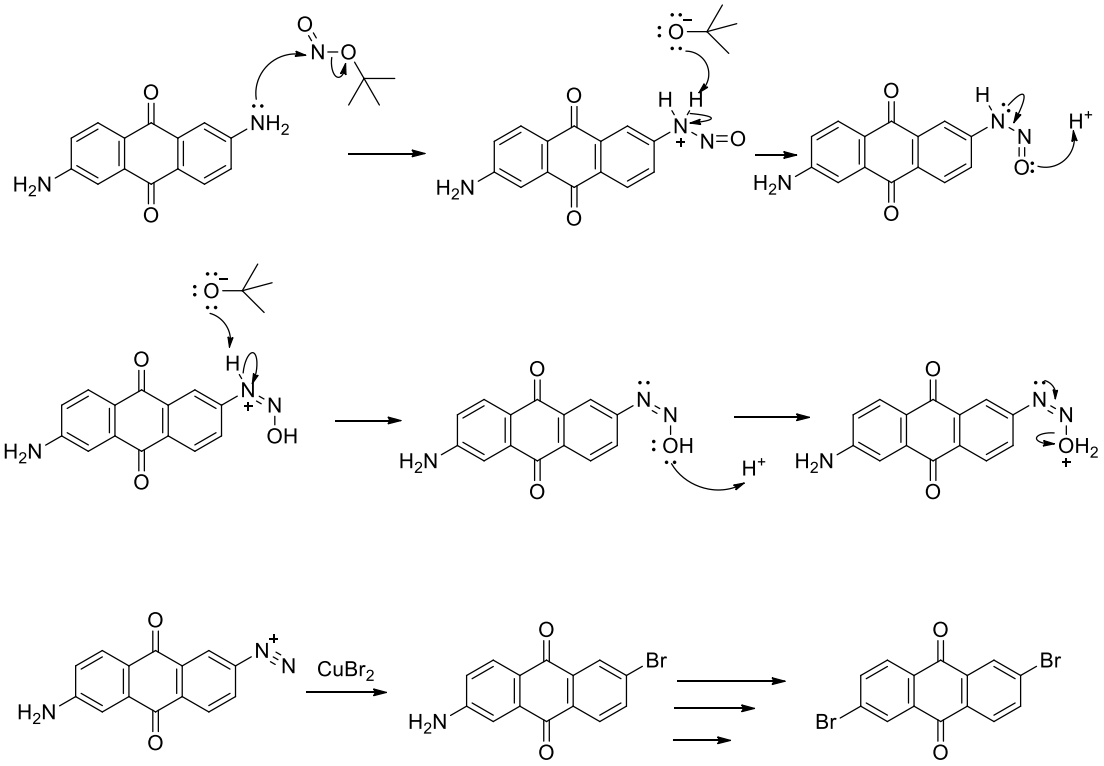


**Scheme 2-2:** Schematic representation of the postulated mechanism by which the Sandmeyer reaction proceeds.

We then synthesised the substituents that will be attached to the 9,10 positions of compound (**2**). First, thiophene (**3**) was lithiated which afterward reacted with either dodecyl bromide or 2-butyl octyl bromide to give (**4A**) or (**4B**), respectively, as described in **Scheme 2-3**.

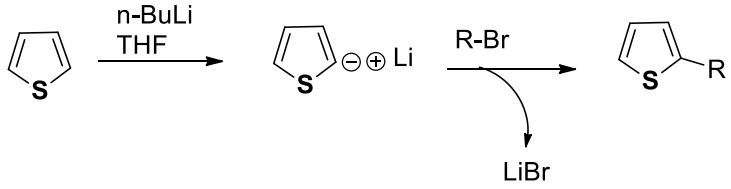


**Scheme 2-3:** the proposed reaction mechanism for preparation of (**4A**) and (**4B**).

Compounds (**5A**) or (**5B**) were obtained after treating (**4A**) or (**4B**) with *N*-bromosuccinimide in acetic acid/chloroform mixture. The suggested mechanism for these reactions involve an electrophilic aromatic substitution, where the 2-position of the thiophene ring is more nucleophilic compared to other sites which is attacked by the electrophilic bromine of NBS. Then, the proton on the 2-position of thiophene is removed by the succinimide anion to produce the brominated ring. The mechanism of the reaction is shown in **Scheme 2-4**.

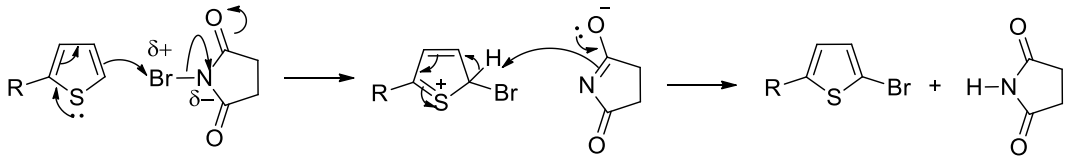


**Scheme 2-4:** The proposed mechanism for the preparation of (**5A**) or (**5B**).

The Sonogashira coupling reaction of the synthesised compounds (**5A**) and (**5B**) with 2-methylbut-3-yn-2-ol in the presence of $Pd(OAc)_2$, $(o\text{-tolyl})_3P$, triethylamine and CuI in freshly distilled THF yielded the desired compounds (**6A**) and (**6B**). The mechanism of Sonogashira coupling reaction was discussed in chapter 1.

To obtain (**7A**) and (**7B**), a solution of 2-(2-methylbut-3-yn-2-ol)-5-alkyl thiophene in toluene was treated with an inorganic base, KOH, at elevated temperatures to give the desired products. The suggested mechanism for the reaction is shown in**Scheme 2-5**.

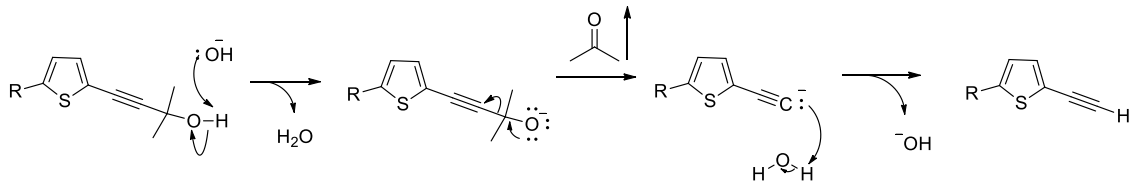

**Scheme 2-5:** The suggested mechanism for preparation of compounds (**7A**) and (**7B**).

Finally, the addition of 2,6-dibromo-9,10-anthrquinone to 2 equivalents of ethynyl compounds, (**7A**) or (**7B**), in the presence of *n*-BuLi afforded the corresponding enediols intermediates which readily reduced to the desired anthracene-based monomers **M1** and **M2** using $SnCl_2$ in acidic medium. The outline of the mechanism is given **Scheme 2-6**. First, the nucleophilic carbon in the organometallic reagent attacked the electrophilic carbon of the polar carbonyl group of compound (**2**) to give an intermediate alkoxide. In the next step, water protonates the alkoxide oxygen leading to the formation of the diol product. According to Pramanik *et al.* [22] using concentrated HCl facilitates the conversion of diol intermediates to compounds **M1** or **M2** through the protonation of the hydroxyl groups followed by elimination of water creating electron deficient carbocations that act as electron acceptors. On the other hand, HCl could change $SnCl_2$ to a good electron donor species such as, $SnCl_4^{2-}$ or $SnCl_6^{4-}$ which donate electrons to the carbocations leading to the final monomers.

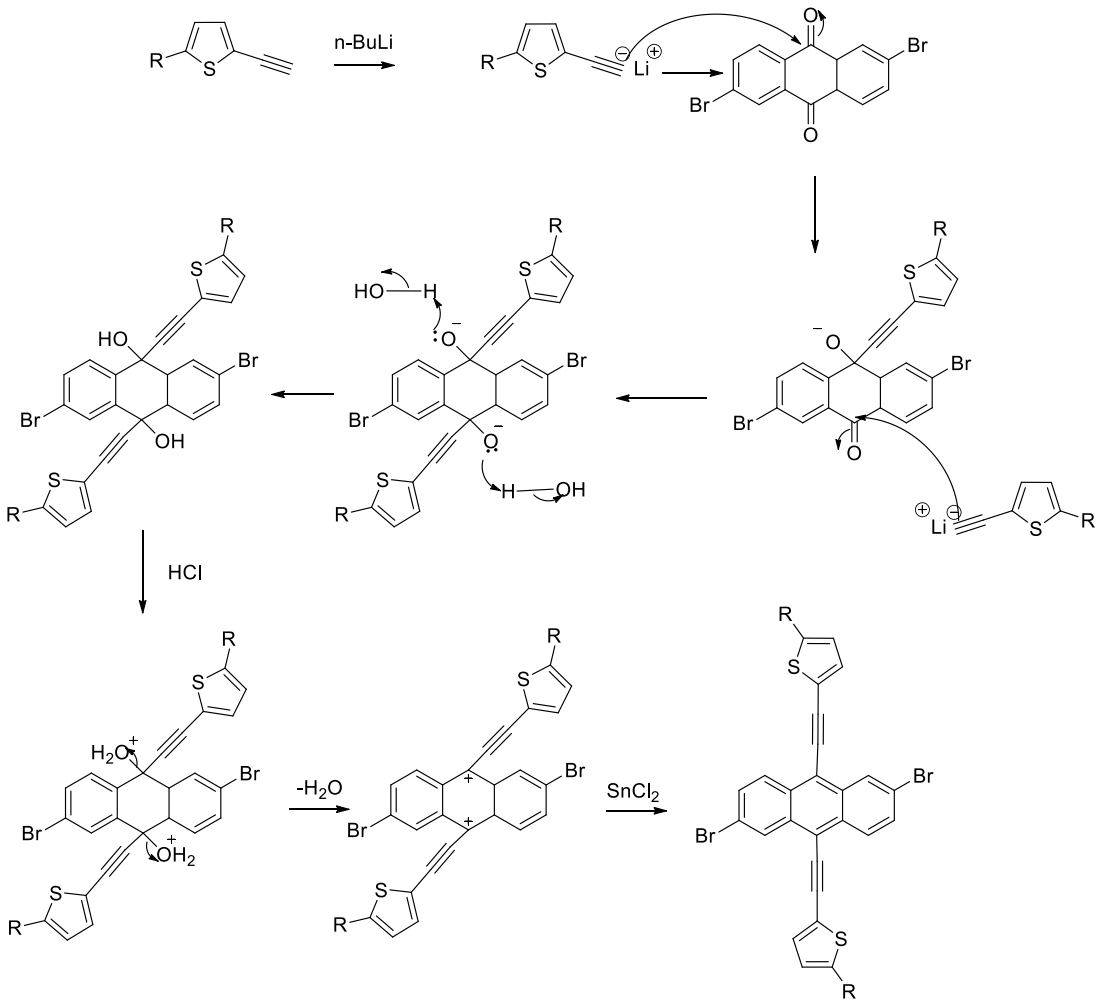


**Scheme 2-6:** The suggested mechanism for preparation of monomers **M1** and **M2**.

The synthetic route to the monomer 2,6-dibromo-9,10-di-(3-pentylundec-1-yne)-anthracene **M3** is started with the preparation of the solubilising side chains 3-pentylundec-1-yne (**9**). Formation of the product required the substitution of an octyl group at the 3-position of 1-octyne. The reaction proceeded through deprotonation using n-BuLi, to produce an anion at the C3 site of the alkyne which attacks 1-bromooctane to substitute bromine. It is important to use two equivalents of n-BuLi for this reaction because the most acidic proton of the octyne is the one attached to the terminal alkyne at the C1 site (p$K_a$~ 25) and not the C3 site (p$K_a$ ~ 35). Thus, two equivalents of n-BuLi are required for this reaction as the C1 site will be deprotonated at first, and then the second equivalent will deprotonate the next most acidic proton at the C3 site.

However, when only one equivalent of the 1-bromooctane is used only one alkyne product is produced. The reason behind that is the deprotonated $C_3$ site has a higher p$K_a$, making it a stronger nucleophile. As a result, it is more favorable for the reaction to occur at this site rather than the $C_1$ position. The mechanism of the reaction is shown in**Scheme 2-7**.

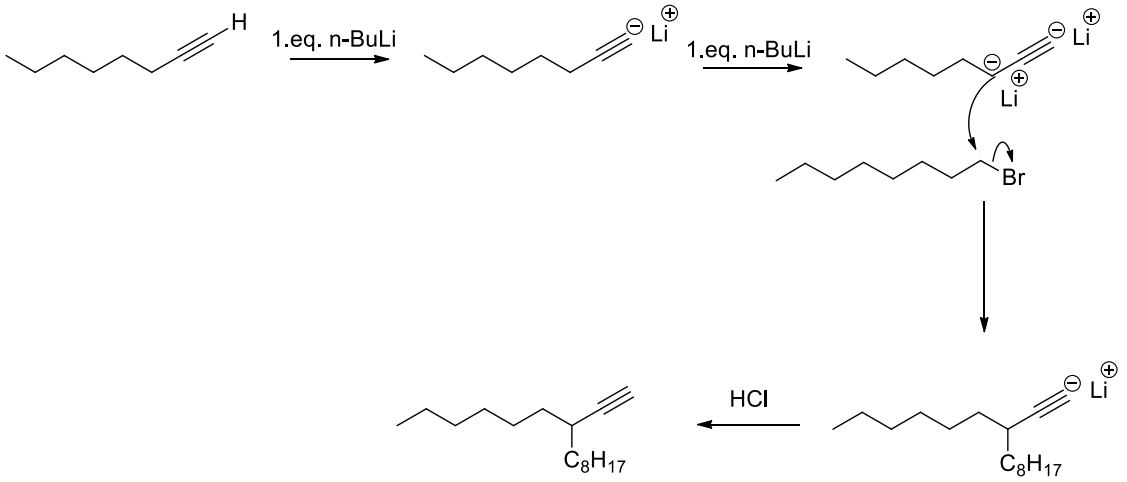


**Scheme 2-7:** Schematic representation of the mechanism by which compound (**9**) is synthesised.

2,6-Dibromo-9,10-di-(3-pentylundec-1-yne)-anthracene **M3** is synthesised by a similar method to that described for anthracene monomers **M1** and **M2**. The reaction first proceeded by deprotonation of the 3-pentylundec-1-yne using *n*-BuLi. Then the resulted nucleophile attacked the electrophilic carbonyl of compound **2**. $SnCl_2$ was added to the reaction mixture in the presence of $HCl_{(aq)}$ to reduce alcohol and reform aromaticity within the molecule.

### 2.2.2 Polymers Synthesis:

**Scheme 2-1** outlines the synthesis of polymers **PATA(D)TBT**, **PATA(BO)TBT**, and **PAA(PU)TBT** which were synthesised *via* direct arylation polymerisation in yields between 22% and 43%. $Pd(OAc)_2$ and tri(*o*-tolyl)phosphine were used as the catalyst in the presence of $Cs_2CO_3$ base and pivalic acid and toluene as the solvent. All the polymers were purified by Soxhlet extraction and toluene fractions were collected, reduced in *vacuo,* and precipitated in methanol. The rather low yields of these polymers are ascribed to their low solubility. Incorporating the arylethynyl and alkynyl

substituents on the anthracene units did not provide high solubilities to these polymers. This suggested that the incorporation of these substituents on the anthracene units *via* acetylene spacers led to enhance the planarity of the resulting polymers leading to strong π-π stacking between polymer chains which affected their solubility in common organic solvents. It is worth to note that, even the quantities of these polymers which were extracted in toluene fractions, exhibited very low solubility at room temperature in common organic solvents such as chlorobenzene and chloroform. This is why it was only possible to fabricate photovoltaic devices from **PATA(D)TBT**.

All polymers were characterised by $^{1}$H-NMR, IR, and elemental analysis to confirm their chemical structures ($^{1}$H-NMR of the polymers are shown in the Chapter 7, Figure 7-11 and 7-12). The number average molecular weights ($M_n$) of the polymers were determined using gel permeation chromatography (GPC) relative to polystyrene standards using 1,2,4-trichlorobenzene as the eluent (**Table 2-1** and **Figure 2-5**). The three polymers displayed low $M_n$ in the range (2200–3300 Da) indicating the low solubility of these polymers because of the absence of solubilising groups on the **TBT** units. Polymer **PPATBT**, prepared by Iraqi et al.[15], (an analogous polymer to our polymers which has 4-dodecyloxy-phenyl substituents on the anthracene units) had an $M_n$ of 3500 Da which is very close to the molecular weights of the new polymers prepared in this study. Surprisingly, polymer **PTADTBT** prepared by Jung *et al.*[18] showed a higher $M_n$ value of 41100 Da compared to those obtained for polymers presented in this work. This difference in the $M_n$ can be attributed to the twisting out of planarity of the bulky branched 2-hexyldecyl-thienyl substituents attached to the anthracene units at its 9,10 positions and the anthracene units in **PTADTBT**. As a result, the π-π stacking between the polymers chains was disrupted leading to more soluble polymer in the normal organic solvents even with higher $M_n$ values.

**Table 2-1:** GPC data and TGA data of the polymers.

| Polymer | Yield (%) | $M_n$ (Da)[a] | $M_w$ (Da)[a] | PD[b] | DP[c] | Td ($^oC$) |
|---|---|---|---|---|---|---|
| PATA(D)TBT | 22 | 3600 | 4000 | 1.2 | 4 | 332 |
| PATA(BO)TBT | 23 | 2100 | 3200 | 1.56 | 2 | 401 |
| PAA(PU)TBT | 43 | 2200 | 3300 | 1.52 | 2 | 353 |

[a] Measurements conducted on the polymers using a differential refractive index (DRI) detection method. [b] Polydispersity index. [c] Degree of Polymerisation.

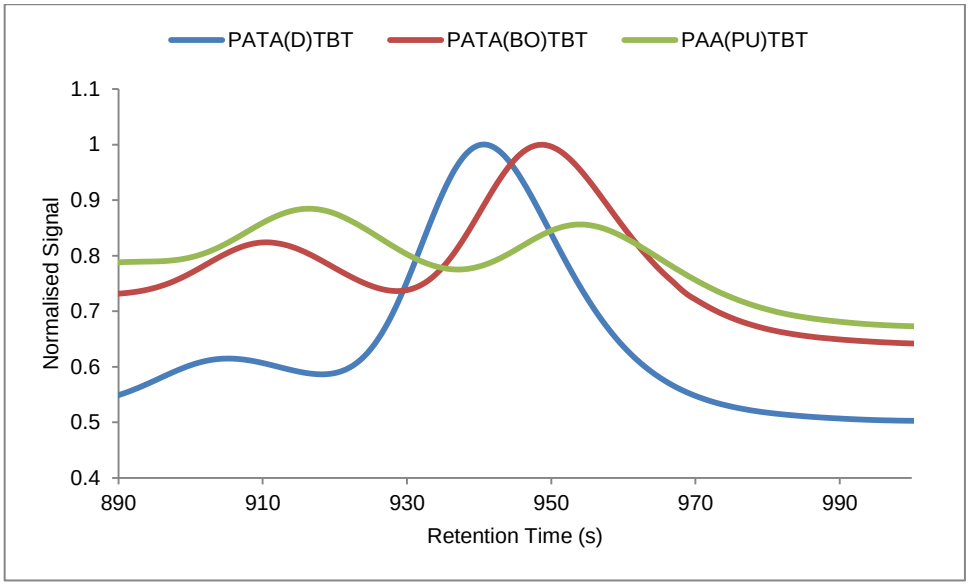


**Figure 2-5**: The GPC traces by RI detector of **PATA(D)TBT**, **PATA(BO)TBT** and **PAA(PU)TBT.**

### 2.2.3 Thermal Analysis

Thermal stability of the polymers was investigated *via* thermal gravimetric analysis (TGA) in a $N_2$ atmosphere. The three polymers displayed high thermal stability with 5% loss in excess of 300 °C as shown in **Figure 2-6**. Polymers, **PTAT(D)TBT** and **PTAT(BO)TBT** show degradation temperatures of 332 and 401 °C, respectively. Whereas, **PAA(PU)TBT** with alkynyl substituents attached to the anthracene moiety has a degradation temperature of 352 °C. This indicates that all the polymers are thermally stable enough to be fabricated into organic photovoltaic devices.

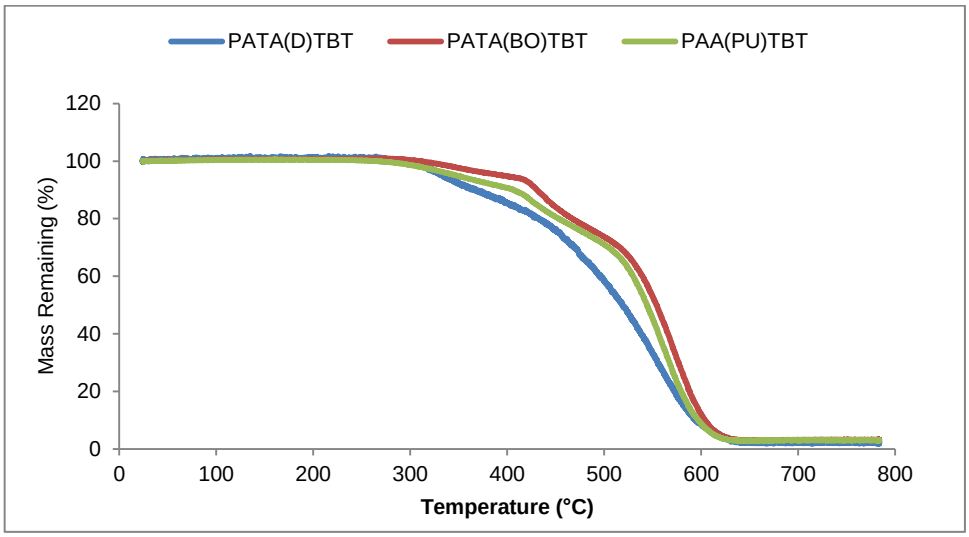


**Figure 2-6:** TGA plots of **PATA(D)TBT**, **PATA(BO)TBT** and **PAA(PU)TBT**.

### 2.2.4 Optical Properties

The UV-Vis spectra of the three polymers in chloroform solutions and as thin films are displayed in **Figure 2-7**, and all their optical data are summarised in **Table 2-2**. The three polymers show multiple absorption bands in the range 300-650 nm either in the solution phase or as thin films. The absorption bands in the higher energy region are attributed to the π-π* transitions [23], while the low-energy absorptions are originated from intramolecular charge transfer between the anthracene dithienyl donor units and BT acceptor units [24]. These absorption bands are bathochromicly shifted in the case of thin films due to the enhancement in the interchain packing in the solid state. **PATA(BO)TBT** and **PAA(PU)TBT** have shown clear shoulder peaks already in dilute solutions at long-wavelengths around 642 and 517 nm respectively, indicating the existence of aggregation in the solution phase due to stacking of polymer chains [15]. This provides a good evidence for the backbone planarisation enhancement upon the use of acetylenic substituents into the polymer backbones. Also, the existence of these shoulders in the solution phase can explain the low solubility of these polymers as well as their low molecular weights. These shoulder absorption peaks become more pronounced in the spectra of the thin films of the three polymers.

**Table 2-2:** UV-Vis data and optical band gaps of the polymers **PATA(D)TBT**, **PATA(BO)TBT** and **PAA(PU)TBT**.

| Polymer | $\lambda_{max}$ Solution (nm) | $\varepsilon^a$ ($M^{-1}$ $cm^{-1}$) | $\lambda_{max}$ film (nm) | $E_g^{opt}$ film (eV)[b] |
|---|---|---|---|---|
| PATA(D)TBT | 330, 382, 475 | $3.90 \times 10^{+4}$ | 384, 493, 638 | 1.75 |
| PATA(BO)TBT | 333, 377, 470 | $3.90 \times 10^{+4}$ | 393, 493, 634 | 1.80 |
| PAA(PU)TBT | 359, 448, 516 | $3.48 \times 10^{+4}$ | 370, 560 | 1.85 |

[a] Molar absorptivity measured at $\lambda_{max}$ in chloroform. [b]($E_g^{opt}$) optical bandgap, calculated from the onset of the absorption s band on solid films.

The nature of the three ethynyl substituents (**7A**), (**7B**) and (**9**) attached to the backbone of the polymers seem to have an influence in their optical properties. In films, the peak of absorption ($\lambda_{max}$) of the polymer **PAA(PU)TBT** is about 560 nm, whereas, the $\lambda_{max}$ of the polymers **PATA(D)TBT** and **PATA(BO)TBT** show red shifts by 78 and 74 nm, respectively. The red-shifted absorptions of **PATA(D)TBT** and **PATA(BO)TBT** can be ascribed to the additional thienyl units attached to the acetylene substituents as side chains on the anthracene units, which extend the electronic conjugation laterally on these polymers. Using the linear alkylthienylethynyl (**7A**) substituents in **PATA(D)TBT** resulted in the enhancement of the stacking of polymer backbones leading to a reduced optical band gap relative to those of **PATA(BO)TBT** and **PAA(PU)TBT**. The optical band gaps ($E_g^{opt}$) of the polymers with different substituents were (**7A**) (1.75 eV) < (**7B**) (1.80 eV) < (**9**) (1.85eV).

It is worth to mention, the molar absorption coefficients of the polymers **PATA(D)TBT** and **PATA(BO)TBT** ($3.90 \times 10^{+4}$ $M^{-1}cm^{-1}$ for both) are higher than that of **PAA(PU)TBT** ($3.48 \times 10^{+4}$ $M^{-1}cm^{-1}$) indicating that the amount of photons absorbed by the former polymers are higher. All these results suggest that introducing arylethynyl groups to the polymer backbone helps in delocalising π-electrons to the conjugated side substituents which enlarged the π-conjugation more effectively. As a result, **PATA(D)TBT** and **PATA(BO)TBT** with conjugated side groups will have larger conjugated area compare to **PAA(PU)TBT** resulted in more effective interchain π-π overlapping leading better optical properties [25].

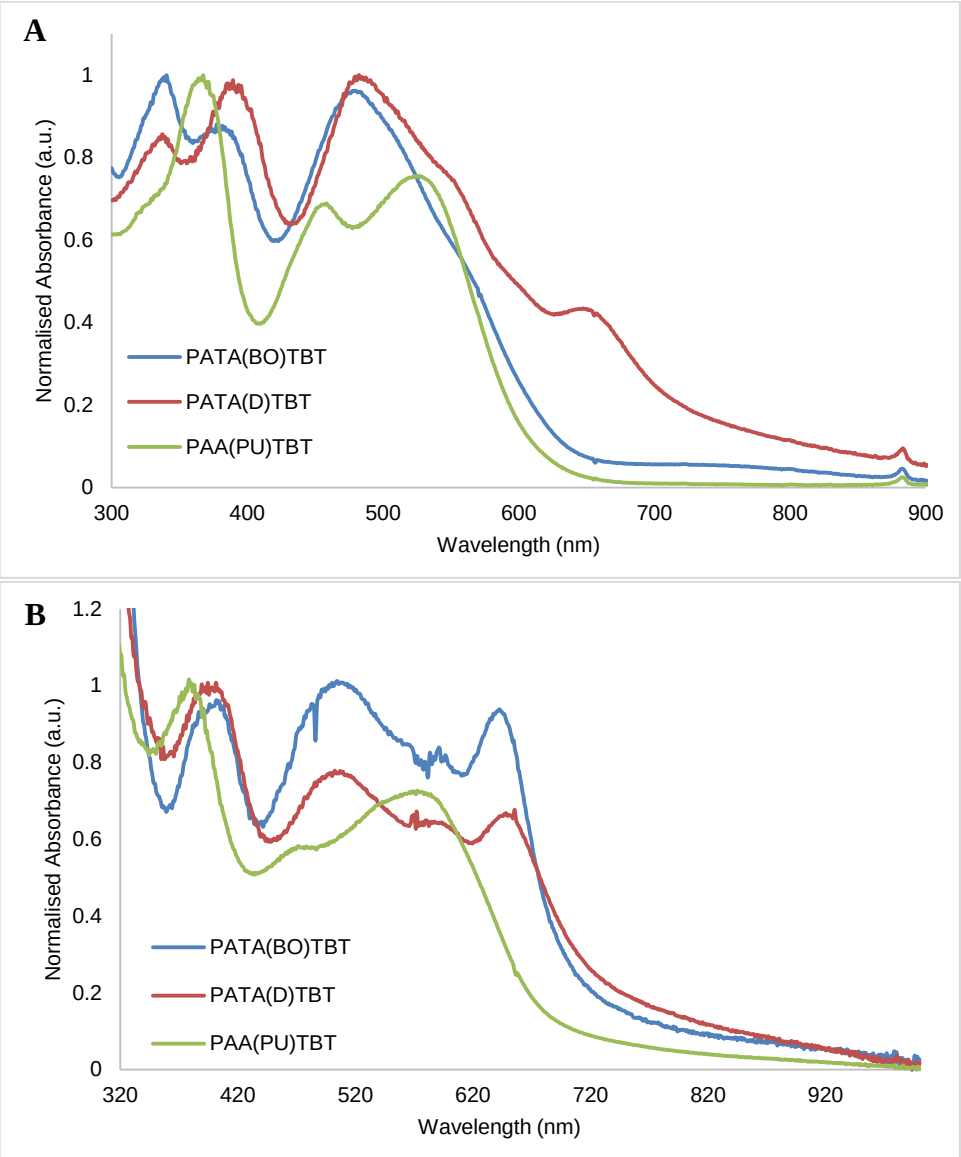


**Figure 2-7:** Normalised UV-Vis absorption spectra of **PATA(D)TBT**, **PATA(BO)TBT** and **PAA(PU)TBT** in : (A) chloroform solutions; and (B) thin films.

These polymers **PATA(D)TBT** and **PATA(BO)TBT** are analogous to polymers previously prepared by Iraqi group [15] (**PPATBT**) as well as **PTADTBT** synthesised by Jung and co-workers [18]. **PPATBT** and **PTADTBT** have optical band gaps of 1.84 and 1.78 eV, respectively which are close to the optical band gaps ($E_g^{opt}$) of this new series of polymers.

### 2.2.5 Electrochemical Characterisation

The optical properties of conjugated polymers can provide the energy separation of their frontier orbitals i.e their energy band gaps. However, to get more details on the

positions of their HOMO and LOMO levels, we need to measure the reduction and oxidation potentials of the conjugated polymers using cyclic voltammetry (CV). It is a very important tool which provides us with very important information for a better understanding of their photovoltaic performances [26].

The HOMO and LUMO energy levels of the polymers were determined by cyclic voltammetry measurements which were achieved under argon by using a solution of tetrabutylammonium perchlorate in acetonitrile as the supporting electrolyte with a Pt disc as a working electrode, reference electrode and counter electrode, Ferrocene was used as the reference redox standard. According to the literature, the redox potential of $Fc/Fc^+$ is –4.8 eV below the vacuum level [27]. The half-way potential of $Fc/Fc^+$ was measured to be 0.083 eV with respect to $Ag/Ag^+$ reference electrode. Therefore, the HOMO and LUMO energy level were calculated using the following equations:

$$E_{LUMO} = -[(E_{red,onset} - E_{1/2(ferrocene)}) + 4.8] \text{ eV}$$

$$E_{HOMO} = -[(E_{ox,onset} - E_{1/2(ferrocene)}) + 4.8] \text{ eV}$$

where $E_{red,onset}$ and $E_{ox,onset}$ are the onsets of reduction and oxidation of the polymers, respectively, relative to $Ag/Ag^+$ reference electrode. The cyclic voltammograms of the three polymers are displayed in **Figure 2-8** and the detailed electrochemical data is summarised in**Table 2-3**.

The $E_{HOMO}/E_{LUMO}$ levels of the polymers **PATA(D)TBT**, **PATA(BO)TBT** and **PAA(PU)TBT** were calculated to be –5.39/–3.52, –5.41/–3.55 and –5.42/–3.50 eV, respectively. This obvious similarity in the electrochemical properties of the polymers indicates that there was no significant impact of the attached substituents into the backbone of these polymers. The values of the HOMO levels of these polymers are comparable to similar polymers with anthracene repeat units having alkylaryl substituents on their 9,10-positions and benzothiadiazole units (**PPATBT**, HOMO at –5.44 eV and **PTADTBT**, HOMO at –5.40 eV) [15, 18].

**Table 2-3:** The energy levels and electrochemical band gaps of the polymers.

| Polymers | HOMO (eV) [a] | LUMO (eV) [b] | $E_g^{elece}$ (eV) [c] |
|---|---|---|---|
| PATA(D)TBT | –5.39 | –3.52 | 1.87 (±0.03) |
| PATA(BO)TBT | –5.41 | –3.55 | 1.86 (±0.03) |
| PAA(PU)TBT | –5.42 | –3.50 | 1.92 (±0.04) |

[a] HOMO position (*vs. vacuum*) determined from onset of oxidation. [b] LUMO position (*vs. vacuum*) determined from onset of reduction. [c] Electrochemical energy gap of the polymers.

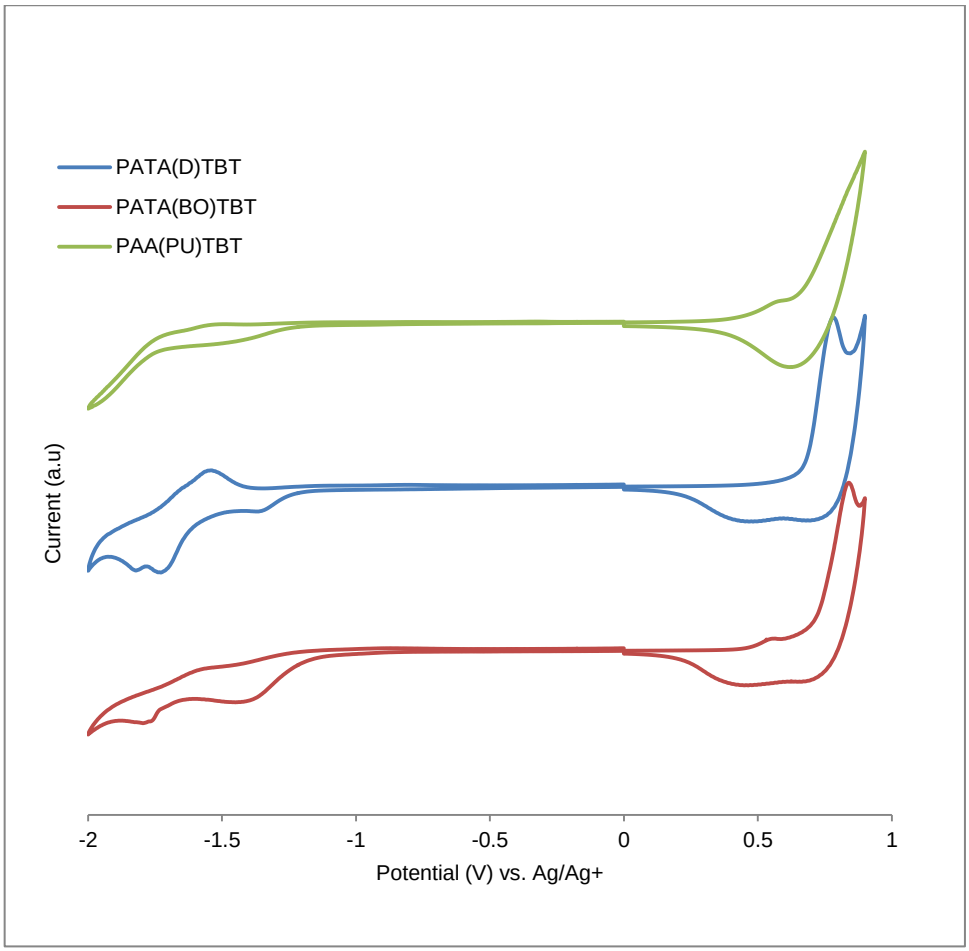


**Figure 2-8:** Cyclic voltammograms of **PATA(D)TBT**, **PATA(BO)TBT** and **PAA(PU)TBT**.

However, the LUMO levels of the three polymers are relatively higher than **PTADTBT** (LUMO at –3.62 eV) synthesised by Jung and co-workers [18]. We think that the high molecular weight of **PTADTBT** is responsible for this difference. According to a previous literature, the LUMO level of a polymer become much deeper when compared

to the HOMO level as the molecular weight increases [28, 29]. Kim *et al*, ascribed that to the molecular orbital hybridisation of the donor and acceptor units which resulted in localisation of the LUMO level on the electron-rich unit as the $M_n$ of the polymer increases [29].

On the other hand, **PPATBT** synthesised by Iraqi *et al.*[15] had a LUMO level of –3.21 eV higher than the LUMO levels of the polymers presented in this work; even though the polymers have a comparable low molecular weight. Clearly, modification of these polymers by replacing 4-dodecyloxyphenyl groups attached to the anthracene units with arylethynyl or alkynyl groups resulted in improving the electronic properties of this new class of polymers. It seems that using acetylene units to connect alkylthienyl groups and the polymer backbone leads to an extension of the conjugation of the polymer in 2-D which enhance the resonance effect. Therefore, our polymers which incorporate alkylthienylethynyl or alkynyl groups induce efficient intramolecular charge separation leading to a considerable decline in their LUMO energy levels [28].

### 2.2.6 X-ray Diffraction studies

The crystallinity of the three polymers was investigated by X-ray powder diffraction (XRD) (**Figure 2-9**). Diffraction peaks for **PATA(D)TBT**, **PATA(BO)TBT** and **PAA(PU)TBT** appeared in the wide angle region at $2\theta$ of 22.01, 20.74$^o$ and 22.33$^o$, respectively, reflecting the π-π stacking distances between the polymer chains which are calculated to be 4.03, 4.28 and 3.98 Å, respectively. The intensity of the diffraction peak of **PATA(BO)TBT** in the wide angle region is larger than the other two polymers indicating that **PATA(BO)TBT** has better crystallinity [30]. Also it is worth to mention that, **PATA(BO)TBT** display a sharp peak at $2\theta$ value of 4.13$^o$ which corresponds to a distance of 21.37 Å. According to previous studies on different conjugated polymers, this value could be attributed to the distance between polymer backbones separated by the alkyl chains [30, 31]. We proposed that the incorporation of the substituents through acetylene groups resulted in enhanced π-π stacking and intermolecular interactions of these polymers. These results provide a good explanation for the low solubility of these polymers in common organic solvents and hence their low molecular weights. We also anticipate that the miscibility of these polymers with electron acceptor $PC_{70}BM$ will be

very low, and therefore it might be difficult to fabricate them into organic solar cells in view of their low solubility

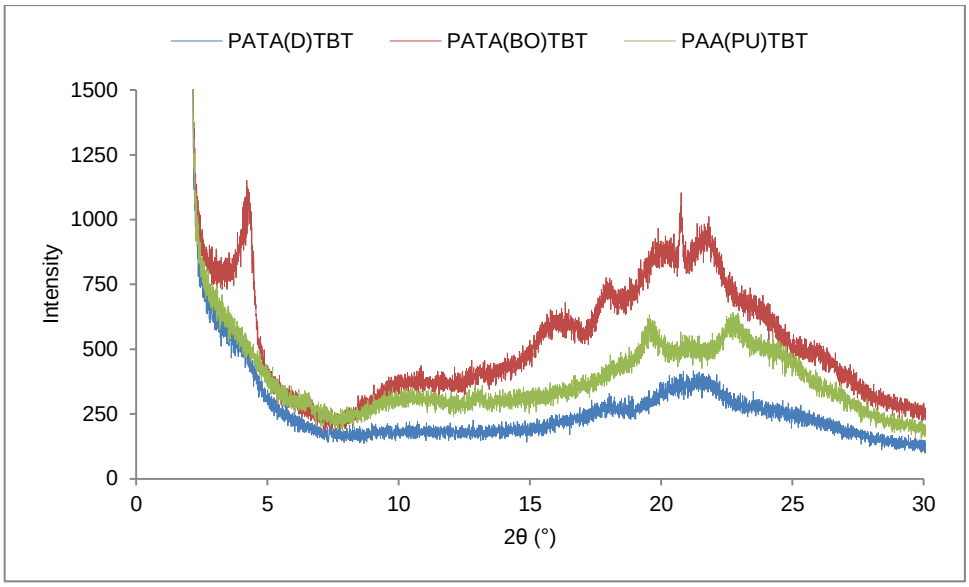


**Figure 2-9:** Powder X-ray diffraction scans of the polymers **PATA(D)TBT**, **PATA(BO)TBT** and **PAA(PU)TBT.**

### 2.2.7 Photovoltaic Device Properties

The photovoltaic performance of the polymers were evaluated using a series of glass/ITO/PEDOT:PSS/polymer : $PC_{70}BM$ (1 : 3)/Ca/Al polymer solar cells devices. A detailed device fabrication method is given in the Experimental section. Preparation of uniform films from **PATA(BO)TBT** and **PAA(PU)TBT** were difficult to achieve as the polymers formed aggregates at the surface of the film after spin coating due to their low solubilities. **PATA(D)TBT** was the only polymer in the series that was possible to process into devices. The *J–V* curve of the **PATA(D)TBT** device is shown in **Figure 2-10**, and the device parameters are listed in **Table 2-4**. The performance of the device was quite modest in comparison to its counterparts **PTADTBT** prepared by Jung and co-worker [18] and **PPATBT** prepared by Iraqi group [15]. The polymer provided a device with an open circuit voltage ($V_{oc}$) of 0.80 V, a short circuit current density ($J_{sc}$) of 3.38 mA/cm$^2$, a fill factor (FF) of 31% and a power conversion efficiency of 0.84%.

**Table 2-4:** Photovoltaic performance of **PATA(D)TBT** measured under a simulated photovoltaic light with 1000 $Wm^{-2}$ the illumination (AM 1.5).

| Polymer | Polymer : $PC_{71}BM$[a] (w/w) | Solvent | $J_{sc}$ (mA $cm^{-2}$) | $V_{oc}$ (V) | FF (%) | PCE (%) |
|---|---|---|---|---|---|---|
| PATA(D)TBT | 1 : 3 | CB[b] | –3.38 | 0.80 | 0.31 | 0.84 |

[a] Polymer : $PC_{71}BM$ weight ratio. [b] chlorobenzene.

We believe that the low $V_{oc}$ of **PATA(D)TBT** compared to **PTADTBT** ($V_{oc}$ = 0.92 V) can be ascribed to its poor solubility which resulted in formation of a non-uniform film. To support the previous assumption by comparison between the two devices through the so-called fill factor (FF), we find that the *FF* of **PATA(D)TBT** device (*FF* = 0.31) is lower than that of **PTADTBT** (FF = 0.65). The lower fill factor of **PATA(D)TBT** seemingly due to the poor packing of the polymer chains in the device and probably a low charge mobility [15]. In addition, according to Hoppe *et al.* not only the materials' energy levels can affect the $V_{oc}$ values, it is also a sensitive function of the energy level alignments between organic-metal electrodes interfaces [32]. So, the other possible reason that can be attributed to it this difference in $V_{oc}$ values between **PATA(D)TBT** and **PTADTBT** is the device structures used to investigate the photovoltaic properties. In fact, the $V_{oc}$ of **PATA(D)TBT** is very close to the $V_{oc}$ of **PPATBT** ($V_{oc}$ = 0.59 V) prepared in Iraqi group where they have used a similar device structure to measure the photovoltaic performance of their polymer [15].

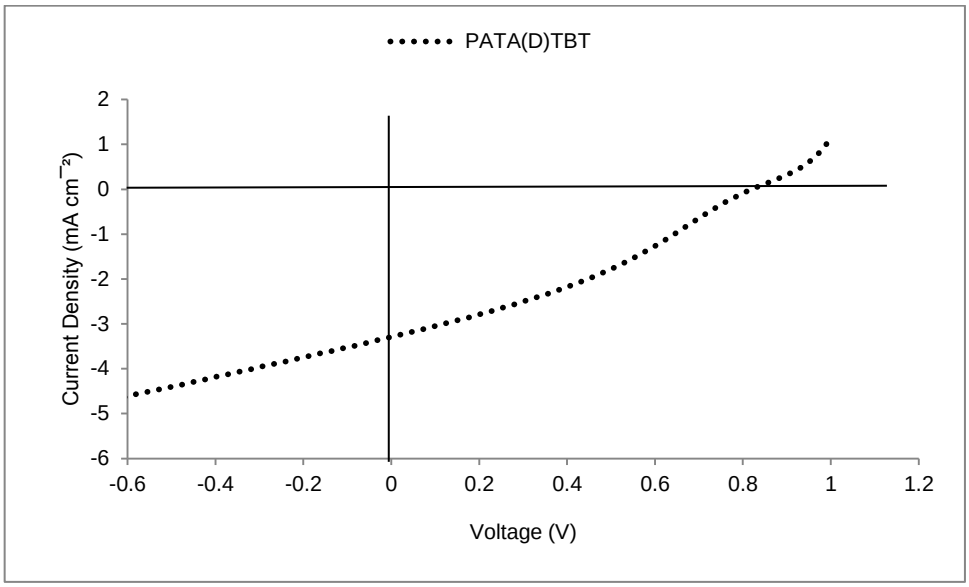


**Figure 2-10:** *J-V* characteristic curve of the organic solar cell device fabricated from **PATA(D)TBT**.

Further studies are needed to optimise the performance of this polymer. It is very important to use different polar solvents to cast the active layer of devices and different polymer:$PC_{70}BM$ weight ratios to investigate the influence of the morphology in the performance of the polymer.

## 2.3 Summary

In summary, a series of 2,6-linked anthracene derivatives based polymers were synthesised by direct arylation polymerisation with dithienyl-benzo[*c*]-[1,2,5]thiadiazole to yield **PATA(D)TBT**, **PATA(BO)TBT** and **PAA(PU)TBT**. The influence of the attached groups into the 9,10 positions of the anthracene unit was studied by UV-visible spectroscopy, cyclic voltammetry and X-ray diffraction techniques. The three polymers display a limited solubility in common organic solvent at room temperature; a consequence of the absence of solubilising groups on the **TBT** units. As a result, the fabrication of photovoltaic devices using **PATA(BO)TBT** and **PAA(PU)TBT** through solution processing were not possible. A comparison between **PAA(PU)TBT** which possesses alkynyl groups at 9,10-positions of anthracene repeat units, and the polymers with arylethynyl substituents (**PATA(D)TBT** and **PATA(BO)TBT**) indicates that the later polymers have greater electronic conjugation and lower optical band gaps. The electrochemical properties of the polymers were

highly comparable; an indication of the lack of a significant influence of these attached groups on the position of the HOMO and LUMO energy levels of the polymers. Polymer solar cell based on **PATA(D)TBT** blended with $PC_{70}BM$ has shown a PCE of 0.84% and $V_{oc}$ of 0.80 V. These low values can be attributed to the low solubility of the polymer which presents processing difficulties and a poor morphology of active layers in polymer photovoltaic devices.

The processability of this class of polymers is clearly an issue that needs to be addressed. Addition of solublising groups on the benzothiadiazole repeat units could help in the preparation of polymers with enhanced processability. This option is investigated in the next chapter of this thesis.

## 2.4 Experimental Section:

### 2.4.1 Materials:

Unless otherwise stated, all chemicals, reagents and solvents were obtained from commercial sources (Sigma-Aldrich, Fisher, Acros Organics and Alfa Aesar) in the highest purities possible and used as received. Regent grade solvents were purchased from the internal stores which were used for some reactions, extraction, recrystallization and chromatography. However, most of the reactions were carried out using anhydrous solvents which were obtained from the Grubbs solvent system within the chemistry department. Acids, bases, drying agents and salts were obtained from the internal stores. Reactions proceeded under an argon atmosphere as standard unless stated otherwise. Column chromatography was carried out on silica gel (200-300 mesh) or alumina as stated.

4,7-Dithien-2-yl-2,1,3-benzothiadiazole (**M4**), 5-(bromomethyl)undecane were prepared by A. Almaliky and R. Vanga of the Iraqi group, respectively, according to a procedure by Fu *et al* [20].

### 2.4.2 Analytical Techniques:

Elemental analyses were analysed by using the Perkin Elmer 2400 CHN Elemental Analyser for CHN analysis, and the Schoniger oxygen flask combustion method for

sulphur and halides. In both methods, the weights submitted for the analysis were 10 mg. Fourier transform infrared spectroscopy (FTIR) and attenuated total reflectance (ATR) were recorded on a Perkin Elmer Spectrum 65 spectroscopy.

$^{13}C$ and $^{1}H$-NMR spectra of the monomers were recorded on Bruker AV 250 (250 MHz), and Bruker AV 400 (400 MHz) NMR spectrometers at room temperature in chloroform-d ($CDCl_3$) solution. NMR spectra of the polymers were recorded using Bruker Avance III HD 500 (500 MHz) at 100 °C in 1,1,2,2-tetrachloroethane-d2 solution. As an internal standard, tetramethylsilane (TMS) was used for calibrating chemical shifts (δ). The chemical shifts were measured in part per million (ppm), while the coupling constant (*J*) were given in Hertz (Hz).

GC-MS spectra were recorded on Perkin Elmer Turbomass Mass Spectrometer equipped with a Perkin Elmer Autosystem XL Gas Chromatograph. Mass spectra were obtained by the electron impact method (EI) and MALDI-TOF mass spectrometry.

GPC analysis were recorded on the equipment consisted of a Viscotek $GPC_{max}$ VE 2001 GPC solvent/sample module, a Waters 410 Differential Refractometer and a PLgel 5 μm Mixed Column (650 mm set length) using chloroform as the eluent at rate of 1 mL/min. Polymer samples were made up as a solutions in chloroform (2 mg/mL) spiked with toluene as a reference. The RI-detection method was used to obtain the GPC curves, which was calibrated with a series of polystyrene narrow standards. Degree of polymerisation (DP) was calculated using the below equation:

$$\chi_n = \frac{M_n}{M_R}$$

where $\chi_n$ is the DP, $M_n$ is the number average molecular weight of the polymer and $M_R$ is the molecular mass of the repeat unit of the polymer. Perkin Elmer TGA-7 Thermogravimetric Analyser was used to determine TGA curves at a scan rate of 10 °C/minute under nitrogen atmosphere.

Powder X-ray diffraction were conducted on a Bruker D8 advance diffractometer with a CuKα radiation source (1.5418 A, rated as 1.6 kW). The scanning angle was recorded over the range 2–30°.

Hitachi U-2010 Double Beam UV-Visible Spectrophotometer has been used to evaluate the optical properties of the polymers. The absorbance of the polymers was measured in a solution of chloroform at room temperature using quartz cuvette ($l$ = 10 mm). Thin films of the polymers were prepared by dip coating quartz plates into around 1 mg/mL solutions in chloroform, then dried in the air and the UV-Vis absorption spectra measurements were run at room temperature.

Cyclic voltammograms were conducted using Princeton Applied Research Model 263A Potentiostat/Galvanostat. The analyses were recorded under Argon protection at approximately room temperature. A three electrode system was used for the measurements consisting of an $Ag/Ag^+$ reference electrode (Ag wire in 0.01 *M* $AgNO_3$ solution in the electrolyte solution), a Pt working electrode, and Pt counter electrode (Pt wire). Measurements were done in tetrabutylammonium perchlorate acetonitrile solution (0.1 *M*) on polymer thin films which made by drop casting polymer solution onto the working electrode which were left to dry in air. According to the IUPAC's recommendation, ferrocene was used as a reference redox system [33]. The energy level of $Fc/Fc^+$ was assumed at –4.8 eV to vacuum. The half-wave potential of Fc/Fc+ redox couple was found to be 0.08 V *vs*. $Ag/Ag^+$ reference electrode. the HOMO and LUMO energy level were calculated using the following equations:

$$E_{LUMO} = -[(E_{red,onset} - E_{1/2(ferrocene)}) + 4.8] \text{ eV}$$

$$E_{HOMO} = -[(E_{ox,onset} - E_{1/2(ferrocene)}) + 4.8] \text{ eV}$$

where $E_{red,onset}$ and $E_{ox,onset}$ are the onset of reduction and oxidation, respectively, relative to $Ag/Ag^+$ reference electrode [34].

### 2.4.3 Fabrication and testing of polymer solar cells:

The polymer and $PC_{70}BM$ were mixed at (1:3) polymer : fullerene blending ratio and were dissolved in CB. Photovoltaic device was fabricated onto pre-patterned ITO glass substrate (20 Ohms per square) that were supplied by Ossila Limited. The ITO/glass substrate was cleaned by sonication in $NaOH_{(aq)}$ followed by IPA. A 30 nm thick PEDOT:PSS layer was spin-coated onto the ITO substrate. This was then transferred to a hot plate held at a temperature of 120 °C for 5 min. In a glove-box, the active layer was spin cast onto the glass/ITO/PEDOT:PSS substrate, which was then transferred into a thermal evaporator for deposition of OPV cathode (5 nm of calcium capped by a 100 nm of aluminium evaporated at a base pressure of ~$10^{-7}$ mbar). PCE was measured using a Newport 92251A-1000 AM 1.5 solar simulator. An NREL calibrated silicon cell was used to calibrate the power output to 100 mW $cm^{-2}$ at 25 °C. An aperture mask having an area of 2.06 $mm^2$ was placed over devices to define the test area.

## 2.5 Synthesis of Monomers and Polymers:

### 2.5.1 Synthesis of 2,6-dibromo-9,10-antharaquinone (2): [21]

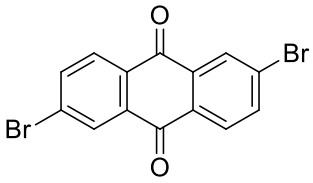


2,6-Diamino-9,10-antharaquinone **(1)** (9.6 g, $4.0\times10^{-2}$ mol) was added to a reaction mixture of *tert*-butyl nitrate (10.4 g, 12.0 mL, 0.10 mol) and $CuBr_2$ (22.2 g, 0.10 mol) in a one-neck flask containing 170 mL of dry acetonitrile. The reaction mixture was stirred for 2 hours at 65 °C, and then quenched by adding 100 mL of 35% HCl. The resulting product was filtered, washed with acetonitrile and recrystallised from 1,4-dioxane to afford a pale yellow solid: yield 7.98 g (54%). $^1$H-NMR (250 MHz, *CDCl*$_3$) $\delta_H$/ppm: 8.45 (d, *J* = 3.0 Hz, 2H), 8.18 (d, *J* = 8.5 Hz, 2H), 7.90 (dd, *J* = 8.5, 3.0 Hz, 2 H). Elemental Analysis (%) Calculated for $C_{14}H_6O_2Br_2$: C, 45.94; H, 1.65; Br, 43.66. Found: C, 45.74; H, 1.24; Br, 44.76. Mass (EI); (*m/z*) 366 ($M^+$). FT-IR ($cm^{-1}$): 3080 (aromatic C–H stretch), 1675 (C=O stretch), 1580 (C=C stretch), 730 (C–Br stretch).

### 2.5.2 Synthesis of 2-dodecyl thiophene (4A): [35]

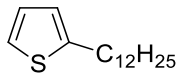


Thiophene (8.4 g, 8.0 mL, 0.10 mol) was dissolved in dry THF (60 mL) under $N_2$ protection. *N*-Butyl lithium (62.5 mL, 0.10 mol, 1.6 mol/L in Hexane) was then added to the mixture dropwise. The reaction mixture was stirred for 1 hour, followed by the addition of 1-bromododecane (22.6 g, 21.8 mL, 0.20 mol) and stirred at room temperature overnight. The reaction mixture was poured into 200 mL cold water, extracted with diethyl ether and the organic layers were collected, washed with water and dried over $MgSO_4$. The solvent was evaporated and the resulting product was distilled under vacuum to give a pale yellow oil: yield 12.3 g (49%). $^1$H-NMR (250 MHz, *CDCl$_3$*) $\delta_H$/ppm; 7.12 (d, *J* = 1.0 Hz, 1 H), 6.94 (t, *J* = 2.0 Hz, 1 H), 6.80 (d, *J* = 1.0 Hz, 1 H), 2.85 (t, *J* = 3.0 Hz, 2 H), 1.69 (p, 2 H), 1.40-1.18 (m, 18 H), 0.92 (t, 2.0 Hz, 3H). $^{13}$C-NMR (250 MHz,$CDCl_3$): δ 145.75, 126.23, 123.75, 122.6, 31.89, 31.8, 29.94, 29.87, 29.59, 29.52, 29.4, 29.36, 29.31, 29.13, 22.54, 14.08 Elemental Analysis (%) Calculated for $C_{16}H_{28}S$: C, 76.12; H, 11.18; S, 12.70. Found: C, 76.14; H, 11.95; S, 10.83. Mass (EI); (m/z) 252. FT-IR ($cm^{-1}$): 2955-2852 (C–H stretch for $sp^3$ carbon).

### 2.5.3 Synthesis of 2-(2-butyl-octyl) thiophene (4B): [35]

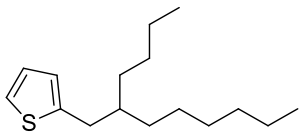


2-(2-Butyl-octyl)thiophene was synthesised from thiophene (8.4 g, 0.10 mol) and 5-(bromomethyl)undecane (22.3 g, 8.9 × $10^{-2}$ mol) using a synthetic method similar to that used to synthesised 2-dodecylthiophene (**4A**). The product was collected by vacuum distillation to give a colourless oil. Yield 9.5 g (37%). $^1$H-NMR (400 MHz, $CDCl_3$) $\delta_H$/ppm; 7.14 (dd, *J* = 5.0, 1.0 Hz, 1 H), 6.94 (dd, *J* = 5.0, 3.5 Hz, 1 H), 6.77 (d, *J* = 3.5 Hz, 1 H), 2.78 (d, *J* = 7.0 Hz, 2 H), 1.69-1.61 (bm, 1 H), 1.37-1.20 (bm, 16 H), 0.92 (t, 7.0 Hz, 6H). $^{13}$C-NMR (250 MHz, *CDCl$_3$*): δ 144.35, 126.52, 124.95, 122.89, 40.03, 34.27, 33.23, 32.91, 31.89, 29.64, 28.86, 26.59, 23.01, 22.67, 14.09 Elemental Analysis (%) Calculated for $C_{16}H_{28}S$: C, 76.12; H, 11.18; S, 12.70. Found: C, 75.65; H,

11.54; S, 12.29. Mass (EI); (m/z) 248. FT-IR ($cm^{-1}$): 2958-2856 (aliphatic C–H stretch), 1540 (C=C stretch), 1377 ($CH_2$ bending), 724 ($CH_2$ bending).

### 2.5.4 Synthesis of 2-bromo-5-dodecyl thiophene (5A): [35]

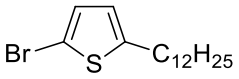


In a two necks round bottom flask, 2-dodecylthiophene (8.00 g, $3.2\times10^{-2}$ mol) was dissolved in 350 mL of chloroform. A mixture of acetic acid (350 mL) and *n*-bromosuccinimide (6.79 g, $3.8\times10^{-2}$ mol) was added to the reaction mixture dropwise at 0 °C. The reaction mixture was stirred for 24 hours at room temperature under light protection. Thereafter, the reaction mixture was poured in $NaHCO_3$ solution and extracted with chloroform. The organic layers were collected and dried over $MgSO_4$. Removal of the solvent gave a pale brownish oily product, which was then purified on silica gel column chromatography eluting with petroleum ether. The product was collected as colourless oil, yield of 10.32 g, (98%). $^1$H-NMR (250 MHz, *CDCl*$_3$) $\delta_H$/ppm: 6.86 (d, *J* = 3.5 Hz, 1H), 6.55 (d, *J* = 3.5 Hz, 1H), 2.73 (t, *J* = 7.5 Hz, 2 H), 1.73-1.59 (m, 2 H), 1.42-1.23 (m, 18 H) 0.95-0.89 (t, *J* = 6.5 Hz, 3 H). $^{13}$C-NMR (250 MHz, *CDCl*$_3$): δ 147.59, 129.33, 124.28, 108.61, 41.41, 31.91, 31.48, 30.36, 29.69, 29.58, 29.40, 29.10, 22.73, 20.48, 14.30, 11.40. Elemental Analysis (%) Calculated for $C_{16}H_{27}BrS$: C, 58.00; H, 8.20; Br, 24.10; S, 9.67. Found: C, 58.32; H, 8.09; Br, 24.27; S, 8.86. Mass (EI); (*m/z*) 330 ($M^+$). FT-IR ($cm^{-1}$): 2921-2851 (aliphatic C–H stretch), 1446 (C=C stretch), 1377 ($CH_2$ bending), 721 ($CH_2$ bending) 789 (C–Br stretch).

### 2.5.5 Synthesis of 2-bromo-5-(2-butyl-octyl) thiophene (5B): [35]

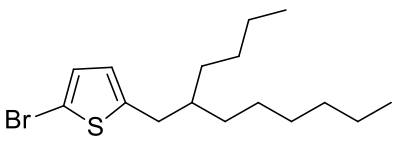


This compound was prepared using the same method as described for 2-bromo-5-dodecylthiophene using with 2-(2-butyl-octyl) thiophene (4.61 g, $1.8\times10^{-2}$ mol) and *n*-

bromosuccinimide (3.20 g, 1.8 × $10^{-2}$ mol). The crude product was purified on silica gel column chromatography eluting with petroleum ether. The product was collected as colourless oil. Yield 5.08 g (85%). $^{1}$H-NMR (250 MHz, *CDCl$_3$*) $\delta_H$/ppm: 6.87 (d, *J* = 3.5 Hz, 1H), 6.53 (d, *J* = 3.5 Hz, 1H), 2.70 (d, *J* = 7.0 Hz, 2 H), 1.63-1.54 (bm, 1 H), 1.36-1.22 (bm, 16 H) 0.93-0.88 (t, *J* = 7.0 Hz, 6 H). $^{13}$C-NMR (250 MHz, *CDCl$_3$*): δ 146.20, 129.33, 125.42, 108.68, 39.77, 34.70, 33.09, 32.77, 31.87, 29.60, 28.80, 26.54, 22.98, 22.67, 14.12. Elemental Analysis (%) Calculated for $C_{16}H_{27}BrS$: C, 58.00; H, 8.20; Br, 24.10; S, 9.67. Found: C, 58.52; H, 8.48; Br, 23.20; S, 9.14. Mass (EI); (*m/z*) 330 ($M^+$). FT-IR ($cm^{-1}$): 2957-2854 (aliphatic C–H stretch), 1560 (C=C stretch), 1377 ($CH_2$ bending), 724 ($CH_2$ bending) 787 (C–Br stretch).

### 2.5.6 Synthesis of 2-(2-methylbut-3-yn-2-ol)-5-dodecyl thiophene (6A): [36]

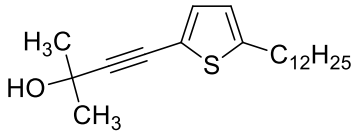


2-Bromo-5-dodecyl thiophene (10.6 g, 3.0×$10^{-2}$ mol) was dissolved in 150 mL of triethylamine ($Et_3N$) in a round bottom flask. To the reaction mixture, CuI (570 mg, 3.0×$10^{-3}$ mol), palladium acetate (340 mg, 1.5 × $10^{-3}$ mol), triphenylphosphine (400 mg, 1.5×$10^{-3}$ mol) and 2-methylbut-3-yn-2-ol (5.05 g, 6.0 × $10^{-2}$ mol) were added under $N_2$ protection and refluxed overnight. The mixture was filtered and solvent was evaporated by rotatory evaporator. The resulting residue was purified *via* silica gel column chromatography using petroleum ether/ethyl acetate (7.5:2.5) as an eluent. The desired product was obtained as a greenish solid crystals: yield 6.15 g (61%). $^{1}$H-NMR (250 MHz, *CDCl$_3$*) $\delta_H$/ppm: 7.02 (d, *J* = 3.5 Hz, 1H), 6.63 (d, *J* = 3.5 Hz, 1H), 2.78 (t, *J* = 7.5 Hz, 2H), 2.33 (s, 1H), 1.70-1.60 (m, 8H), 1.38-1.25 (m, 18H) 0.95-0.89 (t, *J* = 6.5 Hz, 3H). $^{13}$C-NMR (250 MHz, *CDCl$_3$*): δ 148.11, 132, 123.97, 119.84, 96.63, 76.03, 65.77, 31.91, 31.54, 31.39, 30.14, 29.62, 29.53, 29.33, 29, 22.86, 14.10. Elemental Analysis (%) Calculated for $C_{21}H_{34}OS$: C, 75.39; H, 10.24; S, 9.58. Found: C, 73.32; H, 9.67; S, 9.27. Mass (EI); (*m/z*) 334 ($M^+$). FT-IR ($cm^{-1}$):3490 (O–H stretch), 2985-2849 (aliphatic C–H stretch), (C,C triple bond stretch) at 2215 $cm^{-1}$, 1434 (C=C stretch), 1370 ($CH_2$ bending), 1215 (C–O stretch).

### 2.5.7 Synthesis of 2-(2-methylbut-3-yn-2-ol)-5-(2-butyl-octyl) thiophene (6B): [36]

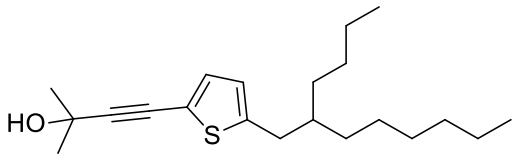


Compound **6B** was prepared, following a procedure similar to that used for compound **6A** using 2-bromo-5-(2-butyl-octyl) thiophene (5.08 g, 1.5 × $10^{-2}$ mol) and 2-methylbut-3-yn-2-ol (2.58 g, 3.0 × $10^{-2}$ mol). The crude product was purified on silica gel column chromatography using petroleum ether. The product was collected as dark green oil. Yield, 3.51 g (69%). $^{1}$H-NMR (250 MHz, *CDCl$_3$*) $\delta_H$/ppm: 7.02 (d, *J* = 3.5 Hz, 1H), 6.6 (d, *J* = 3.5 Hz, 1H), 2.72 (d, *J* = 6.5 Hz, 2H), 2.02 (s, 1H), 1.65-1.55 (m, 7H), 1.32-1.22 (m, 16H) 0.94-0.83 (bm, 6H). $^{13}$C-NMR (250 MHz, *CDCl$_3$*): δ 146.69, 131.94, 125.02, 120.03, 96.69, 65.78, 39.96, 34.52, 33.17, 32.84, 31.86, 31.39, 29.59, 28.83, 26.57, 22.97, 22.65, 14.08. Elemental Analysis (%) Calculated for $C_{21}H_{34}OS$: C, 75.39; H, 10.24; S, 9.58. Found: C, 75.02; H, 9.99; S, 8.60. Mass (EI); (*m/z*) 334 ($M^+$). FT-IR ($cm^{-1}$):3490 (O–H stretch), 2985-2849 (aliphatic C–H stretch), (C,C triple bond stretch) at 2215 $cm^{-1}$, 1634 (C=C stretch), 1370 ($CH_2$ bending), 1215 (C–O stretch).

### 2.5.8 Synthesis of 2-ethynyl-5-dodcylthiophene (7A): [36]

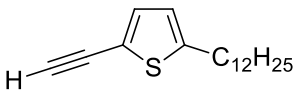


To a solution of 2-(2-methyl-3-butyne)-5-dodecyl thiophene (5.8 g, 1.7×$10^{-2}$ mol) in toluene (80 mL), finely powdered KOH (1.9 g, 3.4×$10^{-2}$ mol) was added. The mixture was refluxed overnight, cooled to room temperature, filtered, and the solvent evaporated. The resulting residue was purified *via* flash chromatography on a silica gel column, eluting with petroleum ether to afford 2-ethynyl-5-dodcylthiophene (**7A**) as pale yellow oil (3.70 g, 79%). $^{1}$H-NMR (250 MHz, *CDCl$_3$*) $\delta_H$/ppm: 7.12 (d, *J* = 3.5 Hz, 1H), 6.65 (d, *J* = 3.5 Hz, 1H), 3.30 (s, 1H), 2.80 (t, *J* = 7.5 Hz, 2H), 1.70-1.64 (m, 2H), 1.38-1.25 (m, 18H), 0.95-0.89 (t, *J* = 6.5 Hz, 3H). $^{13}$C-NMR (250 MHz, *CDCl$_3$*): δ

148.53, 133.05, 129.04, 128.23, 125.32, 123.91, 119.34, 80.31, 41.41, 36.13, 31.97, 31.56, 30.16, 29.68, 29.37, 29.07, 22.72, 14.10. Elemental Analysis (%) Calculated for $C_{18}H_{28}S$: C, 78.20; H, 10.21; S, 11.60. Found: C, 76.44, H, 10.26; S, 10.94. Mass (EI); (*m/z*) 276 ($M^+$). FT-IR ($cm^{-1}$): 3311 (acetylenic C–H stretch), 2957-2853 (aliphatic C–H stretch), 2099 (carbon, carbon triple bond stretch), 1461 (C=C stretch), 731 ($CH_2$ bending).

### 2.5.9 Synthesis of 2-ethynyl-5-(2-bytyl-octyl) thiophene (7B):[36]

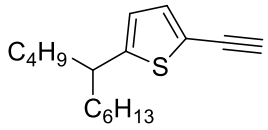


This compound was synthesised using the same procedure used to prepare **7A** starting with 2-(2-methylbut-3-yn-2-ol)-5-(2-butyl-octyl) thiophene (3.64 g, $1.1 \times 10^{-2}$ mol) and KOH (1.25 g, $2.2\times 10^{-2}$ mol). The resulting residue was purified by flash chromatography on a silica gel column, eluting with petroleum ether. The product was obtained as dark brown oil. Yield, 2.3 g (76%). $^1$H-NMR (250 MHz, *CDCl$_3$*) $\delta_H$/ppm: 7.12 (d, *J* = 3.5 Hz, 1H), 6.63 (d, *J* = 3.5 Hz, 1H), 3.32 (s, 1H), 2.73 (d, *J* = 6.5 Hz, 2H), 1.68-1.53 (bm, 1H), 1.38-1.17 (m, 16H), 0.95-0.84 (t, *J* = 6.5 Hz, 6H). $^{13}$C-NMR (250 MHz, *CDCl$_3$*): δ 147.20, 133.02, 124.97, 119.44, 80.37, 39.96, 34.52, 33.18, 31.86, 29.59, 28.83, 26.57, 22.97, 22.66, 14.08. Elemental Analysis (%) Calculated for $C_{18}H_{28}S$: C, 78.20; H, 10.21; S, 11.60. Found: C, 76.44, H, 10.26; S, 10.94. Mass (EI); (*m/z*) 276 ($M^+$). FT-IR ($cm^{-1}$): 3311 (acetylenic C–H stretch), 2957-2853 (aliphatic C–H stretch), 2099 (carbon, carbon triple bond stretch), 1661 (C=C stretch), 731 ($CH_2$ bending).

### 2.5.10 Synthesis of 3-pentylundec-1-yne (9): [37]

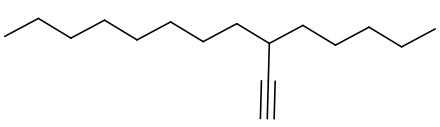

This synthesis was conducted under an argon atmosphere. 1-octyne (16.56 g, 22.2 mL, 0.15 mol) and dry hexane (150 mL) were added to a 500 mL round bottom flask. The

reaction mixture was cooled to –78 °C and *n*-BuLi (25 M in hexanes, 132 mL, 0.33 mol) was added dropwise via a dropping funnel. The solution was stirred for 30 minutes. The solution was allowed to warm to –42 °C using an acetonitrile/dry ice bath and then stirred for a further 1 hour. 1-Bromooctane (29.01 g, 23 mL, 0.15 mol) was added to the reaction mixture and was left to warm to room temperature overnight. HCl (6 M, 150 mL) was added drop-wise to the solution in an ice/water bath. The organic phase was separated, washed with water and dried ($MgSO_4$). After removal of the solvent under reduced pressure, the residual oil was purified by distillation to give 3-Pentylundec-1-yne as a yellow oil (9.68 g, 29 %). $^1$H NMR (400 MHz, $CDCl_3$) δ 2.32 (m,1H), 2.06 (d, *J* = 2.5 Hz, 1H), 1.48 – 1.26 (m, 22H), 0.91 (td, *J* = 7.0, 5.0 Hz, 6H). $^{13}$C NMR (400 MHz, *CDCl*$_3$) $\delta_C$/ppm: 88.37, 68.88, 35.00, 34.96, 31.94, 31.90, 31.72, 31.53, 30.20, 29.71, 29.67, 29.55, 29.53, 29.38, 29.31, 27.29, 26.96, 22.69, 22.61, 14.12, 14.08.Elemenatl analysis (%) Calculated for $C_{16}H_{30}$: C, 86.39; H, 13.60. Found: C, 82.16; H, 13.12. Mass (EI) (*m/z*) 222. FT-IR ($cm^{-1}$): 3310 (acetylenic C–H stretch), 2958-2851 (aliphatic C–H stretch), 2105 (carbon, carbon triple bond stretch).

### 2.5.11 Synthesis of 2,6-dibromo-9,10-bis[2-ethynyl-5-dodcylthiophen-2-yl] anthracene (M1): [13, 38]

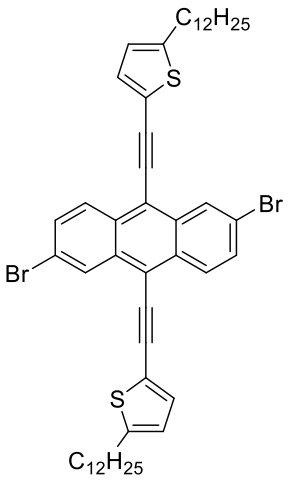


In a dried round bottom flask, 2-ethynyl-5-dodcylthiophene (1.8 g, $6.5 \times 10^{-3}$ mol) was dissolved in 120 mL of dry THF. *N*-BuLi (4.06 mL, $6.5 \times 10^{-3}$ mol, 1.6 *M* solution in hexane) was added dropwise over 5 minutes at –78 °C. The reaction mixture was stirred for 30 minutes at room temperature, followed by the addition of 2,6-dibromo-9,10-antharaquinone (1.07 g, $3.3 \times 10^{-3}$ mol) to the mixture at –78 °C. The mixture was

stirred at room temperature overnight. The reaction mixture was quenched by adding a solution of $SnCl_2$ (3.70 g, $2.0 \times 10^{-2}$ mol) in 10% HCl (15 mL) and the mixture was stirred for 30 minutes at 60 °C. After completing the reaction, the solution was precipitated into MeOH and the product was collected as an orange solid. (2.45 g, 85%). $^1$H-NMR (250 MHz, *CDCl$_3$*) $\delta_H$/ppm: 8.69 (s, 2H), 8.41 (d, *J* = 9.0 Hz, 2H), 7.67 (d, *J* = 8.5 Hz, 2H), 7.37 (d, *J* = 3.5 Hz, 2H), 6.80 (d, *J* = 3.5 Hz, 2H), 2.90 (t, *J* = 7.5 Hz, 4H), 1.82-1.70 (m, 4H), 1.45-1.23 (m, 36H) 0.89 (t, *J* = 6.5 Hz, 6H). Elemental Analysis (%) Calculated for $C_{50}H_{60}Br_2S_2$: C, 67.86; H, 6.84; Br, 18.05; S, 7.23. Found: C, 67.21; H, 6.63; Br, 19.09; S, 7.37. Mass (MALDI-TOF); (*m/z*) 884 ($M^+$). FT-IR ($cm^{-1}$): 2957-2846 (aliphatic C–H stretch), 2180 (carbon, carbon triple bond stretch), 1544 and 1464 (aromatic C=C stretch), 792 (C–Br stretch), 725 ($CH_2$ bending).

### 2.5.12 Synthesis of 2,6-dibromo-9,10-bis-[2-ethynyl-5-(2-butyl-octyl) thiophen-2-yl]-anthracene (M2): [13, 38]

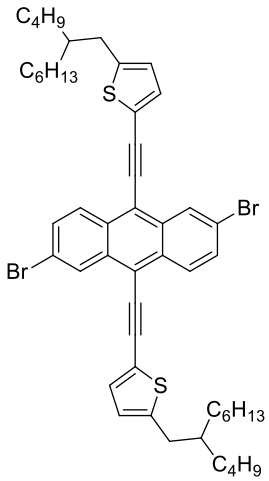


This product was synthesised by the same method described above for 2,6-dibromo-9,10-bis[2-ethynyl-5-dodcylthiophen-2-yl]anthracene **(M1)**. Materials used to prepare the product were; 2-ethynyl-5-(2-bytyl-octyl) thiophene (2.5 g, $9.0 \times 10^{-3}$ mol), n-BuLi (2.5 M in hexane, 3.5 mL, $8.7 \times 10^{-3}$ mol), 2,6-dibromo-9,10-antharaquinone (1.65 g, $4.5 \times 10^{-3}$ mol) and a solution of $SnCl_2$ (3.43 g, $1.8 \times 10^{-2}$ mol) in 10%HCl (15 mL). The product was collected as dark red solid. Yield of 2.3 g (58%). $^1$H-NMR (250 MHz, *CDCl$_3$*) $\delta_H$/ppm: 8.53 (s, 2H), 8.25 (d, *J* = 9.0 Hz, 2H), 7.58 (dd, *J* = 2.5, 9.0 Hz, 2H), 7.34 (d, *J* = 3.5 Hz, 2H), 6.79 (d, *J* = 3.5, 2H), 2.84 (d, *J* = 7.0, 4H), 1.80-1.68 (bm, 2H), 1.44-1.26 (bm, 32H) 0.99-0.90 (bm, 12 H). $^{13}$C-NMR (250 MHz, *CDCl$_3$*): δ

148.43, 132.80, 132.14, 130.53, 130.10, 129.04, 128.80, 125.71, 121.82, 120.30, 117.48, 97.04, 88.86, 40.13, 34.82, 33.28, 32.96, 31.93, 29.68, 28.89, 26.64, 23.06, 22.72, 14.18, 14.16. Elemental Analysis (%) Calculated for $C_{50}H_{60}Br_2S_2$: C, 67.86; H, 6.84; Br, 18.05; S, 7.23. Found: C, 67.06; H, 6.88; Br, 19.42; S, 6.93. Mass (MALDI-TOF); (*m/z*) 884 ($M^+$). FT-IR ($cm^{-1}$): 2958-2847 (aliphatic C–H stretch), 2180 (carbon, carbon triple bond stretch), 1541 and 1461 (aromatic C=C stretch), 785 (C–Br stretch), 720 ($CH_2$ bending).

### 2.5.13 Synthesis of 2,6-dibromo-9,10-di-(3-pentylundec-1-yne)-anthracene (M3): [13, 38]

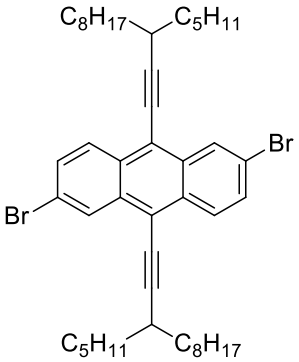


This product was synthesised by the same method described for 2,6-dibromo-9,10-bis[2-ethynyl-5-dodcylthiophen-2-yl]anthracene **M1**. Materials used to prepare the product were; 3-pentylundec-1-yne (7.5 g, $3.4 \times 10^{-2}$ mol), n-BuLi (2.5 M in hexane, 10 mL, $2.5 \times 10^{-2}$ mol), 2,6-dibromo-9,10-antharaquinone (2.75 g, $7.5 \times 10^{-3}$ mol) and a solution of $SnCl_2$ (4.04 g, $1.1 \times 10^{-2}$ mol) in 10%HCl (15 mL). The product was purified *via* silica gel column chromatography using petroleum ether as an eluent. Yield 2.10 g, (36%). $^1$H-NMR (400 MHz, *CDCl$_3$*) $\delta_H$/ppm: 8.72 (d, *J*= 2.0, 2H), 8.41 (d, *J* = 9.0 Hz, 2H), 7.62 (dd, *J* = 2.0, 9.0 Hz, 2H), 2.89 (m, 2H), 1.82-1.60 (bm, 14H), 1.52-1.25 (bm, 30H) 0.97 (t, *J* = 7.0 Hz, 6H) 0.89 (t, *J* = 7.0, 6H). $^{13}$C-NMR (400 MHz, *CDCl$_3$*): δ 132.95, 130.77, 130.26, 129.40, 129.14, 121.41, 118.20, 108.16, 77.68, 35.39, 35.34, 33.40, 31.95, 31.84, 29.69, 29.38, 27.92, 27.58, 22.75, 22.72, 14.16. Elemental Analysis (%) Calculated for $C_{46}H_{64}Br_2$: C, 71.12; H, 8.29; Br, 20.57. Found: C, 70.45; H, 8.18; Br, 21.89. Mass (MALDI-TOF); (*m/z*) 776 ($M^+$). FT-IR ($cm^{-1}$): 2957-2846 (aliphatic C–H stretch), 2180 (carbon, carbon triple bond stretch), 1605 and 1464 (aromatic C=C stretch), 800 (C–Br stretch), 725 ($CH_2$ bending).

### 2.5.14 Poly[9,10-bis[2-ethynyl-5-dodcylthiophene]-anthracene-2,6-diyl-alt-4,7-di (thiophene-2-yl)benzo[c][1,2,5]thiadiazole] (PATA(D)TBT): [39]

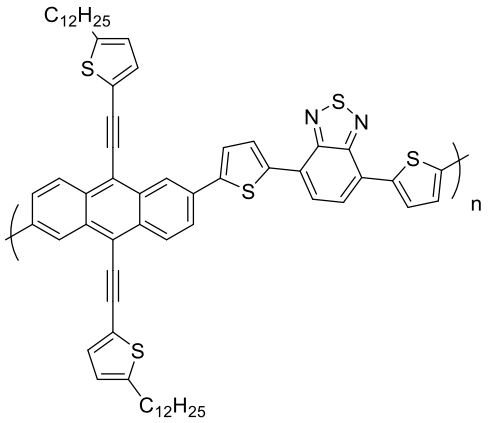


An oven-dry sealed tube was charged with dibromo-9,10-bis[2-ethynyl-5-dodcylthiophene]anthracene (0.124 g, 0.14 × $10^{-3}$ mol), 4,7-di-2-thienyl-2,1,3-benzothiadiazole (0.079 g, 0.14 × $10^{-3}$ mol), (*o*-OMePh)$_3$P (0.0025 g, 0.0112 × $10^{-3}$ mol) and Pd(OAc)$_2$ (0.0026 g, 0.0028 × $10^{-3}$ mol), pivalic acid (0.014 g, 0.14 × $10^{-3}$ mol) and $Cs_2CO_3$ (0.14 g, 0.420× $10^{-3}$ mol). The tube was subjected to several cycles of vacuum followed by refilling with argon. Then, dry toluene (1.0 mL) was added and the mixture was degassed again. The polymerization was carried out at 100 °C for 2 hours under argon protection. The reaction was cooled to room temperature, diluted with 300 mL of chloroform followed by addition of ammonia to remove residual catalyst before precipitating the reaction contents into methanol. The raw product was collected by filtration and purified using Soxhlet extraction with solvents in the order; methanol (250 mL), acetone (250 mL), hexane (250 mL), toluene (250 mL), chloroform (250 mL). The toluene fraction was concentrated (≈ 50 mL) and then poured into methanol (500 mL). The resulting mixture was stirred overnight and the solid was collected by filtration through a membrane filter to yield a dark purple powder (32 mg, 22%).

GPC (TCB): $M_w$ = 4000, $M_n$ = 3600, PD = 1.1. $^1$H-NMR ($C_2D_2Cl_4$): ($\delta_H$/ppm): signals were not clear due to low solubility. Elemental Analysis (%) calculated for $C_{64}H_{68}N_2S_5$: C, 74.95; H, 6.68; N, 2.72; S, 15.63. Found: C, 82.36; H, 13.44; N and S, sample was not enough to detect them. FT-IR ($cm^{-1}$): 3070-3045 (aromatic C–H stretch), 2951-

2849 (aliphatic C–H stretch), 2114 (carbon, carbon triple bond stretch), 1531 and 1484 (aromatic C=C stretch). 1462 (C–H bending aliphatic).

### 2.5.15 Poly[9,10-bis[2-(ethynyl-5-butyl-octyl)thiophene]-anthracene-2,6-diyl-alt-4,7-di(thiophene-2-yl)benzo[c][1,2,5]thiadiazole] (PATA(BO)TBT): [39]

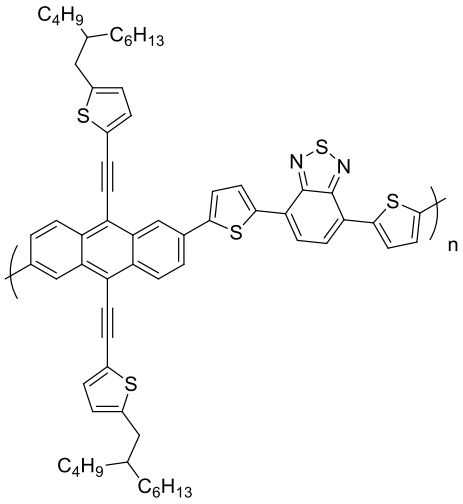


The procedure for preparation of (**PATA(D)TBT**) was followed to prepare (**PATA(BO)TBT**) from **M2** (0.124 g, 0.14 × $10^{-3}$ mol) and **M4** (0.079 g, 0.14 × $10^{-3}$ mol)**.** The polymer was collected from toluene fraction as dark purple solid. Yield 33 mg (23%). GPC (TCB): $M_w$ = 3200, $M_n$ = 2100, PD = 1.56. $^1$HNMR ($C_2D_2Cl_4$): ($\delta_H$/ppm); 8.79 (d, *J* = 1.5 Hz, 2H); 8.53 (d, *J* = 9.0 Hz, 2H); 8.13 (d, *J* = 4.0 Hz, 2H); 7.90 (bm, *J* = 9.0, 2.0 Hz, 2H); 7.59 (d, *J* = 4.0 Hz, 2H); 7.43 (t, *J* = 4.0 Hz, 2H); 7.17 (dd, *J* = 5.0, 1.5 Hz, 2H); 6.84 (d, *J* = 3.5 Hz, 2H); 2.87 (d, *J* = 6.5 Hz, 4H); 1.79-1.73 (m, 2H); 1.45-1.28 (bm, 32H); 0.95-0.86 (bm, 12H). Elemental Analysis (%) calculated for $C_{64}H_{66}N_2S_5$: C, 75.10; H, 6.50; N, 2.73; S, 15.66. Found: C, 69.67; H, 5.71; N, 3.78; S, 17.90. FT-IR ($cm^{-1}$): 3073-3051 (aromatic C–H stretch), 2951-2852 (aliphatic C–H stretch), 2182 (carbon, carbon triple bond stretch), 1615-1484 (aromatic C=C stretch). 1462 (C–H bending aliphatic).

### 2.5.16 Poly[9,10-di-(3-pentylundec-1-yne)-anthracene-2,6diyl-alt-4,7-di (thiophene-2-yl)benzo[c][1,2,5]thiadiazole](PAA(PU)TBT): [39]

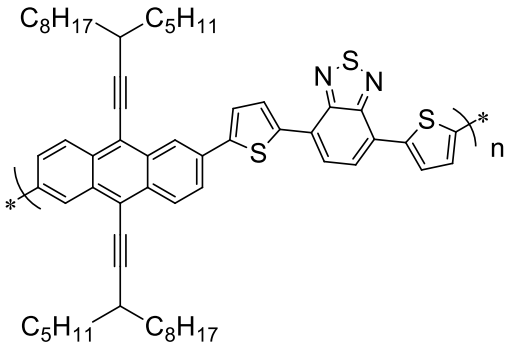


The procedure for the synthesis of (**PATA(D)TBT**) was followed to synthesis (**PAA(PU)TBT**) from **M3** (0.11 g, $0.14 \times 10^{-3}$ mol) and **M4** (0.079 g, $0.14 \times 10^{-3}$ mol)**.** The polymer was collected from chloroform fraction as dark purple solid. Yield 55 mg (43%). GPC (TCB): $M_w$ = 3300, $M_n$ = 2200, PD = 1.52. $^1$HNMR ($C_2D_2Cl_4$): ($\delta_H$/ppm); 8.89 (d, *J* = 1.5 Hz, 2H); 8.59 (d, *J* = 9.0 Hz, 2H); 8.19 (d, *J* = 4.0 Hz, 2H); 7.89 (bm, 2H); 7.61 (d, *J* = 4.0 Hz, 2H); 7.22 (dd, *J* = 5.0, 3.5 Hz, 2H); 3.03-2.88 (bm, 2H); 1. 93-1.18 (bm, 46H); 0.99-0.78 (bm, 12H). Elemental Analysis (%) calculated for $C_{60}H_{70}N_2S_3$: C, 78.73; H, 7.71; N, 3.06; S, 10.50. Found: C, 73.83; H, 6.93; N, 3.57; S, 12.28. FT-IR ($cm^{-1}$): 3048 (aromatic C–H stretch), 2954-2849 (aliphatic C–H stretch), 2107 (carbon, carbon triple bond stretch), 1615-1488 (aromatic C=C stretch). 1465 (C–H bending aliphatic).

## 2.6 References


1. H. Choi, H. M. Ko, N. Cho, K. Song, J. K. Lee and J. Ko, *ChemSusChem*, 2012, **5**, 2045-2052.
2. Y. Sun, B. Lin, H. Yang and X. Gong, *Polymer*, 2012, **53**, 1535-1542.
3. C. Liu, W. Cai, X. Guan, C. Duan, Q. Xue, L. Ying, F. Huang and Y. Cao, *Polym. Chem.*, 2013, **4**, 3949-3958.
4. A. Cardone, C. Martinelli, M. Losurdo, E. Dilonardo, G. Bruno, G. Scavia, S. Destri, P. Cosma, L. Salamandra and A. Reale, *J. Mater. Chem. A*, 2013, **1**, 715-727.
5. L. Bian, E. Zhu, J. Tang, W. Tang and F. Zhang, *Prog. Polym. Sci.*, 2012, **37**, 1292-1331.
6. P. Sista, B. Xue, M. Wilson, N. Holmes, R. S. Kularatne, H. Nguyen, P. C. Dastoor, W. Belcher, K. Poole and B. G. Janesko, *Macromolecules*, 2012, **45**, 772-780.
7. D. SungáChung, D. HoonáLee, N. SungáCho and C. EonáPark, *Chem. Commun.*, 2010, **46**, 1863-1865.
8. P. Ding, C. C. Chu, Y. Zou, D. Xiao, C. Pan and C. S. Hsu, *J. App. Polym. Sci.*, 2012, **123**, 99-107.
9. L. Dou, C.-C. Chen, K. Yoshimura, K. Ohya, W.-H. Chang, J. Gao, Y. Liu, E. Richard and Y. Yang, *Macromolecules*, 2013, **46**, 3384-3390.
10. C. Liu, W. Xu, X. Guan, H.-L. Yip, X. Gong, F. Huang and Y. Cao, *Macromolecules*, 2014.
11. D. A. Egbe, S. Turk, S. Rathgeber, F. Kuhnlenz, R. Jadhav, A. Wild, E. Birckner, G. Adam, A. Pivrikas and V. Cimrova, *Macromolecules*, 2010, **43**, 1261-1269.
12. J. B. Lee, K. H. Kim, C. S. Hong and D. H. Choi, *J. Polym. Sci. Part A: Polym. Chem.*, 2012, **50**, 2809-2818.
13. W. Cui, Y. Zhao, H. Tian, Z. Xie, Y. Geng and F. Wang, *Macromolecules*, 2009, **42**, 8021-8027.
14. J. Sun, J. Chen, J. Zou, S. Ren, H. Zhong, D. Zeng, J. Du, E. Xu and Q. Fang, *Polymer*, 2008, **49**, 2282-2287.
15. A. Abdulaziz, *Chem. Commun.*, 2013, **49**, 2252-2254.

16. J. Y. Ma, H. J. Yun, S. O. Kim, G. B. Lee, H. Cha, C. E. Park, S. K. Kwon and Y. H. Kim, *Journal of Polymer Science Part A: Polym. Chem.*, 2014, **52**, 1306-1314.
17. J. W. Jung and W. H. Jo, *Polym. Chem.*, 2015, **6**, 4013-4019.
18. J. W. Jung, F. Liu, T. P. Russell and W. H. Jo, *Adv. Energ. Mater.*, 2015.
19. H. Medlej, H. Awada, M. Abbas, G. Wantz, A. Bousquet, E. Grelet, K. Hariri, T. Hamieh, R. C. Hiorns and C. Dagron-Lartigau, *Euro. Polym. J.*, 2013, **49**, 4176-4188.
20. B. Fu, J. Baltazar, Z. Hu, A.-T. Chien, S. Kumar, C. L. Henderson, D. M. Collard and E. Reichmanis, *Chem. of Mater.*, 2012, **24**, 4123-4133.
21. M. P. Doyle, B. Siegfried and J. F. Dellaria Jr, *J. Org. Chem.*, 1977, **42**, 2426-2431.
22. C. Pramanik and G. P. Miller, *Molecules*, 2012, **17**, 4625-4633.
23. C. Liu, W. Xu, X. Guan, H.-L. Yip, X. Gong, F. Huang and Y. Cao, *Macromolecules*, 2014, **47**, 8585-8593.
24. R. Qin, W. Li, C. Li, C. Du, C. Veit, H.-F. Schleiermacher, M. Andersson, Z. Bo, Z. Liu and O. Inganas, *J. Am. Chem. Soc.*, 2009, **131**, 14612-14613.
25. L. Ye, S. Zhang, L. Huo, M. Zhang and J. Hou, *Acc. Chem. Res.*, 2014, **47**, 1595-1603.
26. K. Haubner, E. Jaehne, H. J. Adler, D. Koehler, C. Loppacher, L. Eng, J. Grenzer, A. Herasimovich and S. Scheinert, *Phys. Status Solidi (a)*, 2008, **205**, 430-439.
27. P. Deng, L. Liu, S. Ren, H. Li and Q. Zhang, *Chem. Commun.*, 2012, **48**, 6960-6962.
28. L. Cartwright, L. J. Taylor, H. Yi, A. Iraqi, Y. Zhang, N. W. Scarratt, T. Wang and D. G. Lidzey, *RSC Advances*, 2015, **5**, 101607-101615.
29. B. G. Kim, X. Ma, C. Chen, Y. Ie, E. W. Coir, H. Hashemi, Y. Aso, P. F. Green, J. Kieffer and J. Kim, *Adv. Funct. Mater.*, 2013, **23**, 439-445.
30. C. Kang, J. Zhang, H. Dong, W. Hu and Z. Bo, *J. Mater. Chem. C*, 2015, **3**, 12083-12089.
31. L. Cartwright, A. Iraqi, Y. Zhang, T. Wang and D. G. Lidzey, *RSC Advances*, 2015, **5**, 46386-46394.
32. H. Hoppe and N. S. Sariciftci, *J. Mater. Res.*, 2004, **19**, 1924-1945.

33. G. Gritzner, *Pure App. Chem.*, 1990, **62**, 1839-1858.
34. L. Cartwright, H. Yi and A. Iraqi, *New J. Chem.*, 2016, **40**, 1655-1662.
35. M. Kirkus, S. Knippenberg, D. Beljonne, J. r. m. Cornil, R. A. Janssen and S. C. Meskers, *J. Phys. Chem. A*, 2013, **117**, 2782-2789.
36. B. Shaik, J. H. Park, T. K. An, Y. R. Noh, S. B. Yoon, C. E. Park, Y. J. Yoon, Y.-H. Kim and S.-G. Lee, *Tetrahedron*, 2013, **69**, 8191-8198.
37. Z. Li, J. Lu, S.-C. Tse, J. Zhou, X. Du, Y. Tao and J. Ding, *J. Mater. Chem.*, 2011, **21**, 3226-3233.
38. S. Jo, J. Shin, S. Y. Bae, K. H. Kim, T. W. Lee, S. Son, K. Kim and D. H. Choi, *Synth. Met.*, 2011, **161**, 833-843.
39. P.-O. Morin, T. Bura, B. Sun, S. I. Gorelsky, Y. Li and M. Leclerc, *ACS Macro Lett.*, 2014, **4**, 21-24.

# Chapter 3

***New Series of Medium Band Gap Conjugated Polymers Derived From 2,6-Linked Anthracene and 5,6-Bis(octyloxy)-4,7-di (thiophene-2-yl)benzothiadiazole: Preparation and OPV Applications***

# Chapter 3

## 3.1 Introduction

In the last few decades, bulk heterojunction (BHJ) organic solar cells made from conjugated polymers as p-type materials blended with n-type materials commonly fullerene derivatives have displayed reasonable power conversion efficiencies (PCEs) and attracted much attention of the scientific community. This interest in organic photovoltaics is due to their advantages such as light weight, low cost and flexibility when compared to silicon-based photovoltaics [1-3].

However, the PCEs of polymer solar cells (PSCs) are believed to be influenced by the photoactive layer of the PSCs. Fullerene derivatives are used widely for BHJ organic solar cells and can be considered as near ideal n-type materials [4]. Therefore, most research groups tend to focus attention on designing and developing efficient p-type materials for organic photovoltaic (OPV) applications. The most important criteria that should be taken in account when these photoactive materials are designed and synthesised are related to how narrow is their optical band gap, how high are their hole mobilities and absorption coefficients, and the positions of their energy levels [4]. Up to date, the most effective approach for controlling these criteria in a polymer is the use of the donor-acceptor (D–A) polymer framework [5].

The electron rich units in an alternating donor-acceptor conjugated polymer should be relatively weak electron donors to ensure a low-lying HOMO levels of the resulting polymer. This is crucial for achieving high open circuit voltages as well as stability to oxidation in air. Charge transport of the polymer is also an important factor and could be enhanced if there is a close π-π stacking between polymer backbones which can be attained through molecular rigidity and planarity [6]. During the last few years, 2,6-linked anthracene derivatives units were used as electron donating moieties for the design and synthesis of medium band gap polymers [4, 6-9]. Incorporating fused heteroarenes such as anthracene in the polymer backbone is thought to induce a strong π-π stacking affording good crystallinity to the polymer leading to a reduction in the energy needed for charge carrier transport. In addition, because of the weak electron-donating ability

of anthracene compared to other heteroarenes, anthracene based conjugated polymers are assumed to have a low-lying HOMO energy levels. Therefore, a combination of benzothiadiazole (BT) derivatives and anthracene moieties could lead to high $V_{oc}$ and $J_{sc}$ [10].

Recently, as discussed in chapter 2, we have synthesised three polymers containing alternating 2,6-linked anthracene derivatives and BT units which offered materials with low band gaps and low-laying HOMO energy levels. However, using BT units without solubilizing groups led to polymers with limited solubility and low processability. To overcome this problem, we have decided to use benzothiadiazole with two lateral octyloxy substituents on the 5,6- positions. Side chains incorporated to the polymer backbone play an important role in enhancing the solubility of the polymer in common organic solvents which is important for device fabrication. These types of electron donating side chains could utilize intermolecular interactions through S(thienyl)–O–(alkoxy) leading to coplanar conjugated polymers [11]. However, some drawbacks of using these alkoxy groups could also be expected which could affect the overall performance of the prepared polymers. Du *et al* found that, the use of dioctyloxy substituted BT unit is a weaker electron acceptor when compared to the non-substituted BT unit. This in turn affects the optical band gap and LUMO energy level position of the polymer [12]. It was also found that when the alkoxy groups are bulkier than methoxy units, the π-π stacking can be disrupted **[11]**.

During the course of this work, Jung *et al* reported a copolymer **PTADTBTO** based on 2,6-linked anthracene units flanked by thienyl donor units and BT with octyloxy substituents as acceptor moieties (**Figure 3-1**) [13]. **PTADTBTO** exhibited a high optical band gap of 2.10 eV and a high-lying LUMO energy level due to the reduced electron accepting properties of dioctyloxy-substituted BT because of the existence of strong electron donating alkoxy groups. In addition, the X-ray diffraction indicates that, these long alkoxy groups may cause steric hindrance which affect the crystallinity of the polymer.

Iraqi and co-workers synthesised a polymer using 2,6-linked anthracene flanked by thienyl as donor moieties and benzothiadiazole units substituted with octyloxy groups **PPATBT-8** [6] as shown in **Figure 3-1**. The polymer showed a high band gap of 1.96 eV

as well as high-lying LUMO energy level compare to its counterpart **PPATBT**. However, polymer **PPATBT-8** provided device with a better efficiency of 3.92% compare to that made **PPATBT**.

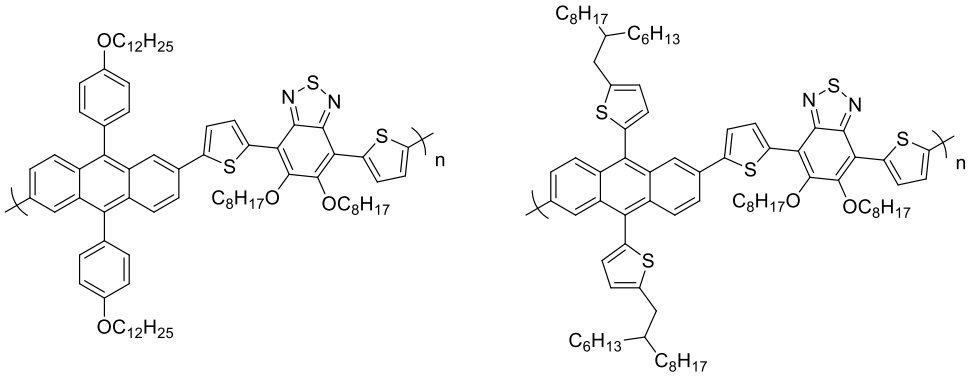


**PPATBT-8** **PTADTBTO**

**Figure 3-1:** The chemical structures of the copolymers **PPATBT-8** and **PTADTBTO.**

In order to address this point, a series of donor-acceptor conjugated polymers based on 2,6-linked anthracene derivatives with various substituents such as 2-ethynyl-5-dodecylthiophene, 2-ethynyl-5-(2-butyl-octyl)-thiophene and 3-pentylundec-1-yne appended through the 9,10-positions of the anthracene, and dioctyloxy-substituted benzo[c][1,2,5]thiadiazole (BT) flanked with thienyl groups as the acceptor moiety were prepared in this project (**Figure 3-2**). The optical, electrochemical and photovoltaic properties of these polymers in blends with [6,6]-phenyl $C_{71}$-butyric acid methyl ester ($PC_{71}BM$) were studied and are discussed along with their preparation in this chapter.

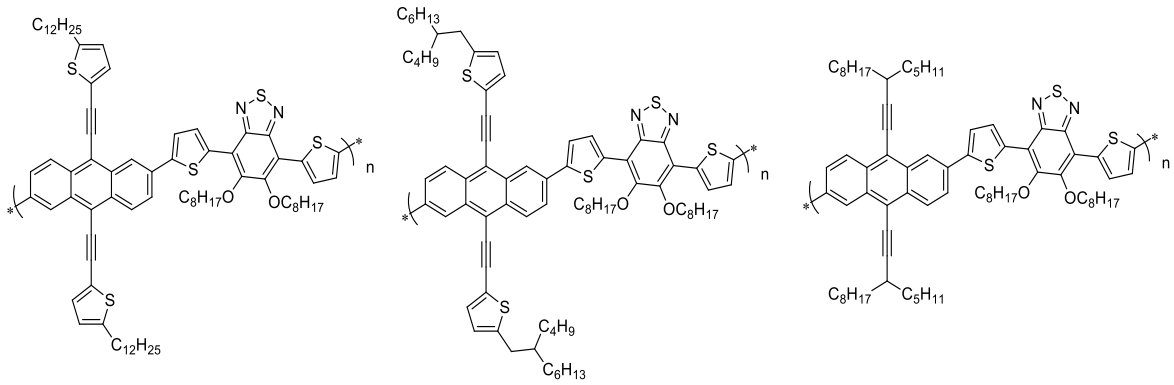


**Figure 3-2:** Structures of **PATA(D)TBT-8**, **PATA(BO)TBT-8**, and **PAA(PU)TBT-8**.

## 3.2 Results and Discussion

### 3.2.1 Synthesis of the Monomers

The synthetic route of 4,7-bis-(5-trimethylstannylthiophen-2-yl)-5,6-bis(octyloxy) benzo-[c][1,2,5]-thiadiazole **M5** which is a key monomer for all polymers targeted in this study, is displayed in **Scheme 3-1**. The preparation of 2,6-linked anthracene monomers, **M1**, **M2**, and **M3**, also required in the preparation of the target polymers, were discussed already in chapter 2.

The preparation of monomers **10-16** was carried out by following modified procedures by Ding and co-workers [14]. The final monomers 4,7-bis[(5-trimethylstannyl)thiophene-yl]-5,6-bis(octyloxy)benzo[c][1,2,5]thiadiazole **M5** was synthesised according to a modified procedure by Saadeh *et al* [15].

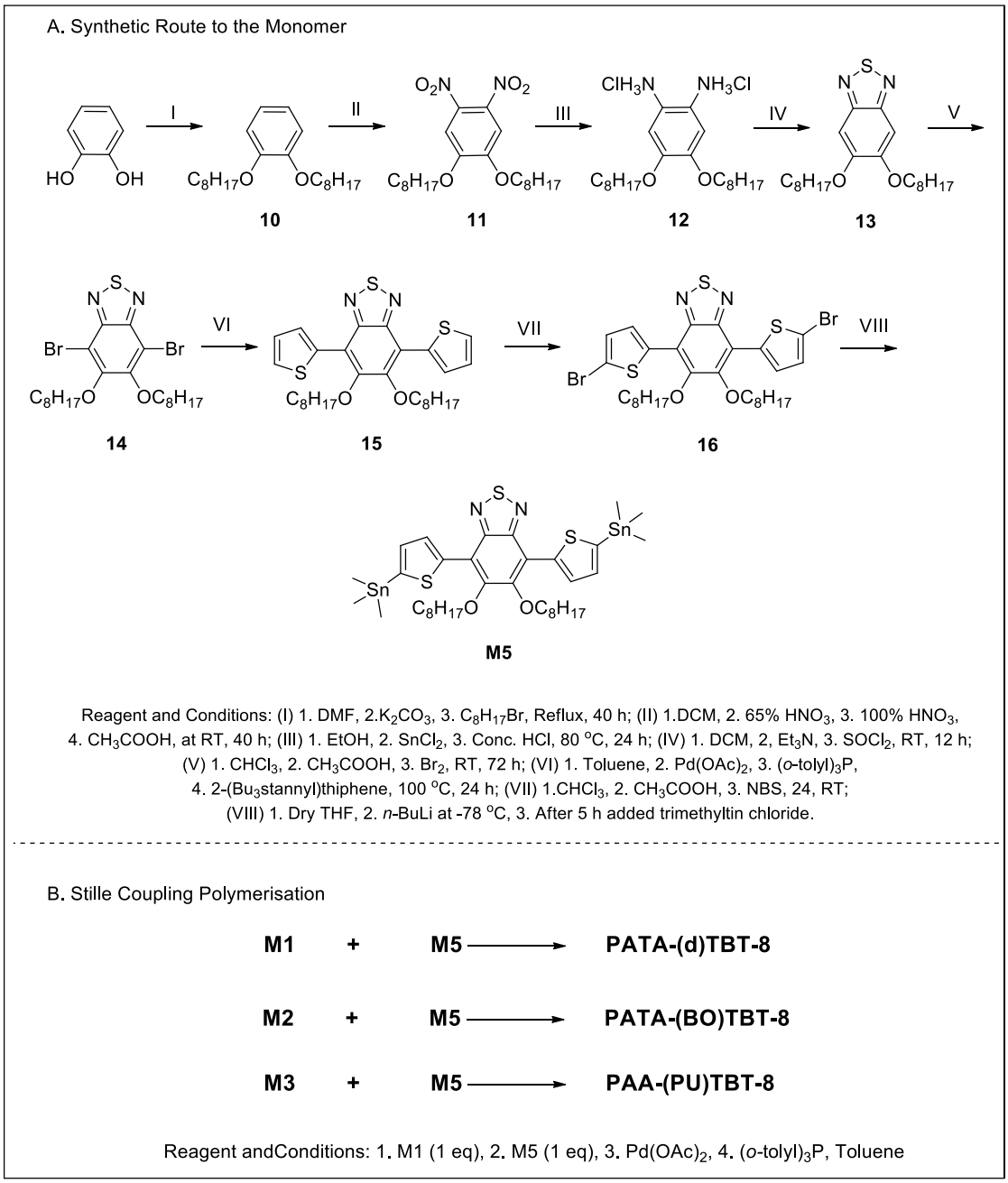


**Scheme 3-1:** A. Synthetic route to the final monomer **M5** and (B). Synthesis of the polymers *via* Stille coupling polymerisation.

1,2-Bis(octyloxy)benzene was prepared by using $K_2CO_3$ to deprotonate the two hydroxyl groups of 1,2-dihydroxybenzene. The resulting alkoxide groups attacked 1-bromooctane to afford the product **10** (**Scheme 3-2**).

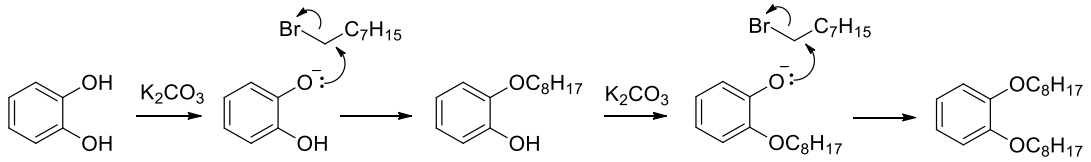


**Scheme 3-2:** The mechanism of preparation compound **10** *via* nucleophillic substitution.

Synthesis of 1,2-dinitro-4,5-bis(octyloxy)benzene (**11**) was performed in the presence of nitric acid 65 %, fuming nitric acid and acetic acid. The mixture was stirred at room temperature for 40 hours. The first step in the reaction involves the formation of a strong electrophile (a nitronium ion $NO_2^+$) by the reaction of acetic acid and nitric acid which releases water. Then the rest of the reaction proceeds *via* electrophilic aromatic substitution mechanism as outlined in **Scheme 3-3**.

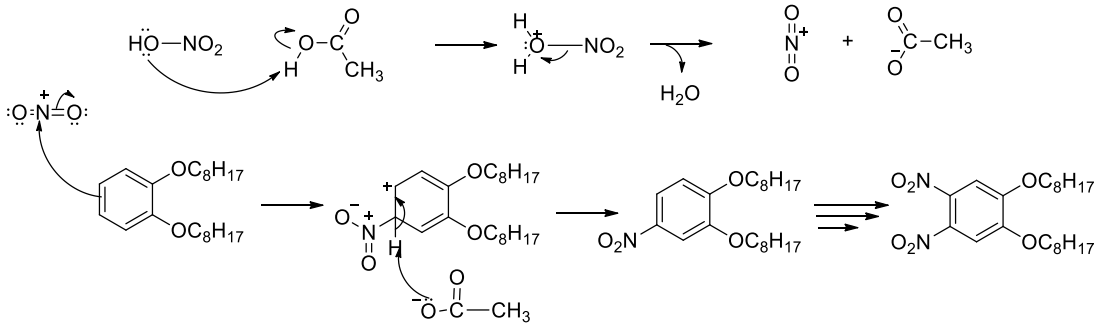


**Scheme 3-3:** Nitration reaction mechanism.

Reduction of the nitro groups in 1,2-dinitro-4,5-bis(octyloxy)benzene was performed using $SnCl_2$ in the presence of concentrated HCl leading to form the product (**12**) as diammonium chloride salt which was used immediately due to its unstable nature.

Ring-closure was carried out for compound (**12**) using thionyl chloride in the presence of triethylamine to afford 5,6-bis(octyloxy)benzo[c][1,2,5]thiadiazole (**13**). Triethylamine was used to remove the hydrogen chloride from 4,5-bis(octyloxy)benzene-1,2-diammonium chloride as triethylamine hydrochloride salt.

After that, the nucleophillic amine groups attack the sulphur in thionyl chloride initiating the ring-closure leading to the desired product as stated in the **Scheme 3-4**.

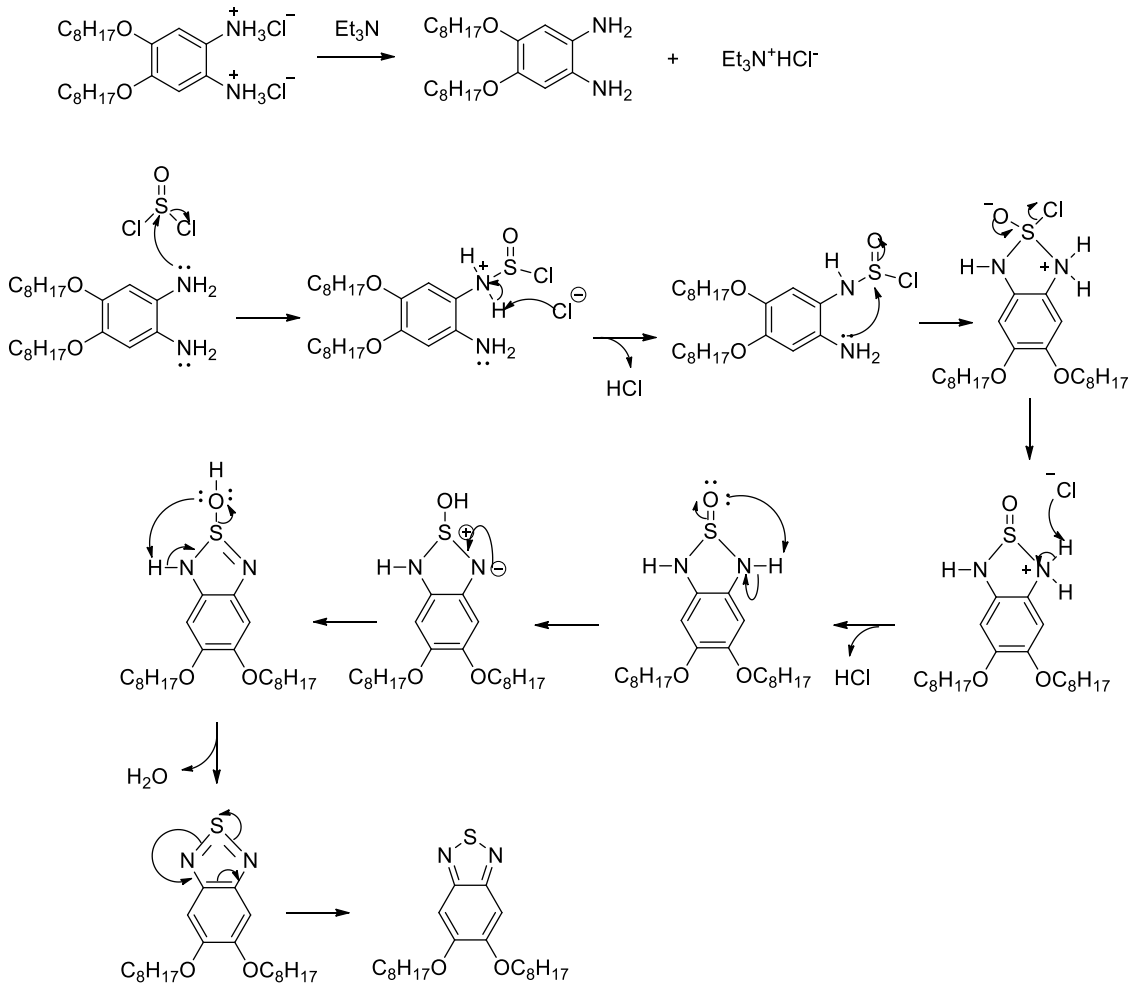

**Scheme 3-4:** The reaction mechanism for the synthesis of compound (**13**)

Starting from compound (**13**), 4,7-dibromo-5,6-bis(octyloxy)benzo[c][1,2,5]thiadiazole (**14**) was prepared by bromination of 5,6-bis(octyloxy)benzo[c][1,2,5]thiadiazole using bromine in acetic acid/chloroform mixture. The reaction was performed at room temperature for 72 hours. The reaction mechanism involved electrophilic aromatic substitution as shown in **Scheme 3-5**.

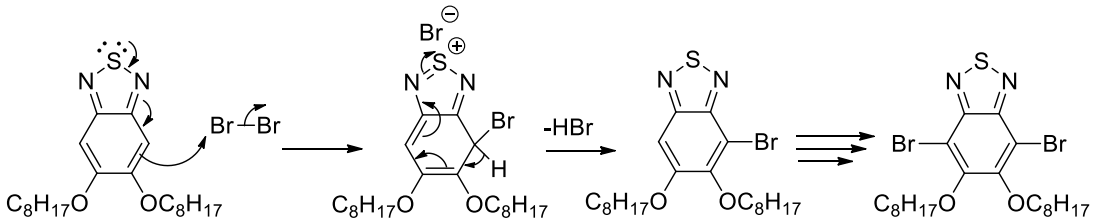


**Scheme 3-5:** The mechanism of bromination 5,6-bis(octyloxy)benzo[c][1,2,5]thiadiazole.

Stille coupling reaction was used to synthesise 5,6-bis(octyloxy)-4,7-di(thiophene-2-yl)benzo[c][1,2,5]thiadiazole (**15**). One equivalent of compound (**14**) was reacted with two equivalents of 2-(tributylstannyl)thiophene using the catalyst system consisting of tris(dibenzylideneacetone) dipalladium (0) ($Pd_2dba_3$) and tri-o-tolylphosphine ($(o\text{-tolyl})_3P$. The mechanism of Stille coupling reaction has been discussed in chapter 1 in detail.

Bromination of compound (**15**) was carried out in a mixture of acetic acid/chloroform using two equivalents of *N*-bromosuccinimide. The resulting product, 4,7-bis(5-dibromothiophen-2-yl)-5,6-(octyloxy)benzo[c][1,2,5]thiadiazole (**16**), was then reacted with *n*-BuLi (3 eq.) in dry THF under inert atmosphere of nitrogen at -78 °C for 2 hours. The reaction mixture was then quenched by the addition of trimethyltin chloride (2.5 eq.) to afford the final monomer **M5**. The mechanism of the reaction proceeds through two steps. In the beginning, the metal-halogen interchange occurred through nucleophillic attack of the *n*-BuLi on the bromine of compound **(16)** [16]. Then, the mechanism of the second part of the reaction will involve a nucleophilic substitution by attack on the tin in trimethyltin chloride as described in **Scheme 3-6**.

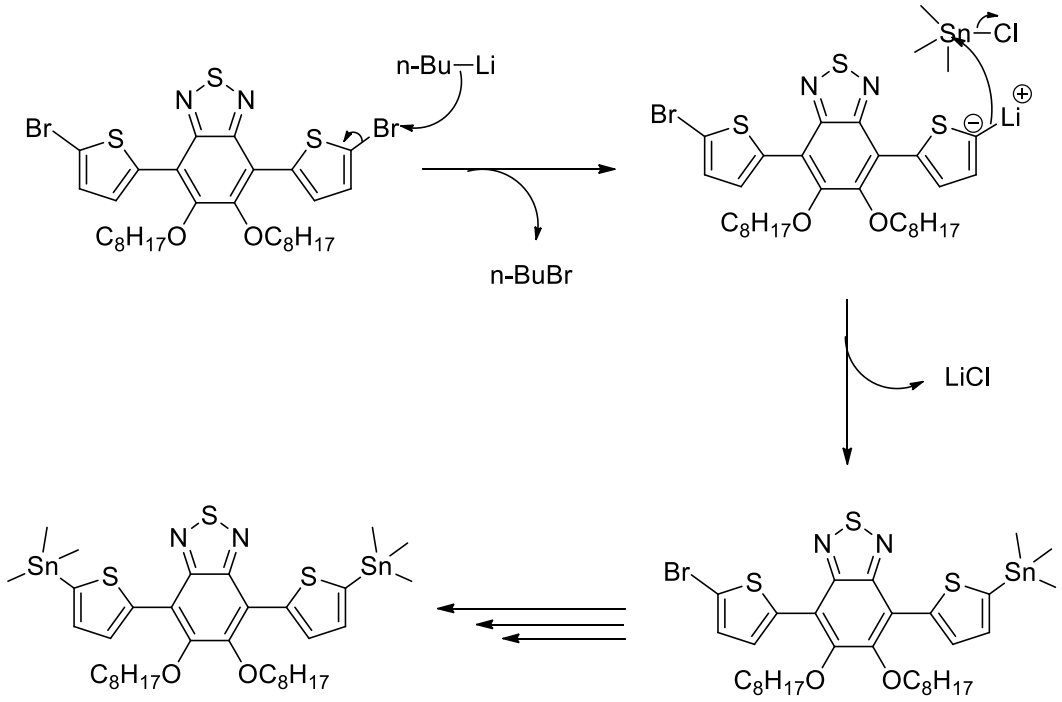


**Scheme 3-6:** Proposed mechanism reaction of compound **M5**.

### 3.2.2 Polymers Synthesis

**PATA(D)TBT-8**, **PATA(BO)TBT-8**, and **PAA(PU)TBT-8** were synthesised by Stille coupling polymerisation between the corresponding monomers using $Pd(OAc)_2$ and $(o\text{-tolyl})_3P$ as a catalyst system (**Scheme 3-1**). The polymers were purified by Soxhlet extraction with methanol, acetone, hexane and toluene. **PATA(D)TBT-8** and **PATA(BO)TBT-8** were isolated form their toluene fractions with yields of 37% and 39% respectively. Whereas, the hexane fraction contained most of polymer **PAA(PU)TBT-8** upon Soxhlet extraction with 95 mg representing a 42 % yield. The enhancement in the solubility of these polymers versus their counterpart polymers **PATA(D)TBT**, **PATA(BO)TBT** and **PAA(PU)TBT** was apparent as they were extracted in the toluene or hexane fractions.

The average molecular weights ($M_n$) of the three polymers are represented in **Table 3-1** which are obtained by gel permeation chromatography (GPC) in TCB at high temperature relative to polystyrene standards (**Figure 3-3**). As expected, introduction of octyloxy substituents on the BT units has indeed improved the solubility of the resulting polymers in comparison to their counterparts polymers without solubilizing

groups on the BT units. **PATA(D)TBT-8** and **PATA(BO)TBT-8** exhibit improvement in their molar mass with $M_n$ of 8200 and 9900 Da respectively, compared to their equivalent polymers **PATA(D)TBT** and **PATA(BO)TBT**. However, **PAA(PU)TBT-8** shows a low $M_n$ of 3200 Da relative to **PATA(D)TBT-8** and **PATA(BO)TBT-8**, which may be attributed to steric hindrance resulted from the bulky substituents on the anthracene units and the alkoxy groups on the BT that impede polymer chain growth. All polymers in this work were soluble enough to be fabricated into photovoltaic devices.

**Table 3-1:** GPC data and TGA data of the polymers.

| Polymer | Yield (%) | $M_n$ (Da)[a] | $M_w$ (Da)[a] | PD[b] | DP[c] | Td (°C) |
|---|---|---|---|---|---|---|
| PATA(D)TBT-8 | 37 | 8100 | 18800 | 2.3 | 6 | 335 |
| PATA(BO)TBT-8 | 39 | 9900 | 19100 | 1.9 | 8 | 347 |
| PAA(PU)TBT-8 | 42 | 3200 | 6400 | 2.8 | 3 | 352 |

[a] Measurements conducted on the polymers using a differential refractive index (DRI) detection method. [b] Polydispersity index. [c] Degree of polymerisation.

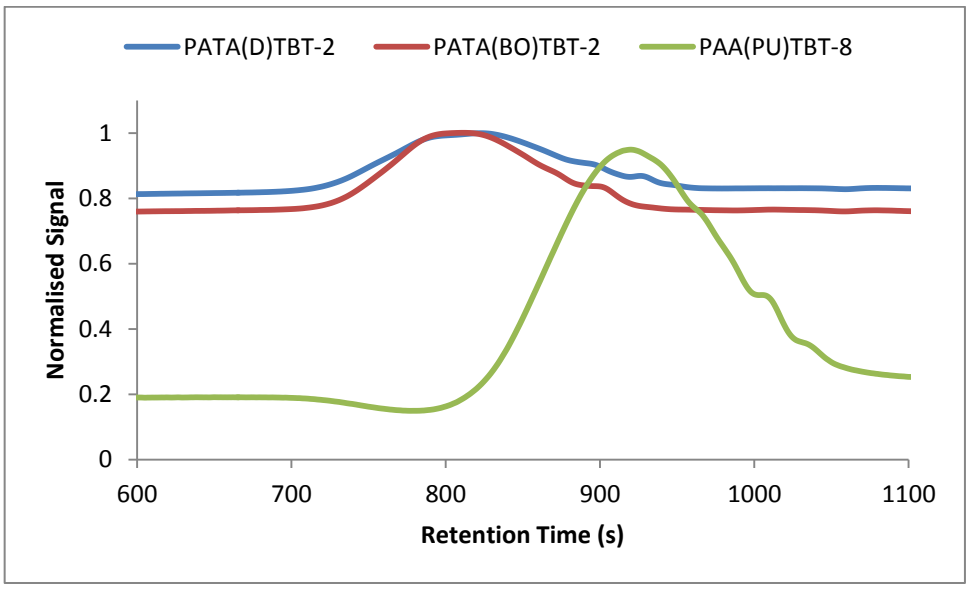


**Figure 3-3:** The GPC traces by RI detector of **PATA(D)TBT-2**, **PATA(BO)TBT-2** and **PAA(PU)TBT-2.**

### 3.2.3 Thermal Analysis

The thermal stability of the synthesised polymers **PATA(D)TBT-8**, **PATA(BO)TBT-8** and **PAA(PU)TBT-8** was evaluated with thermogravimetric analysis TGA under a nitrogen atmosphere as shown in **Figure 3-4**. The TGA thermograms show that the three polymers undergo thermal degradation with the 5% weight loss beginning at 335 °C for **PATA(D)TBT-8**, 347 °C for **PATA(BO)TBT-8** and 320 °C for **PAA(PU)TBT-8**. The degradation temperatures of these polymers are lower than their corresponding polymers **PATA(D)TBT**, **PATA(BO)TBT** and **PAA(PU)TBT** mainly because of the removal of the octyloxy groups. These TGA results indicate that these polymers are nevertheless, thermally stable enough to be applied in PSCs applications.

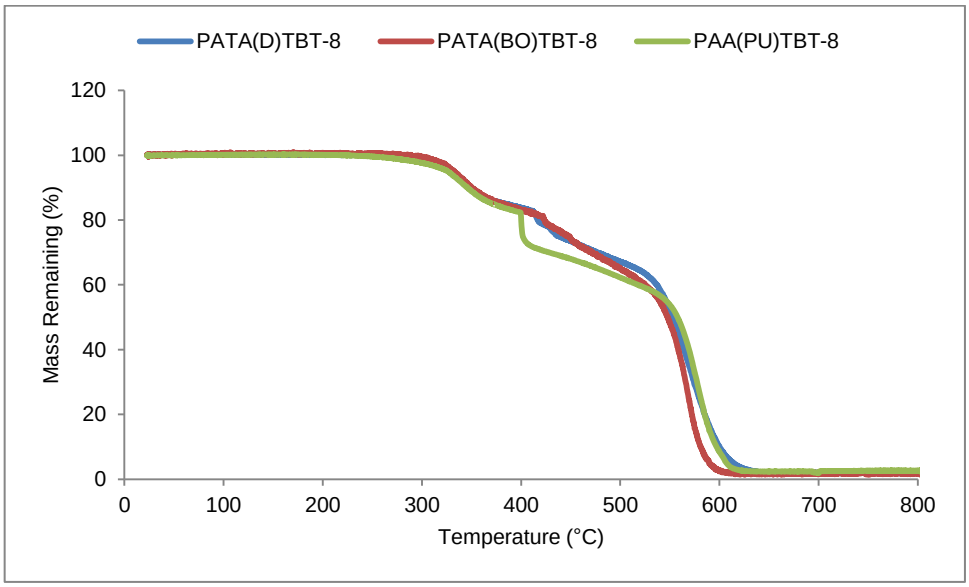


**Figure 3-4:** TGA plots of **PATA(D)TBT-8**, **PATA(BO)TBT-8** and **PAA(PU)TBT-8**.

### 3.2.4 Optical Properties

The UV-Vis absorption spectra of polymers **PATA(D)TBT-8**, **PATA(BO)TBT-8** and **PAA(PU)TBT-8** in chloroform solutions and thin films are displayed in **Figure 3-5**, and all the data are summarised in **Table 3-2**. The three polymers reveal multi-absorption bands; the bands in the lower wavelength region are ascribed to the π-π* transitions of the polymer backbone. While, the bands in the higher wavelength region between 450 and 600 nm are due to intramolecular charge transfer interactions (ICT) between dithienyl anthracene electron donors and benzothiadiazole acceptors.

Importantly, the ICT absorption in polymer **PATA(D)TBT-8** has similar intensity to its π-π* band, in comparison with the other two polymers which have ICT bands with lower intensities than their π-π* bands. This is suggesting that **PATA(D)TBT-8** has a more planer structure than the other two polymer counterparts because the magnitude of ICT mainly rely on the planarity of the polymer backbone [17].

**Table 3-2:** UV-Vis data and optical band gaps of the polymers **PATA(D)TBT-8**, **PATA(BO)TBT-8** and **PAA(PU)TBT-8**.

| Polymer | $\lambda_{max}$ Solution (nm) | $\varepsilon^{a}$ ($M^{-1}$ $cm^{-1}$) | $\lambda_{max}$ film (nm) | $E_g^{opt}$ film (eV)[b] |
|---|---|---|---|---|
| PATA(D)TBT-8 | 331, 474 | $5.23 \times 10^{+4}$ | 365, 482 | 1.85 |
| PATA(BO)TBT-8 | 331, 380, 474 | $5.80 \times 10^{+4}$ | 380, 480 | 1.88 |
| PAA(PU)TBT-8 | 353, 508 | $4.22 \times 10^{+4}$ | 358, 529 | 1.97 |

[a] Molar absorptivity measured at $\lambda_{max}$ in chloroform. [b]($E_g^{opt}$) optical bandgap, calculated from the onset of the absorption s band on solid films.

The absorption maxima of the polymers **PATA(D)TBT-8**, **PATA(BO)TBT-8** and **PAA(PU)TBT-8**, exhibited red-shifts of about 52, 46 and 37 nm compared with their values in solution, with onsets of absorption $\lambda_{onset}$ at 670, 659 and 630 nm, respectively. These red-shift values indicate a more coplanar structure as well as a stronger Van der Waals interactions between polymer backbones in the solid state. Using the absorption onsets, the optical band gaps of the polymers were calculated to be 1.85, 1.88 and 1.97 eV respectively. It can be noticed that polymers containing thienyl aromatic side groups attached to the acetylene substituents on the anthracene units possess red-shifted and broader absorption bands in comparison to the polymer with only an aliphatic side group attached to the acetylene substituent (**PAA(PU)TBT-8**). **PAA(PU)TBT-8** shows the largest band gap relative to its counterpart polymers which can be attributed to two reasons; its low molecular weight which affects its conjugation length and the absence of aromatic side groups attached to the acetylene substituents on the polymer backbone. Attaching thienyl-ethynyl groups to the polymer backbone seems to help in delocalising π-electrons on the conjugated side substituents resulting in the enlargement of the π-conjugation more effectively. As a result, **PATA(D)TBT-8** and **PATA(BO)TBT-8** with conjugated side groups will have larger conjugated area

compared to **PAA(PU)TBT-8** and results in more effective interchain π-π overlap leading to better optical properties [18].

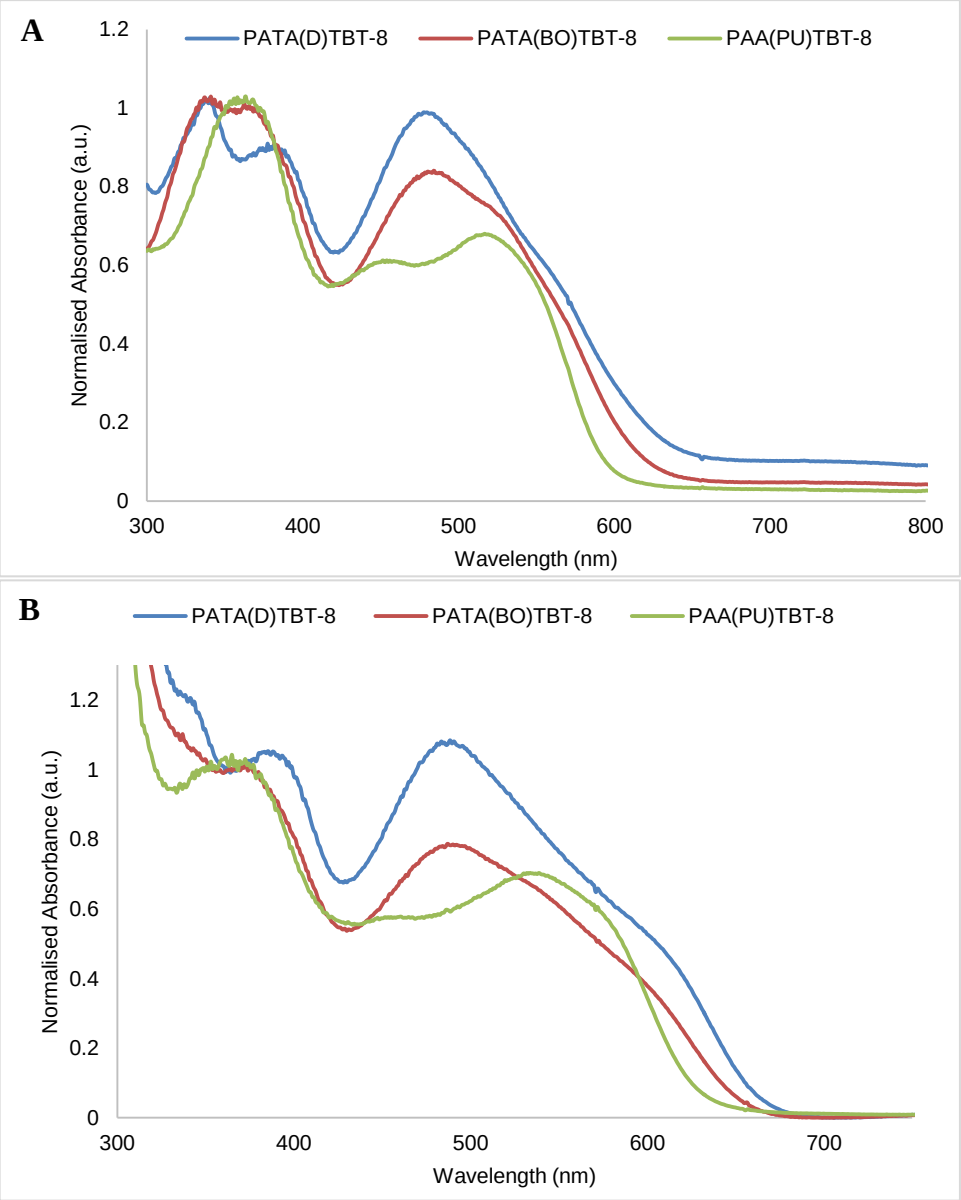


**Figure 3-5:** Normalised UV-Vis absorption spectra of **PATA(D)TBT-8**, **PATA(BO)TBT-8** and **PAA(PU)TBT-8** in : (A) chloroform solutions; and (B) thin films.

A comparison of the current set of polymers to the analogous polymers, **PATA(D)TBT**, **PATA(BO)TBT** and **PAA(PU)TBT**, discussed in chapter 2, and in which the BT units have no alkoxy substituents, indicates that their optical properties are affected by introduction of the alkoxy substituents on BT units. Absorption onset and absorption maxima of **PATA(D)TBT-8**, **PATA(BO)TBT-8** and **PAA(PU)TBT-8** are blue shifted compared to former polymer counterparts both in solution and thin

films. Also, their optical band gaps are wider than polymers without octyloxy substituents attached on their BT repeat units. This effect on the optical properties of the **PATA(D)TBT-8**, **PATA(BO)TBT-8** and **PAA(PU)TBT-8** when compared to their counterparts polymers having the same backbone but without alkoxy substituents on the BT repeat units is probably due to the electron donating alkoxy groups which reduce the electron accepting characteristics of benzothiadiazole moieties [6, 13, 19].

Iraqi and co-workers synthesised a series anthracene-based polymers containing 2,6-linked anthracene and dithienyl-benzo[c]-[1,2,5]thiadiazole alternate repeat units [6]. They found that polymer **PPATBT-8**, which is an analogous polymer to our polymers presented in this work, has a higher optical band gap reported by the group around 1.96 eV. They speculated that this high optical band gap of the octyloxy-substituted polymer is due to the lower electron accepting nature of the octyloxy-substituted BT units because of the attached electron donating alkoxy groups [6]. A similar conclusion was obtained by Jung *et al*. where they synthesised a range of anthracene-benzothiadiazole based polymers, including **PTADTBTO** (**Figure 3-1**) which reveals the highest optical band gaps reported by the group [13].

### 3.2.5 Electrochemical Characterisation

Cyclic voltammetry studies were conducted on thin films of all polymers to determine their energy levels as shown in **Figure 3-6**. The HOMO and LUMO energy levels of the polymers were calculated from their oxidation and reduction onset values, respectively (**Table 3-3**). The HOMO/LUMO energy levels of **PATA(D)TBT-8**, **PATA(BO)TBT-8** and **PAA(PU)TBT-8** are at −5.39/−3.39, −5.41/−3.44, and −5.41/−3.09 eV, respectively. Accordingly, their band gaps measured from CV are 2.00, 1.97, and 2.32 eV, respectively.

**Table 3-3:** The energy levels and electrochemical band gaps of the polymers.

| Polymers | HOMO (eV)[a] | LUMO (eV)[b] | $E_g^{elece}$ (eV)[c] |
|---|---|---|---|
| PATA(D)TBT-8 | –5.39 | –3.39 | 2.00 (±0.04) |
| PATA(BO)TBT-8 | –5.41 | –3.44 | 1.97 (±0.03) |
| PAA(PU)TBT-8 | –5.41 | –3.09 | 2.32 (±0.03) |

[a] HOMO position (*vs. vacuum*) determined from onset of oxidation. [b] LUMO position (*vs. vacuum*) determined from onset of reduction. [c] Electrochemical energy gap of the polymers.

Polymers **PATA(D)TBT-8**, **PATA(BO)TBT-8** and **PAA(PU)TBT-8**, exhibited predominantly the same HOMO energy levels as their counterpart polymers **PATA(D)TBT**, **PATA(BO)TBT** and **PAA(PU)TBT**, which do not have alkoxy substituents on their BT units. Their HOMO levels are also comparable to polymers with similar backbone but with different substituents on the anthracene moieties (e.g. **PPATBT-8**, HOMO level at –5.48 and **PTADTBTO**, HOMO level at –5.38) [6, 13].

However, substituting benzothiadiazole units with alkoxy groups in this new series of polymers, has led to a rise of their LUMO energy levels when compared to their corresponding polymers **PATA(D)TBT** (–3.52 eV), **PATA(BO)TBT** (–3.55 eV) and **PAA(PU)TBT** (–3.50 eV). These high-lying LUMO energy levels can be ascribed to the lower electron-deficiency of benzothiadiazole units upon attachment of electron-rich octyloxy groups as discussed in section 3.2.4. This result is in agreement with the previously published works by Iraqi *et al.*[6] and Jung *et al.*[13]. Nevertheless, polymers **PATA(D)TBT-8** and **PATA(BO)TBT-8** exhibited shallower LUMO level in comparison to **PPATBT-8** (LUMO level at –3.11 eV) prepared by Iraqi and co-worker and **PTADTBTO** (LUMO level at –3.28 eV) prepared by Jung and co-worker. Clearly, modifying the polymers by replacing the attached groups incorporated into anthracene unit with arylethynyl groups help to improve the electronic properties of our polymers. It seems that using acetylene bond to connect between the alkylthienyl and polymer backbone lead to extend the conjugation of the polymer in two dimensions which enhance the resonance effect. Therefore, **PATA(D)TBT-8** and **PATA(BO)TBT-8** incorporate alkylthienylethynyl groups induce efficient intramolecular charge separation leading to a considerable decline in the LUMO level [4].

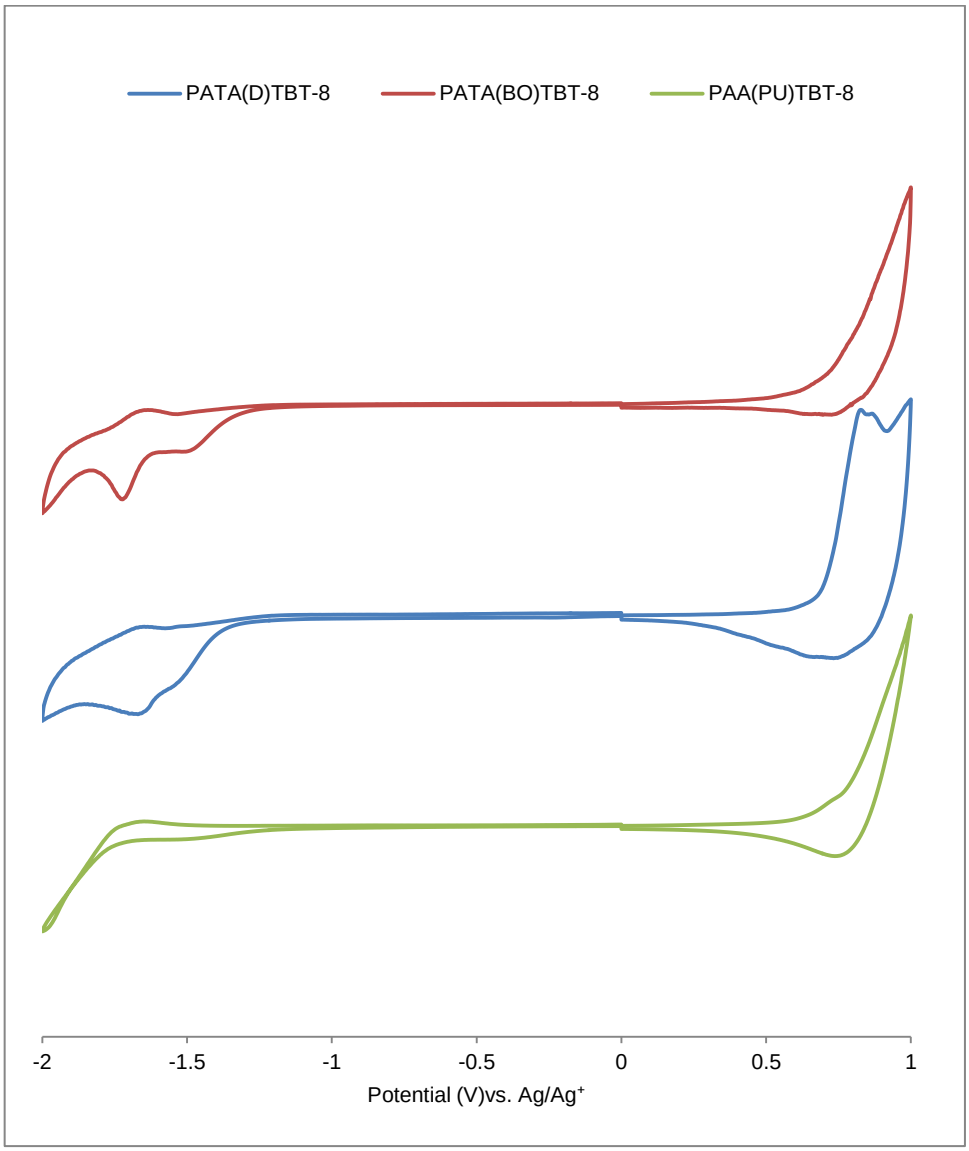


**Figure 3-6:** Cyclic voltammograms of **PATA(D)TBT-8**, **PATA(BO)TBT-8** and **PAA(PU)TBT-8**.

### 3.2.6 X-ray Diffraction studies

The crystallinity and molecular packing of all polymers was studied by powder X-ray diffraction (XRD) (**Figure 3-7** and **Table 3-4**).

The X-ray diffractograms of the polymers exhibit a single broad peak in the wide angle region which shows that the polymers are amorphous. Also we notice that the absence of any peaks in the low angle region indicating that these polymers do not have any long range translational order. This is another evidence that these polymers possess an

amorphous structure in the solid state. This is a good indication that the miscibility of these polymers will be enhanced when they are mixed with the electron acceptor $PC_{70}BM$, and hence it will enable us to measure the power conversion efficiencies of these polymers.

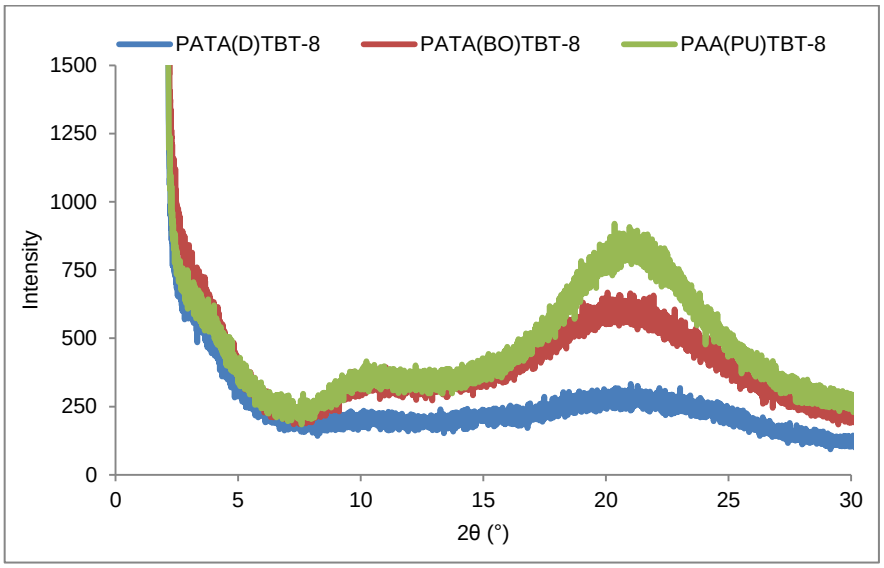


**Figure 3-7:** Powder X-ray diffraction diagram of the anthracene-based polymers **PATA(D)TBT-8**, **PATA(BO)TBT-8** and **PAA(PU)TBT-8**.

In comparison to polymers **PATA(D)TBT**, **PATA(BO)TBT** and **PAA(PU)TBT** discussed in the previous chapter, the amorphous structure of the present polymers are attributed to the larger and more sterically demanding octyloxy groups attached to the benzothiadiazole moiety [4].

**Table 3-4:** Powder X-ray diffraction data for anthracene-based polymers **PATA(D)TBT-8**, **PATA(BO)TBT-8** and **PAA(PU)TBT-8**.

| Polymers | 2θ (°) | *d*-spacing (Å) |
|---|---|---|
| PATA(D)TBT-8 | 20.11 | 4.41 |
| PATA(BO)TBT-8 | 20.26 | 4.38 |
| PAA(PU)TBT-8 | 20.54 | 4.32 |

### 3.2.7 Photovoltaic Device Properties

The photovoltaic performance of the **PATA(D)TBT-8** and **PATA(BO)TBT-8** was examined in bulk heterojunction type PSC in preliminary studies. The polymers were fabricated with a conventional pattern of glass/ITO/PEDOT:PSS/polymer : $PC_{70}BM$ /Ca/Al using blends of polymers : $PC_{70}BM$ in a weight ratio of 1 : 3. A detailed device fabrication method is given in the Experimental section. The current density (*J*) – voltage (*V*) curves of polymer devices are shown in **Figure 3-8**, and the device parameters are listed in **Table 3-5**.

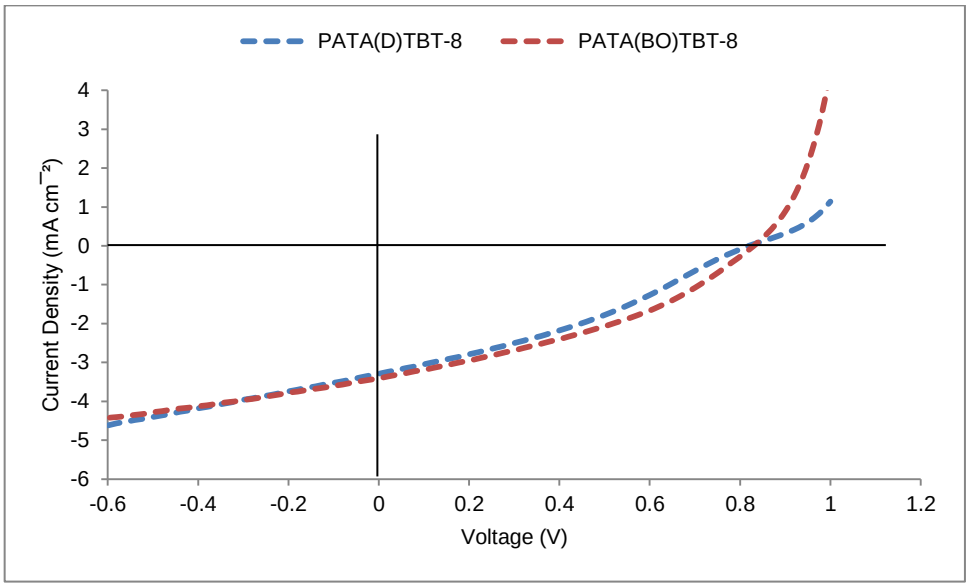


**Figure 3-8:** *J-V* characteristic curve of the organic solar cell device fabricated from **PATA(D)TBT-8** and **PATA(BO)TBT-8**.

The $V_{oc}$ for the blended **PATA(D)TBT-8** and **PATA(BO)TBT-8** devices was measured to be 0.82 and 0.83V, respectively. In comparison to **PATA(BO)TBT-8**, the little decline in the $V_{oc}$ of **PATA(D)TBT-8** was in agreement with its slightly higher HOMO energy level. The $V_{oc}$ values of these two polymers are comparable with their corresponding polymers **PPATBT-8** prepared by Iraqi group ($V_{oc}$ = 0.84 V) and **PTADTBTO** prepared by Jung and co-worker ($V_{oc}$ = 0.85 V) [6, 13]. This indicates that these polymers possess almost similar HOMO energy levels.

**Table 3-5:** Photovoltaic performance of **PATA(D)TBT-8** and **PATA(BO)TBT-8** measured under a simulated photovoltaic light with 1000 $Wm^{-2}$ the illumination (AM 15).

| Polymer | Polymer : $PC_{71}BM$[a] (w/w) | Solvent | $J_{sc}$ (mA $cm^{-2}$) | $V_{oc}$ (V) | FF (%) | PCE (%) |
|---|---|---|---|---|---|---|
| PATA(D)TBT-8 | 1 : 3 | CB[b] | –3.29 | 0.82 | 33 | 0.90 |
| PATA(BO)TBT-8 | 1 : 3 | CB | –3.41 | 0.83 | 36 | 1.04 |

[a] Polymer : $PC_{71}BM$ weight ratio. [b] chlorobenzene.

The $J_{sc}$ for the polymers devices was measured to be 3.29 mA $cm^{-2}$ for **PATA(D)TBT-8** and 3.41 mA $cm^{-2}$ for **PATA(BO)TBT-8**. These $J_{sc}$ values are much lower than that of their corresponding polymers **PPATBT-8** ($J_{sc}$ = 9.70 mA $cm^{-2}$) and **PTADTBTO** ($J_{sc}$ = 11.02 mA $cm^{-2}$) [6, 13]. We believe this to be mainly attributed to the film morphology which usually has a crucial role on the photo-induced charge generation and so their transport to the electrodes [20]. However, further studies and characterizations are required to clarify this assumption like atomic force microscopy (AFM). In addition, we expected that the higher molecular weight of **PPATBT-8** and **PTADTBTO** relative to **PATA(D)TBT-8** and **PATA(BO)TBT-8** could result in higher molar extinction coefficient of these polymers. As a result, this will enable a stronger photon absorption even with a similar active layer thickness [20].

The power conversion efficiencies of both polymers were modest. Polymer **PATA(D)TBT-8** provides a device with a PCE of 0.90%, while **PATA(BO)TBT-8** provides a device with a PCE of 1.04%. The slight improvement in the fill factor (FF) of **PATA(BO)TBT-8** (FF = 36.6%) in comparison to **PATA(D)TBT-8** (FF = 33.3%) help to obtain device with better performance. This suggests that optimizing the morphology of the active layers in devices could help in overall performances of these polymers. Furthermore, a change in the polymer: PCBM weight ratios could also lead to significant improvements in devices made out of these polymers.

## 3.3 Summary

In conclusion, we have prepared a new series of D-A conjugated polymers **PATA(D)TBT-8**, **PATA(BO)TBT-8** and **PAA(PU)TBT-8** containing dithienyl

anthracene derivatives as donor units and 5,6-bis(octyloxy)-benzothiadiazole as acceptor units *via* Stille cross-coupling reaction. The acceptor monomer (**BT**) with octyloxy substituents was selected on the basis that it will provide an enhanced solubility to the resulting polymers than the BT unit without octyloxy groups. All the polymers have good thermal stability and high solubility on common organic solvents. **PAA(PU)TBT-8** shows a low $M_n$, which may be attributed to the bulky substituents on the anthracene units and the alkoxy groups on the **BT** unit. The **PATA(D)TBT-8** and **PATA(BO)TBT-8** exhibited moderate optical band gap of 1.85 and 1.88 eV, respectively, whereas, **PAA(PU)TBT-8** has a quite large band gap of 1.97 due to its low molecular weight. Substituting **BT** units with octyloxy groups lead to a rise of the LUMO energy levels of these polymers when compared to their corresponding polymers without the octyloxy groups. The X-ray diffractograms of the polymers indicate that the polymers are amorphous. Preliminary photovoltaic studies were undertaken on these polymers. The photovoltaic performance of devices of **PATA(D)TBT-8** and **PATA(BO)TBT-8 (**PCE values of 0.90 and 1.04%, respectively) are quite modest, however, we believe that further studies to optimise device performance are warranted in order to explore the potential properties of these materials in bulk heterojunction solar cells.

## 3.4 Experimental Section:

### 3.4.1 Materials:

Unless otherwise stated, all chemicals, reagents and solvents were obtained from commercial sources (Sigma-Aldrich, Fisher, Acros Organics and Alfa Aesar) in the highest purities possible and used as received. Regent grade solvents were purchased from the internal stores which were used for some reactions, extraction, recrystallization and chromatography. However, most of the reactions were carried out using anhydrous solvents which were obtained from the Grubbs solvent system within the chemistry department. Acids, bases, drying agents and salts were obtained from the internal stores. Reactions proceeded under an argon atmosphere as standard unless stated otherwise. Column chromatography was carried out on silica gel (200-300 mesh) or alumina as stated.

### 3.4.2 Analytical Techniques:

Elemental analyses were analysed by using the Perkin Elmer 2400 CHN Elemental Analyser for CHN analysis, and the Schoniger oxygen flask combustion method for sulphur and halides. In both methods, the weights submitted for the analysis were 10 mg. Fourier transform infrared spectroscopy (FTIR) and attenuated total reflectance (ATR) were recorded on a Perkin Elmer Spectrum 65 spectroscopy.

$^{13}C$ and $^{1}H$-NMR spectra of the monomers were recorded on Bruker AV 250 (250 MHz), and Bruker AV 400 (400 MHz) NMR spectrometers at room temperature in chloroform-d ($CDCl_3$) solution. NMR spectra of the polymers were recorded using Bruker Avance III HD 500 (500 MHz) at 100 °C in 1,1,2,2-tetrachloroethane-d2 solution. As an internal standard, tetramethylsilane (TMS) was used for calibrating chemical shifts (δ). The chemical shifts were measured in part per million (ppm), while the coupling constant (*J*) were given in Hertz (Hz).

GC-MS spectra were recorded on Perkin Elmer Turbomass Mass Spectrometer equipped with a Perkin Elmer Autosystem XL Gas Chromatograph. Mass spectra were obtained by the electron impact method (EI) and MALDI-TOF mass spectrometry.

GPC analysis were recorded on the equipment consisted of a Viscotek $GPC_{max}$ VE 2001 GPC solvent/sample module, a Waters 410 Differential Refractometer and a PLgel 5 μm Mixed Column (650 mm set length) using chloroform as the eluent at rate of 1 mL/min. Polymer samples were made up as a solutions in chloroform (2 mg/mL) spiked with toluene as a reference. The RI-detection method was used to obtain the GPC curves, which was calibrated with a series of polystyrene narrow standards. Degree of polymerisation (DP) was calculated using the below equation:

$$\chi_n = \frac{M_n}{M_R}$$

where $\chi_n$ is the DP, $M_n$ is the number average molecular weight of the polymer and $M_R$ is the molecular mass of the repeat unit of the polymer. Perkin Elmer TGA-7 Thermogravimetric Analyser was used to determine TGA curves at a scan rate of 10 °C/minute under nitrogen atmosphere.

Powder X-ray diffraction were conducted on a Bruker D8 advance diffractometer with a CuKα radiation source (1.5418 A, rated as 1.6 kW). The scanning angle was recorded over the range 2–30°.

Hitachi U-2010 Double Beam UV-Visible Spectrophotometer has been used to evaluate the optical properties of the polymers. The absorbance of the polymers was measured in a solution of chloroform at room temperature using quartz cuvette ($l$ = 10 mm). Thin films of the polymers were prepared by dip coating quartz plates into around 1 mg/mL solutions in chloroform, then dried in the air and the UV-Vis absorption spectra measurements were run at room temperature.

Cyclic voltammograms were conducted using Princeton Applied Research Model 263A Potentiostat/Galvanostat. The analyses were recorded under Argon protection at approximately room temperature. A three electrode system was used for the measurements consisting of an $Ag/Ag^+$ reference electrode (Ag wire in 0.01 *M* $AgNO_3$ solution in the electrolyte solution), a Pt working electrode, and Pt counter electrode (Pt wire). Measurements were done in tetrabutylammonium perchlorate acetonitrile solution (0.1 *M*) on polymer thin films which made by drop casting polymer solution onto the working electrode which were left to dry in air. The energy level of $Fc/Fc^+$ was assumed at –4.8 eV to vacuum. The half-wave potential of Fc/Fc+ redox couple was found to be 0.08 V *vs*. $Ag/Ag^+$ reference electrode. the HOMO and LUMO energy level were calculated using the following equations:

$$E_{LUMO} = -[(E_{red,onset} - E_{1/2(ferrocene)}) + 4.8] \text{ eV}$$

$$E_{HOMO} = -[(E_{ox,onset} - E_{1/2(ferrocene)}) + 4.8] \text{ eV}$$

where $E_{red,onset}$ and $E_{ox,onset}$ are the onset of reduction and oxidation, respectively, relative to $Ag/Ag^+$ reference electrode.

### 3.4.3 Fabrication and testing of polymer solar cells:

The polymers and $PC_{70}BM$ were mixed at (1:3) polymer : fullerene blending ratio and were dissolved in CB. The solutions were then put on a hotplate held at 50 °C overnight

with stirring to allow dissolution. Photovoltaic devices were fabricated onto pre-patterned ITO glass substrate (20 Ohms per square) that were supplied by Ossila Limited. The ITO/glass substrates were cleaned by sonication in $NaOH_{(aq)}$ followed by IPA. A 30 nm thick PEDOT:PSS layer was spin-coated onto the ITO substrates. These were then transferred to a hot plate held at a temperature of 120 °C for 5 min. In a glove-box, the active layer was spin cast onto the glass/ITO/PEDOT:PSS substrates, which were then transferred into a thermal evaporator for deposition of OPV cathode (5 nm of calcium capped by a 100 nm of aluminium evaporated at a base pressure of ~$10^{-7}$ mbar). PCEs were measured using a Newport 92251A-1000 AM 1.5 solar simulator. An NREL calibrated silicon cell was used to calibrate the power output to 100 mW $cm^{-2}$ at 25 °C. An aperture mask having an area of 2.06 $mm^2$ was placed over devices to define the test area.

## 3.5 Synthesis of Monomers and Polymers:

The synthesis procedures of 2,6-linked anthracene monomers, **M1**, **M2**, and **M3** were given already in chapter 2.

### 3.5.1 Synthesis of 1,2-bis(octyloxy)benzene (10): [14, 21, 22]

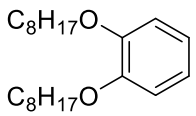


1-Bromooctane (80.5 g, 0.42 mol) was added to a solution of 1,2-dihydroxybenzene (20 g, 0.18 mol) and $K_2CO_3$ (76 g, 0.55 mol) in dry DMF (100 mL) under $N_2$ protection. Subsequently, the reaction mixture was refluxed for 40 hours at 100 °C. Then, the reaction mixture was poured into distilled water, extracted with DCM. The organic layers were combined and dried over $MgSO_4$. Solvent was evaporated and the resulting product was recrystallised twice from EtOH to obtain the product as needle-like crystals (47 g, 78%). $^1$H NMR (250 MHz, *CDCl$_3$*) $\delta_H$/ppm: 6.94 (s, 4H), 4.05 (t, *J* = 6.55 Hz, 4H), 1.94-1.83 (m, 4H), 1.62-1.34 (m, 20H), 0.98 (t, *J* = 6.7 Hz, 6H). $^{13}$C NMR (250 MHz, *CDCl$_3$*) $\delta_C$/ppm: 149.3, 121.0, 114.3, 69.4, 31.8, 29.4, 29.3, 26.0, 22.6, 14.1. Elemental Analysis (%) calculated for $C_{22}H_{38}O_2$: C, 78.99; H, 11.45. Found: C, 79.10; H, 11.61. Mass (EI); (*m/z*): 334 ($M^+$). FT-IR (ATR): ($cm^{-1}$) 2953-2871

(aliphatic C–H stretch), 1594 and 1466 (aromatic C=C stretch), 1454 ($CH_2$ bend), 1387 ($CH_3$ bend), 1255 and 1120 (C–O–C stretch).

### 3.5.2 Synthesis of 1,2-dinitro-4,5-bis(octyloxy)benzene (11): [14, 21, 22]

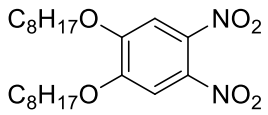


In a 2 neck round-bottom flask, 1,2-bis(octyloxy)benzene (30 g, $9.0 \times 10^{-2}$ mol) was dissolved in mixture of DCM (560 mL) and acetic acid (560 mL). At 0 °C, 65% nitric acid (80 mL) was added dropwise to reaction mixture. The reaction was stirred for 1 hour at room temperature. The reaction mixture was cooled again to 0 °C and fuming nitric acid (200ml) was added dropwise. The reaction was stirred for 40 hours at room temperature. After completing the reaction, the mixture was poured into ice-water and the organic layer was separated. The water phase was extracted with DCM. The organic layers were collected together and washed with water, $NaHCO_3$ solution, and NaCl solution then dried over anhydrous $MgSO_4$. The solvent was evaporated and the crude product was recrystallised from ethanol. The product was obtained as yellow powder (34.2 g, 90%). $^1$H NMR (250 MHz, *CDCl$_3$*) $\delta_H$/ppm: 7.31 (s, 2H), 4.12 (t, *J* = 6.63 Hz, 4H), 1.92-1.86 (m, 4H), 1.53-1.46 (m, 4H), 1.40-1.30 (m, 16H) 0.91 (t, *J* = 6.81 Hz, 6H). $^{13}$C NMR (250 MHz, *CDCl$_3$*) $\delta_C$/ppm: 151.8, 136.4, 107.9, 70.2 31.7, 29.1, 28.7, 25.8, 22.6, 14.0. Elemental Analysis (%) calculated for $C_{22}H_{36}N_2O_2$: C, 62.42; H, 8.55; N, 6.60. Found: C, 62.32; H, 8.36; N, 6.50. Mass (EI); (*m/z*): 424 ($M^+$). FT-IR ($cm^{-1}$): 3071 (aromatic C–H stretch), 2956-2872 (aliphatic C–H stretch), 1597 and 1464 (aromatic C=C stretch), 1540 (N–O stretch), 1454 ($CH_2$ bend), 1387 ($CH_3$ bend), 1355 (N–O stretch), 1255 and 1120 (C–O–C stretch).

### 3.5.3 Synthesis of 4,5-bis(octyloxy)benzene-1,2-diaminium chloride (12): [14, 21]

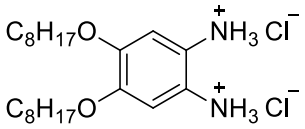

$SnCl_2$ (17.87 g, 9.4 × $10^{-2}$ mol) and HCl (175 mL, 35%) were added to the solution of 1,2-dinitro-4,5-bis(octyloxy)benzene (5 g, 1.2 × $10^{-2}$ mol) dissolved in ethanol (175 mL). The reaction mixture was heated to 85 °C overnight. On cooling to room temperature the solution afforded a white product which was filtered and washed with water and methanol. The product was dried at room temperature under a storm of nitrogen for 6 hours and used directly for the next reaction (unstable). The product was collected as off-white solid (4.48 g, 87%).

### 3.5.4 Synthesis of 5,6-bis(octyloxy)benzo[c][1,2,5]thiadiazole (13):[14, 21]

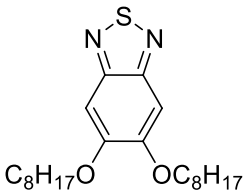

A mixture of 4,5-bis(octyloxy)benzene-1,2-diaminium chloride (4.48 g, 1.0 × $10^{-2}$ mol) and triethylamine (10.8 g, 15.0 mL, 0.11 mol) in dry DCM was placed in 2 neck round bottom flask. A solution of thionyl chloride (2.47 g, 2.0 × $10^{-2}$ mol, 1.51 mL) in 22 mL dry DCM was added slowly to the reaction mixture under $N_2$ protection and refluxed overnight. The reaction mixture was poured in 300 mL water and 300 mL DCM. The organic layer was washed with water (300 x 5) and dried over anhydrous $MgSO_4$. Solvent was evaporated and the crude product was recrystallised from ethanol. The product was obtained as white off powder. (4.50 g, 92%). $^1$H NMR (250 MHz, *CDCl$_3$*) $\delta_H$/ppm: 7.15 (s, 2H), 4.10 (t, *J* = 6.51 Hz, 4H), 1.96-1.89 (m, 4H), 1.57-1.50 (m, 4H), 1.43-1.27 (m, 16H), 0.91 (t, *J* = 6.80, 6H). $^{13}$C NMR (250 MHz, *CDCl$_3$*) $\delta_C$/ppm: 154.1, 151.4, 98.4, 69.1, 31.7, 29.3, 29.2. 28.7, 26.0, 22.6, 14.0. Elemental Analysis (%) calculated for $C_{22}H_{36}N_2O_2S$: C, 67.30; H, 9.24; N, 7.14. Found: C, 66.50; H, 8.65; N, 7.42. Mass (EI); (*m/z*): 392 ($M^+$). FT-IR ($cm^{-1}$): 3118-3052 (aromatic C–H stretch),

2950-2958 (aliphatic C–H stretch), 1460 (C=C stretch), 1195 and 1065 (=C–O–R stretch), 724 ($CH_2$ bending).

### 3.5.5 Synthesis of 4,7-dibromo-5,6-bis(octyloxy)benzo[c][1,2,5]thiadiazole (14):[14, 21]

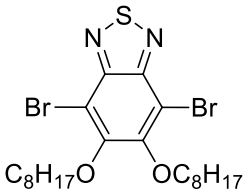


To a solution of 5,6-bis(octyloxy)benzo[c][1,2,5]thiadiazole (3.29 g, $8.4 \times 10^{-3}$ mol) in a mixture of DCM (165 mL) and acetic acid (75 mL) was added a bromine (6.8g, 2.2 mL, $4.3 \times 10^{-2}$ mol). The mixture was stirred in dark for 72 hours at room temperature. The reaction mixture was added to 500 mL of water and extracted with DCM. The organic layer was washed with water, saturated $NaHCO_{3(aq)}$ and $Na_2S_2O_{3(aq)}$. Then, the solvent was evaporated and the crude product was purified on a silica gel column chromatography eluting with petroleum ether/ ethyl acetate (8:2). The product was further purified by recrystallisation from ethanol to give a white powder (3.8 g, 82%). $^1$H NMR (250 MHz, *CDCl$_3$*) $\delta_H$/ppm: 4.18 (t, *J* = 6.65 Hz, 4H), 1.93-1.87 (m, 4H), 1.59-1.51 (m, 4H), 1.44-1.30 (m, 16H) 0.91 (t, *J* = 7.05, 6H). $^{13}$C NMR (250 MHz, *CDCl$_3$*) $\delta_C$/ppm: 154.5, 106.3, 75.16, 31.8, 30.3, 29.9, 29.3, 26.00, 22.7, 14.1. Elemental Analysis (%) calculated for $C_{22}H_{34}N_2O_2Br_2S$: C, 48.01; H, 6.23; Br, 29.04; N, 5.09; S, 5.82. Found: C, 47.89; H, 5.93; Br, 29.02; N, 7.42; S, 6.01. Mass (EI); (*m/z*): 550 ($M^+$). FT-IR ($cm^{-1}$): 2950-2958 (aliphatic C–H stretch), 1470 (C=C stretch), 1285 and 1059 (=C–O–R stretch), 724 ($CH_2$ bending), 797 (C–Br stretch).

### 3.5.6 Synthesis of 4,7-di(thiophen-2-yl)-5,6-Bis(octyloxy)benzo[c][1,2,5] thiadiazole (15):[14, 21]

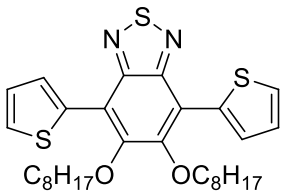


To a solution of 4,7-dibromo-5,6-bis(octyloxy)nenzo[c][1,2,5]thiadiazole (4.00 g, 7.3 × $10^{-3}$ mol), $Pd_2(dpa)_3$ (0.27 g, 0.29 × $10^{-3}$ mol) and tri(o-tolyl)phosphine (0.71 g, 2.3 × $10^{-3}$ mol) in anhydrous toluene (80 mL) was added 2-(tributylstannyl) thiophene (6.82 g, 18.2 × $10^{-3}$ mol). The reaction mixture was refluxed for 24 hours under argon atmosphere. Thereafter, the solvent was evaporated under reduced pressure. The residue was purified on a silica gel column chromatography eluting with $CHCl_3$/hexane (gradient $CHCl_3$ 1-10%) to afford the product as an orange oil (2.3 g, 57 %). $^1$H NMR (250 MHz, *CDCl$_3$*) $\delta_H$/ppm: 8.49 (dd, *J* = 3.82, 1.25 Hz, 2), 7.52 (dd, *J* = 5.3, 1.25 Hz, 2), 7.25 (dd, *J* = 5.2, 3.8 Hz, 2), 4.13 (t, *J* = 7.10 Hz, 4H), 2.00-1.87 (m, 4H), 1.53-1.24 (m, 20H), 0.96-0.84 (m, 6H). $^{13}$C NMR (250 MHz, *CDCl$_3$*) $\delta_C$/ppm: 152.02, 151.05, 134.15, 130.55, 127.29, 126.73, 117.65, 74.38, 31.82, 30.33, 29.49, 29.26, 25.96, 22.65, 14.07. Elemental Analysis (%) calculated for $C_{30}H_{40}N_2O_2S_3$: C, 64.71; H, 7.24; N, 5.03; S, 17.27. Found: C, 62.99; H, 6.99; N, 4.74; S, 15.91. Mass (EI); (*m/z*): 556 ($M^+$). FT-IR ($cm^{-1}$): 3077 (aromatic C–H stretch), 2958-2956 (aliphatic C–H stretch), 1558 and 1466 (C=C stretch), 1283 and 1033 (C–O–R stretch), 724 ($CH_2$ bending).

### 3.5.7 Synthesis of 4,7-Bis(5-bromothiophen-2-yl)-5,6-bis(octyloxy)benzo[c] [1,2,5]thiadiazole (16):[14, 21]

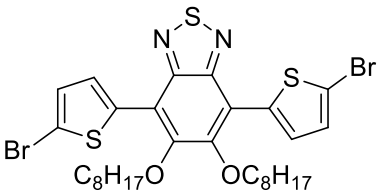


A mixture of 5,6-bis(octyloxy)-4,7-di(thiophene-2-yl)benzo[c][1,2,5]-thidiazole (0.88 g, 1.6 × $10^{-3}$ mol), *n*-bromosuccinimide (NBS) (0.30 mg, 3.1 × $10^{-3}$ mol), glacial acetic acid (40 mL) and chloroform (40 mL) was stirred at room temperature in dark for 24

hours. The solvent was evaporated using rotatory evaporator, the residue was purified on a silica gel column chromatography eluting with $CHCl_3$/hexane (gradient $CHCl_3$ 1-10%) to afford the product as orange crystals (0.56 g, 50%). $^1$H NMR (250 MHz, *CDCl$_3$*) $\delta_H$/ppm: 8.38 (d, *J* = 4.14, 2H), 7.18 (d, *J* = 4.14, 2H), 4.13 (t, *J* = 7.30 Hz, 4H), 2.02-1.91 (m, 4H), 1.50-1.29 (m, 20H), 0.92 (t, *J* = 6.70, 6H). $^{13}$C NMR (250 MHz, *CDCl$_3$*) $\delta_C$/ppm: 151.5, 150.4, 135.7, 131.0, 129.7, 117.0, 115.5, 74.6, 31.8, 30.3, 29.5, 29.3, 25.9, 22.68, 14.1. Elemental Analysis (%) calculated for $C_{30}H_{38}Br_2N_2O_2S_3$: C, 50.42; H, 5.36; N, 3.92; Br, 22.36; S, 13.46. Found: C, 50.34; H, 5.35; N, 4.22; Br, 22.18; S, 13.47. Mass (MALDI-TOF); (*m/z*): 714 ($M^+$). FT-IR ($cm^{-1}$): 3180-3080 (aromatic C–H stretch), 2954-2950 (aliphatic C–H stretch), 1466 (C=C stretch), 1285 and 1031 (=C–O–R stretch), 724 ($CH_2$ bending), 790 (C–Br stretch).

### 3.5.8 Synthesis of 4,7-bis-(5-trimethylstannylthiophene-2-yl)-5,6-bis (octyloxy)benzo[c][1,2,5]thiadiazole (M5): [15]

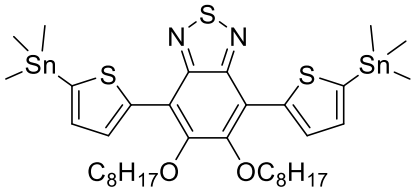


4,7-bis(5-bromothiophen-2-yl)-5,6-bis(octyloxy)benzo-[c][1,2,5]-thiadiazole (0.75 g, $1.05 \times 10^{-3}$ mol) was dissolved in dry THF (30 mL) under argon atmosphere. The solution was cooled to -78 °C and 2.5 M *n*-BuLi (1.30 mL, $3.3 \times 10^{-3}$ mol in hexane) was added dropwise. After stirring for 5 hours at –78 °C, 1M $SnMe_3Cl$ (3.15 mL, $3.15 \times 10^{-3}$ mol in hexane) was added dropwise and allowed to stir at –78 °C overnight. The mixture was poured into $H_2O$ and extracted with diethyl ether. The organic layer was extracted three times with $H_2O$, dried over $MgSO_4$ and solvent evaporated to give a green oil product (0.82 g, 75%). $^1$H NMR (250 MHz, *CDCl$_3$*) $\delta_H$/ppm: 8.54 (d, *J* = 3.6, 2H), 7.35 (d, *J* = 3.6, 2H), 4.13 (t, *J* = 7.05 Hz, 4H), 1.98-1.91 (m, 4H), 1.52-1.45 (m, 4H), 1.38-1.30 (m, 16H), 0.92 (t, *J* = 7.0, 6H), 0.45 (s, 18H). $^{13}$C NMR (250 MHz, *CDCl$_3$*) $\delta_C$/ppm: 151.9, 151.0, 140.19, 139.9, 134.8, 131.3, 127.2, 126.7, 117.6, 74.1, 31.8, 30.4, 29.6, 29.3, 26.1, 22.7, 14.1. Elemental Analysis (%) calculated for $C_{36}H_{56}N_2O_2S_3Sn_2$: C, 49.00; H, 6.40; N, 3.17; S, 10.90. Found: C, 52.80; H, 6.55; N, 3.33; S, 10.92. Mass (MALDI-TOF); (*m/z*): 882 ($M^+$). FT-IR ($cm^{-1}$): 3172-3078

(aromatic C–H stretch), 2954-2854 (aliphatic C–H stretch), 1464 (C=C stretch), 1283 and 1027 (C–O–R stretch), 734 ($CH_2$ bending), 531 and 515 (C–Sn stretch).

### 3.5.9 Poly[9,10-bis[2-ethynyl-5-dodcylthiophene]-anthracene-2,6-diyl-alt-5,6-bis(octyloxy)-4,7-di(thiophene-2-yl)benzo[c][1,2,5]thiadiazole] (PATA(D)TBT-8): [21, 23, 24]

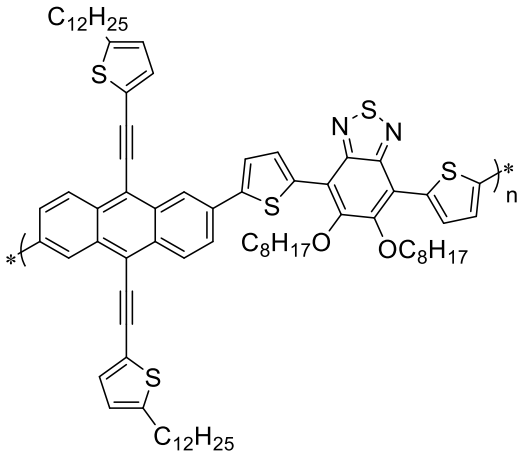


4,7-bis-(5-trimethylstannyl)thiophene-2-yl)-5,6-bis(octyloxy)benz[c][1,2,5]thiadiazole (**M5**) (180 mg, 0.204 × $10^{-3}$ mol) was weighed into a dry 100 mL round-bottom flask. 2,6-dibromo-9,10-bis[2-ethynyl-5-dodcylthiophene]anthracene (**M1**) (181 mg, 0.204 × $10^{-3}$ mol), (*o*-tolyl)$_3$P (9.00 mg, 0.0296 × $10^{-3}$ mol) and $Pd(OAc)_2$ (3.30 mg, 0.0148 × $10^{-3}$ mol) were added. The flask was subjected to several cycles of vacuum followed by refilling with argon gas. Then, dry toluene (10 mL) were added and degassed again. The polymerization was carried out at 100 °C for 24 hour under argon protection. The mixture was cooled to room temperature and 2-(tributylstannyl) thiophene (0.30 mL) was added. The mixture was degassed and heated at 100 °C for 1 hour. The mixture was cooled to room temperature and 2-bromothiophene (0.30 mL mg) was added, degassed and heated to 100 °C for 1 hours. The reaction cooled to room temperature and the raw product was precipitated into methanol and collected by filtration. The resulting solid was purified using Soxhlet extraction with solvents in the order; methanol (250 mL), acetone (250 mL), hexane (250 mL), chloroform (250 mL) and chlorobenzene (250 mL). The chloroform fraction was concentrated (≈ 50 mL) and then poured into methanol (500 mL). The resulting mixture was stirred overnight and the solid was collected by filtration through a membrane filter to yield a red powder (97 mg, 37%).

GPC (TCB): $M_w$ = 18800, $M_n$ = 8100, PD = 2.3. $^1$HNMR ($C_2D_2Cl_4$): ($\delta_H$/ppm) 8.90 (bs, 2H); 8.72-8.37 (bm, 4H); 8.00 (bs, 2H); 7.68 (bm, 2H), 7.40 (bm, 2H); 6.80 (bs, 2H); 4.25 (bm,4H); 2.86 (bs, 4H); 2.02-1.66 (bm); 1.30-1.17(bm); 0.88-0.80 (bs). Elemental analysis (%) calculated for $C_{80}H_{100}N_2O_2S_5$: C, 74.95; H, 7.86; N, 2.19; S, 12.50. Found; C, 71.59; H, 7.47; N, 1.88; S, 11.04. FT-IR ($cm^{-1}$): 3067 (aromatic C–H stretch), 2951-2849 (aliphatic C–H stretch), 2188 (carbon, carbon triple bond stretch), 1615 (aromatic C=C stretch), 1459 (C–H bending aliphatic), 1282 (C–O stretch), 721 ($CH_2$ bending).

### 3.5.10 Poly[9,10-bis[2-(ethynyl-5-butyl-octyl)thiophene]-anthracene-2,6-diyl-alt-5,6-bis(octyloxy)-4,7-di(thiophene-2-yl)benzo[c][1,2,5] thiadiazole] (PATA(BO)TBT-8):[21, 23, 24]

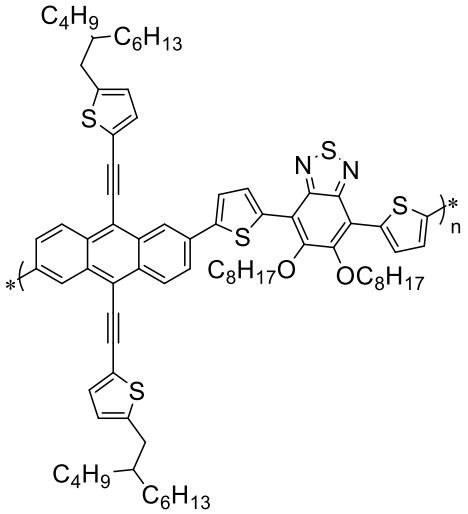


(**PATA(BO)TBT-8**) was prepared following a procedure similar to (**PATA(D)TBT-8**) from monomer 4,7-bis-(5-trimethylstannyl)thiophene-2-yl)-5,6-bis(octyloxy)benz [c][1,2,5]thiadiazole (**M5**) (126 mg, 0.143 × $10^{-3}$ mol), and monomer 2,6-dibromo-9,10-bis[2-(ethynyl-5-butyl-octyl)thiophene]anthracene (**M2**) (126 mg, 0.143 × $10^{-3}$ mol). The product was collected form toluene fraction as dark purple solid. Yield: 71 mg. (39%).

GPC (TCB): $M_w$ = 19100, $M_n$ = 9900, PD = 1.9. $^1$HNMR ($C_2D_2Cl_4$): ($\delta_H$/ppm) 8.92 (bs, 2H); 8.62-8.45 (bm, 4H); 8.00 (bd, 2H); 7.68 (bm, 2H); 7.45-7.32 (bm, 2H); 6.78 (bs, 2H); 4.3-4.02 (bm, 4d); 2.86-2.73 (bd, 4H); 2.02-1.86 (bm); 1.72-1.63 (bs); 1.55-1.12(bm); 0.92-0.60 (bs). Elemental analysis (%) calculated for $C_{80}H_{100}N_2O_2S_5$: C, 74.95; H, 7.86; N, 2.19; S, 12.50. Found; C, 74.62; H, 7.78; N, 1.56; S, 10.81. FT-IR

($cm^{-1}$): 3072 (aromatic C–H stretch), 2951-2851 (aliphatic C–H stretch), 2184 (carbon, carbon triple bond stretch), 1618 (aromatic C=C stretch), 1457 (C–H bending aliphatic), 1233 (C–O stretch), 723 ($CH_2$ bending).

### 3.5.11 Poly[9,10-di-(3-pentylundec-1-yne)-anthracene-2,6diyl-alt-5,6-bis (octyloxy)-4,7-di(thiophene-2-yl)benzo[c][1,2,5]thiadiazole] (PAA-(PU)TBT-8): [21, 23, 24]

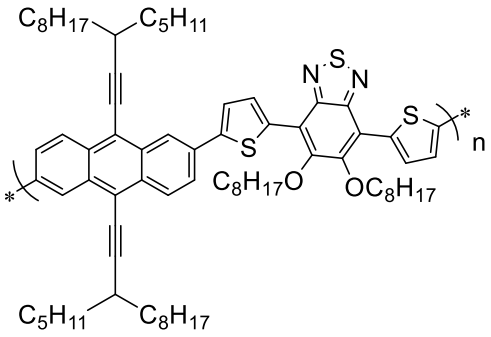


(**PAA(PU)TBT-8**) was prepared following a procedure similar to (**PATA(D)TBT-8**) from monomer 4,7-bis-(5-trimethylstannyl)thiophene-2-yl)-5,6-bis(octyloxy) benzo[c][1,2,5]thiadiazole (**M5**) (0.17 g, 0.19 × $10^{-3}$ mol), 2,6-dibromo-9,10-di-(3-pentylundec-1-yne)-anthracene (**M3**) (0.15 g, 0.19 × $10^{-3}$ mol). The product was collected form hexane fraction as a red solid. Yield: 95 mg. (42%). GPC (TCB): $M_w$ = 6400, $M_n$ = 3200, PD = 2.75. $^1$HNMR ($CDCl_3$): ($\delta_H$/ppm): 8.98 (bs, 2H), 8.61 (bm, 4H), 7.98 (bm, 2H), 7.73 (bs, 2H), 4.31-4.13 (bm, 4H); 3.05-2.91 (bm, 2H); 2.11-1.98 (bm, 4H); 1.52-1.13 (bm, 64H); 1.02-0.77 (bm, 18H). FT-IR ($cm^{-1}$): 3057 (aromatic C–H stretch), 2955-2855 (aliphatic C–H stretch), 2207 (carbon, carbon triple bond stretch), 1618 (aromatic C=C stretch), 1459 (C–H bending aliphatic), 1235 (C–O stretch), 721 ($CH_2$ bending).

## 3.6 References


1. M. H. Choi, K. W. Song, S. W. Heo, Y. W. Han and D. K. Moon, *J. Ind. Eng. Chem.*, 2015, **26**, 173-181.
2. V. Tamilavan, J. B. Park, I.-N. Kang, D.-H. Hwang and M. H. Hyun, *Synth. Met.*, 2014, **198**, 230-238.
3. E. Bundgaard and F. C. Krebs, *Sol. Energ. Mater. Sol. Cells*, 2007, **91**, 954-985.
4. L. Cartwright, L. J. Taylor, H. Yi, A. Iraqi, Y. Zhang, N. W. Scarratt, T. Wang and D. G. Lidzey, *RSC Advances*, 2015, **5**, 101607-101615.
5. C. Kitamura, S. Tanaka and Y. Yamashita, *Chem. Mater.*, 1996, **8**, 570-578.
6. A. Abdulaziz, *Chem. Commun.*, 2013, **49**, 2252-2254.
7. W. Cui, Y. Zhao, H. Tian, Z. Xie, Y. Geng and F. Wang, *Macromolecules*, 2009, **42**, 8021-8027.
8. C. Liu, W. Cai, X. Guan, C. Duan, Q. Xue, L. Ying, F. Huang and Y. Cao, *Polym. Chem.*, 2013, **4**, 3949-3958.
9. J. Y. Ma, H. J. Yun, S. O. Kim, G. B. Lee, H. Cha, C. E. Park, S. K. Kwon and Y. H. Kim, *J. Polym. Sci. Part A: Polym. Chem.*, 2014, **52**, 1306-1314.
10. J. W. Jung and W. H. Jo, *Polym. Chem.*, 2015, **6**, 4013-4019.
11. J. Mei and Z. Bao, *Chem. Mater.*, 2013, **26**, 604-615.
12. C. Du, W. Li, C. Li and Z. Bo, *J. Polym. Sci. Part A: Polym. Chem.*, 2013, **51**, 383-393.
13. J. W. Jung, F. Liu, T. P. Russell and W. H. Jo, *Adv. Energy Mater.*, 2015.
14. P. Ding, C. C. Chu, Y. Zou, D. Xiao, C. Pan and C. S. Hsu, *J. App. Polym. Sci.*, 2012, **123**, 99-107.
15. H. A. Saadeh, L. Lu, F. He, J. E. Bullock, W. Wang, B. Carsten and L. Yu, *ACS Macro Lett.*, 2012, **1**, 361-365.
16. W. F. Bailey, T. V. Ovaska and T. K. Leipert, *Tetrahedron Lett.*, 1989, **30**, 3901-3904.
17. K. Kranthiraja, K. Gunasekar, N. Chakravarthi, M. Song, J. H. Moon, J. Y. Lee, I.-N. Kang and S.-H. Jin, *Dyes Pigm.*, 2015, **123**, 100-111.
18. L. Ye, S. Zhang, L. Huo, M. Zhang and J. Hou, *Acc. Chem. Res.*, 2014, **47**, 1595-1603.
19. J. W. Jung, F. Liu, T. P. Russell and W. H. Jo, *Adv. Energy Mater.*, 2015, **5**.

20. M. A. Uddin, T. Kim, S. Yum, H. Choi, S. Hwang, J. Y. Kim and H. Y. Woo, *Curr. App. Phys.*, 2015, **15**, 654-661.
21. M. Helgesen, S. A. Gevorgyan, F. C. Krebs and R. A. Janssen, *Chem. Mater.*, 2009, **21**, 4669-4675.
22. P. Ding, C. Zhong, Y. Zou, C. Pan, H. Wu and Y. Cao, *J. Phys. Chem. C*, 2011, **115**, 16211-16219.
23. X. Guo, H. Xin, F. S. Kim, A. D. Liyanage, S. A. Jenekhe and M. D. Watson, *Macromolecules*, 2010, **44**, 269-277.
24. D. Gedefaw, M. Tessarolo, W. Zhuang, R. Kroon, E. Wang, M. Bolognesi, M. Seri, M. Muccini and M. R. Andersson, *Polym. Chem.*, 2014, **5**, 2083-2093.

# Chapter 4

## *Synthesis of Donor-Acceptor Conjugated Polymers Based on 2,6-Linked Anthracene Derivatives for Polymer Solar Cells*

# Chapter 4

## 4.1 Introduction

Research on organic conjugated materials has grown rapidly during the past few decades and received a great attention because of their distinct optoelectronic and electronic properties. Conjugated polymers are used in a variety of applications, such as polymer solar cells (PSCs) [1], organic field-effect transistors (OTFTs) [2] and polymer light-emitting diodes (PLEDs) [3]. All of these applications have contributed to increase and encourage the continuous exploration of organic conjugated materials with new structures. Several soluble π-conjugated polymers based on either simple aromatic units such as thiophene or polymers based on fused aromatic units like fluorenes, carbazoles, dithienosilole and benzodithiophenes have been developed, which show encouraging optoelectronic properties [4, 5].

The donor-acceptor (D–A) structural copolymers approach is one of the most successful strategies for narrowing the optical band gap and tuning the HOMO-LUMO energy levels of the conjugated polymers [4, 6]. One of the advantages of using the D–A copolymerization approach is that, the resulted polymer possesses a broadened absorption spectrum at longer wavelength due to the presence of intramolecular charge transfer absorption bands from the polymer. Furthermore, the (D–A) strategy offers a chance to control and tune the electronic energy levels of the polymer by choosing suitable donor and acceptor monomers where the HOMO and LUMO levels of the polymers mainly depend on the donor and acceptor moieties, respectively [4].

Due to their promising optoelectronic and electronic properties and charge carriers transport properties, anthracene derivatives have been used as donor building blocks for (PSCs) [7, 8], (OTFTs) [9], and (PLEDs) [10]. Anthracene can be incorporated in the polymer backbone either through the 9,10-positions or the 2,6-positions, but the polymers prepared based on 9,10-linked anthracene derivatives are found to suffer a strong twisting

out of planarity in their main chains and hence the conjugation is strongly limited due to high steric hindrance [11]. To overcome this problem and to improve the solar energy absorption, incorporating the anthracene unit into conjugated polymers through its 2,6-positions has been used. Linkage along the polymer through the 2,6-positions of anthracene units can make the backbone of the polymer fully π-conjugated and offers a practical way to tune the optoelectronic properties of the corresponding polymers [12]. The first reported poly(anthracene-2,6-diyl) was synthesised by Hodge *et al.* through a precursor approach as an insoluble polymer [13].

On the other hand, benzothiadiazole electron deficient moieties have attracted a considerable interest due to their high electron accepting ability resulting from the existence of two electron withdrawing imine groups. Leclerc *et al.* and Li *et al.* have reported a series of BT-based copolymers which have shown good photovoltaic properties [14, 15].

Using side chains in the design of new conjugated polymers is a crucial element in their design as it affects their solubility, thin film morphologies and molecular packing motifs. In fact, using side chains including conjugated units (e.g. thiophene) is thought to enhance charge carrier mobility as well as the absorption range for device application [16]. However, introducing solubilizing substituents in the polymer backbone could lead to steric hindrance which affect the planarity of the polymer backbone as well as their electronic delocalisation [17].

In our previous work, we found that introducing linear octyloxy groups on the benzothiadiazole (BT) repeat units was a good solution to enhance the processability of the resulting polymers and avoid solubility problems. However, the optical band gaps of the polymers **PATA(D)TBT-8**, **PATA(BO)TBT-8** and **PAA(PU)TBT-8** indicate a higher value compare to their corresponding polymers **PATA(D)TBT**, **PATA(BO)TBT** and **PAA(PU)TBT** which are without solubilizing alkoxy substituents on the BT unit. The $M_n$ value of polymer **PAA(PU)TBT-8** was also quite low compared to its

counterparts polymers, which could be attributed to the steric hindrance resulting from the bulky groups attached to the anthracene unit and alkoxy groups on the BT. One practical solution to deal with such a problem is to use bithiophene spacers between the donor-acceptor units instead of thiophene.

Previous studies by Iraqi group indicated that, using bithiophene units to separate BT repeat units from the donor moieties enhanced the electronic and photophysical properties of the prepared polymers **PPAT2BT-8** [7] and **PTAT2BT-8** [18] (**Figure 4-1**). There are also another studies that have shown that the use of different π-bridge linkers between the donor and acceptor units could affect the molecular architecture and enhance the optoelectronic and photovoltaic properties of the conjugated polymers [16, 19, 20].

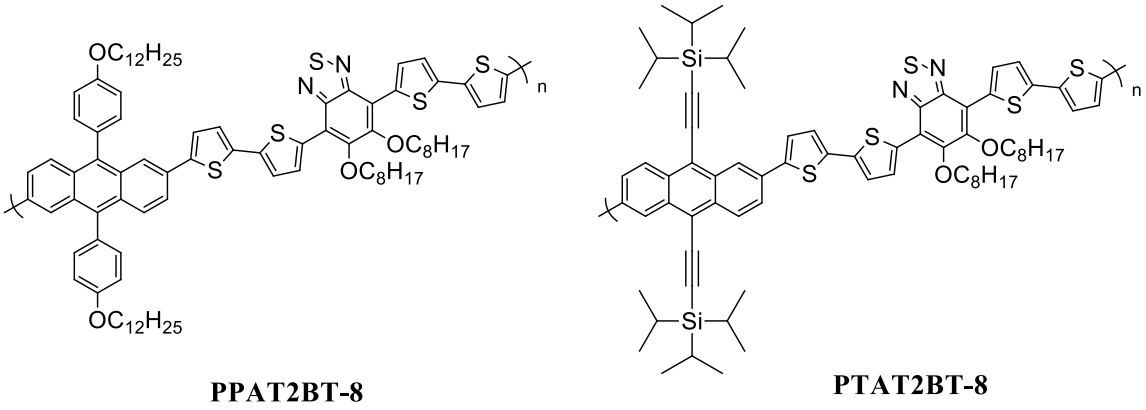


**PPAT2BT-8** **PTAT2BT-8**

**Figure 4-1:** The structure of the conjugated polymers **PPAT2BT-8** and **PTAT2BT-8**.

In this part of our work, we report the synthesis of novel donor–acceptor copolymers comprising alternating 2,6-linked-anthracene repeat units and dioctyloxy substituted benzothiadiazole with two bithiophene π–bridge as outlined in **Figure 4-2**. The electronic, photophysical and photovoltaic properties of the new materials are compared and contrasted to those of the known **PATA(D)TBT-8**, **PATA(BO)TBT-8** and **PAA(PU)TBT-8**.

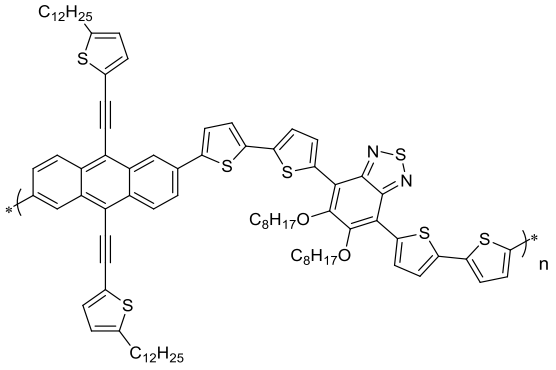

**PATA(D)T2BT-8**

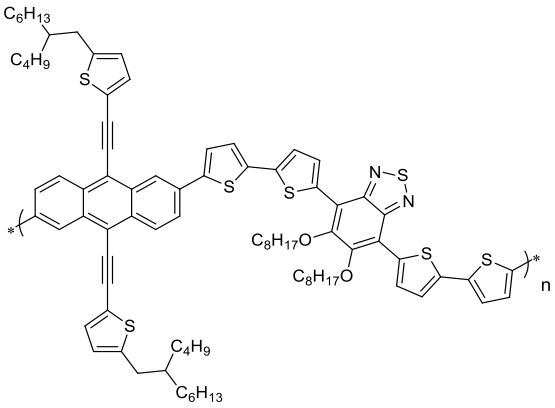

**PATA(BO)T2BT-8**

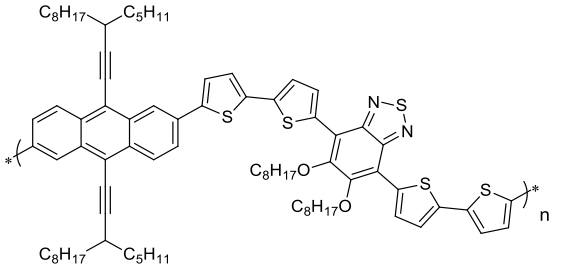

**PAA(PU)T2BT-8**

**Figure 4-2:** Chemical structures of the target anthracene-based conjugated polymers.

## 4.2 Results and Discussion

### 4.2.1 Synthesis of the Monomers

The synthesis of monomer **M6** and conjugated polymers **PATA(D)T2BT-8**, **PATA(BO)T2BT-8**, and **PAA(PU)T2BT-8** are outlined in **Scheme 4-1**. Preparation of monomers **M1-M3** were discussed previously in Chapter 2.

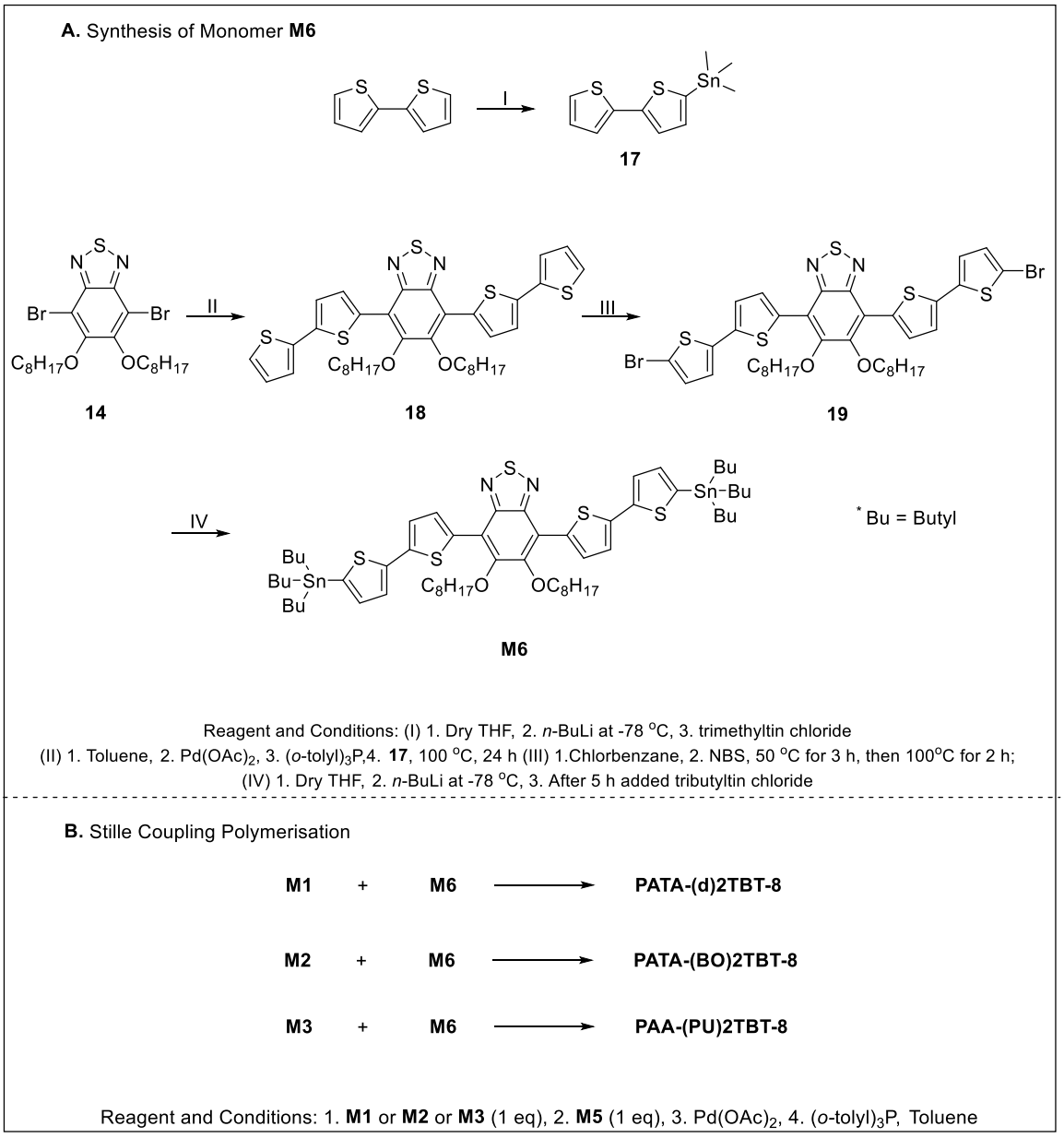


**Scheme 4-1:** Synthetic routes of monomer **M6** and polymers, **PATA(D)T2BT-8**, **PATA(BO)T2BT-8**, and **PAA(PU)T2BT-8**.

4,7-Bis(5-(tributylstannyl)-[2,2']-bithiophen-5-yl)-5,6 bis(octyloxy)benzo[c][1,2,5]thia diazole **M6** was synthesised by a similar method to that described for monomer **M5** in chapter 3. It was obtained upon reacting compound (**14**) and 2,2'-bithiophen-5-yl(trimethyl)stannane in a Stille type reaction to collect 4,7-di(2,2'-bithiophen-5-yl)-5,6-bis(octyloxy) benzo[c][1,2,5]thiadiazole (**15**) as dark orange crystals. Compound (**15)** was then brominated using NBS to afford (**16**), followed by a stannylation reaction of the product on reaction with *n*-BuLi at first, then with tributyltin chloride to afford monomer **M6**.

### 4.2.2 Polymers Synthesis

The polymers, **PATA(D)T2BT-8**, **PATA(BO)T2BT-8**, and **PAA(PU)T2BT-8**, were synthesized by the Stille coupling polymerisation in refluxing toluene catalysed by $Pd(OAc)_2$ and $(o\text{-tolyl})_3P$ (**Scheme 4-1**). The resulting polymers were precipitated in methanol and purified *via* Soxhlet extraction to remove the catalyst, unreacted monomers and low molecular weight materials. All three polymers were extracted with toluene and their chemical structures have been determined by $^1$H-NMR, IR and elemental analysis ($^1$H-NMR spectra of the polymers are provided in Chapter 7, Figure 7-15 and Figure 7-16).

The average molecular weight of the polymers was determined by the gel permeation chromatography (GPC) relative to polystyrene standards using 1,2,4-trichlorobenzene as the eluent, at 140 °C. The $M_n$ of the polymers ranged between 7200 Da to 9700 Da as listed in**Table 4-1**.

**Table 4-1:** GPC data and TGA data of **PATA(D)T2BT-8**, **PATA(BO)T2BT-8** and **PAA(PU)T2BT-8**.

| Polymer | Yield (%) | $M_n$ (Da)[a] | $M_w$ (Da)[a] | PD[b] | DP[c] | Td ($^oC$) |
|---|---|---|---|---|---|---|
| PATA(D)T2BT-8 | 66 | 7200 | 13400 | 2.75 | 5 | 327 |
| PATA(BO)T2BT-8 | 58 | 9700 | 25900 | 2.70 | 7 | 328 |
| PAA(PU)T2BT-8 | 61 | 8200 | 13800 | 290 | 6 | 331 |

[a] Measurements conducted using a differential refractive index (DRI) detection method.

[b] Polydispersity index. [c] Degree of polymerisation.

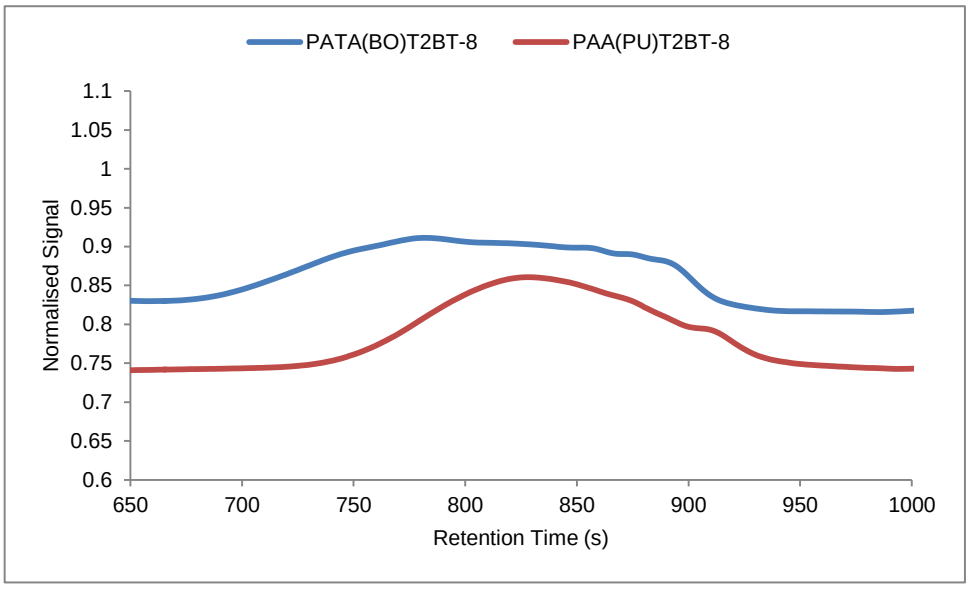


**Figure 4-3:** The GPC traces by RI detector of **PATA(BO)T2BT-2** and **PAA(PU)T2BT-2**.

As expected, the introduction of the bithiophene as a spacer between the anthracene units and the BT units has led to an improve the number average molecular weight ($M_n$) of polymer **PAA(PU)T2BT-8** (8200 Da) when compared to its counterpart **PAA(PU)TBT-8** (3200 Da). We had postulated previously that the low molecular weight of polymer **PAA(PU)TBT-8** can be attributed to steric hindrance resulting from the bulky alkenyl groups attached to anthracene unit and octyloxy groups substituted into BT. However, polymers **PATA(D)T2BT-8**, **PATA(BO)T2BT-8** reveal a slight

decrease in their $M_n$ values with 7200 and 9700 Da, respectively, compared to their counterparts **PATA(D)TBT-8** ($M_n$ of 8100), **PATA(BO)TBT-8** ($M_n$ of 9900). This can be ascribed to incorporation of bithiophene spacer units without adding more solubilizing groups to polymer backbones [18].

### 4.2.3 Thermal Analysis

The thermal properties of the polymers were investigated by thermogravimetric analysis (TGA) under a nitrogen atmosphere as shown in **Figure 4-4**. The thermal decomposition temperatures (corresponding to 5% weight loss in the thermogravimetric analysis) of **PATA(D)T2BT-8**, **PATA(BO)T2BT-8**, and **PAA(PU)T2BT-8** are 327, 328 and 331, respectively. The polymers reveals good thermal stability with decomposition temperatures over 300 °C, which indicates that they are stable enough for photovoltaic applications.

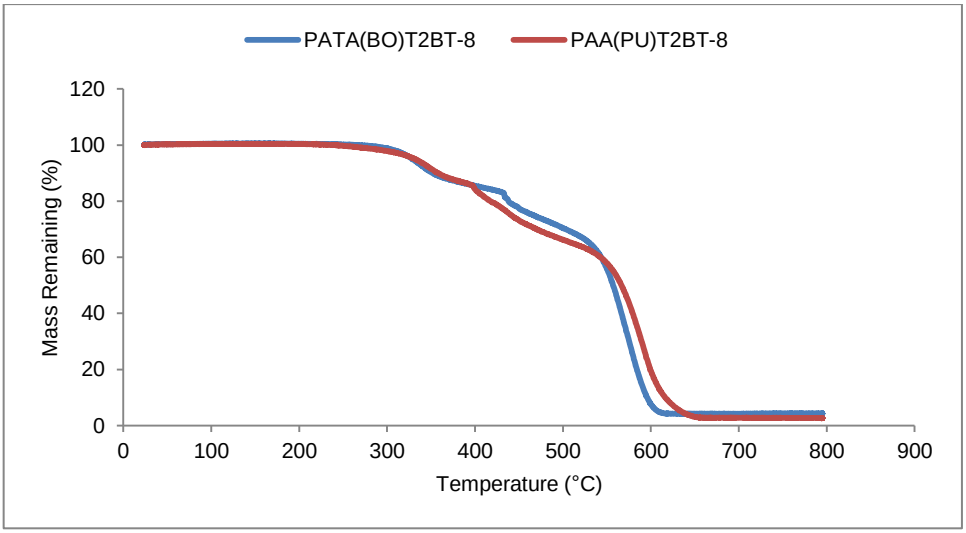


**Figure 4-4:** TGA plots of **PATA(BO)T2BT-8** and **PAA(PU)T2BT-8**.

### 4.2.4 Optical Properties

The optical properties of the three polymers were investigated by UV-Vis absorption spectroscopy in chloroform solutions and films as displayed in **Figure 4-5**. The optical properties of **PATA(D)T2BT-8**, **PATA(BO)T2BT-8**, and **PAA(PU)T2BT-8** are summarised in **Table 4-2**.

**Table 4-2:** UV-Vis data and optical band gaps of polymers **PATA(D)T2BT-8**, **PATA(BO)T2BT-8** and **PAA(PU)T2BT-8**.

| Polymer | $\lambda_{max}$ Solution (nm) | $\varepsilon^{a}$ ($M^{-1}$ $cm^{-1}$) | $\lambda_{max}$ film (nm) | $E_g^{opt}$ film (eV)[b] |
|---|---|---|---|---|
| PATA(D)T2BT-8 | 343, 400, 515 | $5.20 \times 10^{+4}$ | 402, 520 | 1.86 |
| PATA(BO)T2BT-8 | 348, 409, 520 | $5.30 \times 10^{+4}$ | 410, 557 | 1.80 |
| PAA(PU)T2BT-8 | 342, 397, 530 | $4.99 \times 10^{+4}$ | 334, 338, 545 | 1.89 |

[a] Molar absorptivity measured at $\lambda_{max}$ in chloroform. [b]($E_g^{opt}$) optical bandgap, calculated from the onset of the absorption s band on solid films.

The absorption spectrum of **PATA(BO)T2BT-8** in a dilute solution of chloroform showed three absorption maxima in the visible region at 348, 409 and 520 nm. After casting the polymer into a thin-film, the absorption spectrum of **PATA(BO)T2BT-8** was red-shifted and became much broader with two absorption bands at 410 and 557 nm, relative to those observed in solution. This bathochromic shift indicates that the polymer chains form a strong π–π interchain stacking in the solid state and adopt more planar conformations. The optical band gap of **PATA(BO)T2BT-8** was calculated as 1.80 eV.

The analogue of this polymer, **PATA(D)T2BT-8** which has linear dodecylthienylethynyl substituents on the anthracene unit, displays absorption bands at 343, 400 and 515 nm in chloroform solutions. These are slightly red-shifted to 402 and 520 after casting the polymer into a film, indicating that the polymer has a similar conformation in both solution and solid state. However, the optical band gap of **PATA(D)T2BT-8** ($E_g^{opt}$ = 1.89 eV) is higher than that of **PATA(BO)T2BT-8** which can be ascribed to its lower molecular weight.

Polymer **PAA(PU)T2BT-8** with branched alkynyl substituents on anthracene units shows narrower UV-Vis absorption characteristics in chloroform solutions and thin films with a steep slope at long wavelength resulting in an absorption onset in the film state at 655 nm which was hypsochromic shifted by 35 nm comparing to **PATA(BO)T2BT-8**. This has resulted in a wider HOMO-LUMO energy gap of 1.89 eV in comparison to its counterpart polymers. This result suggests that incorporating

arylethynyl groups to the polymer backbone as in the case of polymers **PATA(BO)T2BT-8** and **PATA(D)T2BT-8** will help in delocalising π-electrons to the conjugated side substituents which enlarged the π-conjugation more effectively. As a result, **PAA(PU)T2BT-8** with alkynyl side groups has a lower electronic conjugation compared to **PATA(D)T2BT-8** and **PATA(BO)T2BT-8** resulting in a less effective interchain π-π overlapping leading a higher band gap [21].

As we had anticipated at the introduction of this chapter, using bithiophene spacers between the anthracene units and benzothiadiazole units should help in improving the optical properties of these polymers when compared to polymers synthesised with one thiophene spacers which were discussed in chapter 3. **PATA(BO)T2BT-8**, and **PAA(PU)T2BT-8** have shown lower optical band gap compared to their equivalent polymers **PATA(BO)TBT-8**, and **PAA(PU)TBT-8** while **PATA(D)T2BT-8** has revealed a similar band gap compared to that **PATA(D)TBT-8**. We speculated that polymers presented in this work reveals more extended electronic delocalisation when compared to **PATA(D)TBT-8**, **PATA(BO)TBT-8**, and **PAA(PU)TBT-8** with thiophene spacers due to the incorporation of bithiophene spacers which enhances the intramolecular charge transfer along the backbone of the polymers [7, 18]. This result is in agreement with previous studies conducted in Iraqi group. **PATA(D)T2BT-8**, **PATA(BO)T2BT-8**, and **PAA(PU)T2BT-8** are analogous to two polymers prepared by Iraqi and co-workers (**PPAT2BT-8** and **PTAT2BT-8**) [7, 18]. In **PPAT2BT-8** the anthracene unit was functionalised with 4-dodecyloxybenzene substituents while in **PTAT2BT-8** the anthracene was functionalised with triisopropylsilylacetylene groups. They found that the addition of more thiophene spacer units in these polymers between the anthracene units and benzothiadiazole units increases intramolecular charge transfer along the polymer backbones [18].

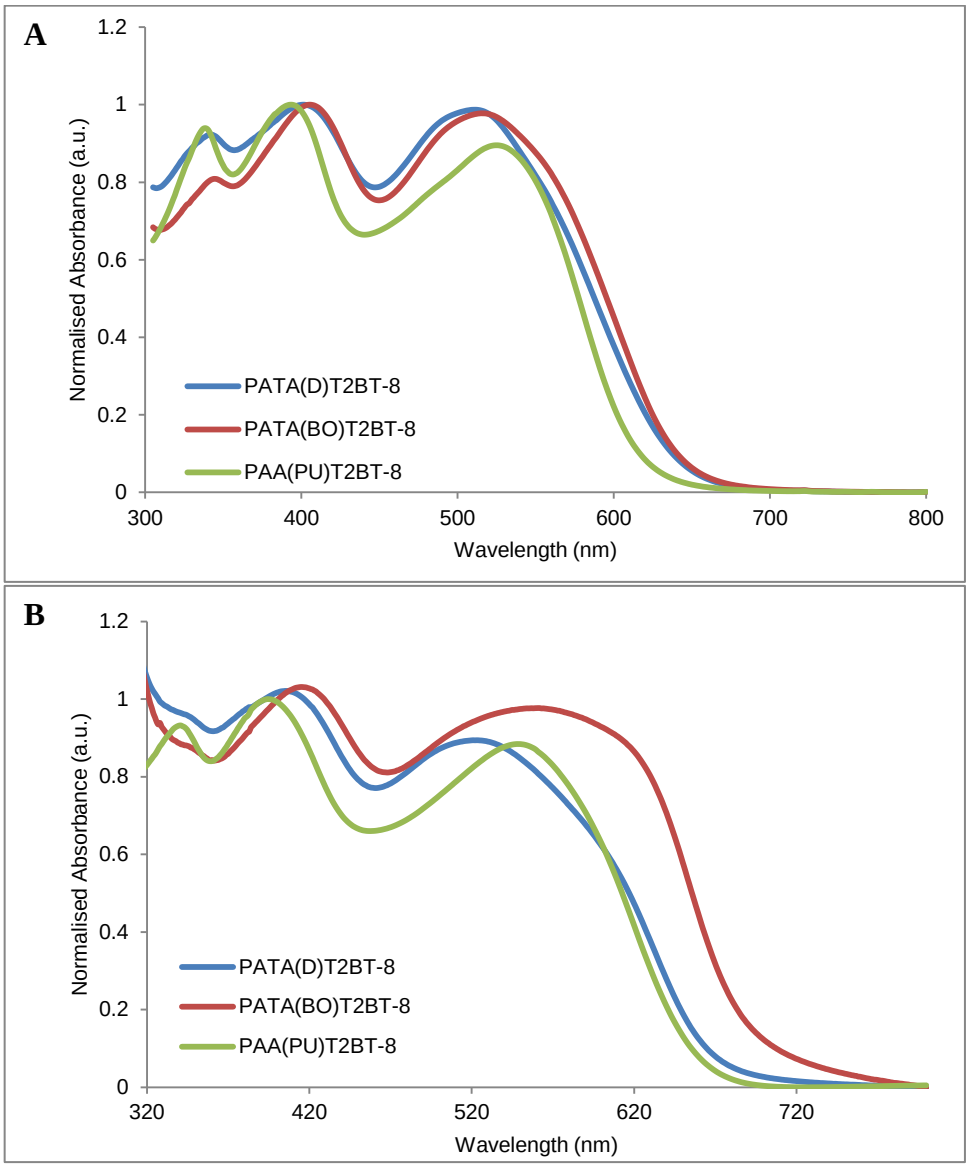


**Figure 4-5:** Normalised UV-Vis absorption spectra of **PATA(D)T2BT-8**, **PATA(BO)T2BT-8** and **PAA(PU)T2BT-8** in : (A) chloroform solutions; and (B) thin films.

### 4.2.5 Electrochemical Characterisation

Cyclic voltammetry studies on polymer films cast onto platinum electrodes, was used to determine the HOMO and LUMO energy levels of the polymers from oxidation and reduction onsets, respectively (**Table 4-3** and **Figure 4-6**). The HOMO/LUMO energy levels of **PATA(D)T2BT-8**, **PATA(BO)T2BT-8**, and **PAA(PU)T2BT-8** were deduced to be –5.36/–3.44 eV, –5.37/–3.44 eV and –5.36/–3.41 eV, respectively.

**Table 4-3:** The energy levels and electrochemical band gaps of the polymers.

| Polymers | HOMO (eV)[a] | LUMO (eV)[b] | $E_g^{elece}$ (eV)[c] |
|---|---|---|---|
| PATA(D)T2BT-8 | –5.36 | –3.44 | 1.92 (±0.04) |
| PATA(BO)T2BT-8 | –5.37 | –3.44 | 1.93 (±0.02) |
| PAA(PU)T2BT-8 | –5.36 | –3.41 | 1.95 (±0.02) |

[a] HOMO position (*vs. vacuum*) determined from onset of oxidation. [b] LUMO position (*vs. vacuum*) determined from onset of reduction. [c] Electrochemical energy gap of the polymers.

All the polymers exhibited shallower HOMO energy levels when compared to those of **PATA(D)TBT-8**, **PATA(BO)TBT-8**, and **PAA(PU)TBT-8** because of enhanced intramolecular charge transfer along the polymer chains [7, 18]. This can be attributed to the incorporation of bithiophene spacer-units between the anthracene unit and benzothiadiazole units instead of one thiophene spacer-units. The bithiophene units are indeed stronger electron donating groups than thiophene units. This result is in agreement with previously reported polymers, **PPAT2BT-8** and **PTAT2BT-8,** by Iraqi and co-workers [7, 18].

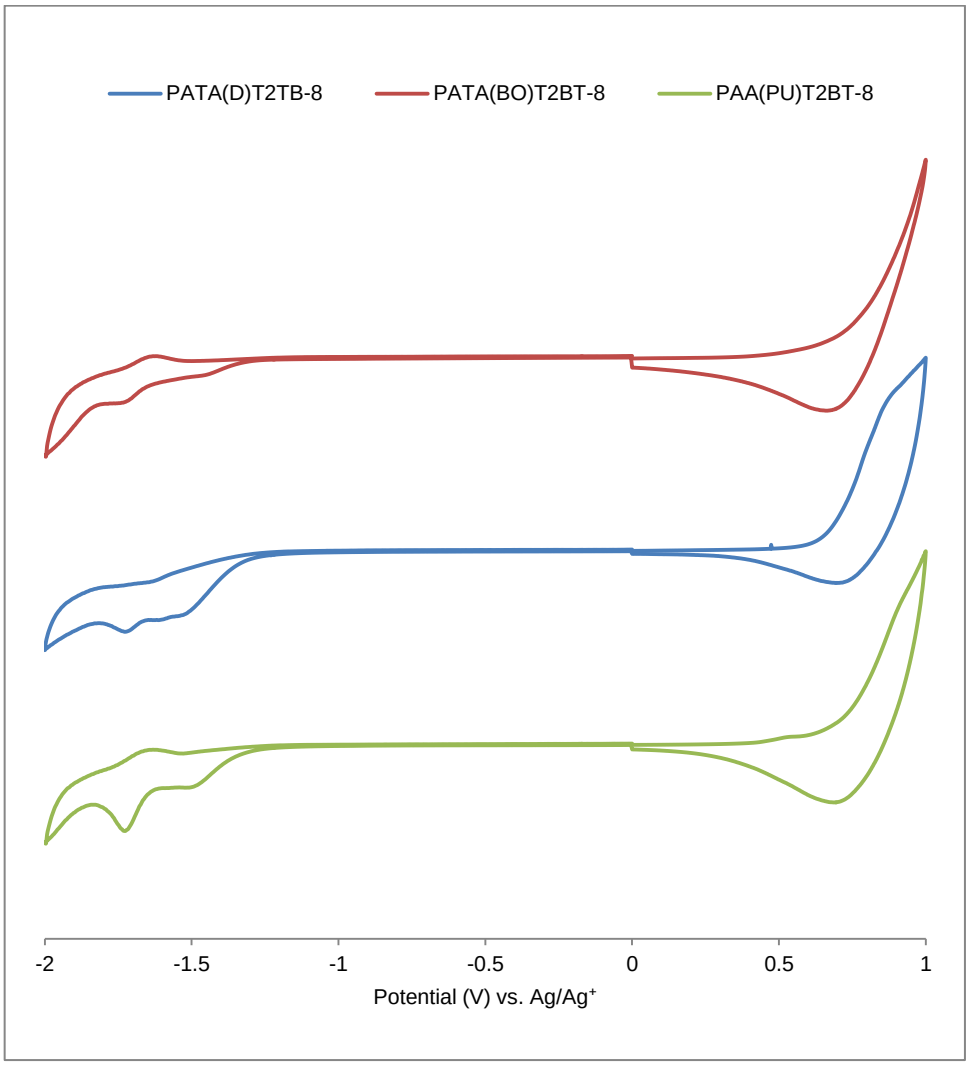


**Figure 4-6:** Cyclic voltammograms of **PATA(D)T2BT-8**, **PATA(BO)T2BT-8** and **PAA(PU)T2BT-8**.

On the other hand, the increase in the molecular weight of **PAA(PU)T2BT-8** in comparison to that of **PAA(PU)TBT-8** resulted in deepening the LUMO energy level for **PAA(PU)T2BT-8** by around 0.32 eV. Previous studies reveals that the LUMO level of a polymer becomes deeper, as the molecular weight of the polymer increases [18, 22]. The other two polymers exhibited comparable LUMO levels with their counterparts polymer **PATA(D)TBT-8** (LUMO level at –3.39 eV) and **PATA(BO)TBT-8** (LUMO level at –3.43 eV). It is worth to mention that, **PPAT2BT-8** synthesised in Iraqi group reveals a LUMO energy level at –3.11 eV which is higher than these polymers [7]. This can be ascribed to the replacement of 4-dodecyloxybenzene groups incorporated into anthracene unit with arylethynyl or alkynyl groups which lead to improved electronic

properties of its counterparts polymers. It is obvious that using acetylene units to connect the alkylthienyl groups and the polymer backbone lead to extended conjugation of the polymer in two dimensions which enhance the resonance effect [18]. This finding agrees with another polymer prepared by the Iraqi group **PTAT2BT-8** using triisopropylsilylacetylene functionalised anthracene units. The polymer displays a LUMO energy level at –3.47 eV, which is very close to its counterpart polymers presented in this work.

### 4.2.6 X-ray Diffraction studies

The packing of copolymer chains in the solid state was studied using powder X-ray diffraction (XRD) technique. As shown in **Figure 4-7**, **PATA(D)T2BT-8**, **PATA(BO)T2BT-8** and **PAA(PU)T2BT-8** displayed broad diffraction peaks at the wide angle region. These peaks are located at 2θ of 20.39° for **PATA(D)T2BT-8**, 21.18$^{o}$ for **PATA(BO)T2BT-8** and 20.86° for **PAA(PU)T2BT-8** correspond to the π-π stacking distances of 4.35, 4.19 and 4.25 Å, respectively, between polymer backbones.

Clearly, these results indicate that these polymers are amorphous. This can be attributed to the sterically demanding octyloxy groups attached to the benzothiadiazole moiety which may disrupt intermolecular interactions and reduce the π-π stacking distances between the polymers chains. The results that we obtained in this project are in agreement to the previous findings by Iraqi and co-workers, where they found that, **PTAT2BT-8** possessed an amorphous structure [18].

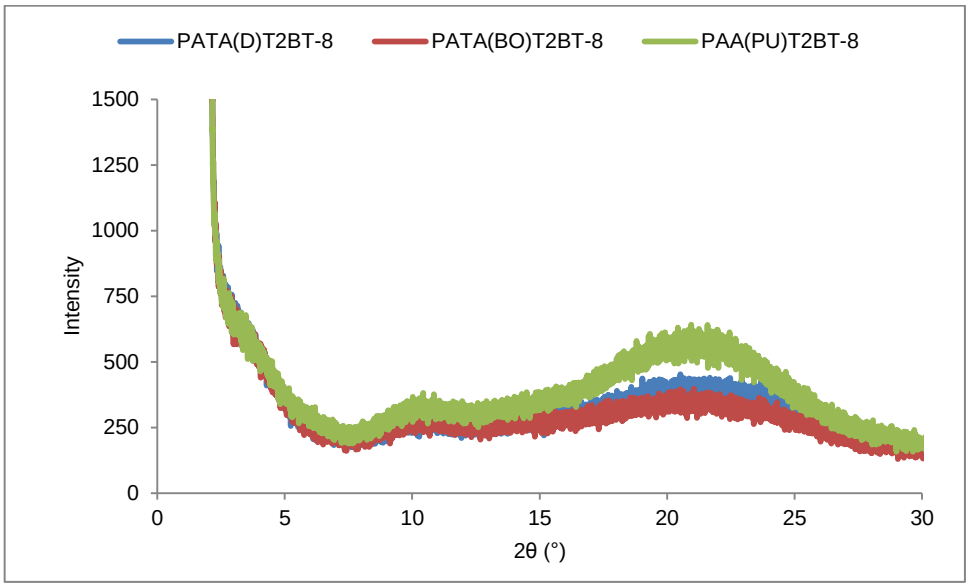


**Figure 4-7:** Powder X-ray diffraction patterns of **PATA(D)T2BT-8**, **PATA(BO)T2BT-8** and **PAA(PU)T2BT-8**.

### 4.2.7 Photovoltaic Device Properties

To explore the photovoltaic properties of polymers **PATA(D)T2BT-8**, **PATA(BO)T2BT-8** and **PAA(PU)T2BT-8**, BHJ polymer solar cells were fabricated with a conventional device configuration glass/ITO/PEDOT:PSS/polymer : $PC_{70}BM$ (1 : 3, w/w) /Ca/Al. The active layer of the corresponding polymers and $PC_{70}BM$ blend was fabricated onto substrates by spin-coated from chlorobenzene solution. A detailed device fabrication method is given in the Experimental section. The *J*–*V* curves of polymers devices are displayed in **Figure 4-8**, and the devices parameters are listed in **Table 4-4**.

By comparing the efficiencies of the devices, the one based on **PATA(D)T2BT-8** and **PAA(PU)T2BT-8** exhibited low performances with PCE of 0.86% and 0.85%, respectively, which can be ascribed to the low $J_{sc}$ and FF. On the other hand, the device based on **PATA(BO)T2BT-8 : $PC_{70}BM$** revealed more than doubled power conversion efficiency (1.80%) as a result of the improvement in the $J_{sc}$ (–4.06 mA $cm^{-2}$) and the FF (55%). We speculate the improvement in $J_{sc}$ and FF of **PATA(BO)T2BT-8** device can be attributed to the formation of an optimal blend film morphology [19], enhanced by

the branching of alkyl chains attached to the thienylethynyl side groups on the 9,10 positions of the anthracene.

**Table 4-4:** Photovoltaic performance of **PATA(D)T2BT-8**, **PATA(BO)T2BT-8** and **PAA(PU)T2BT-8** measured under a simulated photovoltaic light with 1000 $Wm^{-2}$ the illumination (AM 15).

| Polymer | Polymer : $PC_{71}BM$[a] (w/w) | Solvent | $J_{sc}$ (mA $cm^{-2}$) | $V_{oc}$ (V) | FF (%) | PCE (%) |
|---|---|---|---|---|---|---|
| PATA(D)T2BT-8 | 1 : 3 | CB[b] | –2.82 | 0.78 | 39 | 0.86 |
| PATA(BO)T2BT-8 | 1 : 3 | CB | –4.06 | 0.80 | 55 | 1.80 |
| PAA(PU)T2BT-8 | 1 : 3 | CB | –3.61 | 0.79 | 30 | 0.85 |

[a] Polymer : $PC_{71}BM$ weight ratio. [b] chlorobenzene.

**PATA(D)T2BT-8** and **PATA(BO)T2BT-8** devices have lower $V_{oc}$ values relative to their corresponding polymers **PATA(D)TBT-8** and **PATA(BO)TBT-8**, discussed in chapter 4, due to their shallower HOMO levels. **PATA(D)T2BT-8** device revealed a similar performance as its counterpart **PATA(D)TBT-8** device as a result of its low $J_{sc}$ value. On the other hand, **PATA(BO)T2BT-8** displayed the best performance of the devices due to the improvement in its $J_{sc}$ and the FF values. All the polymer devices showed a quite low $J_{sc}$ values with best short circuit current recorded for **PATA(BO)T2BT-8**. This fluctuation in $J_{sc}$ values of the different polymers devices can be affected by a variety of factors including crystallinity, charge carrier mobility, D-A heterojunction morphologies and the amount of photon absorbed by the blending layer [23]. Polymers **PPAT2BT-8** and **PTAT2BT-8** prepared previously in Iraqi group revealed PCEs of 4.17 and 3.15% [7, 18]. These relatively higher efficiencies resulted from the higher $J_{sc}$ and FF values for **PPAT2BT-8** and **PTAT2BT-8** relative to their analogues **PATA(BO)T2BT-8** and **PATA(D)T2BT-8**. However, further studies are required to examine the effect of the morphologies on the performance of these polymers as only one set of devices with polymer:PCBM weight ratios of 1:3 were prepared.

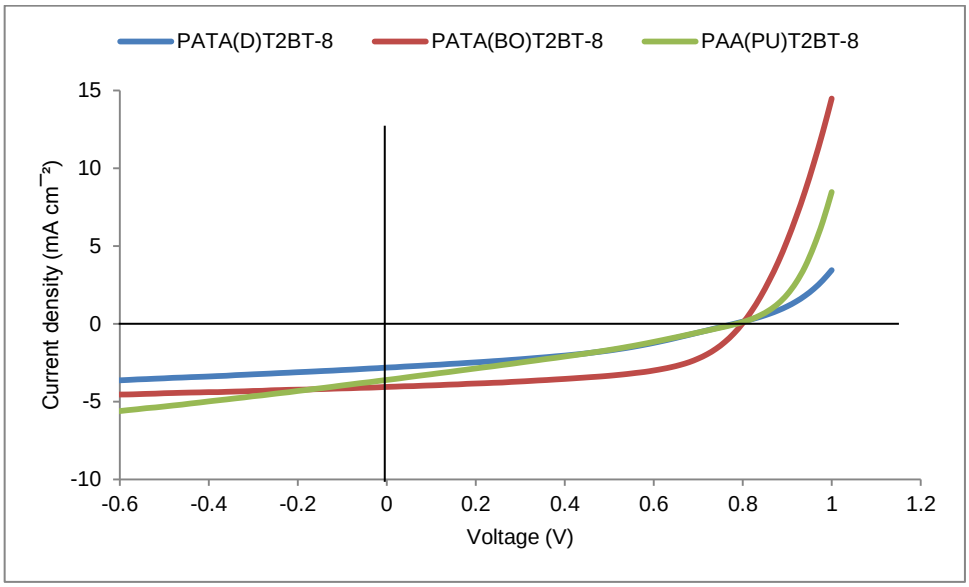


**Figure 4-8:** *J-V* characteristic curve of the organic solar cell device fabricated from **PATA(D)T2BT-8**, **PATA(BO)T2BT-8** and **PAA(PU)T2BT-8**.

## 4.3 Summary

In summary, we designed and synthesised a series of conjugated polymers based on 2,6-linked anthracene flanked by dithienyl groups as donor units and benzo[c]-[1,2,5]thiadiazole as acceptor units using the Stille coupling polymerisation. All the polymers exhibited a high solubility in chlorinated organic solvents such as chloroform and chlorobenzene. Introduction of bithiophene spacers between the anthracene units and benzothiadiazole units help to improve the optical properties of the resulting polymers when compared to polymers with single thiophene spacers., As expected, these polymers displayed shallower HOMO energy levels when compared to their counterparts polymers with single thiophene spacers owing to the enhanced electron donationg properties of bithiophene spacers *vs.* single thiophene spacers. This as a result leads to a stronger intramolecular charge transfer along the polymer chains. Powder X-ray diffraction studies indicate that these polymers are amorphous. Photovoltaic devices using polymer **PATA(BO)T2BT-8** exhibited a higher $J_{sc}$ value than that of **PATA(D)T2BT-8** and **PAA(PU)T2BT-8**. They also showed a relatively similar $V_{oc}$ values due to the similarity into their HOMO energy levels.

**PATA(D)T2BT-8** and **PAA(PU)T2BT-8** devices have low PCEs values than that of **PATA(BO)T2BT-8** as a result of their lower $J_{sc}$ and FF values.

## 4.4 Experimental Section:

### 4.4.1 Materials:

Unless otherwise stated, all chemicals, reagents and solvents were obtained from commercial sources (Sigma-Aldrich, Fisher, Acros Organics and Alfa Aesar) in the highest purities possible and used as received. Regent grade solvents were purchased from the internal stores which were used for some reactions, extraction, recrystallization and chromatography. However, most of the reactions were carried out using anhydrous solvents which were obtained from the Grubbs solvent system within the chemistry department. Acids, bases, drying agents and salts were obtained from the internal stores. Reactions proceeded under an argon atmosphere as standard unless stated otherwise. Column chromatography was carried out on silica gel (200-300 mesh) or alumina as stated.

### 4.4.2 Analytical Techniques:

Elemental analyses were analysed by using the Perkin Elmer 2400 CHN Elemental Analyser for CHN analysis, and the Schoniger oxygen flask combustion method for sulphur and halides. In both methods, the weights submitted for the analysis were 10 mg. Fourier transform infrared spectroscopy (FTIR) and attenuated total reflectance (ATR) were recorded on a Perkin Elmer Spectrum 65 spectroscopy.

$^{13}C$ and $^{1}H$-NMR spectra of the monomers were recorded on Bruker AV 250 (250 MHz), and Bruker AV 400 (400 MHz) NMR spectrometers at room temperature in chloroform-d ($CDCl_3$) solution. NMR spectra of the polymers were recorded using Bruker Avance III HD 500 (500 MHz) at 100 °C in 1,1,2,2-tetrachloroethane-d2 solution. As an internal standard, tetramethylsilane (TMS) was used for calibrating chemical shifts (δ). The chemical shifts were measured in part per million (ppm), while the coupling constant (*J*) were given in Hertz (Hz).

GC-MS spectra were recorded on Perkin Elmer Turbomass Mass Spectrometer equipped with a Perkin Elmer Autosystem XL Gas Chromatograph. Mass spectra were obtained by the electron impact method (EI) and MALDI-TOF mass spectrometry.

GPC analysis were recorded on the equipment consisted of a Viscotek $GPC_{max}$ VE 2001 GPC solvent/sample module, a Waters 410 Differential Refractometer and a PLgel 5 μm Mixed Column (650 mm set length) using chloroform as the eluent at rate of 1 mL/min. Polymer samples were made up as a solutions in chloroform (2 mg/mL) spiked with toluene as a reference. The RI-detection method was used to obtain the GPC curves, which was calibrated with a series of polystyrene narrow standards. Degree of polymerisation (DP) was calculated using the below equation:

$$\chi_n = \frac{M_n}{M_R}$$

where $\chi_n$ is the DP, $M_n$ is the number average molecular weight of the polymer and $M_R$ is the molecular mass of the repeat unit of the polymer. Perkin Elmer TGA-7 Thermogravimetric Analyser was used to determine TGA curves at a scan rate of 10 °C/minute under nitrogen atmosphere.

Powder X-ray diffraction were conducted on a Bruker D8 advance diffractometer with a CuKα radiation source (1.5418 A, rated as 1.6 kW). The scanning angle was recorded over the range 2–30°.

Hitachi U-2010 Double Beam UV-Visible Spectrophotometer has been used to evaluate the optical properties of the polymers. The absorbance of the polymers was measured in a solution of chloroform at room temperature using quartz cuvette ($l$ = 10 mm). Thin films of the polymers were prepared by dip coating quartz plates into around 1 mg/mL solutions in chloroform, then dried in the air and the UV-Vis absorption spectra measurements were run at room temperature.

Cyclic voltammograms were conducted using Princeton Applied Research Model 263A Potentiostat/Galvanostat. The analyses were recorded under Argon protection at

approximately room temperature. A three electrode system was used for the measurements consisting of an $Ag/Ag^+$ reference electrode (Ag wire in 0.01 *M* $AgNO_3$ solution in the electrolyte solution), a Pt working electrode, and Pt counter electrode (Pt wire). Measurements were done in tetrabutylammonium perchlorate acetonitrile solution (0.1 *M*) on polymer thin films which made by drop casting polymer solution onto the working electrode which were left to dry in air. The energy level of $Fc/Fc^+$ was assumed at –4.8 eV to vacuum. The half-wave potential of Fc/Fc+ redox couple was found to be 0.08 V *vs*. $Ag/Ag^+$ reference electrode. the HOMO and LUMO energy level were calculated using the following equations:

$$E_{LUMO} = -[(E_{red,onset} - E_{1/2(ferrocene)}) + 4.8] \text{ eV}$$

$$E_{HOMO} = -[(E_{ox,onset} - E_{1/2(ferrocene)}) + 4.8] \text{ eV}$$

where $E_{red,onset}$ and $E_{ox,onset}$ are the onset of reduction and oxidation, respectively, relative to $Ag/Ag^+$ reference electrode.

### 4.4.3 Fabrication and testing of polymer solar cells:

The polymers and $PC_{70}BM$ were mixed at (1:3) polymer : fullerene blending ratio and were dissolved in CB. The solutions were then put on a hotplate held at 50 °C overnight with stirring to allow dissolution. Photovoltaic devices were fabricated onto pre-patterned ITO glass substrate (20 Ohms per square) that were supplied by Ossila Limited. The ITO/glass substrates were cleaned by sonication in $NaOH_{(aq)}$ followed by IPA. A 30 nm thick PEDOT:PSS layer was spin-coated onto the ITO substrates. These were then transferred to a hot plate held at a temperature of 120 °C for 5 min. In a glove-box, the active layer was spin cast onto the glass/ITO/PEDOT:PSS substrates, which were then transferred into a thermal evaporator for deposition of OPV cathode (5 nm of calcium capped by a 100 nm of aluminium evaporated at a base pressure of $\sim 10^{-7}$ mbar). PCEs were measured using a Newport 92251A-1000 AM 1.5 solar simulator. An NREL calibrated silicon cell was used to calibrate the power output to 100 mW $cm^{-2}$ at 25 °C. An aperture mask having an area of 2.06 $mm^2$ was placed over devices to define the test area.

## 4.5 Synthesis of Monomers and Polymers:

The synthesis procedures of 2,6-linked anthracene monomers, **M1**, **M2**, and **M3** were given already in chapter 2.

### 4.5.1 Synthesis of 2,2'-bithiophen-5-yl(trimethyl)stannane (17): [17, 24]

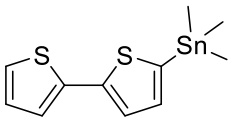


In a two-neck round bottom flask, *n*-BuLi (2.5 M in hexane, 20.8 ml, 0.052 mol) was added to a solution of bithiophene (8.64 g, 0.052 mol) dissolved in 50 ml anhydrous THF at –78 °C. After stirring for 90 minutes at –78 °C, the mixture was returned to the room temperature and stirred for extra 30 minutes. Then, trimethyltin chloride (0.1M in THF, 61 mL, 0.062 mol) was added dropwise to the mixture at –78°C. The mixture was stirred overnight at room temperature and then terminated by adding saturated $NH_4Cl_{(aq)}$. The organic layer was washed with water and extracted with DCM. After removing the solvent, the product was collected as a brown oil which has been used in the following procedure without further purification. (13.97 g, 89 %).

### 4.5.2 Synthesis of 4,7-di(2,2'-bithiophen-5-yl)-5,6-bis(octyloxy)benzo[c] [1,2,5]thiadiazole (18): [17]

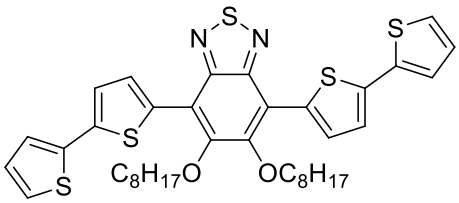


To a solution of 4,7-dibromo-5,6-bis(octyloxy)nenzo[c][1,2,5]thiadiazole (1.41 g, 0.0026 mol), $Pd(OAc)_2$ ($9.4 \times 10^{-3}$ g, $4.25 \times 10^{-5}$ mol) and tri(o-tolyl)phosphine (0.025 g, $8.4 \times 10^{-5}$ mol) in dry toluene (20 mL) was added 2,2'-bithiophen-5-yl(trimethyl)stannane (2.2 g, $6.6 \times 10^{-3}$ mol), and the reaction mixture was refluxed for

24 hours under argon. The solvent was evaporated and the resulting product was purified on a silica gel column chromatography eluting with DCM/petroleum ether (gradient DCM 1-3%) to afford the product as dark orange solid (2.3 g, 57%). $^{1}$H NMR (400 MHz, *CDCl$_3$*) $\delta_H$/ppm: 8.53 (d, *J* = 4.0, 2H), 7.32 (d, *J* = 3.6, 4H), 7.29 (d, *J* = 1.0 Hz, 2H), 7.09 (dd, *J* = 3.6, 1.5 Hz, 2H) 4.20 (t, *J* = 7.05 Hz, 4H), 2.04-1.97 (m, 4H), 1.56-1.48 (m, 4H), 1.43-1.25 (m, 16H), 0.91 (t, *J* = 6.84, 6H). $^{13}$C NMR (400 MHz, *CDCl$_3$*) $\delta_C$/ppm: 151.61, 150.80, 138.87, 137.59, 133.16, 131.64, 127.96, 124.65, 123.75, 123.58, 117.29, 74.55, 31.86, 10.47, 29.60, 29.35, 26.09, 22.71, 14.14. Elemental Analysis (%) calculated for: C, 63.30; H, 6.15; N, 3.88; S, 22.23. Found: C, 63.27; H, 6.04; N, 3.80; S, 22.02. Mass (MALDI-TOF); (*m/z*): 721 ($M^+$). FT-IR ($cm^{-1}$): 3178-3081 (aromatic C–H stretch), 2957-2859 (aliphatic C–H stretch), 1558 and 1464 (C=C stretch), 1282 and 1022 (C–O–R stretch), 772 ($CH_2$ bending).

### 4.5.3 Synthesis of 4,7-di(5-bromo-[2,2']-bithiophen-5-yl)-5,6-bis(octyloxy) benzo[c][1,2 ,5]-thiadiazole (19):[17]

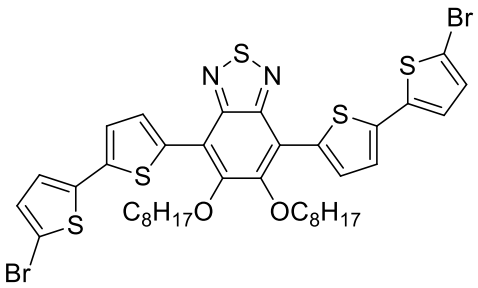


A mixture of 4,7-di(2,2'-bithiophen-5-yl)-5,6-bis(octyloxy)benzo[c][1,2,5]-thiadiazole (0.77 g, 1.06 × $10^{-3}$ mol), *n*-bromosuccinimide (NBS) (0.37 g, 2.1 × $10^{-3}$ mol), chlorobenzene (25 mL) was stirred at 55 °C for 3 hours under light protection, then heated to 100 °C for 20 minutes. After completing the reaction, solvent was evaporated and the residue was purified on a silica gel column chromatography eluting with DCM/hexane (gradient DCM 1-3%) to afford the product as red crystals (0.92 g, 98%). $^{1}$H NMR (400 MHz, *CDCl$_3$*) $\delta_H$/ppm: 8.52 (d, *J* = 3.90, 2H), 7.25 (d, *J* = 4.14, 2H), 7.04 (m, 4H) 4.18 (t, *J* = 6.87 Hz, 4H), 2.02-1.95 (m, 4H), 1.55-1.47 (m, 4H) 1.43-1.26 (m, 16H), 0.91 (t, *J* = 6.60 Hz, 6H). $^{13}$C NMR (400 MHz, *CDCl$_3$*) $\delta_C$/ppm: 151.64, 150.67, 139.07, 137.78, 133.56, 131.68, 130.78, 123.76, 117.22, 111.26, 74.59, 31.86,

30.45, 29.58, 29.35, 26.08, 22.72, 14.14. Elemental Analysis (%) calculated for $C_{38}H_{42}Br_2N_2O_2S_5$: C, 51.93; H, 4.82; N, 3.19; Br, 18.18; S, 18.24. Found: C, 52.16; H, 4.83; N, 3.23; Br, 18.37; S, 18.00. Mass (MALDI-TOF); (*m/z*): 878 ($M^+$). FT-IR ($cm^{-1}$): 3178-3072 (aromatic C–H stretch), 2948-2850 (aliphatic C–H stretch), 1559 and 1463 (C=C stretch), 1282 and 1022 (C–O–R stretch), 791 (C–Br stretch).

### 4.5.4 Synthesis of 4,7-bis(5-(tributylstannyl)-[2,2']-bithiophen-5-yl)-5,6-bis (octyloxy)benzo[c][1,2,5]-thiadiazole (M6): [25]

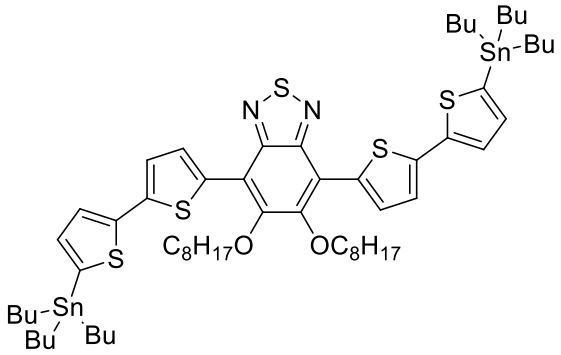


4,7-Bis(5-bromo-[2,2']-bithiophen-5-yl)-5,6-bis(octyloxy)benzo[c][1,2,5]-thiadiazole (0.20 g, $2.26 \times 10^{-4}$ mol) was dissolved in dry THF (30 mL) under argon atmosphere. Subsequently, *n*-BuLi (1.6 M, 0.57 mL, $9.1 \times 10^{-4}$ mol, in hexane) was added dropwise to the reaction mixture at –78 °C. The mixture was stirred for 5 hours at –78 °C. To this, tributyltin chloride (0.28 mL, $1.01 \times 10^{-3}$ mol) was added to the reaction mixture and allowed to stir at –78 °C overnight. The mixture was poured into $H_2O$ and extracted with diethyl ether. The organic layer was extracted three times with $H_2O$, dried over $MgSO_4$ and solvent removed to give a dark brown oil product (0.28 g, 95%). $^1$H NMR (400 MHz, *CDCl*$_3$) $\delta_H$/ppm: 8.53 (d, *J* = 4.0 Hz, 2H), 7.44 (d, *J* = 3.5 Hz, 2H), 7.32 (d, *J* = 4.0 Hz, 2H), 7.14 (d, *J* = 3.36 Hz, 2H), 4.18 (t, *J* = 7.05 Hz, 4H), 2.04-1.97 (m, 4H), 1.78-1.58 (m, ), 1.48-1.28 (m, H), 1.16 (t, *J* = 8.05 Hz, H), 0.94 (t, *J* = 7.4, 6H), 0.45 (s, 18H). $^{13}$C NMR (400 MHz, *CDCl*$_3$) $\delta_C$/ppm: 151.52, 150.87, 142.90, 139.16, 137.17, 136.24, 132.83, 131.64, 124.93, 123.34, 117.3174.51, 31.86, 30.46, 29.59, 29.34, 28.98, 27.97, 27.86, 27.74, 27.29, 27.19, 26.87, 26.08, 22.70, 17.54, 14.14, 13.70, 13.63, 10.91. Elemental analysis (%) calculated for $C_{62}H_{96}N_2O_2S_5Sn_2$: C, 57.32; H,

7.45; N, 2.16; S, 12.34. Found: C, 54.38; H, 7.90; N, 1.56; S, 10.50. Mass (MALDI-TOF); (*m/z*): 1299 ($M^+$). FT-IR ($cm^{-1}$): 3078 (aromatic C–H stretch), 2958-2851 (aliphatic C–H stretch), 1560 and 1468 (C=C stretch), 1285 and 1021 (C–O–R stretch), 734 ($CH_2$ bending), 533 and 516 (C–Sn stretch).

### 4.5.5 Poly[9,10-bis[2-ethynyl-5-dodcylthiophene]-anthracene-2,6-diyl-alt-5,6-bis(octyloxy)-4,7-Di(2.2'-bithiophen-5-yl)benzo[c][1,2,5]-thiadiazole](PATA(D)T2BT-8): [19, 26, 27]

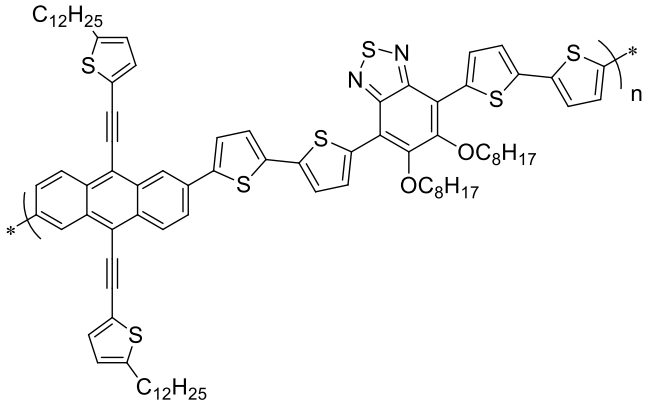


4,7-bis(5-(tributylstannyl)-[2,2']-bithiophen-5-yl)-5,6-bis(octyloxy)benzo[c] [1,2,5]-thiadiazole (**M6**) (176 mg, 0.14 × $10^{-3}$ mol) was weighed into a dry 100 mL round-bottom flask. 2,6-dibromo-9,10-bis[2-ethynyl-5-dodcylthiophene]anthracene (**M1**) (120 mg, 0.14 × $10^{-3}$ mol), (*o*-tolyl)$_3$P (6.0 mg, 0.020 × $10^{-3}$ mol) and $Pd(OAc)_2$ (2.2 mg, 0.010 × $10^{-3}$ mol) were added. The flask was subjected to several cycles of vacuum followed by refilling with argon gas. Then, dry toluene (10 mL) were added and degassed again. The polymerization was carried out at 100 °C for 24 hour under argon protection. The mixture was cooled to room temperature and 2-(tributylstannyl) thiophene (0.30 mL) was added. The mixture was degassed and heated at 100 °C for 1 hour. The mixture was cooled to room temperature and 2-bromothiophene (0.30 mL mg) was added, degassed and heated to 100 °C for 1 hours. The reaction cooled to room temperature and the raw product was precipitated into methanol and collected by filtration. The resulting solid was purified using Soxhlet extraction with solvents in the order; methanol (250 mL), acetone (250 mL), hexane (250 mL), chloroform (250 mL) and chlorobenzene (250 mL). The chloroform fraction was concentrated (≈ 50 mL) and then poured into methanol (500 mL). The resulting mixture was stirred overnight and

the solid was collected by filtration through a membrane filter to yield a red powder (129 mg, 66%).

GPC (TCB): $M_w$ = 13400, $M_n$ = 7200, PD = 2.75. $^1$HNMR ($C_2D_2Cl_4$): ($\delta_H$/ppm) 8.79–8.32 (bm, 6H); 7.86 (bs, 2H); 7.56-7.00 (bm, 8H); 6.80 (bs, 2H); 4.25-4.09 (bm, 4H); 2.93-2.80 (bd, 4H); 2.03-1.90 (bm, 4H); 1.82-1.70 (bm, 4H); 1.56-1.02(bm, 56H); 0.92-0.74 (bs, 12). Elemental analysis (%) calculated for $C_{88}H_{104}N_2O_2S_7$: C, 73.08; H, 7.25; N, 1.94; S, 15.52. Found: C, 71.76; H, 7.11; N, 1.43; S, 13.20. FT-IR ($cm^{-1}$): 3065 (aromatic C–H stretch), 2951-2851 (aliphatic C–H stretch), 2186 (carbon, carbon triple bond stretch), 1613 (aromatic C=C stretch), 1458 (C–H bending aliphatic), 1224 (C–O stretch), 724 ($CH_2$ bending).

### 4.5.6 Poly[9,10-bis[2-(ethynyl-5-butyl-octyl)thiophene]-anthracene-2,6-diyl-alt-5,6-bis(octyloxy)-4,7-Di(2,2'-bithiophen-5-yl)benzo[c][1,2,5]-thiadiazole] (PATA(BO) T2BT-8):[19, 26, 27]

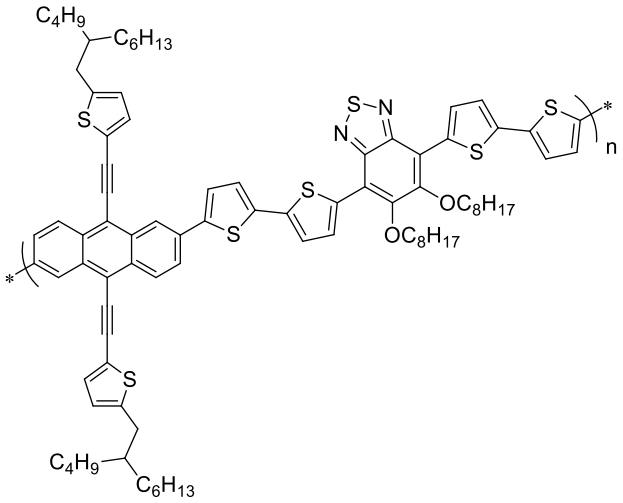


(**PATA(BO)T2BT-8**) was prepared following a procedure similar to (**PATA(D)T2BT-8**) from monomer 4,7-bis(5-(tributylstannyl)-[2,2']-bithiophen-5-yl)-5,6-bis(octyloxy) benzo[c][1,2,5]-thiadiazole (**M6**) (176 mg, 0.14 × $10^{-3}$ mol), 2,6-dibromo-9,10-bis[2-(ethynyl-5-butyl-octyl)thiophene]anthracene (**M2**) (120 mg, 0.14 × $10^{-3}$ mol), (*o*-tolyl)$_3$P (6.0 mg, 0.020 × $10^{-3}$ mol) and Pd(OAc)$_2$ (2.2 mg, 0.010 × $10^{-3}$ mol. The product was collected form toluene fraction as purple solid. Yield: 114 mg. (58%). GPC (TCB): $M_w$ = 25900, $M_n$ = 9700, PD = 2.7. $^1$HNMR ($C_2D_2Cl_4$): ($\delta_H$/ppm) 8.80–

8.37 (bm, 6H); 7.89 (bs, 2H); 7.57–7.05 (bm, 8H); 6.80 (bs, 2H); 4.21(bt, 4H); 2.93-2.80 (bd, 4H); 2.05-1.92 (bm, 4H)1.77-1.65 (bm, 4H); 1.56-1.02(bm, 56H); 0.96-0.72 (bs, 12). Elemental analysis (%) calculated for $C_{88}H_{104}N_2O_2S_7$: C, 73.08; H, 7.25; N, 1.94; S, 15.52. Found: C, 71.09; H, 7.11; N, 1.58; S, 12.62. FT-IR ($cm^{-1}$): 3062 (aromatic C–H stretch), 2951-2851 (aliphatic C–H stretch), 2179 (carbon, carbon triple bond stretch), 1613 (aromatic C=C stretch), 1455 (C–H bending aliphatic), 1258 (C–O stretch), 720 ($CH_2$ bending).

### 4.5.7 Poly[9,10-di-(3-pentylundec-1-yne)-anthracene-2,6diyl-alt-5,6-bis (octyloxy)-4,7-Di(2,2'-bithiophen-5-yl)benzo[c][1,2,5]-thiadiazole] (PAA-(PU)T2BT-8): [19, 26, 27]

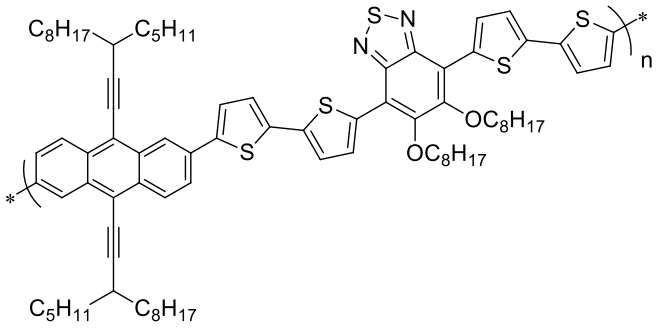


(**PAA(PU)T2BT-8**) was prepared following a procedure similar to (**PATA(D)T2BT-8**) from monomer 4,7-bis(5-(tributylstannyl)-[2,2']-bithiophen-5-yl)-5,6-bis(octyloxy) benzo[c][1,2,5]-thiadiazole (**M6**) (0.15 g, $0.12 \times 10^{-3}$ mol), 2,6-dibromo-9,10-di-(3-pentylundec-1-yne)-anthracene (M3) (0.092 g, $0.12 \times 10^{-3}$ mol), (*o*-tolyl)$_3$P (5.8 mg, $0.019 \times 10^{-3}$ mol) and $Pd(OAc)_2$ (2.1 mg, $0.010 \times 10^{-3}$ mol. The product was collected form toluene fraction. Yield: 98 mg. (61%). GPC (TCB): $M_w$ = 13800, $M_n$ = 8150, PD = 2.9. $^1$HNMR ($CDCl_3$): ($\delta_H$/ppm): 8. 83 (bs, 2H), 8.61-8.53 (bm, 4H), 7.86 (bm, 2H), 7.42–7.16 (bm, 6H) 4.27-4.16 (bm, 4H); 3.03-2.90 (bm, 2H); 2.10-1.98 (bm, 4H); 1.52-1.13 (bm, 64H); 1.02-0.72 (bm, 18H). Elemental analysis (%) calculated for $C_{76}H_{90}N_2O_2S_5$: C, 74.59; H, 7.41; N, 2.29; S, 13.10. Found: C, 73.79; H, 7.96; N, 1.68; S, 10.31. FT-IR ($cm^{-1}$): 3069 (aromatic C–H stretch), 2951-2854 (aliphatic C–H stretch), 2207 (carbon, carbon triple bond stretch), 1615 (aromatic C=C stretch), 1464 (C–H bending aliphatic), 1260 (C–O stretch), 723 ($CH_2$ bending).

## 4.6 References:


1. B. C. Thompson and J. M. Frechet, *Angew. Chem. Int. Ed.*, 2008, **47**, 58-77.
2. J. Zaumseil and H. Sirringhaus, *Chem. Rev.*, 2007, **107**, 1296-1323.
3. J. Żmija and M. Małachowski, *Arch. Mater. Sci. Eng.*, 2009, **40**, 5-12.
4. Y. Li, *Acc. Chem. Res.*, 2012, **45**, 723-733.
5. A. Facchetti, *Chem. Mater.*, 2010, **23**, 733-758.
6. K. Lu, J. Fang, H. Yan, X. Zhu, Y. Yi and Z. Wei, *Org. Electron.*, 2013, **14**, 2652-2661.
7. A. Abdulaziz, *Chem. Commun.*, 2013, **49**, 2252-2254.
8. C. Liu, W. Cai, X. Guan, C. Duan, Q. Xue, L. Ying, F. Huang and Y. Cao, *Polym. Chem.*, 2013, **4**, 3949-3958.
9. J. B. Lee, K. H. Kim, C. S. Hong and D. H. Choi, *J. Polym. Sci. Part A: Polym. Chem.*, 2012, **50**, 2809-2818.
10. H.-Y. Chen, C.-T. Chen and C.-T. Chen, *Macromolecules*, 2010, **43**, 3613-3623.
11. W. Cui, Y. Zhao, H. Tian, Z. Xie, Y. Geng and F. Wang, *Macromolecules*, 2009, **42**, 8021-8027.
12. J. Sun, J. Chen, J. Zou, S. Ren, H. Zhong, D. Zeng, J. Du, E. Xu and Q. Fang, *Polymer*, 2008, **49**, 2282-2287.
13. P. Hodge, G. A. Power and M. Rabjohns, *Chem. Commun.*, 1997, 73-74.
14. N. Blouin, A. Michaud and M. Leclerc, *Adv. Mater.*, 2007, **19**, 2295-2300.
15. W. Li, R. Qin, Y. Zhou, M. Andersson, F. Li, C. Zhang, B. Li, Z. Liu, Z. Bo and F. Zhang, *Polymer*, 2010, **51**, 3031-3038.
16. C.-C. Chiu, H.-C. Wu, C. Lu, J.-Y. Chen and W.-C. Chen, *Polym. Chem.*, 2015, **6**, 3660-3670.
17. H. Yi, S. Al-Faifi, A. Iraqi, D. C. Watters, J. Kingsley and D. G. Lidzey, *J. Mater. Chem.*, 2011, **21**, 13649-13656.
18. L. Cartwright, L. J. Taylor, H. Yi, A. Iraqi, Y. Zhang, N. W. Scarratt, T. Wang and D. G. Lidzey, *RSC Advances*, 2015, **5**, 101607-101615.
19. D. Gedefaw, M. Tessarolo, W. Zhuang, R. Kroon, E. Wang, M. Bolognesi, M. Seri, M. Muccini and M. R. Andersson, *Polym. Chem.*, 2014, **5**, 2083-2093.

20. X. Wang, Y. Sun, S. Chen, X. Guo, M. Zhang, X. Li, Y. Li and H. Wang, *Macromolecules*, 2012, **45**, 1208-1216.
21. L. Ye, S. Zhang, L. Huo, M. Zhang and J. Hou, *Acc. Chem. Res.*, 2014, **47**, 1595-1603.
22. B. G. Kim, X. Ma, C. Chen, Y. Ie, E. W. Coir, H. Hashemi, Y. Aso, P. F. Green, J. Kieffer and J. Kim, *Adv. Funct. Mater.*, 2013, **23**, 439-445.
23. J.-H. Kim, J. B. Park, F. Xu, D. Kim, J. Kwak, A. C. Grimsdale and D.-H. Hwang, *Energy Environ. Sci.*, 2014, **7**, 4118-4131.
24. Z. B. Henson, P. Zalar, X. Chen, G. C. Welch, T.-Q. Nguyen and G. C. Bazan, *J. Mater. Chem. A*, 2013, **1**, 11117-11120.
25. H. A. Saadeh, L. Lu, F. He, J. E. Bullock, W. Wang, B. Carsten and L. Yu, *ACS Macro Lett.*, 2012, **1**, 361-365.
26. X. Guo, H. Xin, F. S. Kim, A. D. Liyanage, S. A. Jenekhe and M. D. Watson, *Macromolecules*, 2010, **44**, 269-277.
27. M. Helgesen, S. A. Gevorgyan, F. C. Krebs and R. A. Janssen, *Chem. Mater.*, 2009, **21**, 4669-4675.

# Chapter 5

## *Synthesis And Properties of 2,6-Linked Anthracene And Thieno[3,4-c]pyrrole-4,6-dione Copolymers*

# Chapter 5

## 5.1 Introduction

Because of their good processability, optoelectronic properties, and flexible fabrication methods into large area devices using solution processing, organic conjugated polymers have been extensively investigated over last few decades by the research community. The active layer of organic solar cells is commonly constituted of a nanoscale bicontinuous interpenetrating network of organic conjugated materials as electron rich materials and fullerene derivatives as electron deficient materials [1]. In order to obtain highly efficient organic solar cells, it is curial to design and synthesise organic conjugated polymers with low HOMO and LUMO energy levels, low optical band gaps and high electron and hole mobilities [2]. The recent trend in designing conjugated materials for organic solar cells applications tend to combine alternating electron rich and electron deficient units along polymer backbones in a so-called donor-acceptor (D–A) arrangement. The alternation of the donor and acceptor moieties can promote intramolecular charge transfer along the polymer chain and control the HOMO-LUMO energy levels resulting in low band gap polymers. Furthermore, using this approach can increase the $J_{sc}$ by increasing the light absorption in the UV–visible range [3, 4].

Thieno[3,4-*c*]pyrrole-4,6-dione (TPD) is widely used as an electron acceptor unit introduced in D–A polymers because of its strong electron withdrawing ability which is attributed to its imide group [5, 6]. Moreover, the TPD repeat unit is a simple, symmetrical and highly planar moiety that could improve electron delocalisation and hence increases interchain interactions, enhancing their hole mobility [3, 5]. So far, TPD-based polymers have been investigated by different research groups for use in photovoltaic applications [5, 7, 8] with device efficiencies which have reached up to 8% [9].

Synthesis of organic conjugated materials is often linked to the use of coupling reactions such as Stille coupling, Suzuki coupling and Sonogashira coupling reactions [10]. Such reactions involve expensive and sometimes toxic organometallic reagents as well as the need for numerous synthetic steps to prepare the final monomers. Recently,

a new synthetic method termed direct (hetero)arylation reaction has been used for the formation of C–C bonds using (hetero)aryl halides and (hetero)arenes without the need for organometallic intermediates. This new synthetic method, minimizes the problems associated with removal of byproducts compared to other coupling reactions. Such byproduct impurities can negatively affect the performance of OPV devices. Furthermore, using the direct arylation reaction reduces the number of synthetic steps required to prepare the final monomers and hence that will be reflected on the reduction of the costs of the whole process [10, 11].

In the present work, we report the synthesis of six alternating copolymers comprising 2,6-linked anthracene units with varying substituents at their 9,10 positions as electron donating moieties and functionalized TPD as electron-acceptor moieties. The six target polymers, which are shown in **Figure 5-1**, were synthesised *via* direct arylation polymerisation. Here we choose to use different substituents in the backbone of the polymers to investigate the influence of these substituents on the processability, optoelectronic properties and the performance of these polymers.

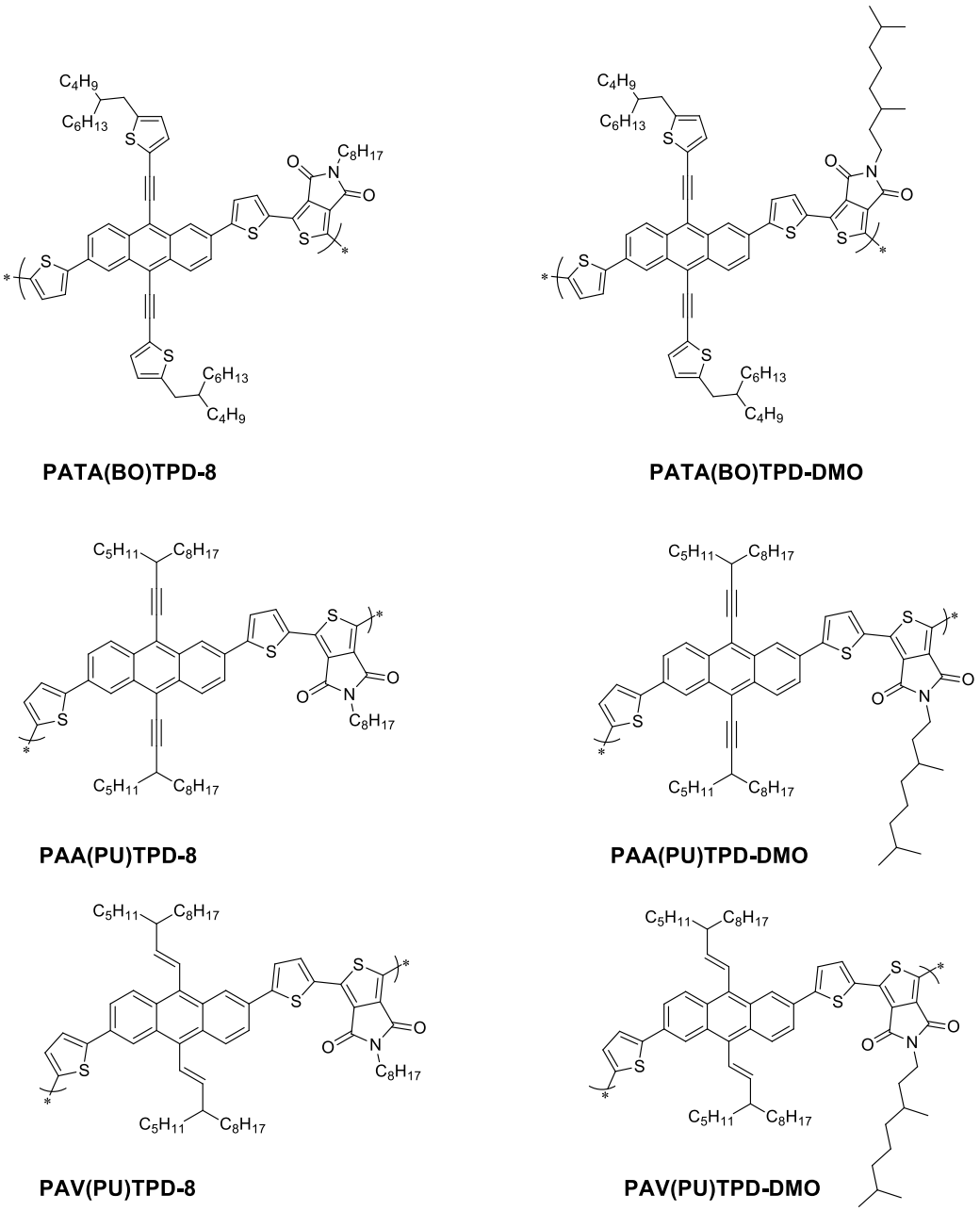


**Figure 5-1:** The chemical structures of the target polymers.

Research work recently published by Iraqi group [3], reported the synthesis of three copolymers, **PTATPD(O)**, **PTATPD(DMO)**, and **PTATPD(BP)** comprising TPD with different substituents as electron accepting units and triisopropylsilylacetylene-functionalized anthracene as electron-rich units (**Figure 5-2**). They found that the optical band gaps of the three polymers exceeded 2.0 eV, which was attributed to steric repulsion between the attached groups on the repeat units of the polymers. As a result, the planarity of the reported polymers was affected and hence decreased their electronic

conjugation leading to these polymers having high optical band gaps [3]. Therefore, to reduce the steric hindrance in our case, we decided to investigate the use of an extra thiophene spacer between the anthracene and TPD units which could increase the electronic conjugation of each repeat unit and thus should narrow the band gap of the resulting polymers.

Recently, Sheng *et al*,[8] synthesised two copolymers, **P1** and **P2**, composed of bulky tertthiophene substituted benzodithiophene and TPD units (**Figure 5-2**). They deduced that, the insertion of a thiophene spacer between donor and acceptor units in the main backbone of the polymers lead to an extention of the conjugated area and a reduction of the steric hindrance between donor and acceptor units. As a result, the photovoltaic performances of the polymers containing thiophene spacers on the backbone should be enhanced due to the expected increase in their $J_{sc}$ values.

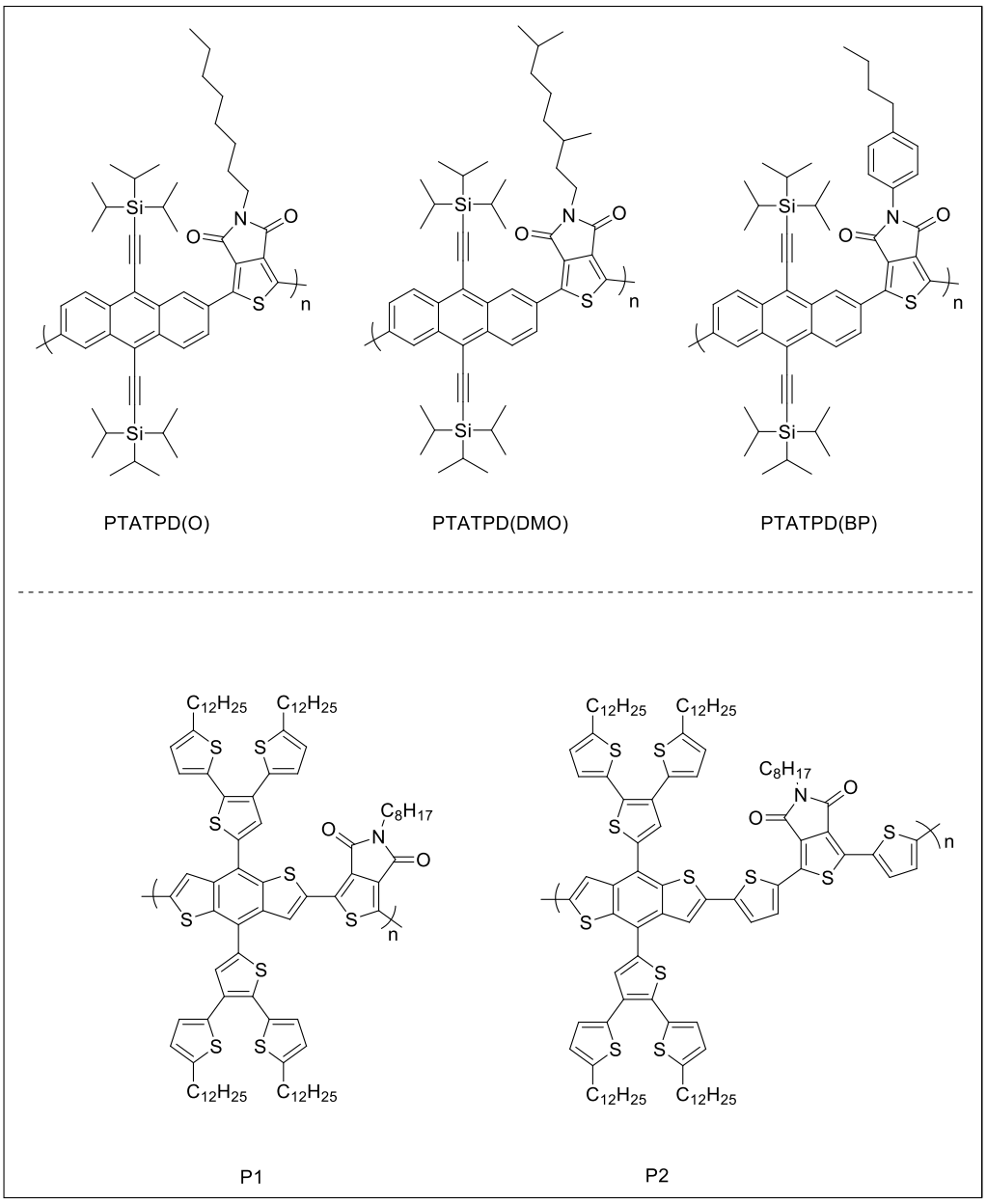


**Figure 5-2:** The chemical structures of polymers; **PTATPD(O)**, **PTATPD(DMO)**, **PTATPD(BP)**, **P1**, and **P2**.

## 5.2 Results and Discussion

### 5.2.1 Synthesis of the Monomers

The synthetic routes toward monomers **M7**, **M8**, **M9**, **M10** and **M11** which are required for the preparation of our target polymers are schematically shown in **Scheme 5-1** below.

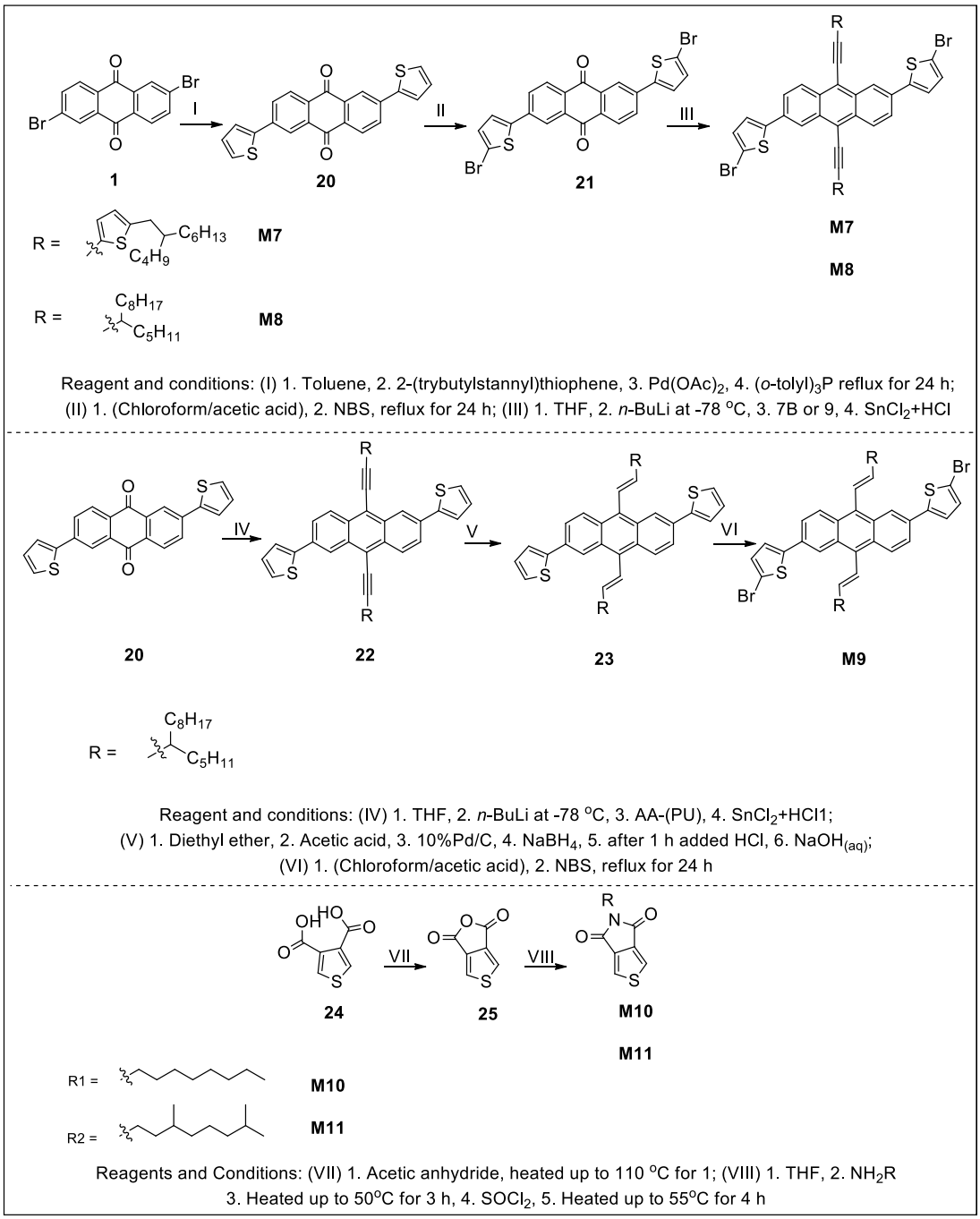


**Scheme 5-1:** Synthetic routes towards monomers; **M7**, **M8**, **M9**, **M10** and **M11**.

Monomers **M7**, **M8** and **M9** were synthesised by a similar method to that described for monomers **M1**, **M2** and **M3** in chapter 2. Compound 2,6-di(thiophen-2-yl)-9,10-anthraqunone (**20**) was synthesised by means of Stille coupling reaction of 2,6-dibromo-9,10-anthraqunone and 2-(tributylstannyl)thiophene in the presence of $Pd(OAc)_2$ and (*o*-tolyl)$_3$P. The resulting product was then brominated using *N*-

bromosuccinimide to afford compound (**21**). To synthesise **M7** and **M8**, arylethynyl derivatives were treated with *n*-BuLi to produce lithiated intermediate compounds, which then reacted with compound (**21**) followed by reduction with $SnCl_2$ to afford the desired monomers.

Compound **M9** was prepared by reduction of the acetylene groups at the 9,10 positions in compound **22** using sodium borohydride in the presence of acetic acid to afford **23**. This indirect hydrogenation using boranes involves the addition of a borane across the acetylene groups, followed by the decomposition of the alkylborane by the acetic acid as describe in **Scheme 5-2** [12, 13].

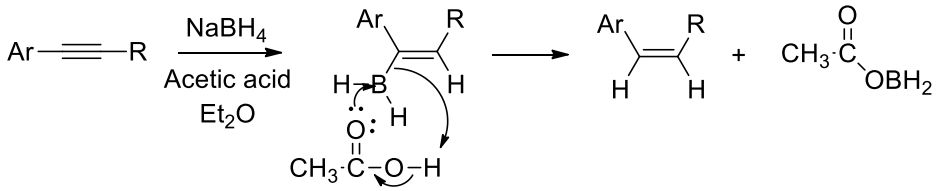


**Scheme 5-2:** The reduction of the acetylene group using $NaBH_4$.

The NMR studies of **23** (Chapter 7, Figure 7-8) reveal that the product exists in two conformations. We speculate these two conformations structure are *anti* and *syn* as drawn in **Figure 5-3**. We believe these two conformations possess *trans* vinylic bonds which are more favorable due to steric issues in comparison to the *cis* form. Previously published analogues molecules with *trans*-ethenyl =C–H possess doublets in the $^1$H-NMR spectra with *J* values at 15–17 Hz range [14-17]. However, due to the overlap of the two conformations of compound **23**, it was difficult to estimate the values of *J* couplings. The final monomer, **M9**, was obtained by the bromination of compound **23** with *N*-bromosuccinimide in acetic acid/chloroform.

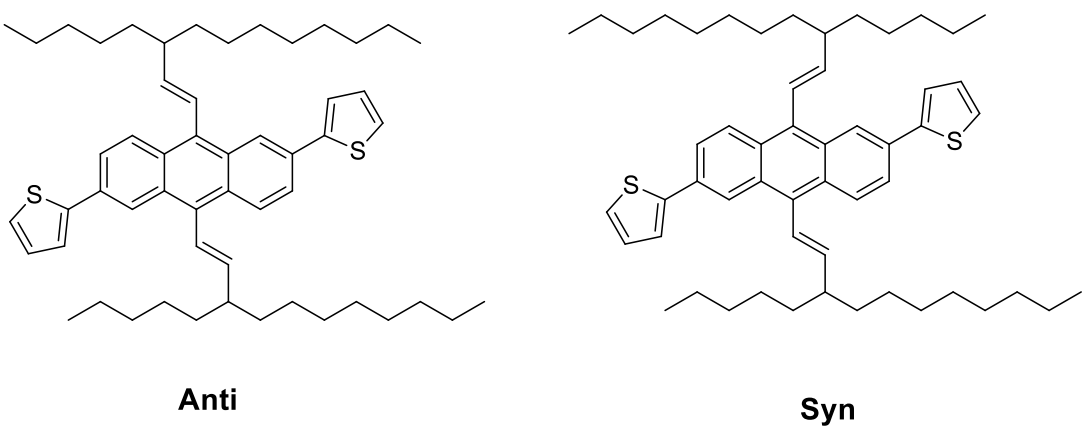


**Figure 5-3:** The proposed chemical structure of the two possible conformations of compound **23**.

Synthesis of TPD monomers began with preparation of the anhydride (**25**) proceeding from thieno-3,4-dicarboxylic acid. The two functionalised TPD monomers **M10** and **M11** were prepared *via* ring opening of (**25**) using alkyl-substituted amine, followed by ring-closure with thionyl chloride [18].

### 5.2.2 Polymers Synthesis

All the six polymers were synthesized *via* the direct arylation polymerisation method using the donating monomers with TPD derivatives. Polymerisation was performed in dry THF as the solvent, $PdCl_2(MeCN)_2$ as the catalyst, $(o\text{-}OMePh)_3P$ as a phosphine ligand, PivOH as a carboxylate source and $Cs_2CO_3$ as the base at 100 °C. The proposed mechanism of the reaction is as described in chapter 1. The obtained crude polymers were collected by precipitation into methanol. They were then purified using a Soxhlet system using methanol, acetone, hexane, toluene and chloroform. Finally, the toluene and/or chloroform fractions were recovered by re-precipitation in methanol, where the yield of the polymers obtained ranged from 41% to 82%. All the polymers can be dissolved easily in common solvents such as chloroform, chlorobenzene, and 1,1,2,2-tetrachloroethane. The chemical structures of the prepared polymers were confirmed using $^1$H-NMR spectroscopy, IR and elemental analysis. The $^1$H-NMR spectra of the polymers are shown in chapter 7 (Figures 7-17, 7-18, 7-19, 7-20, 7-21, 7-22).

The number average molecular weight ($M_n$) of the polymers was determined using gel permeation chromatography (GPC) using 1,2,4-trichlorobenzene as the eluent at room temperature (**Table 5-1** and **Figure 5-4**). As a general trend, polymers with n-octyl substituents, possessed lower $M_n$ values in comparison to their counterparts with 3,7-dimethyloctyl chains. For examples, **PAA(PU)TPD-DMO** displays a higher $M_n$ value (10000 Da) compared to that of **PAA(PU)TPD-8** (6400 Da). The rest of the GPC data is presented in **Table 5-1**. It seems that the use of branched 3,7-dimethyloctyl groups on the TPD units reduces intermolecular interactions in solution leading to more soluble polymers [3].

**Table 5-1:** GPC data and TGA data of the polymers.

| Polymer | Yield (%) | $M_n$ (Da)[a] | $M_w$ (Da)[a] | PD[b] | DP[c] | Td ($^oC$) |
|---|---|---|---|---|---|---|
| PATA(BO)TPD-8 | 65 | 5000 | 7300 | 1.5 | 4 | 330 |
| PATA(BO)TPD-DMO | 67 | 6400 | 11300 | 1.8 | 6 | 324 |
| PAA(PU)TPD-8 | 41 | 6400 | 10000 | 1.6 | 6 | 305 |
| PAA(PU)TPD-DMO | 81 | 10000 | 21800 | 2.2 | 9 | 322 |
| PAV(PU)TPD-8 | 74 | 17100 | 54000 | 3.2 | 16 | 324 |
| PAV(PU)TPD-DMO | 82 | 22000 | 94200 | 4.3 | 20 | 323 |

[a] Measurements conducted using a differential refractive index (DRI) detection method.

[b] Polydispersity index. [c] Degree of polymerisation

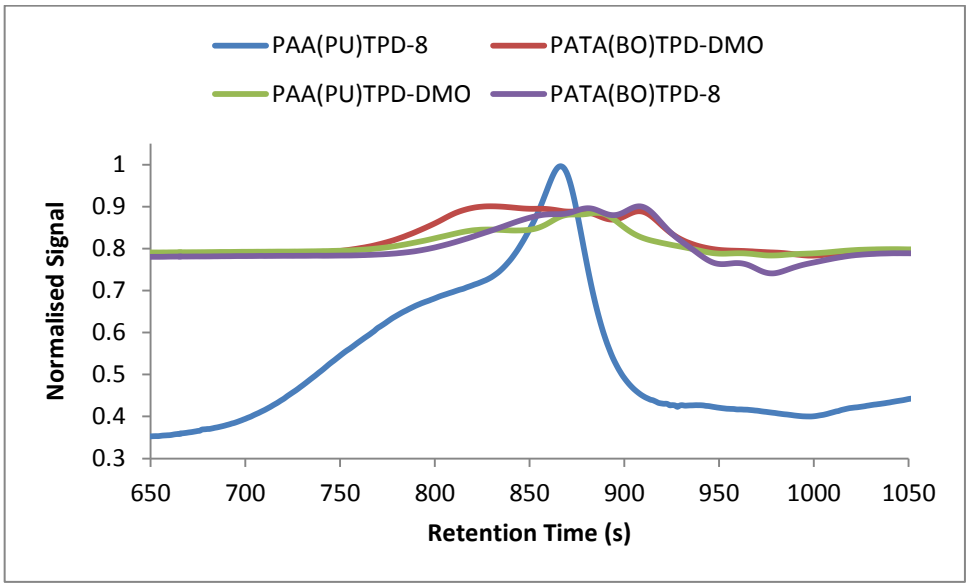


**Figure 5-4:** The GPC traces by RI detector of **PATA(BO)TPD-8, PATA(BO)TPD-DMO** and **PAA(PU)TPD-8** and **PAA(PU)TPD-DMO**

### 5.2.3 Thermal Analysis

The thermal properties of the six new polymers were investigated by thermogravimetric analysis (TGA) conducted under a nitrogen atmosphere at a heating rate of 10 °C/ min. All six polymers revealed good thermal stability with 5% weight loss decomposition temperature around 305 °C for **PAA(PU)TPD-8**, 322 °C for **PAA(PU)TPD-(DMO)**, 330 °C for **PATA(BO)TPD-8**, 324 °C for **PATA(BO)TPD-(DMO)**, 324 °C for **PAV(PU)TPD-8** and 323 °C for **PAV(PU)TPD-(DMO)** (**Figure 5-5**). In the TGA thermograms of the polymers, two-step degradations under $N_2$ atmosphere were observed for all polymers which can be ascribed to the cleavage of the side chains, followed by the rest of the polymer chains. The degradation occurred at a high temperature exceeding 300 $^{o}$C, suggesting that all polymers are thermally stable.

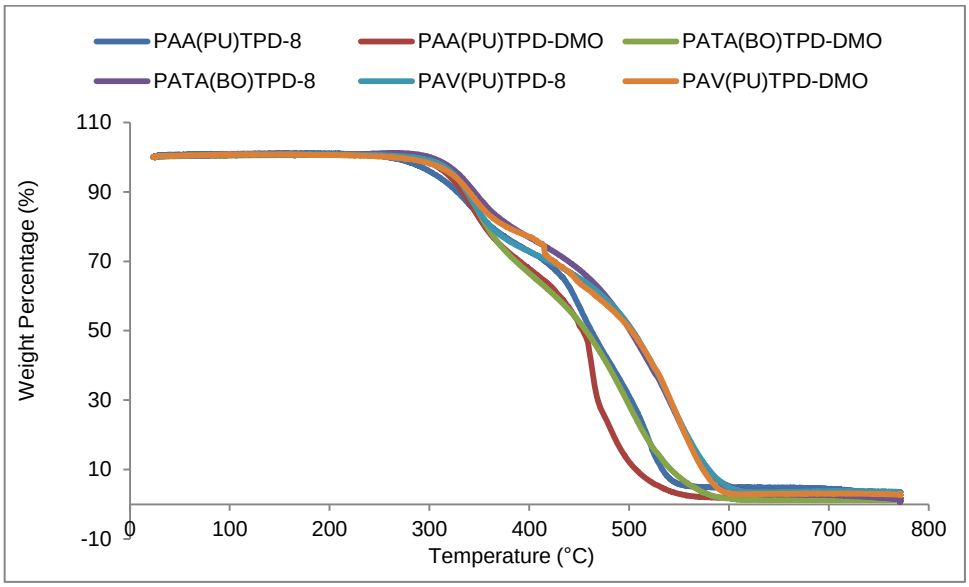


**Figure 5-5:** TGA thermogram of the polymers at a heating temperature rate of 10 °C under $N_2$ atmosphere.

### 5.2.4 Optical Properties

The optical properties of all polymers were measured using UV-Vis spectroscopy in chloroform solutions and on thin films. All the results are summarised in **PATA(BO)TPD-8** and **PATA(BO)TPD-DMO** show absorption maxima at 455 and 452 nm in chloroform solution with absorption onset at 662 and 656 nm, respectively. When cast into thin films, the polymers display the same values for their λmax absorption maxima. Both polymers reveal additional weak shoulder peaks around 618 nm in dilute solutions and films a result that indicates that the polymers tend to aggregate due to the high planarity of the polymer chains enhanced by using acetylenic substituents on anthracene units and non-bulky groups attached to the TPD units. The optical band gaps of **PATA(BO)TPD-8** and **PATA(BO)TPD-DMO** were calculated to be 1.87 eV for both polymers from the onset of their absorptions in thin films. Given the high similarity between the absorption spectra of the polymers both in solution and in the solid state, we speculate that there is a negligible difference in terms of their structure and orientation within the two states indicating that the polymers have similar energetic conformations [3]. The UV-Vis spectra of polymers **PATA(BO)TPD-8** and **PATA(BO)TPD-DMO** are shown in **Figure 5-6**.

**PATA(BO)TPD-8** and **PATA(BO)TPD-DMO** show absorption maxima at 455 and 452 nm in chloroform solution with absorption onset at 662 and 656 nm, respectively. When cast into thin films, the polymers display the same values for their $\lambda_{max}$ absorption maxima. Both polymers reveal additional weak shoulder peaks around 618 nm in dilute solutions and films a result that indicates that the polymers tend to aggregate due to the high planarity of the polymer chains enhanced by using acetylenic substituents on anthracene units and non-bulky groups attached to the TPD units. The optical band gaps of **PATA(BO)TPD-8** and **PATA(BO)TPD-DMO** were calculated to be 1.87 eV for both polymers from the onset of their absorptions in thin films. Given the high similarity between the absorption spectra of the polymers both in solution and in the solid state, we speculate that there is a negligible difference in terms of their structure and orientation within the two states indicating that the polymers have similar energetic conformations [3].

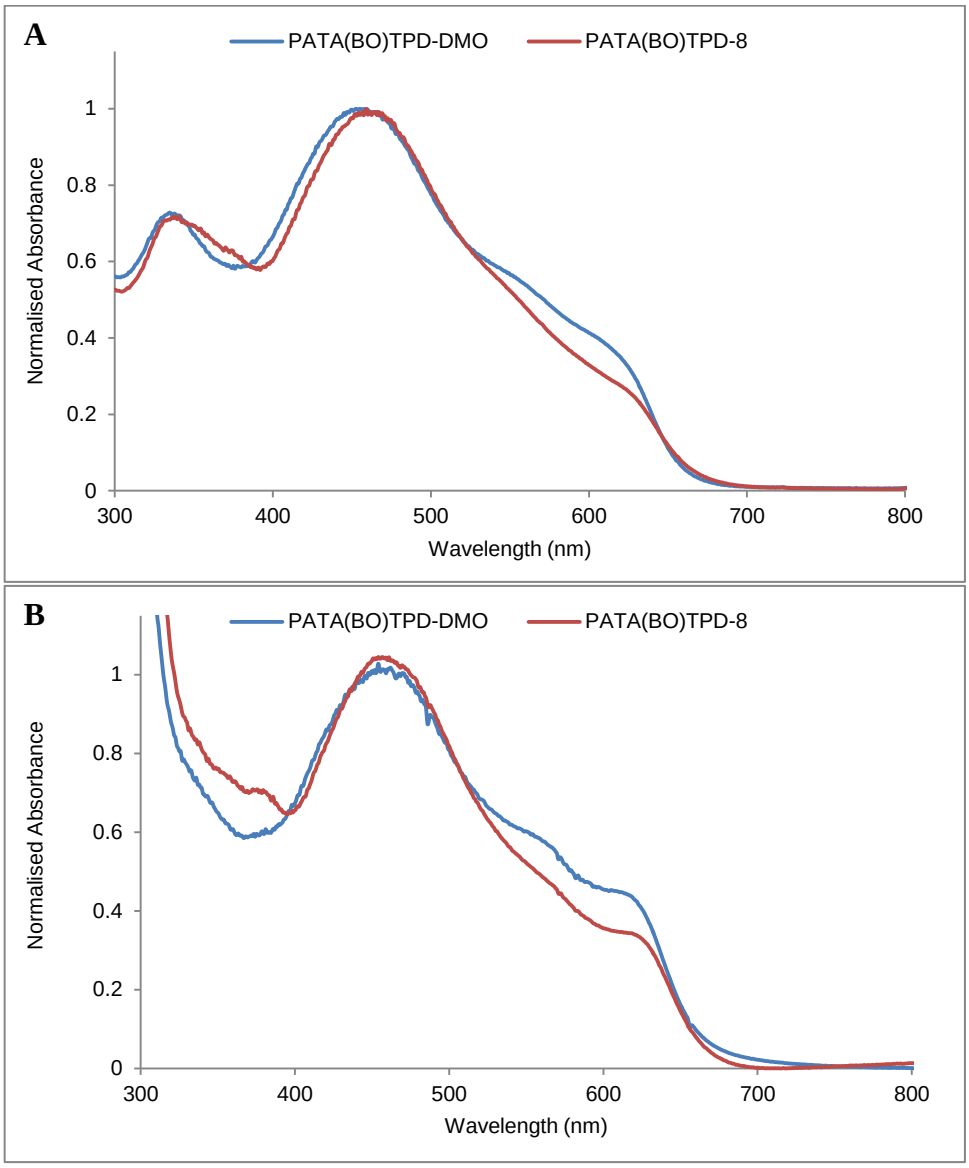


**Figure 5-6:** UV-Vis spectra of the **PATA(BO)TPD-8** and **PATA(BO)TPD-DMO** in; (A) dilute chloroform solution and (B) thin film state.

**Table 5-2:** UV-Vis data and optical band gaps of the polymers

| Polymer | $\lambda_{max}$ Solution (nm) | $\varepsilon^{a}$ ($M^{-1}$ $cm^{-1}$) | $\lambda_{max}$ film (nm) | $E_g^{opt}$ film (eV)[b] |
|---|---|---|---|---|
| PATA(BO)TPD-8 | 455 | $5.81 \times 10^{+4}$ | 455 | 1.87 |
| PATA(BO)TPD-DMO | 452 | $4.12 \times 10^{+4}$ | 452 | 1.87 |
| PAA(PU)TPD-8 | 300, 418, 527 | $2.98 \times 10^{+4}$ | 424, 534, 580 | 1.90 |
| PAA(PU)TPD-DMO | 450 | $3.23 \times 10^{+4}$ | 452 | 1.87 |
| PAV(PU)TPD-8 | 400, 511,553 | $2.67 \times 10^{+4}$ | 318, 398, 518, 565 | 2.03 |
| PAV(PU)TPD-DMO | 400, 511, 553 | $2.20 \times 10^{+4}$ | 318, 398, 518, 565 | 2.03 |

[a] Molar absorptivity measured at $\lambda_{max}$ in chloroform. [b]($E_g^{opt}$) optical bandgap, calculated from the onset of the absorption s band on solid films.

The optical spectra of polymers **PAA(PU)TPD-8** and **PAA(PU)TPD-DMO** are presented in **Figure 5-7**. These polymers are equivalent to **PATA(BO)TPD-8** and **PATA(BO)TPD-DMO**, but the anthracene moiety is functionalised with alkylethynyl groups, instead of thienylethynyl groups.

**PAA(PU)TPD-DMO** has broader absorption bands in the visible region for both solution and film state with $\lambda_{onst}$ at 656 and 662 nm respectively, when compared with **PAA(PU)TPD-8**. This result can be ascribed to the higher molecular weight of **PAA(PU)TPD-DMO** in comparison to that of **PAA(PU)TPD-8**. **PAA(PU)TPD-8** possesses three absorption maxima in chloroform solution at 300, 418 and 527 nm which were red-shifted to 424, 534 and 580 nm in the solid state. Whilst, **PAA(PU)TPD-DMO** has a maximum absorption band at 450 nm in solution state with a shoulder absorption at 625 nm which are shifted slightly to 452 nm and 630 nm in the solid state. This indicates that the polymer adopts a similar conformation in both solution and film states. The optical band gap of the polymers **PAA(PU)TPD-8** and **PAA(PU)TPD-DMO** were calculated form the onset of absorption of thin film spectra

and are found to be 1.90 and 1.87 eV respectively. These results indicate that **PAA(PU)TPD-8** has a higher optical band gap than its counterpart polymers **PATA(BO)TPD-8** and **PATA(BO)TPD-DMO**. This is can be ascribed to the thienylethynyl groups incorporated to polymer backbones which help in delocalising π-electrons to the conjugated side substituents leading to enlarge the π-conjugation more effectively. Therefore, **PATA(BO)TPD-8** and **PATA(BO)TPD-DMO** with 2-dimentional structures possess larger conjugated area compared to **PAA(PU)TPD-8** resulting in more effective interchain π-π overlapping and lower band gaps [19]. Surprisingly, **PAA(PU)TPD-DMO** possesses similar optical properties compare to those **PATA(BO)TPD-8** and **PATA(BO)TPD-DMO**, which can be attributed to the high molecular weight of this polymer. It is also worth noting that the absorption bands of **PAA(PU)TPD-8** at low energy i.e. those that are attributed to intramolecular charge transfer along polymer backbones are much more prominent than those observed for the other polymers pointing to a better intramolecular charge transfer in this particular polymer.

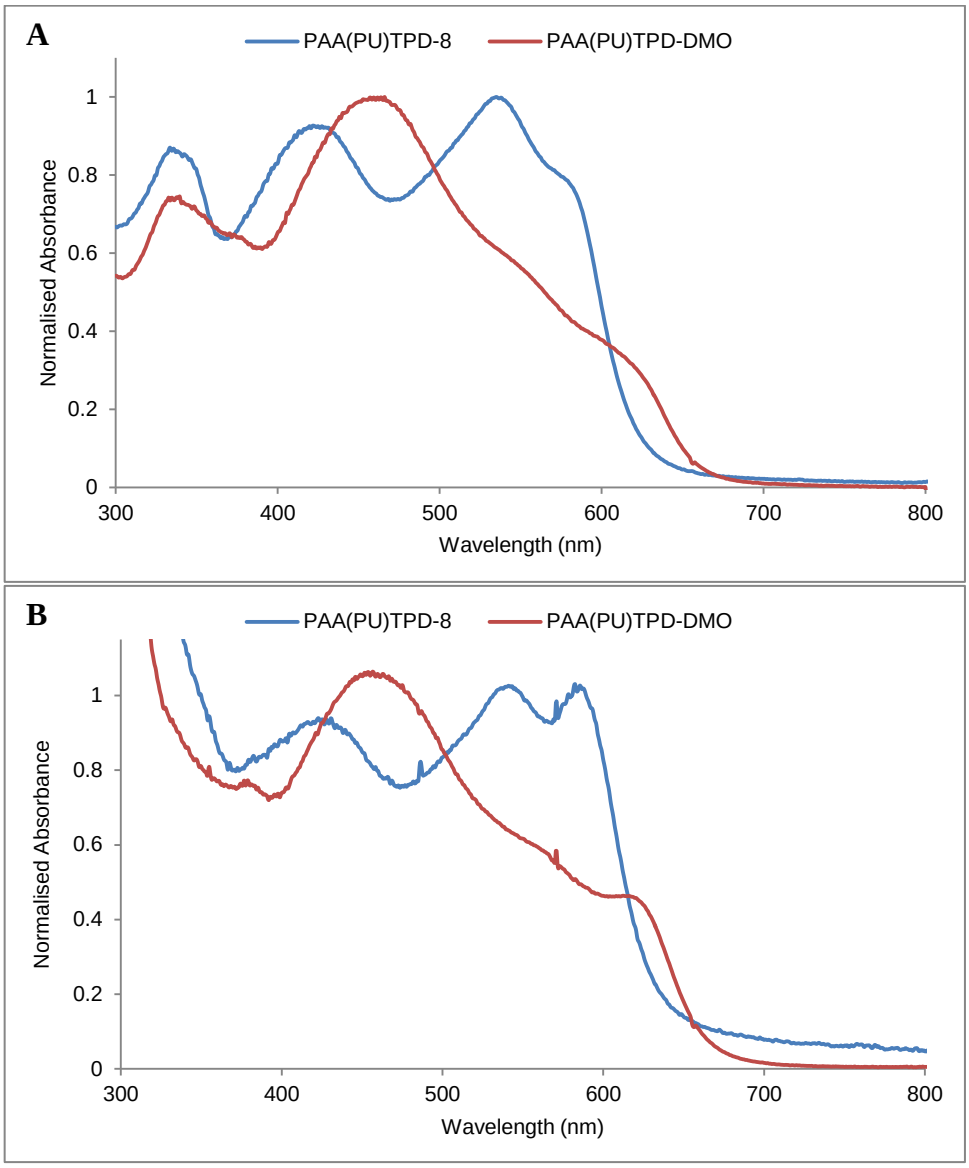


**Figure 5-7:** UV-Vis spectra of the **PAA(PU)TPD-8** and **PAA(PU)TPD-DMO** in; (A) dilute chloroform solution and (B) thin film state.

**Figure 5-8** shows the UV-Vis spectra of polymers **PAV(PU)TPD-8** and **PAV(PU)TPD-DMO** in chloroform solutions and films. The absorption spectra of both polymers in dilute chloroform solutions showed identical patterns with three absorption bands at 400, 511 and 553 nm. In comparison with their solution absorption spectra, those of films of both polymers exhibited a very small bathochromic shift in their absorption maxima $\lambda_{max}$ of about 12 nm with the absorption onset at 612 nm corresponding to an optical band gap of 2.03 eV for both polymers. This similarity in the optical properties of **PAV(PU)TPD-8** and **PAV(PU)TPD-DMO**, indicate that these

polymers are not influenced by the nature of the substituents attached to the TPD units. Furthermore, the high $M_n$ value of **PAV(PU)TPD-DMO** has not affected its optical properties indicating that this polymer as well as **PAV(PU)TPD-8** have both reached their effective conjugation lengths.

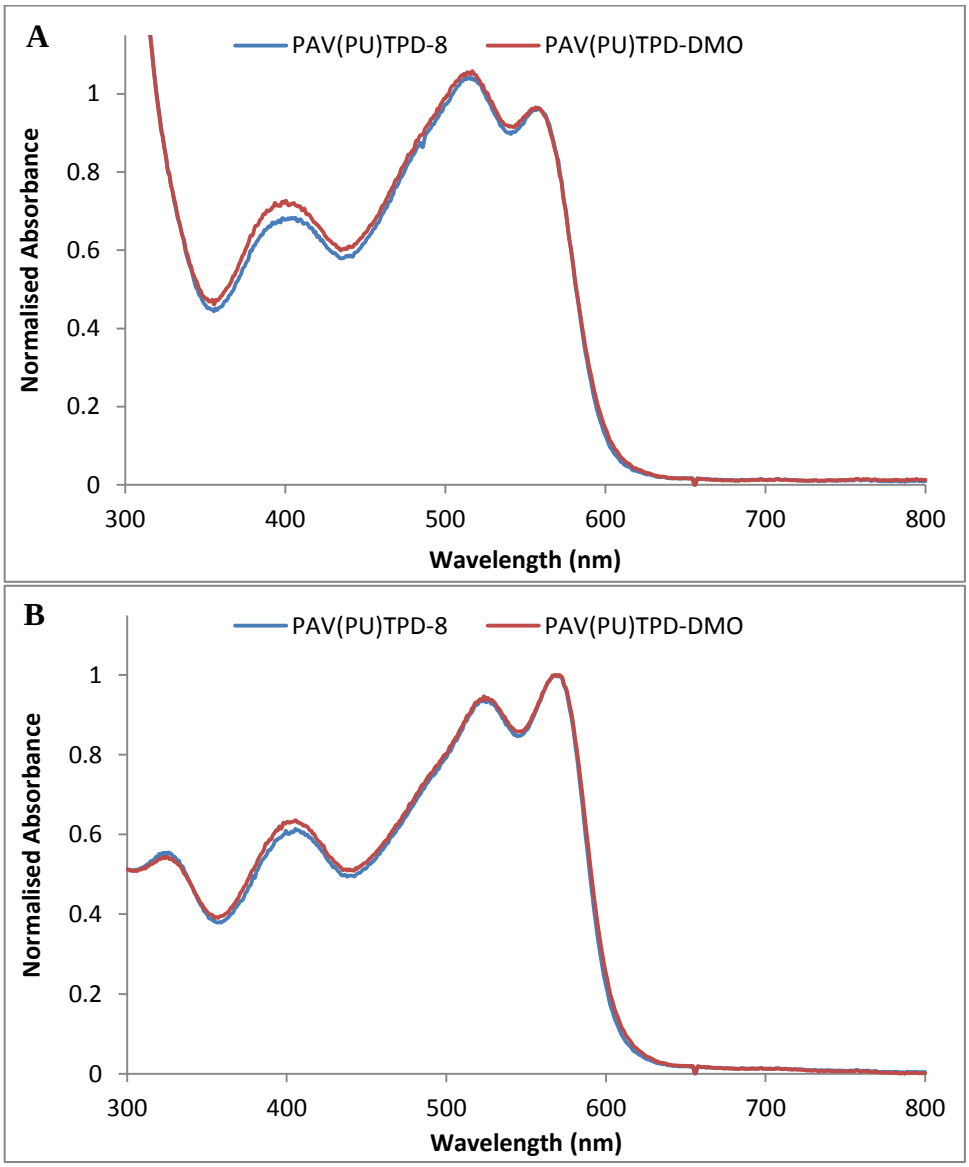


**Figure 5-8:** UV-Vis spectra of the **PAV(PU)TPD-8** and **PAV(PU)TPD-DMO** in; (A) dilute chloroform solution and (B) thin film state.

Results from the optical studies of these two polymers allow for an understanding of the influence of replacing alkylethynyl substituents with alkene substituents on the anthracene units of the polymers. Note from **Figure 5-7** and **Figure 5-8** that the

absorption onsets of **PAA(PU)TPD-8** and **PAA(PU)TPD-DMO** are higher than those of **PAV(PU)TPD-8** and **PAV(PU)TPD-DMO**. Clearly, polymers with alkene substituents on the anthracene units are less conjugated than those with alkylethynyl substituents. We believe that this is caused by a significant out-of-plane twist of the alkylvinyl substituents attached to the anthracene repeat units as a result of significant steric repulsions between olefinic hydrogens of the vinyl substituents and the hydrogens in the 1,4,5,8-postions of anthracene repeat units. This leads to twisting out of planarity about the formal single bonds linking the vinyl substituents to the anthracene units, resulting in disruption of intermolecular interactions of the polymer backbones which explains (i) the higher molecular weights of the resulting vinyl substituted polymers as a result of enhanced solubility (less aggregation) and (ii) the higher optical band gap of alkylvinyl substituted polymers [20, 21].

### 5.2.5 Electrochemical Characterisation

The electrochemical properties of the polymers were investigated by cyclic voltammetry (**Figure 5-10**). Cyclic voltammetry measurements on drop-cast polymer films were conducted in acetonitrile with tetrabutylammonium perchlorate as an electrolyte. The HOMO and LUMO energy levels of the polymers were assessed from the onsets of corresponding first oxidation and reduction peaks as summarised in **Table 5-3**.

In the anodic scan, the oxidation onsets of the polymers **PATA(BO)TPD-8** and **PATA(BO)TPD-DMO** occurred at 0.75 and 0.73 V *vs.* $Ag/Ag^+$ reference electrode, which correspond to HOMO energy levels of –5.47 and –5.45 eV, respectively. This slight difference in the HOMO levels between the two polymers indicates that the nature of alkyl side-chain attached to the TPD repeat units has a minimal effect on the electrochemical properties of the polymers. The HOMO energy levels of the polymers **PAA(PU)TPD-8** (HOMO level at –5.48 eV) and **PAA(PU)TPD-DMO** (HOMO level at –5.46 eV) were very close to those of their corresponding polymers **PATA(BO)TPD-8** and **PATA(BO)TPD-DMO**. However, the HOMO levels of the polymers **PAV(PU)TPD-8** and **PAV(PU)TPD-DMO** found at –5.53 eV for both polymers were deeper than those of the other polymers in this series i.e.

**PATA(BO)TPD-8**, **PATA(BO)TPD-DMO**, **PAA(PU)TPD-8** and **PAA(PU)TPD-DMO**. This can be attributed to a weaker electron donating capability of anthracene units when they are substituted with vinylic substituents in **PAV(PU)TPD-8** and **PAV(PU)TPD-DMO** rather than with ethynylene substituents as for the other polymers in the series. The twisting out of planarity and loss of electronic conjugation in vinylic substituted systems might account for these observations.

The low-lying LUMO energy levels which are around –3.54 eV of all six polymers are due to the strong electron-deficient character of the TPD units [22]. It seems that attaching different substituting groups on the polymers backbone does not have a significant influence on the LUMO levels of the resulting polymers.

**Table 5-3:** A summary of electrochemical data for the polymers.

| Polymers | HOMO (eV)[a] | LUMO (eV)[b] | $E_g^{elec}$ (eV)[c] |
|---|---|---|---|
| PATA(BO)TPD-8 | –5.47 | –3.54 | 1.93 (±0.03) |
| PATA(BO)TPD-DMO | –5.45 | –3.56 | 1.89 (±0.02) |
| PAA(PU)TPD-8 | –5.48 | –3.54 | 1.94 (± 0.03) |
| PAA(PU)TPD-DMO | –5.46 | –3.52 | 1.94 (±0.04) |
| PAV(PU)TPD-8 | –5.53 | –3.54 | 1.99 (±0.02) |
| PAV(PU)TPD-DMO | –5.53 | –3.54 | 1.99 (±0.02) |

[a] HOMO position (*vs. vacuum*) determined from onset of oxidation. [b] LUMO position (*vs. vacuum*) determined from onset of reduction. [c] Electrochemical energy gap of the polymers.

The deep values of the HOMO energy levels for all polymers in this series of materials, should result in devices with high open-circuit voltage ($V_{oc}$) values in applications in PSCs, owing to the fact that the $V_{oc}$ of devices is often proportional to the energy difference between the LUMO of the acceptor (fullerene) and the HOMO of the donor [23]. Moreover, the differences between the LUMO of the donor polymer and that of the acceptor (e.g. the LUMO level of $PC_{70}BM$ at –3.90 eV [24]) affords an appropriate

driving force which is required to ensure an efficient exciton dissociation. **Figure 5-9** shows the electronic energy level diagrams of the donor polymers and $PC_{71}BM$ acceptor in OPV devices.

The higher-lying HOMO energy of the polymers presented in this work compared to the HOMO levels of the polymers synthesised by Iraqi and co-workers (HOMO level at –5.90 eV) (**Figure 5-2**)[3] can be ascribed to the thiophene bridged donor-acceptor. In fact, thiophene is considered as a strong electron donor with a high-lying ionization potential [25]. This result is in agreement with the result found by Sheng *et al*,[8] who synthesised copolymers, **P1** and **P2** (**Figure 5-2**). They found that the insertion of π bridge thiophene in **P2** resulted in raising its HOMO energy level (HOMO level at –5.63 eV) compared to that of **P1** (HOMO level at –5.68 eV).

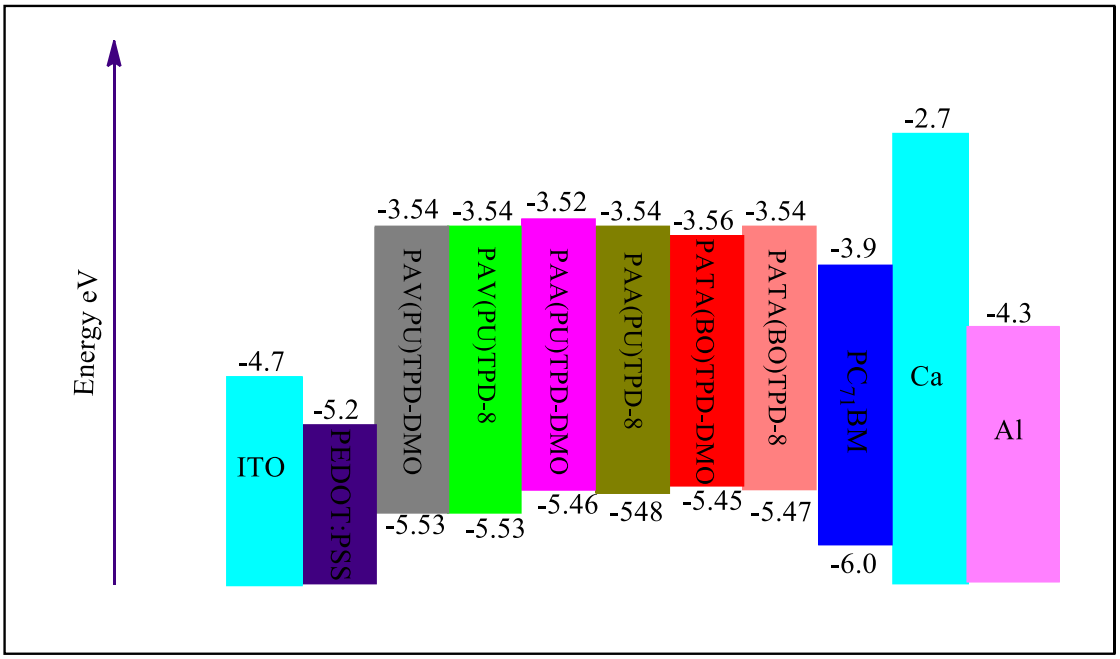


**Figure 5-9:** Energy levels of different components in OPV devices.

In addition, the LUMO energy levels of all six polymers were deeper than those of similar polymers prepared by Iraqi and co-worker by between 0.12 eV and 0.16 eV [3]. We speculate that the use of thiophene spacer units between the anthracene units and TPD units aid to reduce the overall steric hindrance leading to increase the planarity of

the polymer backbone. Hence this helps to increase the π orbital overlap as well as delocalisation of electrons stabilising the LUMO energy levels [26].

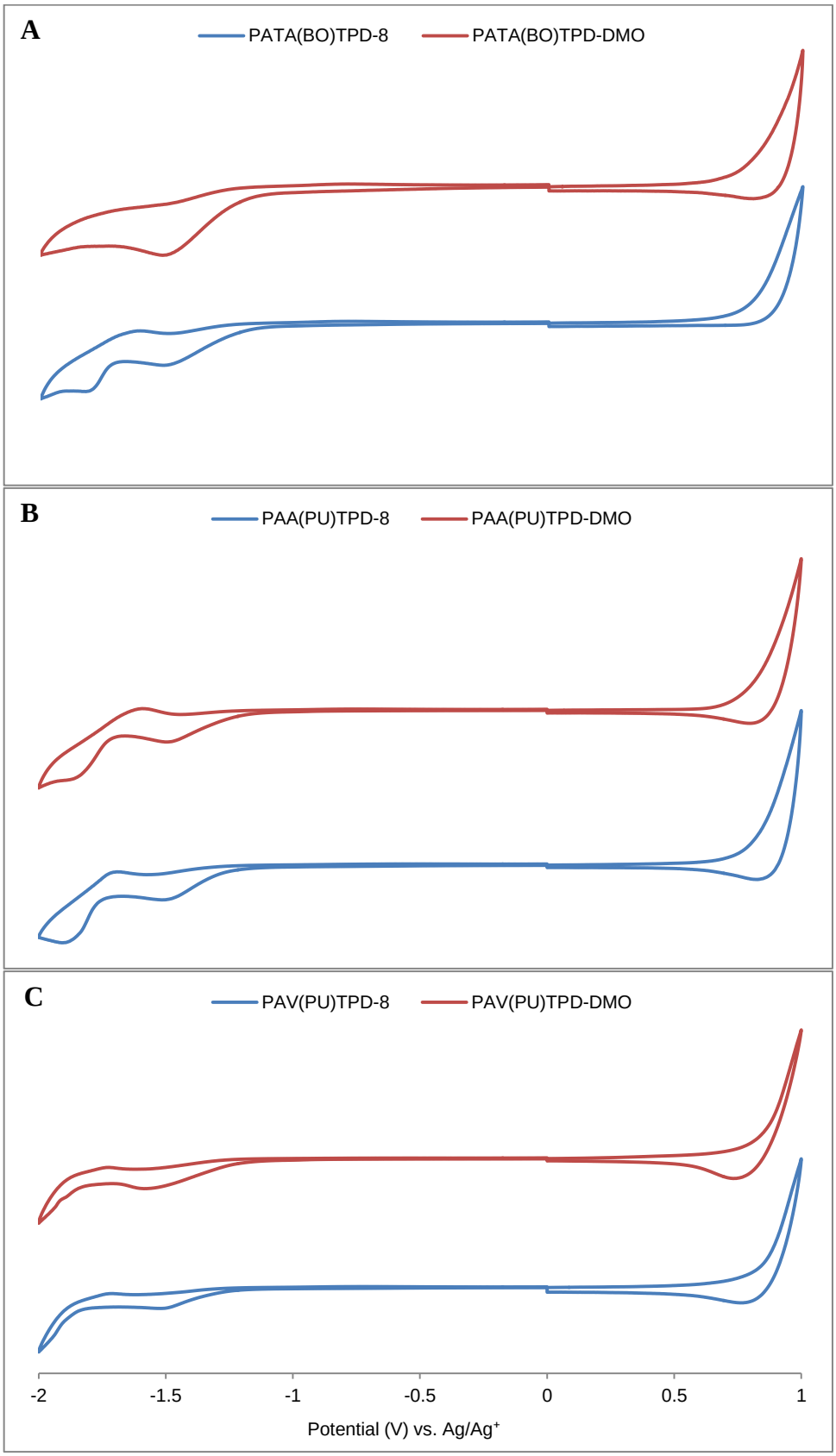


**Figure 5-10:** Cyclic voltammetry curves of the polymers.

### 5.2.6 X-ray Diffraction studies

X-ray diffraction (XRD) was carried out on the polymers powder to study the packing of the polymer backbones in the solid state. The diffractograms are shown in **Figure 5-11** and **Figure 5-12**.

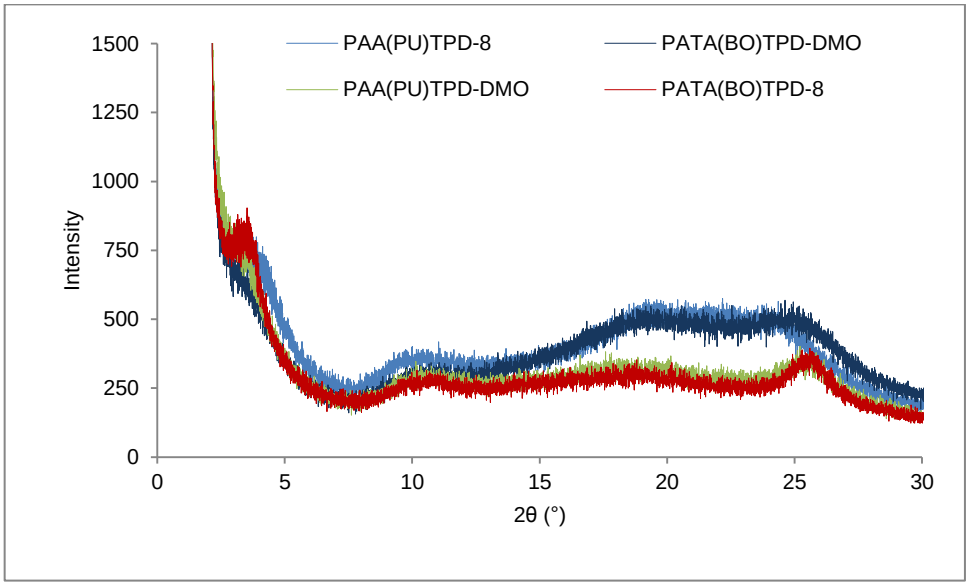


**Figure 5-11:** Powder X-ray diffractogram of **PAA(PU)TPD-8**, **PAA(PU)TPD-DMO**, **PATA(BO)TPD-8** and **PATA(BO)TPD-DMO**.

Polymers **PAA(PU)TPD-8** and **PATA(PU)TPD-8** display weak peaks at low 2θ angle around 3.62° and 3.23° corresponding to $d_1$ spacing of 24.40 Å and 27.35 Å, respectively. These two peaks at low angle region suggest a slight degree of lamellar ordering of neighboring polymer chains lying in the same plane [27]. All the diffractograms show another weak reflection peaks at about 9.77° for **PAA(PU)TPD-8**, 10.04° for **PAA(PU)TPD-DMO**, 10.03° for **PATA(BO)TPD-DMO** and 10.23°. Also these peaks correspond to the inter layer alkyl groups in the lamellar structure as proposed by previous literatures [28, 29]. In addition, the polymers exhibited peaks at the wide angle around 23.99° for **PAA(PU)TPD-8**, 25.15° for **PAA(PU)TPD-DMO**, 25.19° for **PATA(BO)TPD-8** and 24.50° for **PATA(BO)TPD-DMO** corresponds to π-π stacking distance of 3.71 Å, 3.54 Å, 3.53 Å and 3.63 Å respectively. In comparison to the polymers previously prepared in Iraqi group **PTATPD(O)**, **PTATPD(DMO)** and **PTATPD(BP)** (**Figure 5-2**) [3], incorporation thiophene spacer between the anthracene

units and TPD units resulted in enhanced π-π stacking and intermolecular interactions between the polymer strands.

However, replacing the acetylenic substituting system from the polymer backbone with the vinylic system resulted in an amorphous-like structure in the solid state. The X-ray diffractograms (**Figure 5-12**) of **PAV(PU)TPD-8** and **PAV(PU)TPD-DMO** show a broad peak at around 19.78$^{o}$ and 19.00$^{o}$ corresponding to 4.49 Å and 4.67 Å, respectively. We propose that the polymers with alkenes substituents resulted in a significant twist of the attached groups because of steric repulsions between H(olefinic) and the hydrogen in the 1,4,5,8-postions of anthracene. That causes a torsion about the formal single bonds leading to disrupt the intermolecular interactions of the polymer backbones and hence produce an amorphous polymers.

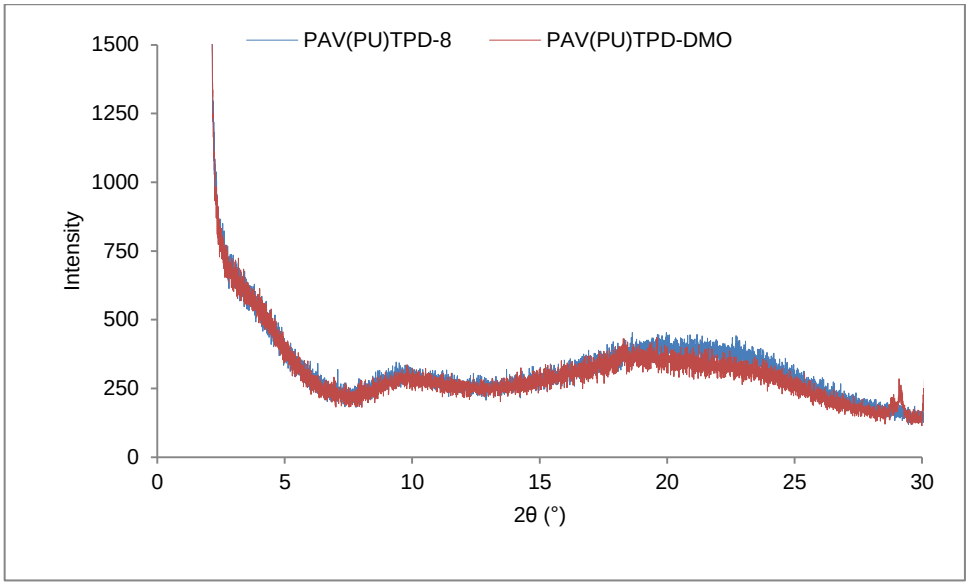


**Figure 5-12:** Powder X-ray diffractogram of **PAA(PU)TPD-8** and **PAA(PU)TPD-DMO**.

## 5.3 Summary

In conclusion, the synthesis of six alternating copolymers comprising 9,10-functionalsied anthracene units and TPD functionalised units using direct arylation polymerisation was reported and yielded the copolymers **PATA(BO)TPD-8**, **PATA(BO)TPD-DMO**, **PAA(PU)TPD-8**, **PAA(PU)TPD-DMO**, **PAV(PU)TPD-8**

and **PAV(PU)TPD-DMO**. All the polymers were soluble in chlorinated solvents. It was recognized that the nature of the substituents on the anthracene units can affect photophysical, electrochemical and the crystallinity of the resulting polymers. Polymers with side chains attached *via* ethynyl groups on the 9,10 positions of the anthracene units are maintained two-dimensional structures that can provide polymers with medium optical band gaps. However, replacing the ethynyl substituents for the alkenes groups on the 9,10 positions of the anthracene unit lead to polymers (**PAV(PU)TPD-8** and **PAV(PU)TPD-DMO**) with higher optical band gaps due to the steric repulsions between H(vinylic) and the hydrogen in the 1,4,5,8-postions of anthracene unit. The planarity of these six polymers was confirmed by X-ray diffraction studies. The polymers with ethynyl groups on the anthracene units **PATA(BO)TPD-8**, **PATA(BO)TPD-DMO**, **PAA(PU)TPD-8** and **PAA(PU)TPD-DMO**) displayed a small sharp peaks at high angle region. These peaks are a good indication of stronger π-π stacking suggesting that the use of the ethynyl groups on the anthracene units improves the planarity of the polymers chains. On the other hand, the X-ray studies of the polymers with alkenes substituents revealed the amorphous nature of these polymers. The HOMO levels of the polymers **PAV(PU)TPD-8** and **PAV(PU)TPD-DMO** were deeper than that of their corresponding polymers **PATA(BO)TPD-8**, **PATA(BO)TPD-DMO**, **PAA(PU)TPD-8** and **PAA(PU)TPD-DMO** because of the vinylic substituents which enhanced the electron donating properties of the anthracene in comparison to the electron withdrawing acetylenic system.

## 5.4 Experimental Section:

### 5.4.1 Materials:

Unless otherwise stated, all chemicals, reagents and solvents were obtained from commercial sources (Sigma-Aldrich, Fisher, Acros Organics and Alfa Aesar) in the highest purities possible and used as received. Regent grade solvents were purchased from the internal stores which were used for some reactions, extraction, recrystallization and chromatography. However, most of the reactions were carried out using anhydrous solvents which were obtained from the Grubbs solvent system within the chemistry department. Acids, bases, drying agents and salts were obtained from the

internal stores. Reactions proceeded under an argon atmosphere as standard unless stated otherwise. Column chromatography was carried out on silica gel (200-300 mesh) or alumina as stated.

### 5.4.2 Analytical Techniques:

Elemental analyses were analysed by using the Perkin Elmer 2400 CHN Elemental Analyser for CHN analysis, and the Schoniger oxygen flask combustion method for sulphur and halides. In both methods, the weights submitted for the analysis were 10 mg. Fourier transform infrared spectroscopy (FTIR) and attenuated total reflectance (ATR) were recorded on a Perkin Elmer Spectrum 65 spectroscopy.

$^{13}C$ and $^{1}H$-NMR spectra of the monomers were recorded on Bruker AV 250 (250 MHz), and Bruker AV 400 (400 MHz) NMR spectrometers at room temperature in chloroform-d ($CDCl_3$) solution. NMR spectra of the polymers were recorded using Bruker Avance III HD 500 (500 MHz) at 100 °C in 1,1,2,2-tetrachloroethane-d2 solution. As an internal standard, tetramethylsilane (TMS) was used for calibrating chemical shifts (δ). The chemical shifts were measured in part per million (ppm), while the coupling constant (*J*) were given in Hertz (Hz).

GC-MS spectra were recorded on Perkin Elmer Turbomass Mass Spectrometer equipped with a Perkin Elmer Autosystem XL Gas Chromatograph. Mass spectra were obtained by the electron impact method (EI) and MALDI-TOF mass spectrometry.

GPC analysis were recorded on the equipment consisted of a Viscotek $GPC_{max}$ VE 2001 GPC solvent/sample module, a Waters 410 Differential Refractometer and a PLgel 5 μm Mixed Column (650 mm set length) using chloroform as the eluent at rate of 1 mL/min. Polymer samples were made up as a solutions in chloroform (2 mg/mL) spiked with toluene as a reference. The RI-detection method was used to obtain the GPC curves, which was calibrated with a series of polystyrene narrow standards. Degree of polymerisation (DP) was calculated using the below equation:

$$\chi_n = \frac{M_n}{M_R}$$

where $\chi_n$ is the DP, $M_n$ is the number average molecular weight of the polymer and $M_R$ is the molecular mass of the repeat unit of the polymer. Perkin Elmer TGA-7 Thermogravimetric Analyser was used to determine TGA curves at a scan rate of 10 °C/minute under nitrogen atmosphere.

Powder X-ray diffraction were conducted on a Bruker D8 advance diffractometer with a CuKα radiation source (1.5418 A, rated as 1.6 kW). The scanning angle was recorded over the range 2–30°.

Hitachi U-2010 Double Beam UV-Visible Spectrophotometer has been used to evaluate the optical properties of the polymers. The absorbance of the polymers was measured in a solution of chloroform at room temperature using quartz cuvette ($l$ = 10 mm). Thin films of the polymers were prepared by dip coating quartz plates into around 1 mg/mL solutions in chloroform, then dried in the air and the UV-Vis absorption spectra measurements were run at room temperature.

Cyclic voltammograms were conducted using Princeton Applied Research Model 263A Potentiostat/Galvanostat. The analyses were recorded under Argon protection at approximately room temperature. A three electrode system was used for the measurements consisting of an $Ag/Ag^+$ reference electrode (Ag wire in 0.01 *M* $AgNO_3$ solution in the electrolyte solution), a Pt working electrode, and Pt counter electrode (Pt wire). Measurements were done in tetrabutylammonium perchlorate acetonitrile solution (0.1 *M*) on polymer thin films which made by drop casting polymer solution onto the working electrode which were left to dry in air. The energy level of $Fc/Fc^+$ was assumed at –4.8 eV to vacuum. The half-wave potential of Fc/Fc+ redox couple was found to be 0.08 V *vs*. $Ag/Ag^+$ reference electrode. the HOMO and LUMO energy level were calculated using the following equations:

$$E_{\text{LUMO}} = -[(E_{\text{red,onset}} - E_{1/2(\text{ferrocene})}) + 4.8] \text{ eV}$$

$$E_{HOMO} = -[(E_{ox,onset} - E_{1/2(ferrocene)}) + 4.8] \text{ eV}$$

where $E_{red,onset}$ and $E_{ox,onset}$ are the onset of reduction and oxidation, respectively, relative to $Ag/Ag^{+}$ reference electrode.

## 5.5 Synthesis of Monomers and Polymers:

### 5.5.1 Synthesis of 2,6-di(thiohen-2-yl)-9,10-anthraqunone (20): [30]

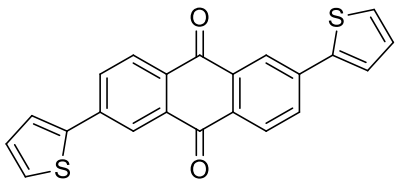


2,6-Dibromo-9,10-anthraqunone (2.00 g, 5.5× $10^{-3}$ mol) and 2-(tributylstannyl*)* thiophene (8.16 g, 6.95 mL, 2.2 × $10^{-2}$ *mol*) were dissolved in 40 mL of anhydrous toluene under argon atmosphere. Subsequently, $Pd(OAc)_2$ (0.062g, 2.75 × $10^{-4}$ mol) and $(o\text{-tolyl})_3P$ (0.168, 5.51 × $10^{-4}$ mol) were added to the reaction mixture and stirred at 110 °C for 24 hours. The reaction mixture was poured in MeOH. A brown shiny crystals was obtained. Yield (1.72 g, 84%). $^{1}$H-NMR (400 MHz, *$CDCl_3$*) $\delta_H$/ppm: 8.55 (d, *J*= 1.9, 2H), 8.36 (d, *J* = 8.1 Hz, 2H), 8.03 (dd, *J* = 2.0, 8.3 Hz, 2H), 7.63 (dd, *J* = 1.02, 3.70, 2H), 7.48 (d, *J* = 5.0 Hz, 2H), 7.02 (dd, *J* = 3.75, 5.0 Hz, 2H). Elemental Analysis (%) Calculated for $C_{22}H_{12}O_2S_2$: C, 70.95; H, 3.25; S, 17.22. Found: C, 69.10; H, 3.46; S, 15.36. Mass (EI); (*m/z*) 372 ($M^{+}$). FT-IR ($cm^{-1}$): 3080 (aromatic C–H stretch), 1665 (C=O stretch), 1580 (aromatic C=C stretch), 730 (C–S–C stretch).

### 5.5.2 Synthesis of 2,6-di-(5-bromothiohen-2-yl)-9,10-anthraqunone (21): [31]

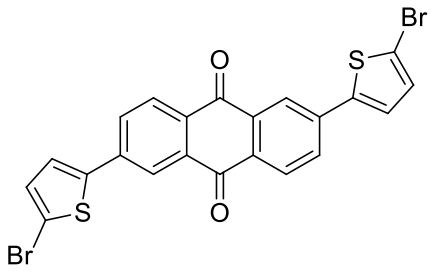


2,6-Di-(thiohen-2-yl)-9,10-anthraqunone (1.00 g, 2.7 × $10^{-3}$ mol) and *n*-bromosuccinimide (0.95 g, 5.3 × $10^{-2}$ mol) were dissolved in a mixture of chloroform (60 mL) / acetic acid (10 mL). The reaction mixture was light protected and stirred overnight at room temperature. The resulting product was precipitated in MeOH. A bright greenish powder was obtained. Yield was 1.25 g (88%). $^{1}$H-NMR (400 MHz, *CDCl*$_3$) $\delta_H$/ppm: 8.45 (d, *J*= 2.0, 2H), 8.36 (d, *J* = 8.0 Hz, 2H), 7.93 (dd, *J* = 2.0, 8.0 Hz, 2H), 7.37 (d, *J* = 4.0 Hz, 2H), 7.16 (d, *J* = 4.0 Hz, 2H). Elemental Analysis (%) Calculated for $C_{22}H_{10}Br_2O_2S_2$: C, 49.83; H, 1.90; Br, 30.14; S, 12.09. Found: C, 51.49; H, 2.10; Br, 29.21; S, 12.31. Mass (MALDI -TOF); (*m/z*) 530 ($M^+$). FT-IR ($cm^{-1}$): 3080 (aromatic C–H stretch), 1665 (C=O stretch), 1580 (aromatic C=C stretch), 791 (C–Br stretch) 730 (C–S–C stretch).

### 5.5.3 Synthesis of 2,6-bis(5-bromothiophen-2-yl)-9,10-bis-[2-(ethynyl-5-butyl-octyl) thiophene-2-yl]anthracene (M7): [32, 33]

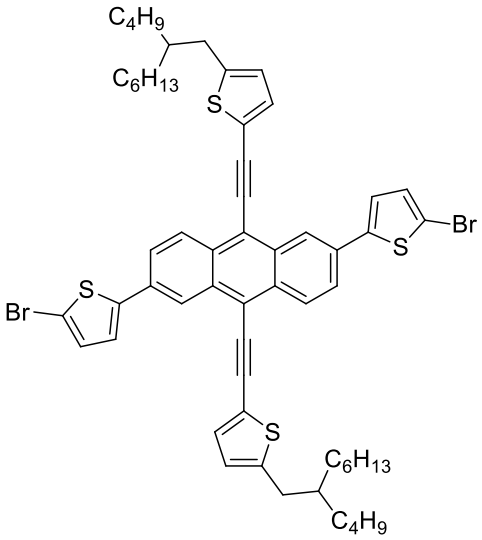


In a dried round bottom flask, 2-ethynyl-5-(2-bytyl-octyl) thiophene (1.0 g, $3.3 \times 10^{-3}$ mol) was dissolved in 80 mL of dry THF. n-BuLi (2.5 M in hexane, 1.3 mL, $3.2 \times 10^{-3}$ mol) was added dropwise over 2 minutes at –78 °C. The reaction mixture was stirred for 30 minutes at room temperature, followed by the addition of 2,6-di-(5-bromothiohen-2-yl)-9,10-anthraqunone (1.21 g, $1.3 \times 10^{-3}$ mol) to the mixture at –78 °C. The mixture was stirred at room temperature overnight. The reaction mixture was quenched by adding a solution of $SnCl_2$ (1.06 g, $5.6 \times 10^{-3}$ mol) in 10% HCl (10 mL) and the mixture was stirred for 30 minutes at 60 °C. After completing the reaction, the solution was precipitated into MeOH and a solid product was collected. This product was further purified on a silica gel column chromatography eluting with DCM/petroleum ether (gradient DCM 0-2 %) to afford the product as dark red powder. Yield 1.72 g (72%). $^1$H-NMR (400 MHz, *CDCl$_3$*) $\delta_H$/ppm: 8.60 (d, *J*= 1.5, 2H), 8.51 (d, *J* = 9.0 Hz, 2H), 7.76 (dd, *J* = 2.0, 9.0 Hz, 2H), 7.37 (d, *J* = 3.5 Hz, 2H), 7.30 (d, *J* = 4.0 Hz, 2H), 7.13 (d, *J* = 4.0 Hz, 2H), 6.82 (d, *J* = 3.5 Hz, 2H), 2.86 (d, *J* = 6.5, 4H), 1.78-1.70 (bm, 2H), 1.42-1.26 (bm, 32H) 0.99-0.85 (bm, 12 H). $^{13}$C-NMR (400 MHz, *CDCl$_3$*): δ 148.19, 145.73, 132.41, 131.61, 131.51, 131.22, 131.17, 128.07, 125.78, 124.71, 124.10, 122.65, 120.62, 118.05, 112.38, 96.95, 89.69, 40.10, 34.80, 33.26, 32.92, 31.94, 29.69, 28.88, 26.64, 23.06, 22.73, 14.22, 14.17. Elemental Analysis (%) Calculated for $C_{58}H_{66}Br_2S_4$: C, 66.27; H, 6.32; Br, 15.20; S, 12.20. Found: C, 67.35; H,

6.96; Br, 17.20; S 12.78. Mass (MALDI-TOF); (*m/z*) 1050 ($M^+$). FT-IR ($cm^{-1}$): 3094-3050 (aromatic C–H stretch), 2955-2850 (aliphatic C–H stretch), 2188 (carbon, carbon triple bond stretch), 1530 and 1463 (aromatic C=C stretch), 794 (C–Br stretch).

### 5.5.4 Synthesis of 2,6-bis(5-bromothiophen-2-yl)-9,10-di-(3-pentylundec-1-yne) thiophene -2-yl]anthracene (M8): [32, 33]

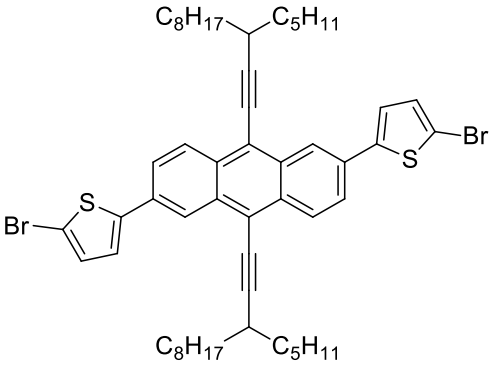


2,6-Bis(5-bromothiophen-2-yl)-9,10-di-(3-pentylundec-1-yne)thiophene-2-yl] anthracene was synthesised from 2,6-di-(5-bromothiohen-2-yl)-9,10-anthraqunone (0.88 g, $1.2 \times 10^{-3}$ mol) and 3-pentylundec-1-yne (0.81 g, $3.7 \times 10^{-3}$ mol) using a synthetic method similar to the method describe above for **M7**. The product was purified on silica gel column chromatography using petroleum ether/DCM eluent (10/0.1) to give yellow powder. Yield 0.42 g (37%). $^1$H-NMR (400 MHz, *CDCl$_3$*) $\delta_H$/ppm: 8.68 (d, *J*= 1.5, 2H), 8.54 (d, *J* = 9.0 Hz, 2H), 7.74 (dd, *J* = 2.0, 9.0 Hz, 2H), 7.26 (d, *J* = 4.0 Hz, 2H), 7.11 (d, *J* = 4.0 Hz, 2H), 2.94 (m, 2H), 1.90-1.63 (bm, 14H), 1.53-1.24 (bm, 30H) 0.97 (t, *J* = 7.0 Hz, 6H) 0.89 (t, *J* = 7.0, 6H). $^{13}$C-NMR (400 MHz, *CDCl$_3$*): δ 145.95, 132.24. 131.91, 131.26, 131.07, 128.25, 124.40, 123.94, 123.25, 118.77, 112.17, 107.87, 78.17, 35.58, 33.56, 31.98, 29.79, 29.70, 29.45, 28.02, 27.70, 22.76, 14.22, 14.15. Elemental Analysis (%) Calculated for $C_{54}H_{68}Br_2S_2$: C, 68.91; H, 7.28; Br, 16.98; S, 6.81. Found: C, 68.65; H, 7.39; Br, 17.20; S 7.07. Mass (MALDI-TOF); (*m/z*) 940 ($M^+$). FT-IR ($cm^{-1}$): 3047 (aromatic C–H stretch), 2952-2847 (aliphatic C–H stretch), 2204 (carbon, carbon triple bond stretch), 1538 and 1461 (aromatic C=C stretch), 788 (C–Br stretch).

### 5.5.5 Synthesis of 2,6-di(thiophen-2-yl)-9,10-bis-(3-pentylundec-1-yne)-anthracene (22): [32, 33]

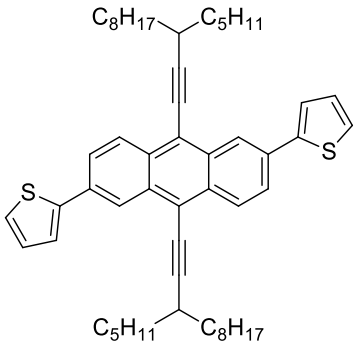


2,6-Dibromo-9,10-di-(3-pentylundec-1-yne)-anthracene (0.85 g, 1.10 × $10^{-3}$ mol) and 2-(tributylstannyl)thiophene (1.22 g, 1.04 mL, 3.3 × 10–3 mol) were dissolved in 20 mL of dry toluene under argon atmosphere. Thereafter, Pd(OAc)2 (0.012g, 5.5 × 10–4 mol) and (o-tolyl)3P (0.033, 1.1 × 10-4 mol) were added to the reaction mixture and stirred at 110 °C for 24 hours. The reaction mixture was poured in MeOH to afford a yellow powder product. Yield (0.82 g, 95%). $^{1}$H-NMR (400 MHz, $CDCl_3$) $\delta_H$/ppm: 8.82 (d, J = 1.5 Hz, 2H), 8.57 (d, J= 9.0 Hz, 2H), 7.86 (dd, J = 2.0, 9.0 Hz, 2H), 7.56 (dd, J = 1.0, 3.5 Hz, 2H), 7.38 (dd, J = 1.0, 5.0 Hz, 2H), 7.18 (dd, J = 3.5, 5.0 Hz, 2H), 2.98-2.91 (m, 2H), 1.90-1.64 (bm, 14H), 1.53-1.24 (bm, 30H) 0.97 (t, J = 7.0 Hz, 6H) 0.89 (t, J = 7.0, 6H). $^{13}$C-NMR (400 MHz, $CDCl_3$): δ 144.59, 132.29, 131.95, 131.86, 128.24, 128.04, 125.35, 125.16, 123.78, 123.28, 118.59, 107.55, 78.32, 35.62, 33.52, 31.97, 29.79, 29.70, 29.45, 27.99, 29.65, 22.74, 14.20, 14.17. Elemental Analysis (%) Calculated for $C_{54}H_{70}S_2$: C, 82.80; H, 9.01; S, 8.19. Found: C, 81.48; H, 9.03; 7.82. Mass (MALDI-TOF); (m/z) 782($M^+$).

### 5.5.6 Synthesis of 2,6-di-(thiophen-2-yl)-9,10-bis-(3-pentylundec-1-yne)-anthracene (23): [34]

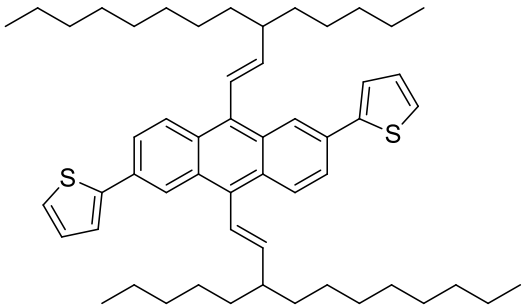

To stirring mixture of 2,6-di(thiophen-2-yl)-9,10-bis-(3-pentylundec-1-yne)-anthracene (1.00 g, $1.3 \times 10^{-3}$ mol), acetic acid (6.14 mL) and 10% Pd/C (1.43 g, $1.34 \times 10^{-3}$ mol) in diethyl ether (80 mL) was added fine sodium borohydride (8.12 g, 0.22 mol) portion wise at room temperature. After stirring the reaction for one hour, a solution of 10% HCl (40 mL) was added dropwise to the mixture at 0 °C, followed by addition of NaOH solution to reaction mixture to adjust the pH to around 10. The reaction mixture was filtered through a Celite pad, the filtrate was extracted with diethyl ether and water. The organic layer was collected and washed with NaCl solution, dried over $MgSO_4$, and filtered. The solvent was evaporated, and the crude product was purified on silica gel column chromatography with petroleum ether as eluent to afford the product as a yellow powder. Yield 0.52 g (52%). $^1$H-NMR (400 MHz, *CDCl*$_3$) $\delta_H$/ppm: 8.46 (s, 2H), 8.27 (d, *J*= 9.0 Hz, 2H), 7.73 (d, *J* = 9.0 Hz, 2H), 7.48 (bd, 2H), 7.33 (bd, 2H), 7.15 (bd, 2H), 7.02 (t, *J* = 11.0 Hz, 2H), 6.13 (bt, 2H), 1.85-1.74 (bm, 2H), 1.37-0.79 (bm, 30H) 0.74-0.68 (bm, 6H) 0.62 (t, *J* = 6.5, 6H). $^{13}$C-NMR (400 MHz, *CDCl*$_3$): δ 146.37, 142.88, 142.73, 132.062, 132.56, 130.92, 129.73, 129.69, 129.38, 129.33, 129.05, 127.98, 127.89, 124.36, 124.20, 123.45, 123.08, 123.02, 122.84, 111.55, 38.32, 38.25, 38.19, 34.99, 34.87, 34.67, 31.16, 31.96, 31.91, 31.83, 31.73, 30.01, 29.76, 29.68, 29.48, 29.36, 29.31, 29.22, 27.39, 27.02, 26.97, 26.69, 22.70, 22.46, 22.39, 14.16, 14.12, 14.02, 19.97, 13.84. Elemental Analysis (%) Calculated for $C_{54}H_{74}S_2$: C, 82.38; H, 9.46; S, 8.14. Found: C, 82.65; H, 9.08; S, 7.36. Mass (MALDI-TOF); (*m/z*) 787 ($M^+$). FT-IR ($cm^{-1}$): 3107-3069 (aromatic C–H stretch), 2955-2854 (aliphatic C–H stretch), 1621 (alkene C=C stretch), 1538 and 1461 (aromatic C=C stretch), 1003 (alkene =C–H stretch), 962 (alkene =C–H bending).

### 5.5.7 Synthesis of 2,6-di-(5-bromothiophen-2-yl)-9,10-bis-(3-pentylundec-1-yne) anthracene (M9): [31, 35]

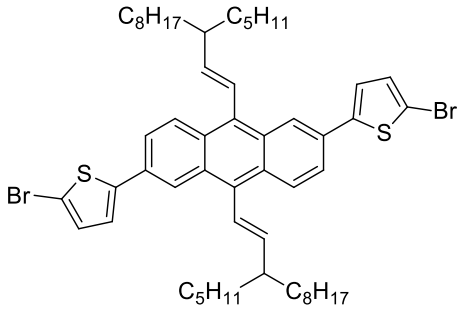


In the absence of light, *n*-bromosuccinimide (0.23 g, $1.3 \times 10^{-3}$ mol) was added to a solution of 2,6-di(thiophen-2-yl)-9,10-bis-(3-pentylundec-1-yne)-anthracene (0.46 g, $5.9 \times 10^{-4}$ mol) in chloroform/acetic acid (20 mL/20 mL). The reaction mixture was stirred at 60 °C overnight, cooled to the room temperature, poured onto cold water and extracted with DCM. The organic layer was washed with $NaHCO_{3(aq)}$, $NaCl_{(aq)}$, water and then dried over $MgSO_4$. After concentrating the solution *in vacuo*, the resultant was precipitated in MeOH. The solid product was further purified on silica gel column chromatography using eluent of petroleum ether/DCM (gradient DCM 0.1-0.3%) and the product was collected as yellow powder after solvent removed. Yield 0.26 g (45%). $^1$H-NMR (400 MHz, *CDCl$_3$*) $\delta_H$/ppm: 8.35 (s, 2H), 8.25 (dd, *J*= 9.0, 4.5 Hz, 2H), 7.63 (d, *J* = 9.0 Hz, 2H), 7.21 (bm, 2H), 7.10 (bm, 2H), 6.98 (t, *J* = 11.0 Hz, 2H), 6.10 (bt, 2H), 1.81-1.71 (bm, 2H), 1.32-0.82 (bm, 50H) 0.72-0.62 (bm, 6H). $^{13}$C-NMR (400 MHz, *CDCl$_3$*): δ 146.37, 142.88, 142.72, 132.62, 132.54, 130.91, 129.73, 129.69, 129.33, 129.05, 127.98, 127.89, 124.36, 124.20, 123.46, 123.08, 123.02, 122.84, 111.55, 38.25, 38.18, 34.87, 34.67, 32.16, 31.96, 31.91, 31.82, 30.01, 29.76, 29.49, 29.36, 29.22, 27.39, 27.02, 26.97, 26.69, 22.70, 22.47, 14.16, 14.12, 14.02, 13.97, 13.84. Elemental Analysis (%) Calculated for $C_{54}H_{72}Br_2S_2$: C, 68.63; H, 7.67; Br, 16.91 S, 6.78. Found: C, 68.74; H, 7.63; Br, 17.24; S, 6.84. Mass (MALDI-TOF); (*m/z*) 945 ($M^+$). FT-IR ($cm^{-1}$): 3047 (aromatic C–H stretch), 2952-2847 (aliphatic C–H stretch), 1621 (alkene C=C stretch), 1532 and 1466 (aromatic C=C stretch), 1007 (alkene =C–H stretch), 966 (alkene =C–H bending) 788 (C–Br stretch).

### 5.5.8 Synthesis of thieno[3,4-c]furan-1,3-dione (24): [3, 7]

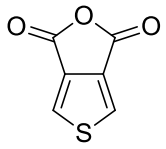

3,4-Thiophenedicarboxylic acid (1.33 g, $7.7 \times 10^{-3}$ mol) was placed in a 500 mL flask and combined with acetic anhydride (110 mL). The mixture was stirred at 110 °C for 1 hour. Then the reaction mixture was cooled to room temperature. A white needles like crystals was deposited on standing overnight. The product was filtered off and dried in air. Yield 0.95 g (80 %). $^{1}$H NMR (400 MHz, *CDCl$_3$*) $\delta_H$/ppm: 8.11 (s, 2H). $^{13}$C NMR (400 MHz, *CDCl$_3$*) $\delta_C$/ppm: 156.33, 135.26, 129.27. Elemental Analysis (%) calculated for $C_6H_2O_3S$: C, 46.75; H, 1.31; S, 20.80. Found: C, 46.70; H, 1.54; S, 20.71. Mass (EI); (*m/z*): 154 ($M^+$). FT-IR ($cm^{-1}$): 3119-3100 (aromatic C–H stretch), 1846-1827 and 1799-1767 (C=O stretch), 1507 and 1466 (aromatic C=C stretch), 1206 (C–O stretch).

### 5.5.9 Synthesis of 5-octyl-4H-thieno[3,4-c]pyrrole-4,6(5H)-dione (M10):[3, 7]

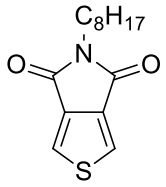

Thieno[3,4-c]furan-1,3-dione (0.15 g, $0.97 \times 10^{-3}$ mol) and octylamine (0.145 g, $1.1 \times 10^{-3}$ mol) were dissolved in dry THF (5 mL) in a round bottom flask and heated to 50 °C for 3 hours. Subsequently, the mixture was cooled to room temperature and thionyl chloride (0.74 mL, 0.011 mol) was added. The reaction contents were stirred at 55 °C for 4 hours. The reaction mixture was cooled to room temperature and poured in distilled water. The organic layer was collected and the aqueous layer was extracted with DCM. The organic layers were combined and dried over $MgSO_4$, filtered and the solvent was evaporated using rotary evaporator. The resultant product was recrystallised from MeOH to obtain the product as white powder. Yield 0.200 g (77.5%). $^{1}$H NMR (400 MHz, *CDCl$_3$*) $\delta_H$/ppm: 7.83 (s, 2H), 3.62 (t, *J* = 7.5 Hz, 2H),

1.66 (m, 2H), 1.35-1.25 (m, 11H), 0.89 (t, *J* = 7.0 Hz, 3H). $^{13}$C NMR (400 MHz, *CDCl*$_3$) $\delta_C$/ppm: 162.69, 136.70, 125.45, 35.51, 31.78, 29.17, 28.48, 26.88, 22.63, 14.08. Elemental Analysis (%) calculated for $C_{14}H_{19}NO_2S$: C, 63.37; H, 7.21; N, 5.28; S, 12.08. Found: C, 63.22; H, 7.16; N, 5.23; S, 11.69. Mass (EI); (*m/z*): 265 ($M^+$). FT-IR ($cm^{-1}$): 3081-3053 (aromatic C–H stretch), 2965-2860 (aliphatic C–H stretch), 1691 (C=O stretch), 1510 and 1460 (aromatic C=C stretch), 1360 and 1181 (C–N stretch).

### 5.5.10 Synthesis of 5-(3,7-dimethyl-octyl)-4H-thieno[3,4-c]pyrrole-4,6(5H)-dione (M11):[3, 7]

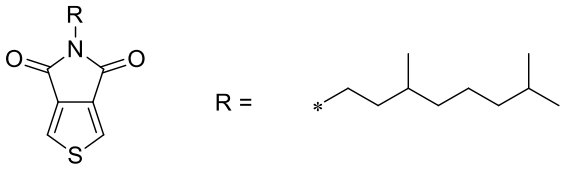


This product was synthesised following the same method described above for 5-Octyl-4H-thieno[3,4-c]pyrrole-4,6(5H)-dione. Chemicals used in reaction were 3,7-dimethloctylamine (0.16 g, 1.5 × $10^{-3}$ mol), Thieno[3,4-c]furan-1,3-dione (0.20 g, 1.3 × $10^{-3}$ mol) and Thionyl chloride (1.08 mL, 0.015 mol). Product was obtained as white powder after recrystallised form MeOH. Yield 0.260 g (68%). $^1$H NMR (400 MHz, *CDCl*$_3$) $\delta_H$/ppm: 7.82 (s, 2H), 3.65 (t, *J* = 7.0 Hz, 2H), 1.74-1.64 (m, 1H),1.57-1.42 (m, 3H ), 1.36-1.12 (m, 6H),0.97 (d, *J* = 6.5 Hz, 3H), 0.87 (d, *J* = 6.5 Hz, 6H). $^{13}$C NMR (400 MHz, *CDCl*$_3$) $\delta_C$/ppm: 162.64, 136.74, 125.41, 39.19, 36.96, 36.79, 35.36, 30.75, 27.92, 24.54, 22.66, 22.59, 19.38. Elemental Analysis (%) calculated for $C_{16}H_{23}NO_2S$: C, 65.49; H, 7.90; N, 4.77; S, 10.93. Found: C, 65.69; H, 7.76; N, 4.76; S, 10.75. Mass (EI); (*m/z*): 293 ($M^+$). FT-IR ($cm^{-1}$): 3082-3053 (aromatic C–H stretch), 2971-2866 (aliphatic C–H stretch), 1691 (C=O stretch), 1513 and 1463 (aromatic C=C stretch), 1362 and 1181 (C–N stretch).

### 5.5.11 Poly[2,6-di-(thiophen-2-yl)-9,10-bis-(3-pentylundec-1-yne)-anthracene-5-diyl-alt-5-octyl-4H-thieno[3,4-c]pyrrole-4,6(5H)-dione[3,4-c]pyrrole-4,6-dione] (PAA(PU)TPD-8): [10, 11]

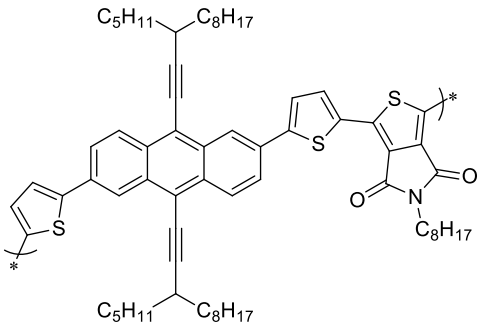


An oven-dry sealed tube was charged with 2,6-bis(5-bromothiophen-2-yl)-9,10-di-(3-pentylundec-1-yne)thiophene-2-yl] anthracene (**M8**) (0.12 g, $0.13 \times 10^{-3}$ mol), 5-octyl-4H-thieno[3,4-c]pyrrole-4,6(5H)-dione (**M10**) (0.034 g, $0.13 \times 10^{-3}$ mol), (*o*-OMePh)$_3$P (0.0036 g, $0.01 \times 10^{-4}$ mol) and $PdCl_2.(MeCN)_2$ (0.00026 mg, $0.001 \times 10^{-4}$ mol), pivalic acid (0.013 g, $0.13 \times 10^{-3}$ mol) and $Cs_2CO_3$ (0.062 g, $0.02\times 10^{-3}$ mol). The tube was sealed and subjected to several cycles of vacuum followed by refilling with argon. Then, dry THF (1.0 mL) was added and the mixture was degassed again. The polymerization was carried out at 100 °C for 2 hours under argon protection. The reaction was cooled to room temperature, diluted with 300 mL of chloroform followed by addition of ammonia to remove residual catalyst before precipitating the reaction contents into methanol. The crude product was collected by filtration and purified using Soxhlet extraction with solvents in the order; methanol (250 mL), acetone (250 mL), hexane (250 mL), toluene (250 mL), chloroform (250 mL). The polymer was collected from chloroform as dark purple. Yield 55 mg (41%). GPC (TCB): $M_w$ = 10000, $M_n$ = 6400, PD = 1.6. $^1$HNMR ($C_2D_2Cl_4$): ($\delta_H$/ppm); 8.89 (d, *J* = 1.5 Hz, 2H); 8.85 (b, 2H); 8.57 (b, 2H); 8.13 (b, 2H); 7.83 (b, 2H); 7.53 (b, 2H); 3.76-3.66 (bm, 2H); 3.04-2.92 (bm, 2H); 1. 93-1.18 (bm, 46H); 0.99-0.78 (bm, 12H). Elemental Analysis (%) calculated for $C_{68}H_{85}NO_2S_3$: C, 78.19; H, 8.20; N, 1.34; S, 9.21. Found: C, 75.82; H, 8.03; N, 1.15; S, 8.52. FT-IR ($cm^{-1}$): 3053 (aromatic C–H stretch), 2951-2852 (aliphatic

C–H stretch), 1696 (C=O stretch), 1510 and 1462 (aromatic C=C stretch), 1369 and 1092 (C–N stretch).

### 5.5.12 Poly[2,6-di-(thiophen-2-yl)-9,10-bis-(3-pentylundec-1-yne)-anthracene-5-diyl-alt-5-(3,7-dimethyl-octyl)-4H-thieno[3,4-c] pyrrole-4,6(5H)-dione[3,4-c]pyrrole-4,6-dione](PAA(PU)TPD-DMO): [10, 11]

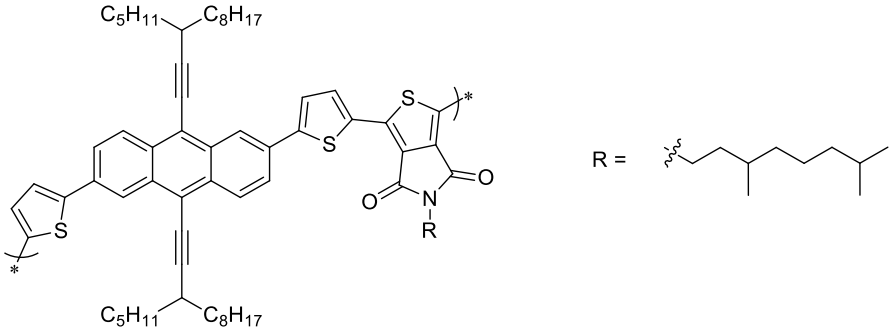


**(PAA(PU)TPD-DMO)** was prepared following a procedure similar to **(PAA(PU)TPD-8)** from monomer 5-(3,7-dimethyl-octyl)-4H-thieno[3,4-c]pyrrole-4,6(5H)-dione **(M11)** (0.037 g, 0.13 × $10^{-3}$ mol) and 2,6-bis(5-bromothiophen-2-yl)-9,10-di-(3-pentylundec-1-yne)thiophene-2-yl] anthracene **M8** (0.12 g, 0.13 × $10^{-3}$ mol). The polymer was collected from chloroform fraction as dark purple solid. Yield 111 mg (81%). GPC (TCB): $M_w$ = 21800, $M_n$ = 10000, PD = 2.2. $^1$HNMR ($C_2D_2Cl_4$): ($\delta_H$/ppm); Peaks were not clear due to aggregation. Elemental Analysis (%) calculated for $C_{70}H_{89}NO_2S_3$: C, 78.38; H, 8.36; N, 1.31; S, 8.97. Found: C, 73.55; H, 7.13; N, 0.88; S, 12.97. FT-IR ($cm^{-1}$): 3067 (aromatic C–H stretch), 2951-2852 (aliphatic C–H stretch), 2182 (carbon, carbon triple bond stretch), 1696 (C=O stretch), 1510 and 1459 (aromatic C=C stretch), 1366 and 1063 (C–N stretch).

### 5.5.13 Poly[2,6-di-(thiophen-2-yl)-9,10-bis[2-(ethynyl-5-butyl-octyl) thiophene]-anthracene-5-diyl-alt-5-octyl-4H-thieno[3,4-c]pyrrole-4,6(5H)-dione [3,4-c]pyrrole-4,6-dione] (PATA(BO)TPD-8): [10, 11]

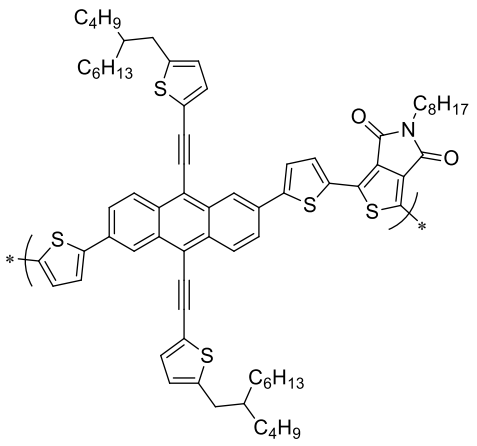


**(PATA(BO)TPD-8)** was prepared following a procedure similar to **(PAA(PU)TPD-8)** from monomer from 2,6-bis(5-bromothiophen-2-yl)-9,10-bis-[2-(ethynyl-5-butyl-octyl) thiophene-2-yl]anthracene (**M7**) (0.10 g, 0.095 × $10^{-3}$ mol) and 5-octyl-4H-thieno[3,4-c]pyrrole-4,6(5H)-dione (**M10**) (0.025 g, 0.095 × $10^{-3}$ mol). The polymer was collected from toluene fraction as dark purple solid. Yield 71 mg (65%). GPC (TCB): $M_w$ = 7300, $M_n$ = 5000, PD = 1.5. $^1$HNMR ($C_2D_2Cl_4$): ($\delta_H$/ppm); 8.74-6.61 (b peak, 14H); 3.84-3.49 (bm, 2H); 3.12-2.72 (bm, 4H); 2.04-1.19 (bm, 46H); 1.16-1.79 (bm, 15H). Elemental Analysis (%) calculated for $C_{72}H_{81}NO_2S_5$: C, 75.02; H, 7.08; N, 1.22; S, 13.91. Found: C, 73.30; H, 6.96; N, 0.93; S, 13.27. FT-IR ($cm^{-1}$): 3067 (aromatic C–H stretch), 2952-2849 (aliphatic C–H stretch), 2182 (carbon, carbon triple bond stretch), 1696 (C=O stretch), 1509 and 1462 (aromatic C=C stretch), 1369 and 1088 (C–N stretch).

### 5.5.14 Poly[2,6-di-(thiophen-2-yl)-9,10-bis[2-(ethynyl-5-butyl-octyl)thiophene]-anthracene-5-diyl-alt-5-(3,7-dimethyl-octyl)-4H-thieno[3,4-c]pyrrole-4,6(5H)-dione[3,4-c]pyrrole-4,6-dione] (PATA(BO)TPD-DMO):[10, 11]

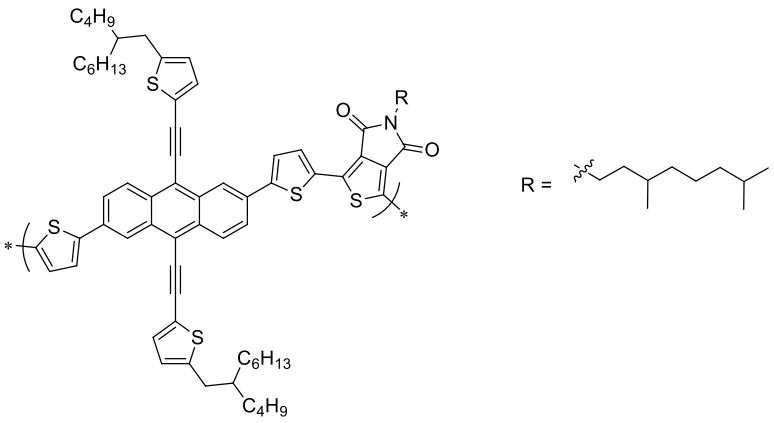


**(PATA(BO)TPD-DMO)** was prepared following a procedure similar to **(PAA(PU)TPD-8)** from monomer from 2,6-bis(5-bromothiophen-2-yl)-9,10-bis-[2-(ethynyl-5-butyl-octyl) thiophene-2-yl]anthracene (**M7**) (0.12 g, $0.11 \times 10^{-3}$ mol) and 5-(3,7-dimethyl-octyl)-4H-thieno[3,4-c]pyrrole-4,6(5H)-dione **(M11)** (0.033 g, $0.11 \times 10^{-3}$ mol). The polymer was collected from toluene fraction as dark purple solid. Yield 90 mg (67%). GPC (TCB): $M_w$ = 11300, $M_n$ = 6400, PD = 1.8. $^1$HNMR ($C_2D_2Cl_4$): ($\delta_H$/ppm); Peaks were not clear due to aggregation. Elemental Analysis (%) calculated for $C_{74}H_{85}NO_2S_5$: C, 75.27; H, 7.26; N, 1.19; S, 13.58. Found: C, 73.35; H, 7.33; N, 1.03; S, 13.18. FT-IR ($cm^{-1}$): 3064 (aromatic C–H stretch), 2955-2855 (aliphatic C–H stretch), 2185 (carbon, carbon triple bond stretch), 1699 (C=O stretch), 1512 and 1459 (aromatic C=C stretch), 1366 and 1054 (C–N stretch).

### 5.5.15 Poly[2,6-di-(thiophen-2-yl)-9,10-bis-(3-pentylundec-1-yne)-anthracene-5-dyil-alt-5-octyl-4H-thieno[3,4-c]pyrrole-4,6(5H)-dione[3,4-c]pyrrole-4,6-dione] (PVA(PU)TPD-8): [10, 11]

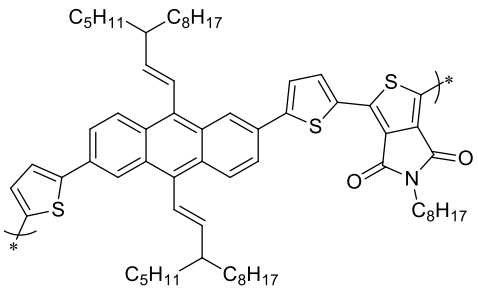


**(PVA(PU)TPD-8)** was prepared following a procedure similar to **(PAA(PU)TPD-8)** from monomer 5-octyl-4H-thieno[3,4-c]pyrrole-4,6(5H)-dione (**M10**) (0.028 g, $0.11 \times 10^{-3}$ mol) and 2,6-di-(5-bromothiophen-2-yl)-9,10-bis-(3-pentylundec-1-yne) anthracene (**M9**) (0.10 g, $0.11 \times 10^{-3}$ mol). The polymer was collected from toluene fraction as dark red solid. Yield 83 mg (74%). GPC ($CHCl_3$): $M_w$ = 54000, $M_n$ = 17100, PD = 3.2. $^1$HNMR ($C_2D_2Cl_4$): ($\delta_H$/ppm); 8.57-7.65 (b, 6H); 7.62-7.15 (b, 4H); 7.13-6.81 (b, 2H); 6.26-6.05 (b, 2H); 3.84-3.57 (bm, 2H); 3.12-2.72 (bm, 4H); 1.98-0.58 (bm, 73H). Elemental Analysis (%) calculated for $C_{68}H_{89}NO_2S_3$: C, 77.89; H, 8.65; N, 1.34; S, 9.17. Found: C, 77.82; H, 8.61; N, 1.26; S, 8.83. FT-IR ($cm^{-1}$): 3080 (aromatic C–H stretch), 2952-2850 (aliphatic C–H stretch), 1700 (C=O stretch), 1610 (alkene C=C stretch), 1516 and 1460 (aromatic C=C stretch), 1364 and 1090 (C–N stretch).

### 5.5.16 Poly[2,6-di-(thiophen-2-yl)-9,10-bis-(3-pentylundec-1-yne)-anthracene -5-dyil-alt-5-(3,7-dimethyl-octyl)-4H-thieno[3,4-c]pyrrole-4,6(5H)-dione [3,4-c]pyrrole-4,6-dione] (PVA(PU) TPD-DMO): [10, 11]

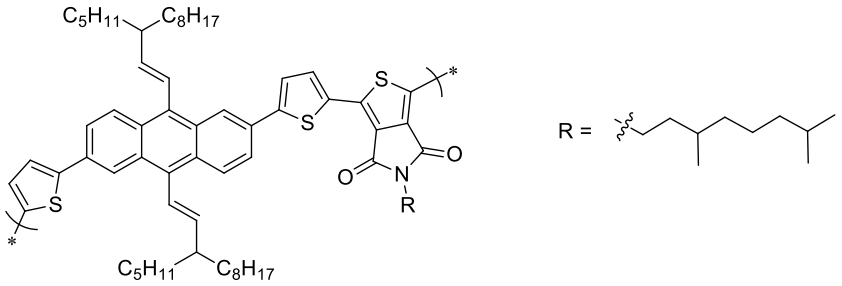


**(PVA(PU)TPD-8)** was prepared following a procedure similar to **(PAA(PU)TPD-8)** from monomer 5-(3,7-dimethyl-octyl)-4H-thieno[3,4-c]pyrrole-4,6(5H)-dione **(M11)** (0.031 g, $0.11 \times 10^{-3}$ mol) and 2,6-di-(5-bromothiophen-2-yl)-9,10-bis-(3-pentylundec-1-yne) anthracene (**M9**) (0.10 g, $0.11 \times 10^{-3}$ mol). The polymer was collected from toluene fraction as dark purple solid. Yield 93 mg (82%). GPC ($CHCl_3$): $M_w$ = 94200, $M_n$ = 22000, PD = 4.3. $^1$HNMR ($C_2D_2Cl_4$): ($\delta_H$/ppm); 8.59-7.65 (b, 6H); 7.63-7.17 (b, 4H); 7.15-6.85 (b, 2H); 6.21-6.03 (b, 2H); 3.94-3.55 (bm, 2H); 1.94-0.52 (bm, 77H). Elemental Analysis (%) calculated for $C_{70}H_{93}NO_2S_3$: C, 78.09; H, 8.71; N, 1.30; S, 8.93. Found: C, 77.62; H, 8.74; N, 1.28; S, 8.51. FT-IR ($cm^{-1}$): 3074 (aromatic C–H stretch), 2950-2850 (aliphatic C–H stretch), 1697 (C=O stretch), 1609 (alkene C=C stretch), 1517 and 1460 (aromatic C=C stretch), 1370 and 1088 (C–N stretch), 1037 (alkene =C–H stretch), 966 (alkene =C–H bending).

## 5.6 References:


1. S. Liu, X. Bao, W. Li, K. Wu, G. Xie, R. Yang and C. Yang, *Macromolecules*, 2015, **48**, 2948-2957.
2. H. Zhang, S. Ying, B. Tieke, J. Zhang and W. Yang, *Polymer*, 2015, **60**, 215-220.
3. L. Cartwright, T. J. Neal, N. J. Rutland and A. Iraqi, *Polym. Adv. Technol.*, 2015.
4. J. Y. Ma, H. J. Yun, S. O. Kim, G. B. Lee, H. Cha, C. E. Park, S. K. Kwon and Y. H. Kim, *J. Polym. Scie. Part A: Polym. Chem.*, 2014, **52**, 1306-1314.
5. W. Liu, D. He, B. Qiu, L. Jiang, G. Chen, H. Peng and Y. Zou, *J. Macromol. Sci., Part A*, 2015, **52**, 752-760.
6. E. Zhu, B. Ni, B. Zhao, J. Hai, L. Bian, H. Wu and W. Tang, *Macromol. Chem. Phys.*, 2014, **215**, 227-234.
7. B. Xia, K. Lu, Y. Zhao, J. Zhang, L. Yuan, L. Zhu, Y. Yi and Z. Wei, *Adv. Sci.*, 2015, **2**.
8. R. Sheng, Q. Liu, W. Chen, M. Sun, H. Zheng, J. Ren and R. Yang, *J. Polym. Sci. Part A: Polym. Chem.*, 2015.
9. C. E. Small, S. Chen, J. Subbiah, C. M. Amb, S.-W. Tsang, T.-H. Lai, J. R. Reynolds and F. So, *Nat. Photonics*, 2012, **6**, 115-120.
10. P.-O. Morin, T. Bura and M. Leclerc, *Mater. Horiz.*, 2016, **3**, 11-20.
11. P.-O. Morin, T. Bura, B. Sun, S. I. Gorelsky, Y. Li and M. Leclerc, *ACS Macro Lett.*, 2014, **4**, 21-24.
12. H. C. Brown and K. Murray, *J. Am. Chem. Soc.*, 1959, **81**, 4108-4109.
13. M. Hudlicky, *Reductions in organic chemistry*, Ellis Horwood Chichester, 1984.
14. Y. Sonoda, Y. Shimoi, M. Goto, N. Tohnai and M. Kanesato, *J. Phys. Chem. A*, 2013, **117**, 566-578.
15. J. Domínguez Chávez, S. Hernandez Ortega and M. Martínez-García, *The Open Organic Chemistry Journal*, 2009, **3**.
16. E. Díez-Barra, J. C. García-Martínez, S. Merino, R. del Rey, J. Rodríguez-López, P. Sánchez-Verdú and J. Tejeda, *J. Org. chem.*, 2001, **66**, 5664-5670.

17. L. Hintermann, M. Schmitz and Y. Chen, *Adv. Synth. Catal.*, 2010, **352**, 2411-2415.
18. J. W. Rumer, C. K. Hor, I. Meager, C. P. Yau, Z. Huang, C. B. Nielsen, S. E. Watkins, H. Bronstein and I. McCulloch, *J. Org. Semiconductors*, 2013, **1**, 30-35.
19. L. Ye, S. Zhang, L. Huo, M. Zhang and J. Hou, *Acc. Chem. Res.*, 2014, **47**, 1595-1603.
20. R. O. Garay, H. Naarmann and K. Muellen, *Macromolecules*, 1994, **27**, 1922-1927.
21. F. Silvestri, A. Marrocchi, M. Seri, C. Kim, T. J. Marks, A. Facchetti and A. Taticchi, *J. Am. Chem. Soc.*, 2010, **132**, 6108-6123.
22. S. Badgujar, S. K. Lee and T. Ahn, *J. Korean Phys. Soc.*, 2015, **67**, 1023-1027.
23. D. Gedefaw, M. Tessarolo, W. Zhuang, R. Kroon, E. Wang, M. Bolognesi, M. Seri, M. Muccini and M. R. Andersson, *Polym. Chem.*, 2014, **5**, 2083-2093.
24. Y. He, J. You, L. Dou, C.-C. Chen, E. Richard, K. C. Cha, Y. Wu, G. Li and Y. Yang, *Chem.l Commun.*, 2012, **48**, 7616-7618.
25. T. T. Do, Y. E. Ha and J. H. Kim, *Org. Electron.*, 2013, **14**, 2673-2681.
26. J. Rumer, Imperial College London, 2014.
27. H. D. Magurudeniya, R. S. Kularatne, E. A. Rainbolt, M. P. Bhatt, J. W. Murphy, E. E. Sheina, B. E. Gnade, M. C. Biewer and M. C. Stefan, *J. Mat. Chem. A*, 2014, **2**, 8773-8781.
28. J.-M. Jiang, M.-C. Yuan, K. Dinakaran, A. Hariharan and K.-H. Wei, *J. Mater. Chem. A*, 2013, **1**, 4415-4422.
29. T. Prosa, M. Winokur, J. Moulton, P. Smith and A. Heeger, *Macromolecules*, 1992, **25**, 4364-4372.
30. S. Wen, M. Xiao, W. Shen, C. Gu, D. Zhu and R. Yang, *New J. Chem.*, 2016, **40**, 5300-5305.
31. J. F. Lee, S. L. C. Hsu, P. I. Lee, H. Y. Chuang, J. S. Chen and W. Y. Chou, *Sol. Energ. Mater. Sol. Cells*, 2012, **96**, 218-225.
32. S. Jo, J. Shin, S. Y. Bae, K. H. Kim, T. W. Lee, S. Son, K. Kim and D. H. Choi, *Synth. Met.*, 2011, **161**, 833-843.

33. W. Cui, Y. Zhao, H. Tian, Z. Xie, Y. Geng and F. Wang, *Macromolecules*, 2009, **42**, 8021-8027.
34. T. Zheng, L. Lu, N. E. Jackson, S. J. Lou, L. X. Chen and L. Yu, *Macromolecules*, 2014, **47**, 6252-6259.
35. M. Helgesen, S. A. Gevorgyan, F. C. Krebs and R. A. Janssen, *Chem. Mater.*, 2009, **21**, 4669-4675.

# Chapter 6

## *Conclusion And Future Work*

# Chapter 6

## 6.1 Conclusion

Development of efficient organic photovoltaic devices, represents a viable approach for the supply of cheap and sustainable energy, capable of satisfying the growing global energy needs in an environmental friendly manner. Major research interest is focussed on bulk heterojunction organic solar cells, in which the active layers consist of blends of conjugated polymers as electron donor materials and fullerene derivatives as electron acceptor materials. This has led to a reasonable enhancement in the performance of organic solar cells [1]. Nowadays, researchers in the field of organic solar cells are focussing their efforts on designing and synthesizing low band gap polymers that can absorb light in the range up-to 800 nm and as a result obtain devices with improved short circuit currents and power conversion efficiencies [2]. Therefore, throughout this dissertation, we have tried to discuss and present three main aspects in detail. Herein, we have designed and synthesised a series of conjugated polymers and characterized their optoelectronic properties, thermal stabilities and molecular orientation in the solid state. We have also evaluated the photovoltaic performance of these polymers in solar cell devices in blends with $PC_{71}BM$.

In order to prepare efficient conjugated polymers for OPV applications, with suitable positions of HOMO and LUMO energy levels when used as electron donors in blends with $PC_{71}BM$, we have designed these materials based on the ‘‘push-pull’’ approach with alternating 2,6-linked anthracene derivatives as electron donor units and benzothiadiazole and TPD units as electron acceptor segments.

The first family of conjugated polymers was based on 2,6-linked anthracene units flanked by thienyl groups as the electron rich segments and benzo[*c*][1,2,5]thiadiazole as the alternate electron acceptor moieties to yield **PATA(D)TBT**, **PATA(BO)TBT** and **PAA(PU)TBT**. The influence of the attached groups into the 9,10-positions of the anthracene units was studied by UV-visible spectroscopy, cyclic voltammetry and powder X-ray diffraction studies. The three polymers display a limited solubility in common organic solvent at room temperature; a consequence of the absence of any solubilising groups on the **BT** units. Polymer solar cell based on **PATA(D)TBT**

blended with $PC_{70}BM$ has shown a PCE of 0.76% and $V_{oc}$ of 0.54 V. These low values can be attributed to the morphology of the active layers in devices.

The second family of polymers was designed to overcome the solubility issues that arose with the first family of polymers. Benzothiadiazole (**BT**) repeat units with octyloxy substituents were used on the basis that they will provide an enhanced solubility to the resulting polymers in comparison to the **BT** units without octyloxy substituents. As expected, all the polymers in the new series have shown high solubility on common organic solvents. However, the low $M_n$ of **PAA(PU)TBT-8** can be ascribed to the bulky substituents on the anthracene units and the alkoxy groups on the BT moieties. As a drawback of substituting **BT** units with octyloxy groups, all the polymers exhibited high lying LUMO levels when compared to their counterpart polymers without alkoxy groups in their backbones. This is believed to originate from the electron releasing octyloxy substituents which reduce the electron accepting properties of the **BT** units they are attached to. The photovoltaic performance of devices of **PATA(D)TBT-8** and **PATA(BO)TBT-8** (PCE values of 0.90 and 1.04%, respectively) are quite modest, however, we believe that further studies to optimise device performance are warranted in order to explore the potential properties of these materials in bulk heterojunction solar cells.

The influence of the spacer between the donor and acceptor in conjugated polymers was investigated in chapter 4. A series of conjugated polymers consisting of 2,6-linked anthracene as donor units and benzo[c][1,2,5]thiadiazole as acceptor units spaced with bithiophene π-bridges has been synthesised by Stille coupling polymerisation. All the polymers exhibited a high solubility in chlorinated organic solvents such as chloroform and chlorobenzene. The presence of bithiophene as spacer makes the polymers backbone planar and more linear which help to improve their optical properties when compared to their corresponding polymers with a single thiophene spacer discussed in chapter 4. However, introducing the bithiophene spacer in these polymers resulted in shallower HOMO energy levels in comparison to their counterpart polymers with one thiophene spacer. The power conversion efficiency of polymer solar cells based on blends of polymers as electron donors and $PC_{71}BM$ as electron acceptor reached 0.85% for **PAA(PU)T2BT-8**, 0.86% for **PATA(B)T2BT-8** and 1.80% for **PATA(BO)T2BT-8**. Obviously, the performance of devices based on **PATA(BO)T2BT-8** : $PC_{71}BM$

revealed more than double the power conversion efficiency of the other two polymers, as a result of the improvement in its $J_{sc}$ (–4.06 mA $cm^{-2}$) and FF (55%).

The last family of conjugated polymers that was investigated in this project was a series of six alternating copolymers comprising 9,10-functionalised anthracene units and **TPD** functionalised units synthesised by direct arylation polymerisation. The photophysical, electrochemical and the crystallinity of the resulting polymers were affected by the nature of the substituents on the anthracene units. Polymers with side chains attached *via* ethynyl groups on the 9,10-positions of the anthracene units (**PATA(BO)TPD-8**, **PATA(BO)TPD-DMO**, **PAA(PU)TPD-8** and **PAA(PU)TPD-DMO**) displayed electronic delocalisation in two-dimensions i.e. both along the polymer chains as well as laterally on the anthracene repeat units and their unsaturated ethynyl-substituents attached at the 9,10-positions, which resulted in materials with moderate optical band gaps. However, replacing the ethynyl substituents with the alkene substituents on the 9,10-positions of the anthracene units lead to polymers (**PAV(PU)TPD-8** and **PAV(PU)TPD-DMO**) with higher optical band gaps due to the steric repulsions between vinylic hydrogens and hydrogens on the 1,4,5,8-postions of anthracene repeat units. The planarity of these six polymers was confirmed by powder X-ray diffraction studies. The polymers with ethynyl groups on the anthracene units **PATA(BO)TPD-8**, **PATA(BO)TPD-DMO**, **PAA(PU)TPD-8** and **PAA(PU)TPD-DMO**) displayed small sharp peaks at the high angle region. These peaks are a good indication of strong π-π stacking suggesting that the use of the ethynyl groups on the anthracene units improves the planarity of the polymers chains. On the other hand, powder X-ray studies of the polymers with alkene substituents revealed the amorphous nature of these polymers. The HOMO levels of the polymers **PAV(PU)TPD-8** and **PAV(PU)TPD-DMO** were deeper than those of corresponding polymers with ethynyl-substituents (**PATA(BO)TPD-8**, **PATA(BO)TPD-DMO**, **PAA(PU)TPD-8** and **PAA(PU)TPD-DMO**) because of the vinylic substituents which enhanced steric hindrance in the resulting polymers and as a result increased their band gaps.

## 6.2 Future Work

We have discussed 2,6-linked anthracene based conjugated polymers as donor materials for the use in organic photovoltaic applications. We believe that the solubility and the photovoltaic properties of these polymers can be further improved through modifying the substituents at the 9,10-positions of the anthracene units. These modifications can be reached by introducing conjugated side chains (such as meta-alkoxyl-phenyl substituents or 2-alkyl-3-fluoro-thienyl substituents) which would allows us to overcome the solubility issues that have arisen in this project. Such substituents on the anthracene repeat units will also at the same time, offer the ability to modulate and tune the molecular energy levels of the anthracene-based polymers. In previous literatures, Huang *et al.* found that using *meta*-alkoxyl phenyl-substituents into benzo[1,2-*b*:4,5-*b*']dithiophene (BDT) repeat units instead of *para*-alkoxyl phenyl substituents resulted in deeper HOMO level which allows to improve the open circuit voltages ($V_{oc}$) and the PCE of OPV devices. Placing alkoxy groups at the *meta*-positions of phenyl substituents, enables to benefit from the solubilising effects of the alkoxy groups without these groups releasing electronic density to the anthracene units on the backbone as would be the case for the *para*-alkoxyl groups [3]. In fact, Iraqi *et al* have recently prepared a series of polymers where the anthracene units were functionalised with 4-dodecyloxy-phenyl groups [4]. Therefore, we can make a good comparison between polymers with regards to the functional groups attached to the anthracene units.

In addition, Zhang and coworkers synthesised a series of donor-acceptor polymers based on BDT and thieno[3,4-b]thiophene (TT), where they added fluorine atoms onto the donor units or/and acceptor moieties. They found that the fluorinated polymers revealed lower HOMO and LUMO levels compared with the non-fluorinated polymer. This is a good indication that fluorination on the donor units and acceptor units could have synergistic effect on lowering the molecular energy levels of the polymer [5]. Relying on these published articles, the chemical structures of the suggested anthracene-based polymers that are shown worth targeting are shown in **Figure 6.1**.

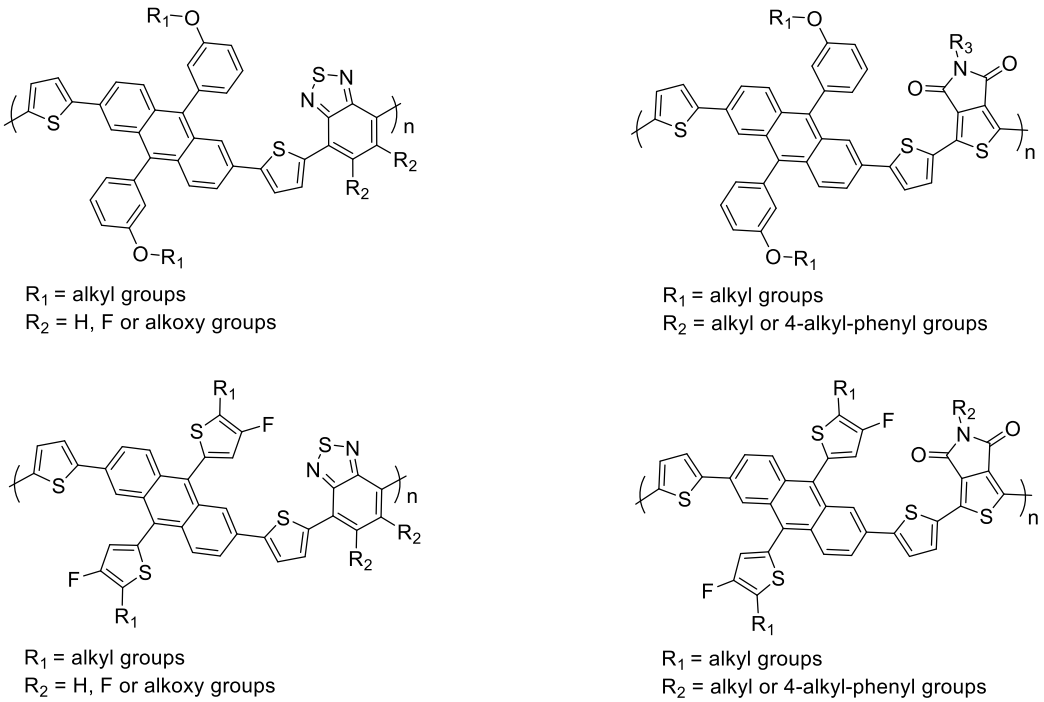


**Figure 6-1:** Proposed new families of anthracene-based donor-acceptor polymers.

The photovoltaic performance of devices of PATA(D)TBT, PATA(D)TBT-8, PATA(BO)TBT-8, PATA(D)T2BT-8, PATA(BO)T2BT-8 and PAA(PU)T2BT-8 studied in this thesis are quite modest. We believe that further investigations can be conducted to optimise the performance of bulk heterojunction polymer photovoltaic devices by a systematic study of the morphology of blends of these polymers with PC71BM. There are several factors and variables that can affect the morphology of active layers of devices and hence influence their power conversion efficiencies. Varying the weight/weight ratios of polymer/PC71BM as well as using different solvents for casting active layers or using additives upon casting films are all parameters that need to be optimised. Varying and controlling the thickness of active layers and using different film casting methods (spin-casting, spray-coating, etc.) in addition to annealing active layer films under different conditions are also parameters that need optimising to achieve optimum efficiencies from OPV devices.

In addition, polymers PATA(BO)TPD-8, PATA(BO)TPD-DMO, PAA(PU)TPD-8, PAA(PU)TPD-DMO, PAV(PU)TPD-8 and PAV(PU)TPD-DMO have shown good optical and electrochemical properties for use as new materials for photovoltaic applications. Future work should include investigations of OPV devices from these

polymers in bulk heterojunction solar cells as electron-rich materials. This will be done in collaboration with the Department of Physics and Astronomy.

## 6.3 References:


1. J. Y. Ma, H. J. Yun, S. O. Kim, G. B. Lee, H. Cha, C. E. Park, S. K. Kwon and Y. H. Kim, *J. Polym. Sci. Part A: Polym. Chem.*, 2014, **52**, 1306-1314.
2. H. Zhou, L. Yang and W. You, *Macromolecules*, 2012, **45**, 607-632.
3. M. Zhang, X. Guo, W. Ma, S. Zhang, L. Huo, H. Ade and J. Hou, *Adv. Mater.*, 2014, **26**, 2089-2095.
4. A. Abdulaziz, *Chem. Commun.*, 2013, **49**, 2252-2254.
5. M. Zhang, X. Guo, S. Zhang and J. Hou, *Adv. Mater.*, 2014, **26**, 1118-1123.

# Chapter 7

*Appendix*

# Chapter 7

## 7.1 Conclusion

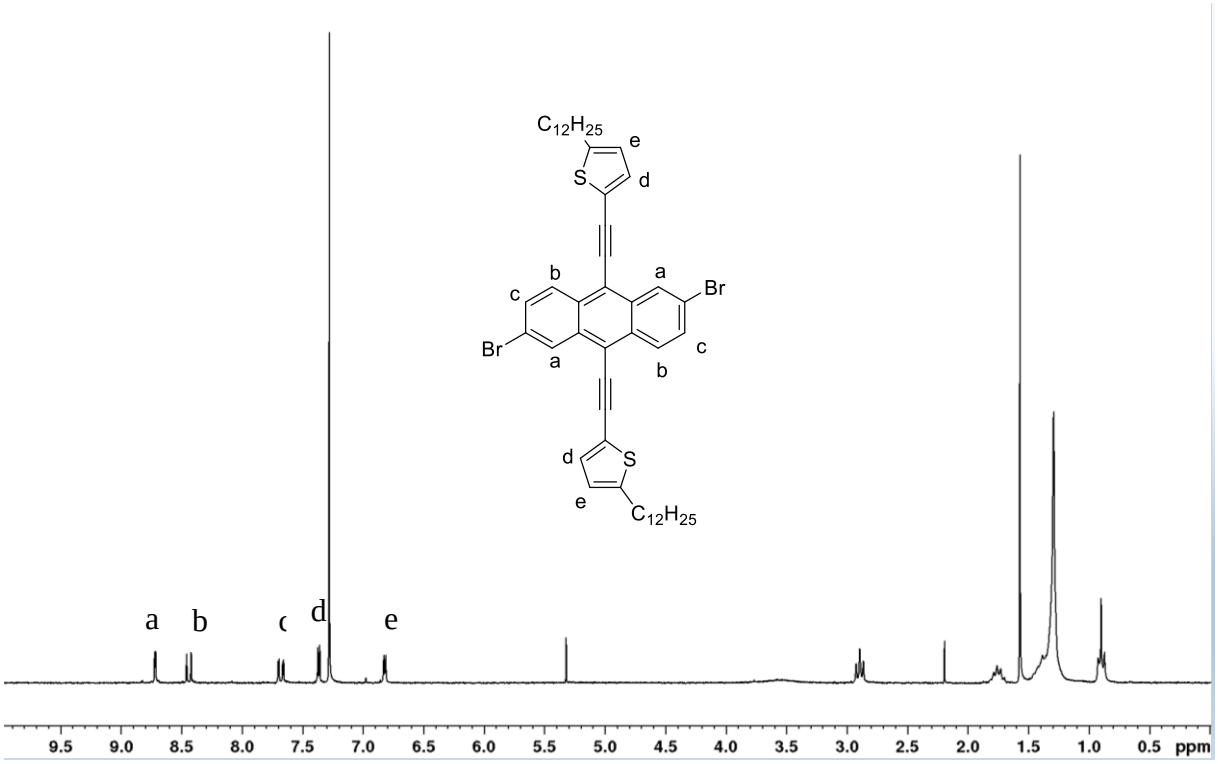


**Figure 7-1:** $^{1}$H-NMR Spectrum of 2,6-dibromo-9,10-bis[2-ethynyl-5-dodcylthiophen-2-yl]anthracene **(M1)**.

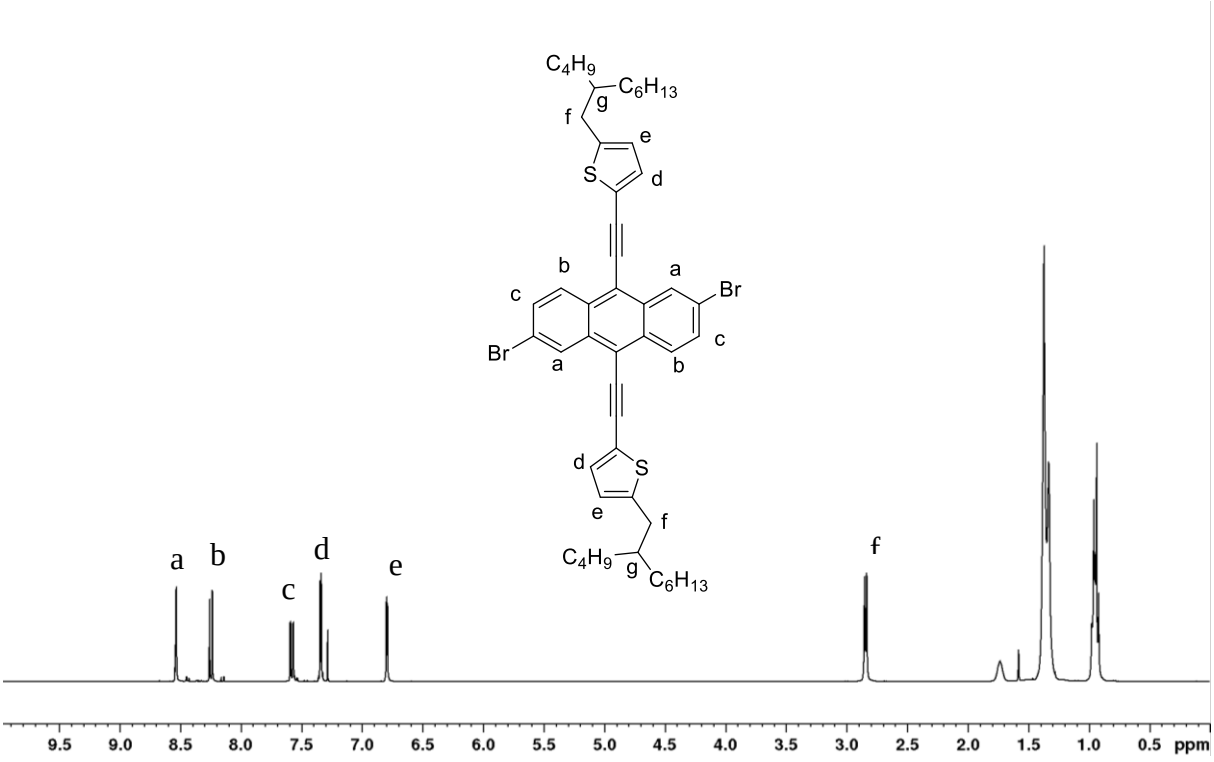


**Figure 7-2:** $^{1}$H-NMR Spectrum of 2,6-dibromo-9,10-bis[2-ethynyl-5-(2-butyl-octyl)-thiophen-2-yl]anthracene **(M2)**.

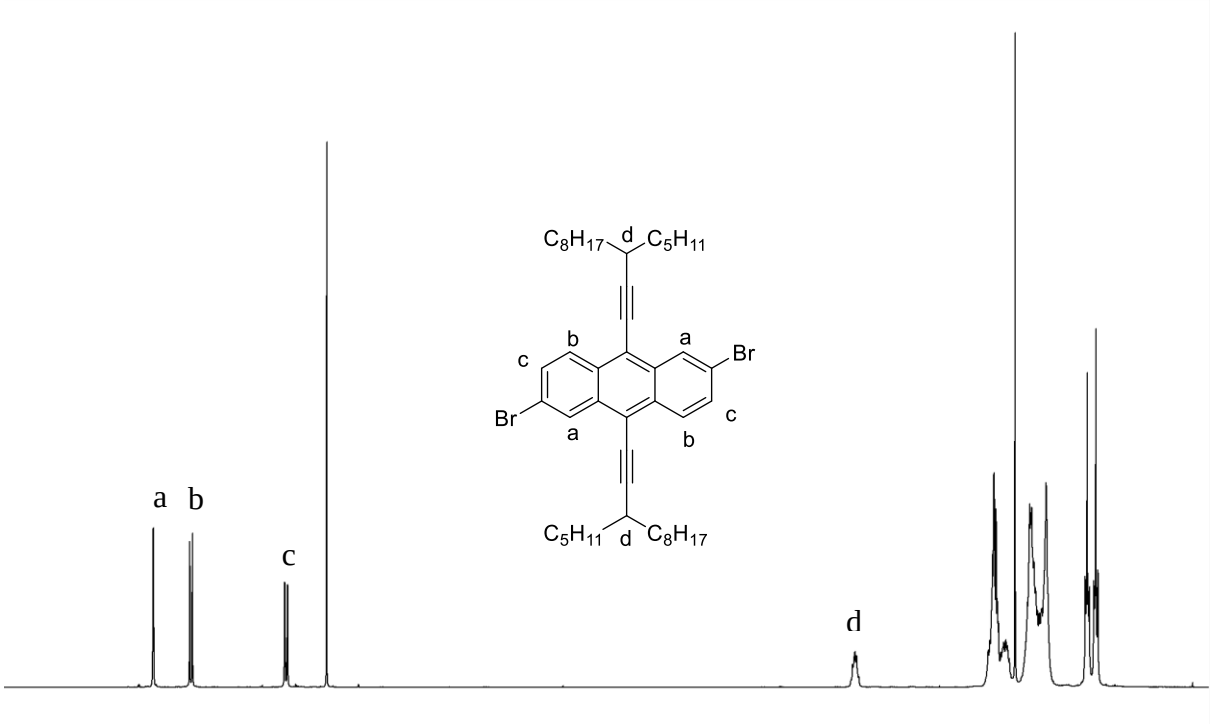


**Figure 7-3:** $^{1}$H-NMR Spectrum of 2,6-dibromo-9,10-di-(3-pentylundec-1-yne)-anthracene (M3).

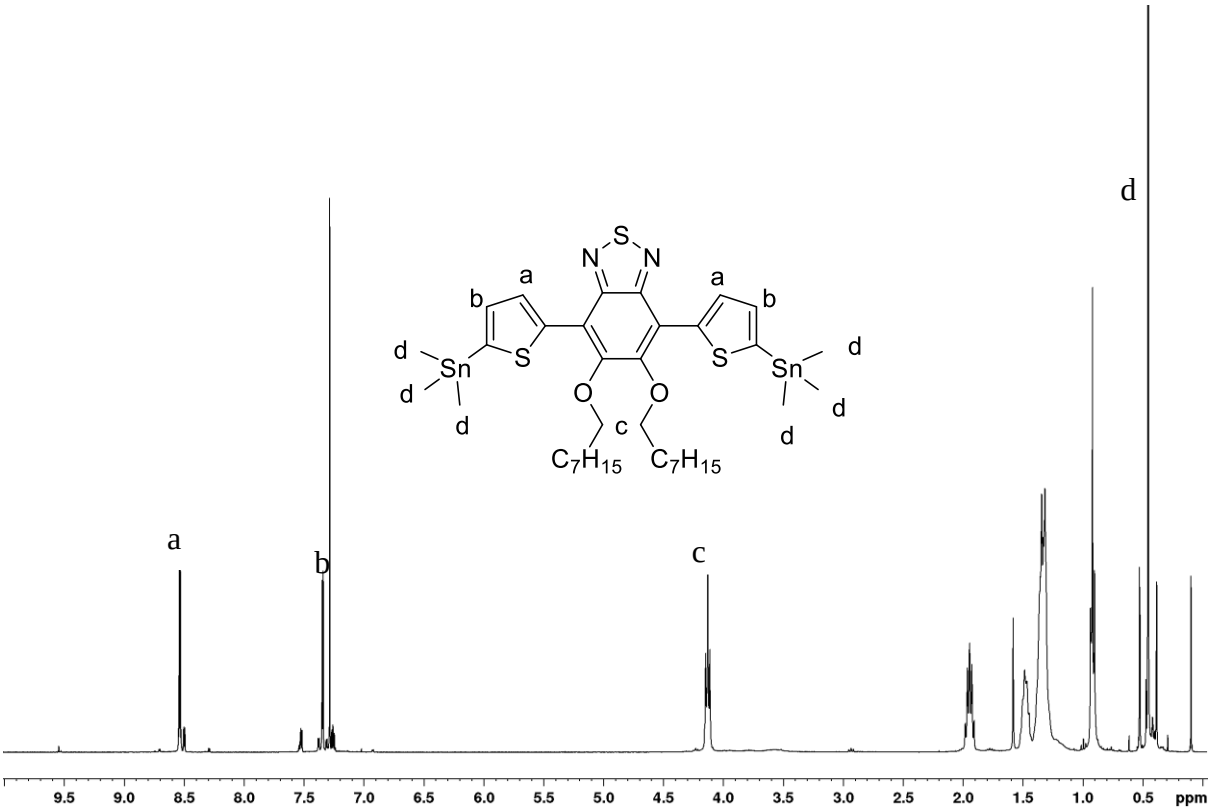


**Figure 7-4:** 1H-NMR Spectrum of 4,7-bis(5-(trimethylstannyl)thiophene-2-yl)-5,6-bis(octyloxy)benzo[c][1,2,5]thiadiazole (M5).

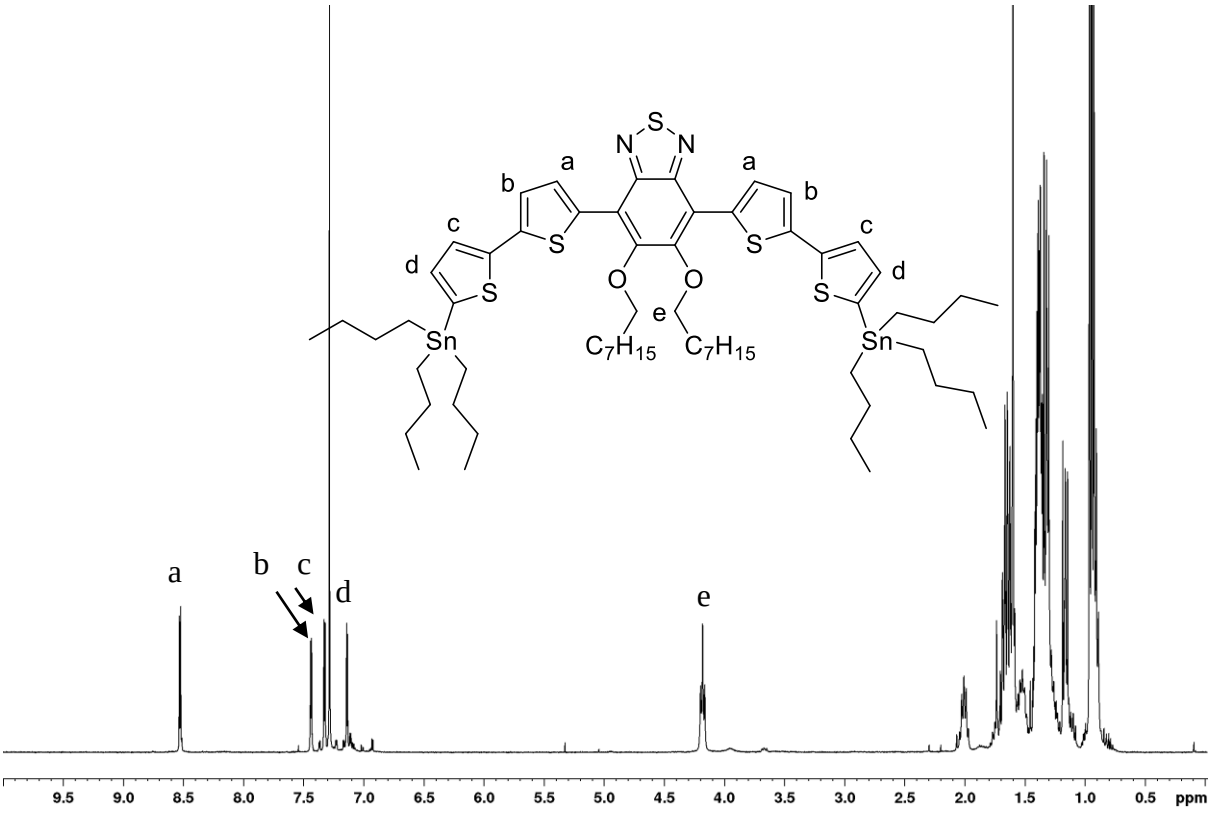


**Figure 7-5:** $^{1}$H-NMR Spectrum of 4,7-bis(5-(tributylstannyl)-[2,2']-bithiophen-5-yl)-5,6-bis (octyloxy)benzo[c][1,2,5]-thiadiazole **(M6)**.

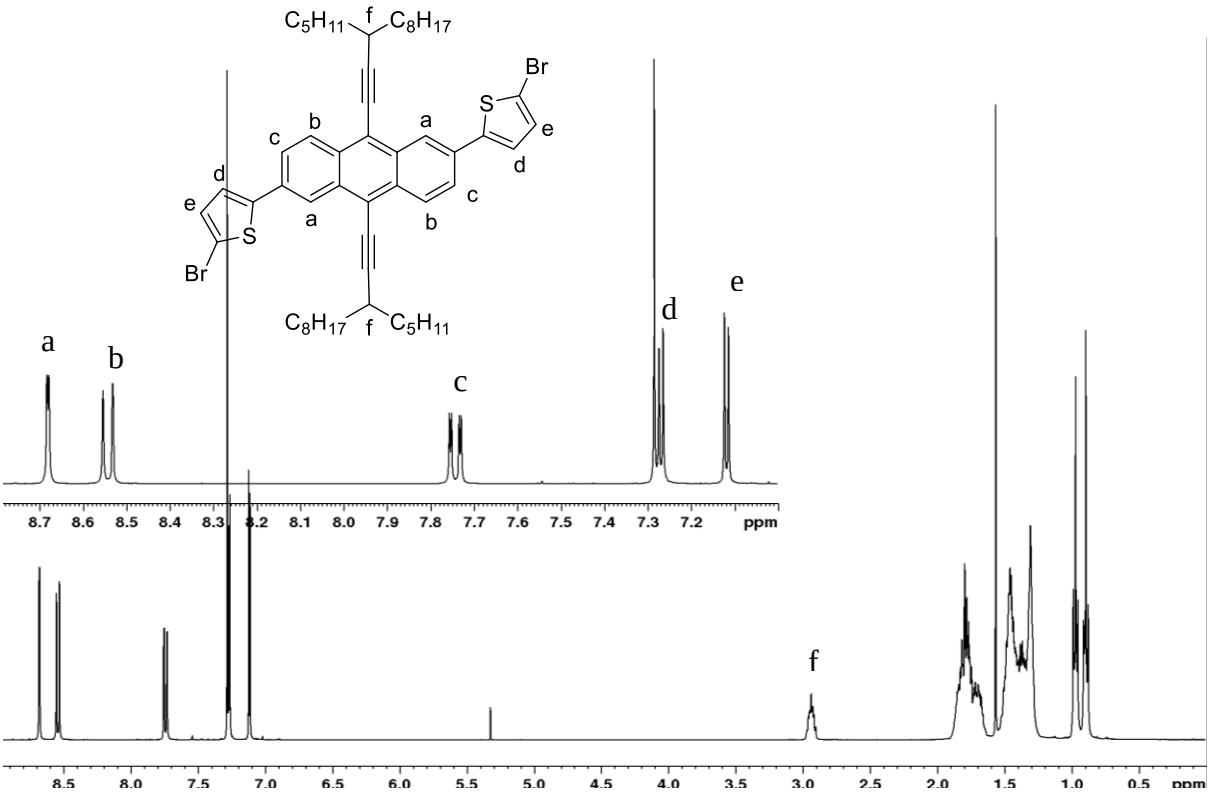


**Figure 7-6:** $^{1}$H-NMR Spectrum of 2,6-bis(5-bromothiophen-2-yl)-9,10-di-(3-pentylundec-1-yne)thiophene-2-yl]anthracene **(M7)**.

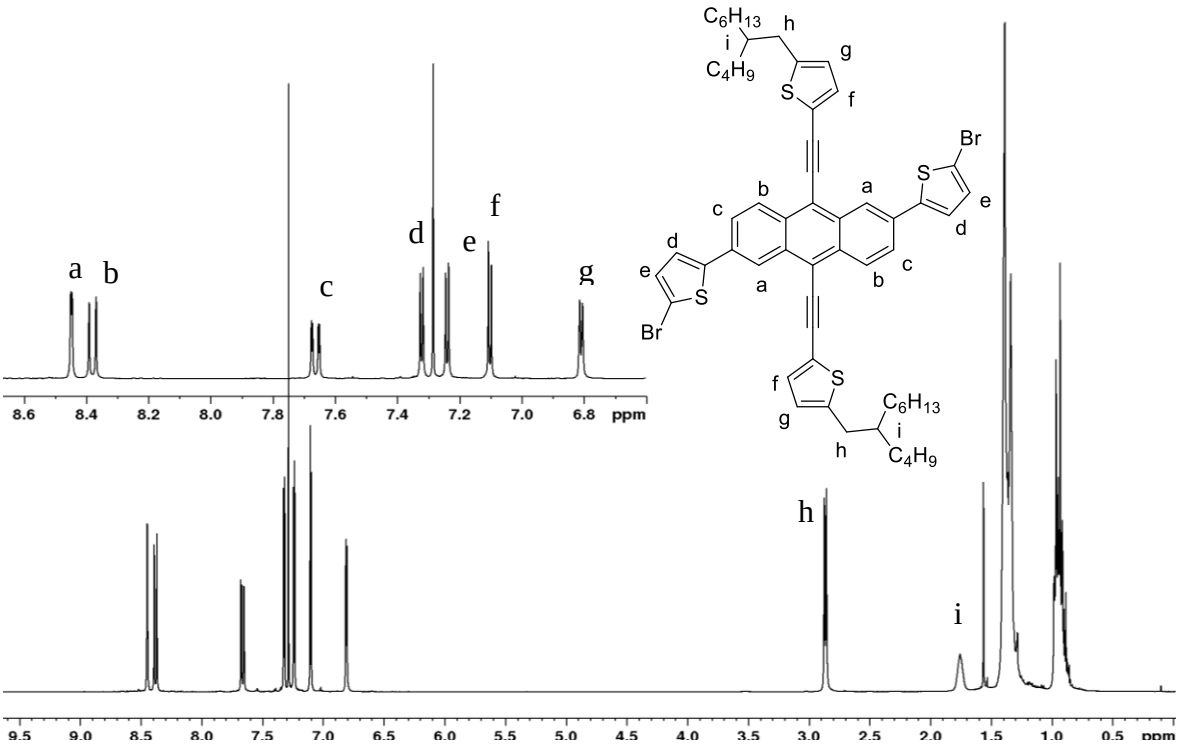


**Figure 7-7:** $^{1}$H-NMR Spectrum of 2,6-bis(5-bromothiophen-2-yl)-9,10-bis-[2-(ethynyl-5-butyl-octyl)thiophene-2-yl]anthracene **(M8)**.

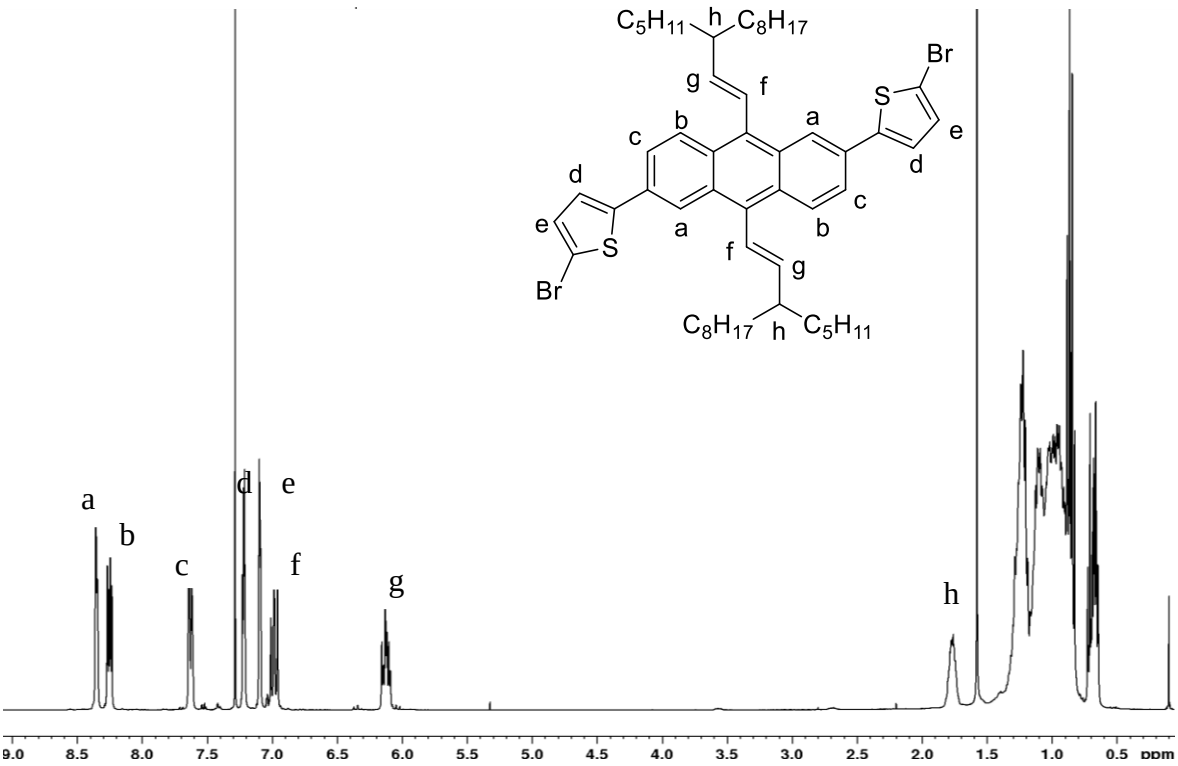


**Figure 7-8:** $^{1}$H-NMR Spectrum of 2,6-di(thiophene-2-yl)-9,10-bis-[3-pentylundcane] anthracene **(M9)**.

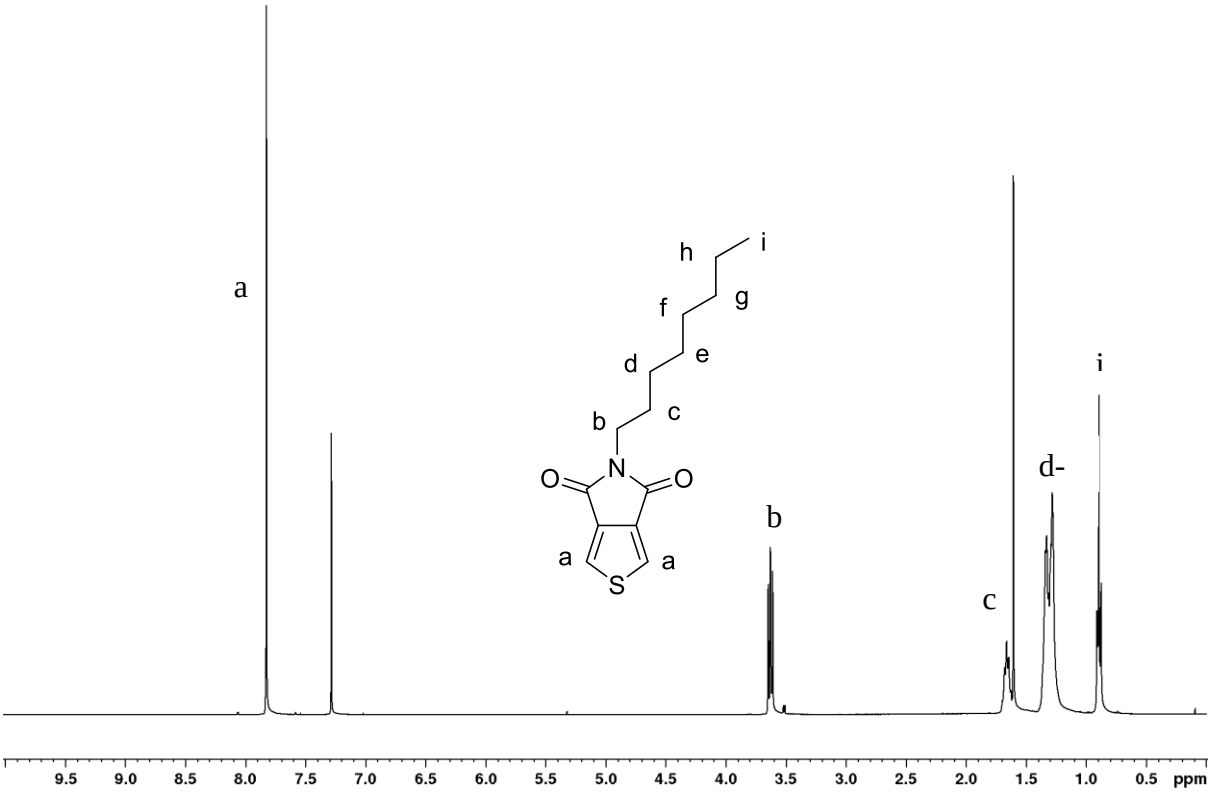


**Figure 7-9:** $^{1}$H-NMR Spectrum of 5-octyl-4H-thieno[3,4-c]pyrrole-4,6(5H)-dione **(M10)**.

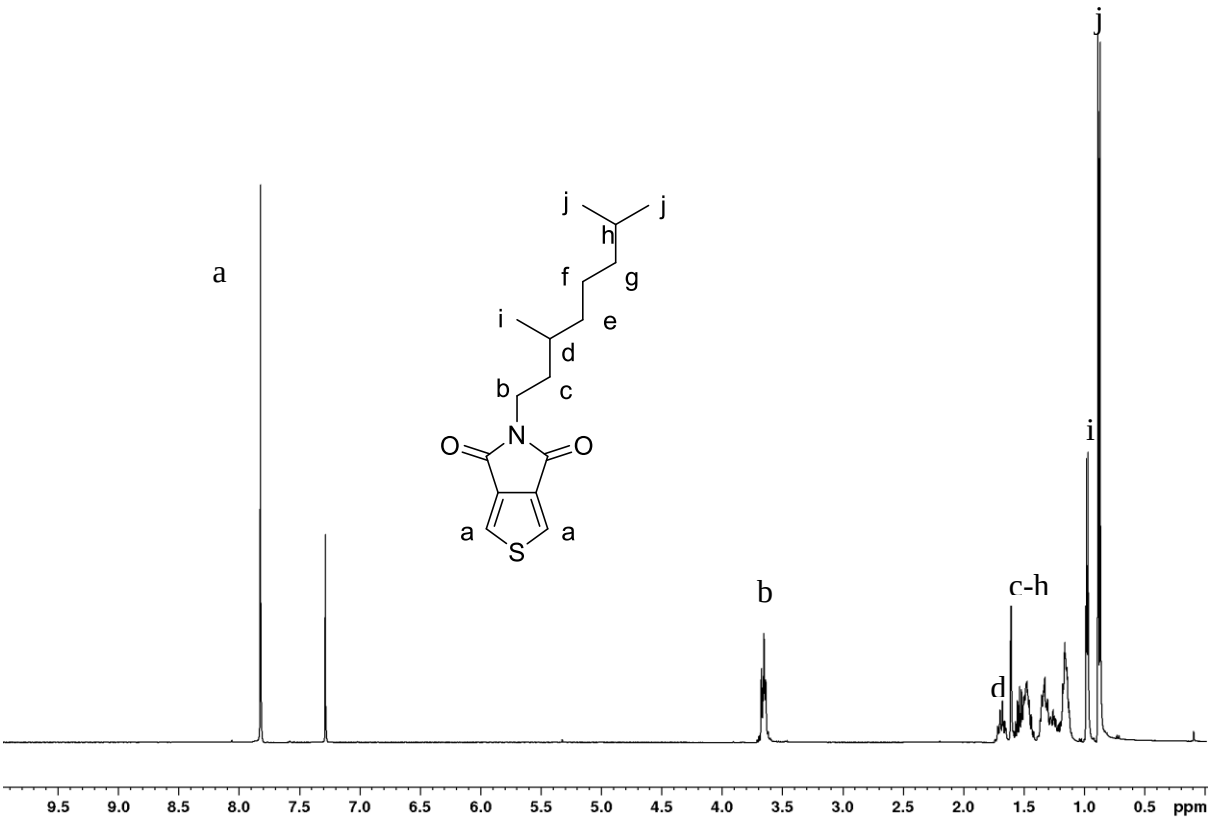


**Figure 7-10:** $^{1}$H-NMR Spectrum of 5-(3,7-dimethyl-octyl)-4H-thieno[3,4-c]pyrrole-4,6(5H)-dione **(M11)**.

## 7.2 $^{1}$H-NMR of the Polymers:

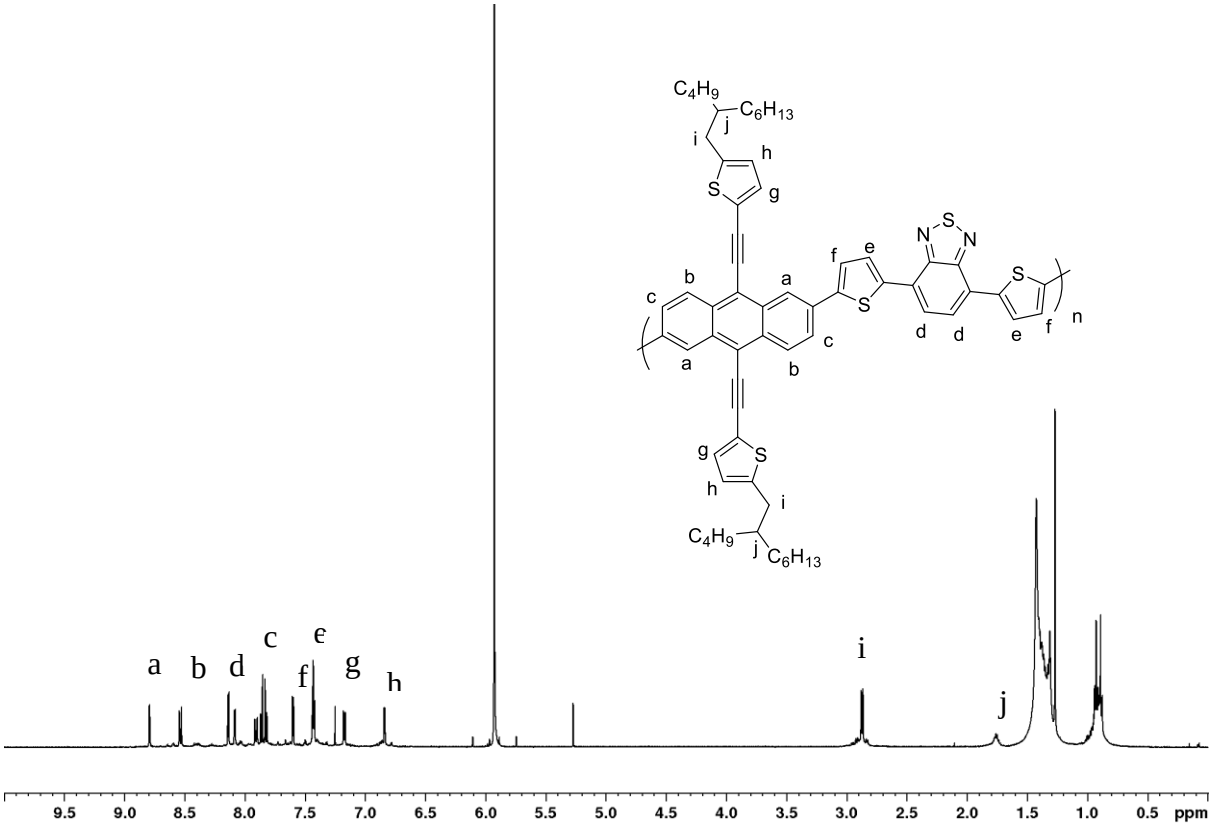


**Figure 7-11:** $^{1}$H-NMR Spectrum of Poly[9,10-bis[2-(ethynyl-5-butyl-octyl)thiophene]-anthracene-2,6-diyl-alt-4,7-di (thiophene-2-yl)benzo[c][1,2,5]thiadiazole] **(PATA(BO)TBT)**.

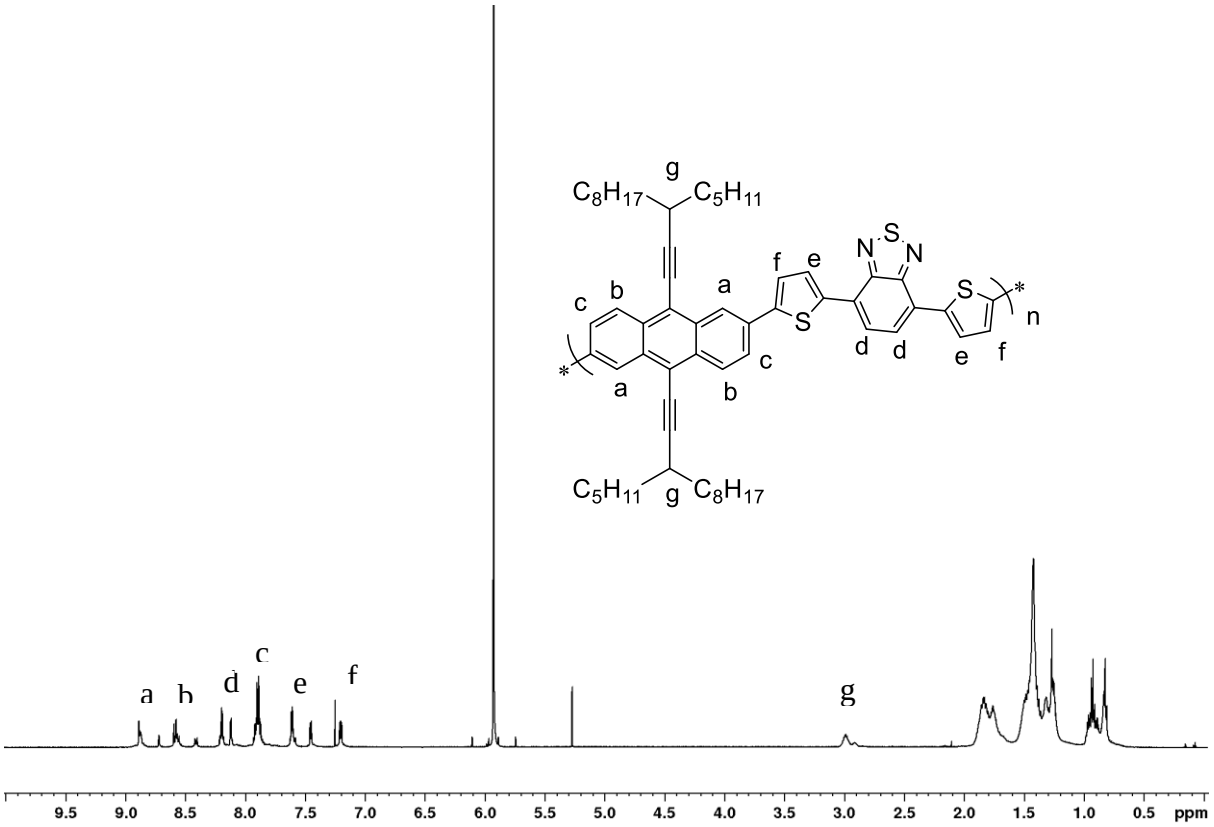


**Figure 7-12:** $^{1}$H-NMR Spectrum of Poly[9,10-di-(3-pentylundec-1-yne)-anthracene-2,6diyl-alt-4,7-di (thiophene-2-yl)benzo[c][1,2,5]thiadiazole] **(PAA(PU)TBT).**

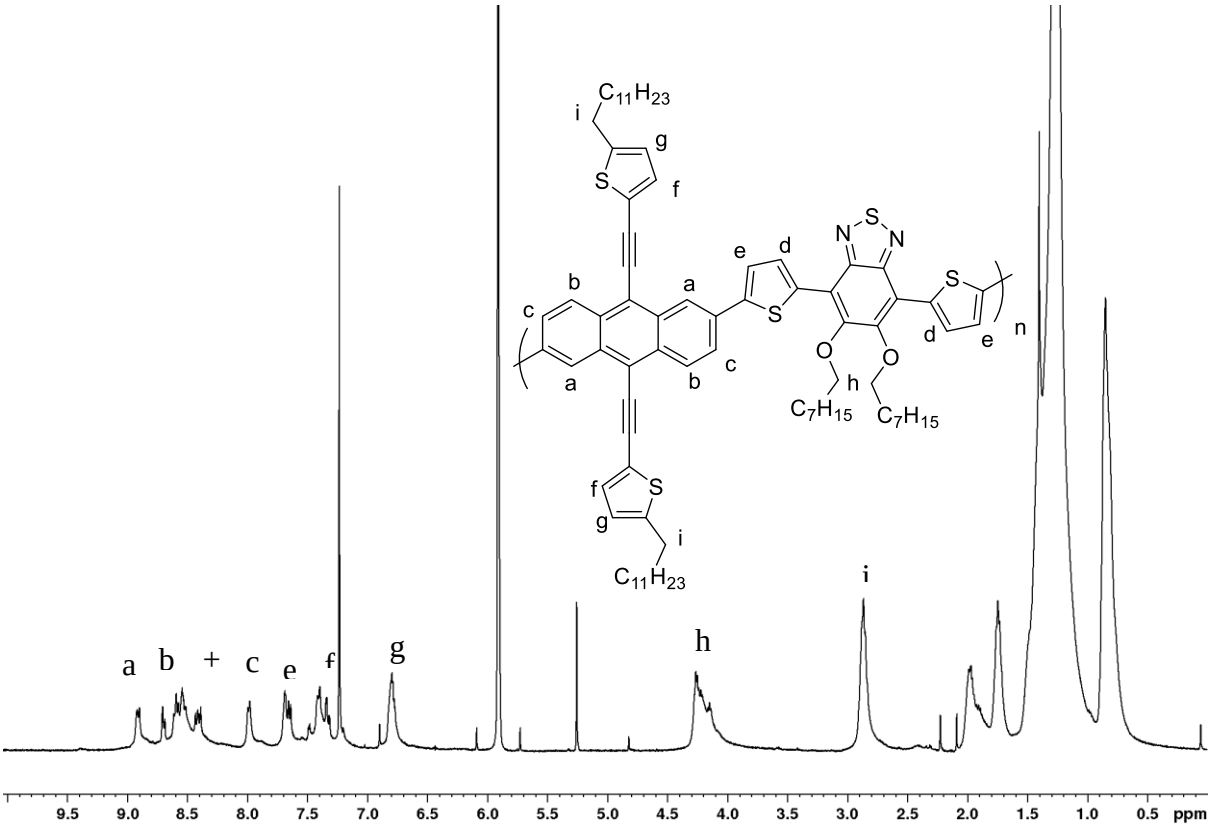


**Figure 7-13: :** $^{1}$H-NMR Spectrum of Poly[9,10-bis[2-ethynyl-5-dodcylthiophene]-anthracene-2,6-diyl-alt-5,6-bis (octyloxy)-4,7-di(thiophene-2-yl)benzo[c][1,2,5]thiadiazole] **(PATA(D)TBT-8).**

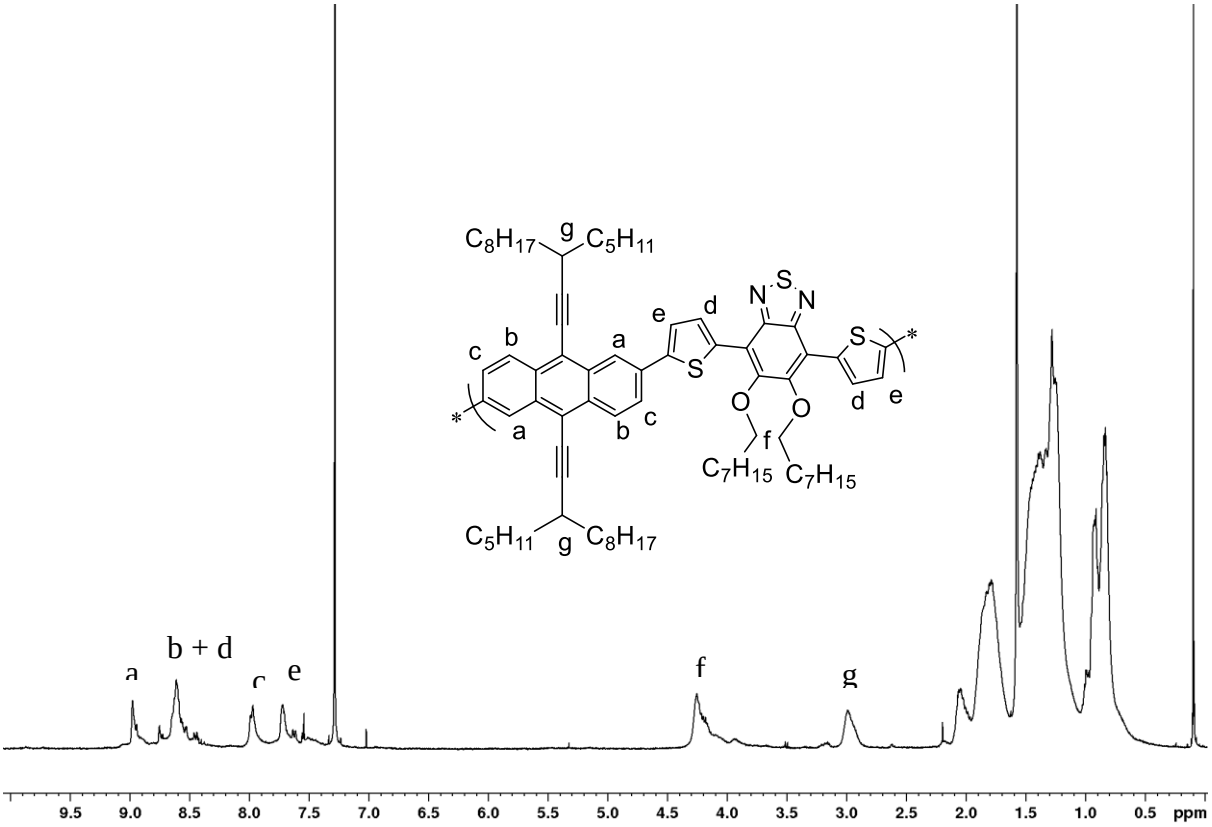


**Figure 7-14: :** $^{1}$H-NMR Spectrum of Poly[9,10-di-(3-pentylundec-1-yne)-anthracene-2,6diyl-alt-5,6-bis (octyloxy)-4,7-di(thiophene-2-yl)benzo[c][1,2,5]thiadiazole] **(PAA(PU)TBT-8).**

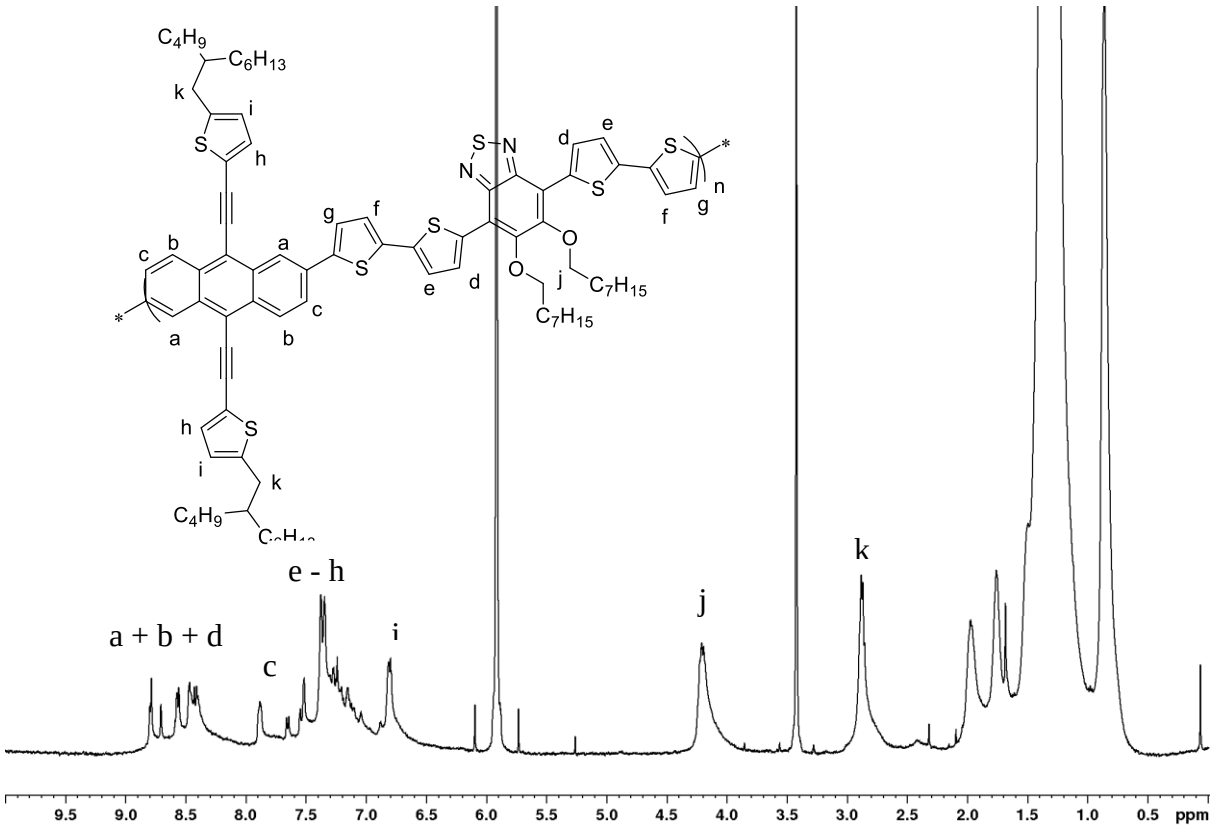


**Figure 7-15: :** $^{1}$H-NMR Spectrum of Poly[9,10-bis[2-(ethynyl-5-butyl-octyl)thiophene]-anthracene-2,6-diyl-alt-5,6-bis (octyloxy)-4,7-Di(2,2'-bithiophen-5-yl)benzo[c][1,2,5]-thiadiazole] **(PATA(BO)T2BT-8).**

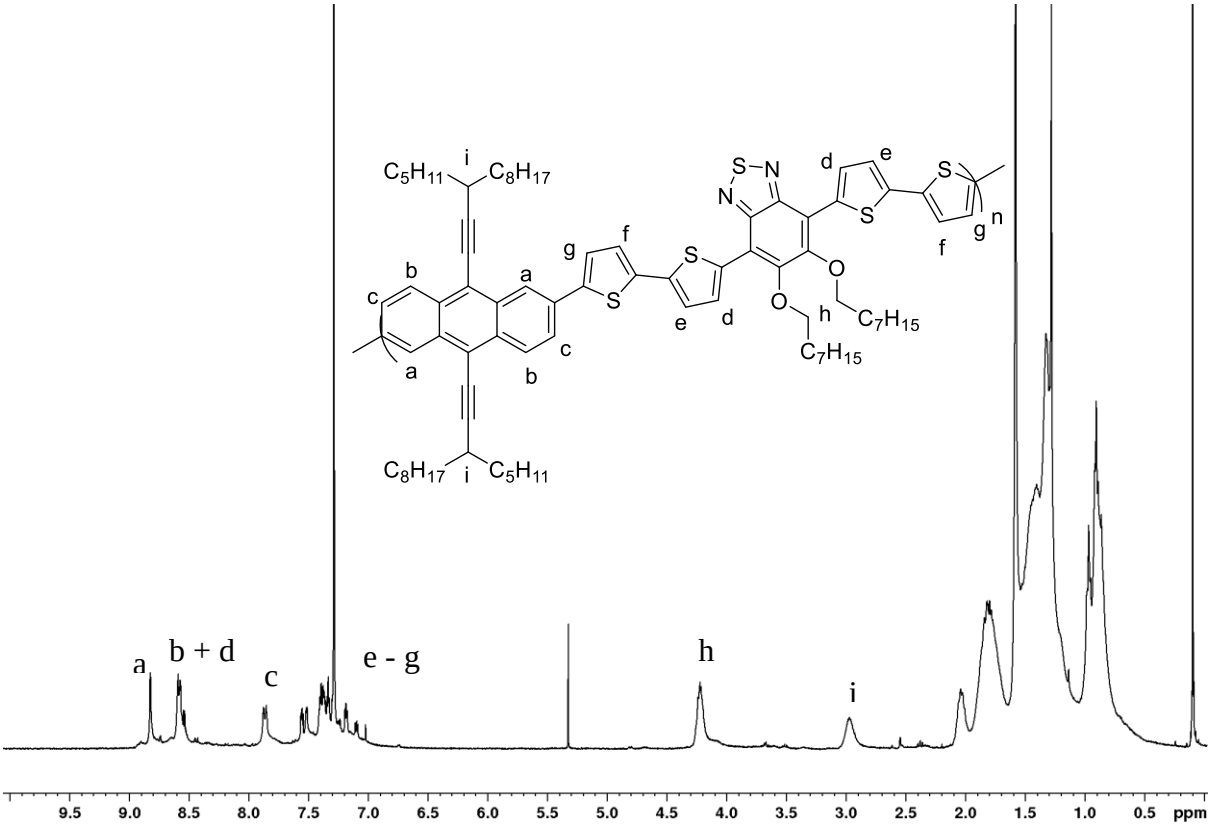


**Figure 7-16:** $^{1}$H-NMR Spectrum of Poly[9,10-di-(3-pentylundec-1-yne)-anthracene-2,6diyl-alt-5,6-bis (octyloxy)-4,7-di(2,2'-bithiophen-5-yl)benzo[c][1,2,5]-thiadiazole] **(PAA(PU)T2BT-8).**

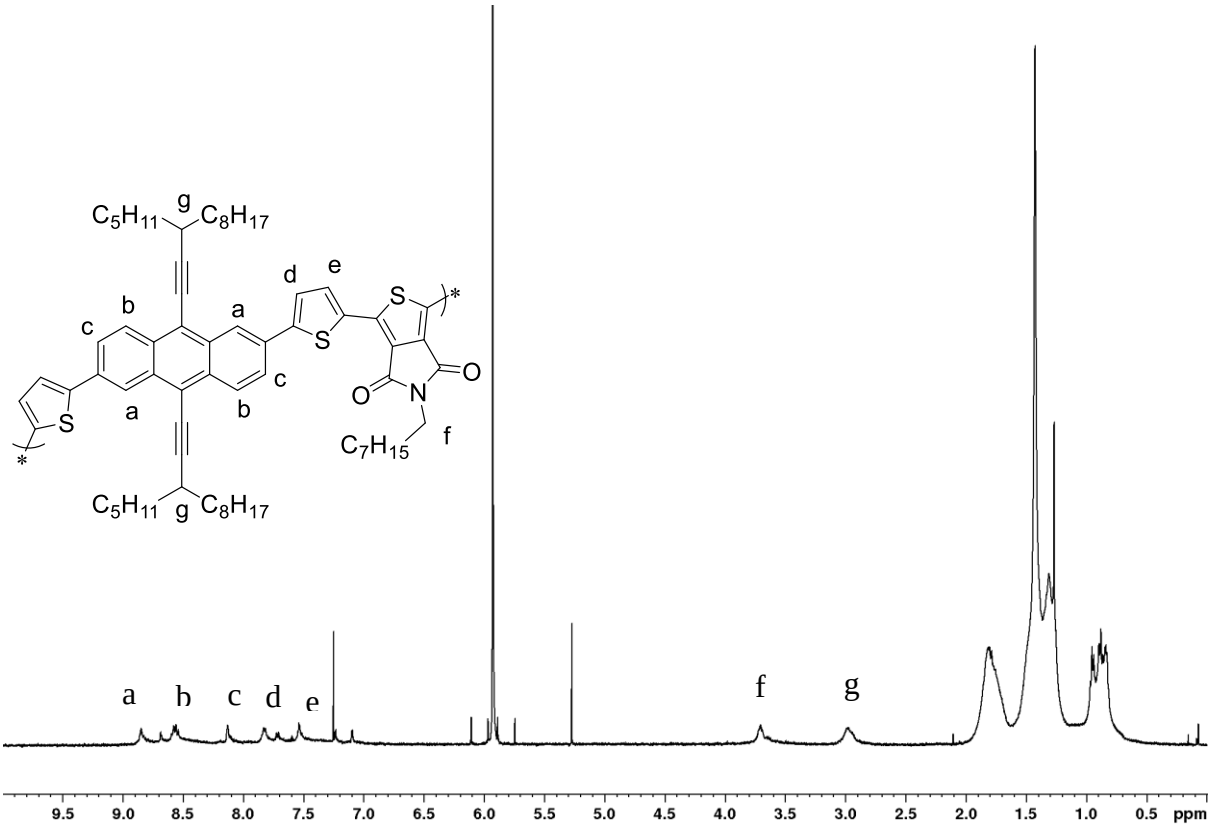


**Figure 7-17:** $^{1}$H-NMR Spectrum of Poly[2,6-di-(thiophen-2-yl)-9,10-bis-(3-pentylundec-1-yne)-anthracene -5-diyl-alt-5-octyl-4H-thieno[3,4-c]pyrrole-4,6(5H)-dione[3,4-c]pyrrole-4,6-dione] **(PAA(PU)TPD-8).**

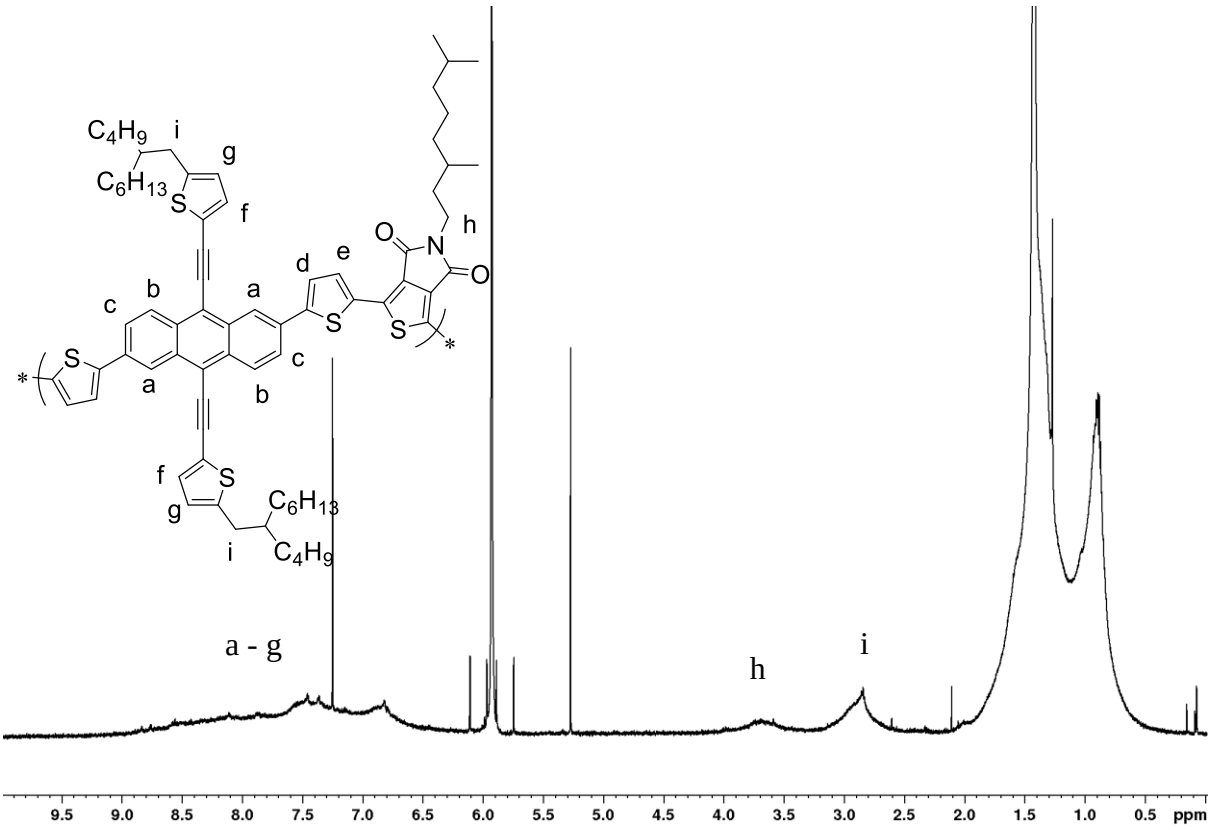


**Figure 7-18:** [1]H-NMR Spectrum of Poly[2,6-di-(thiophen-2-yl)-9,10-bis[2-(ethynyl-5-butyl-octyl) thiophene]-anthracene-5-diyl-alt-5-(3,7-dimethyl-octyl)-4H-thieno[3,4-c] pyrrole-4,6(5H)-dione[3,4-c] pyrrole-4,6-dione] **(PATA(BO)TPD-DMO).**

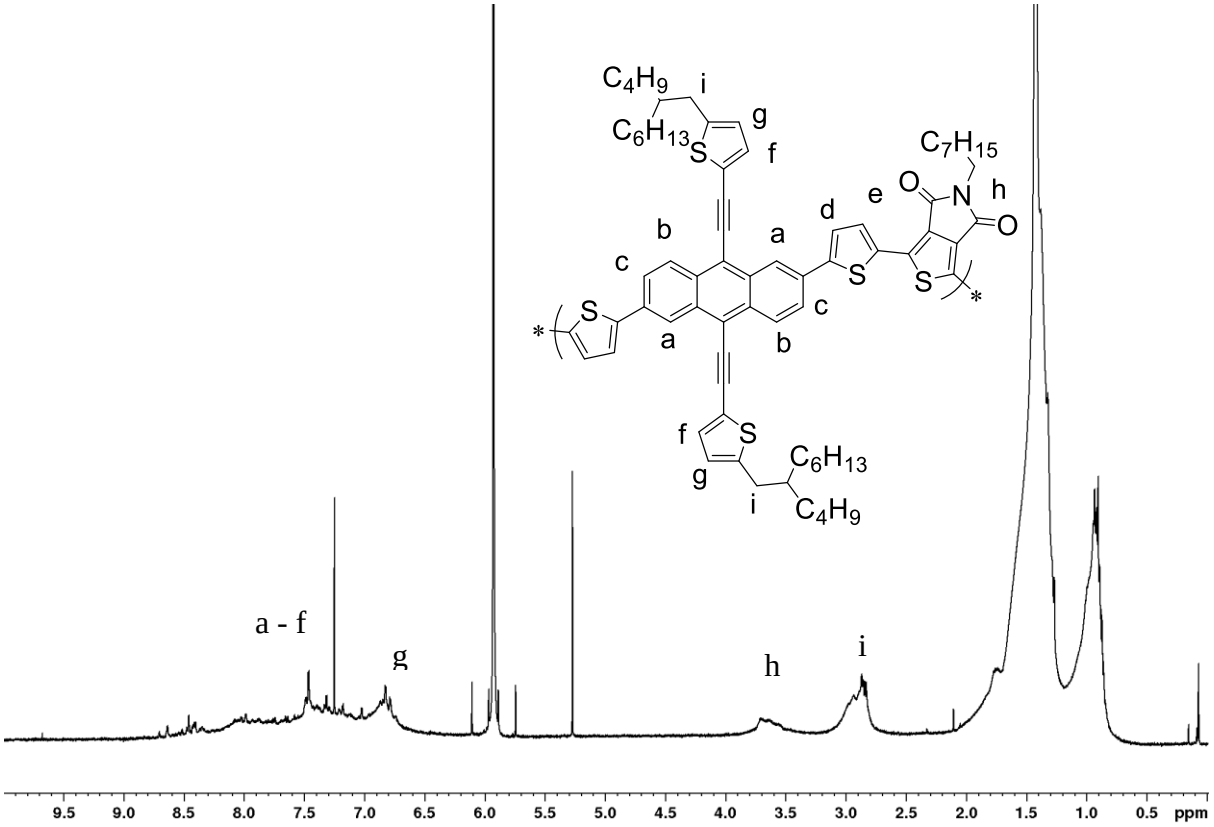


**Figure 7-19:** $^{1}$H-NMR Spectrum of Poly[2,6-di-(thiophen-2-yl)-9,10-bis[2-(ethynyl-5-butyl-octyl) thiophene]-anthracene-5-diyl-alt-5-(octyl)-4H-thieno[3,4-c] pyrrole-4,6(5H)-dione[3,4-c] pyrrole-4,6-dione] **(PATA(BO)TPD-O).**

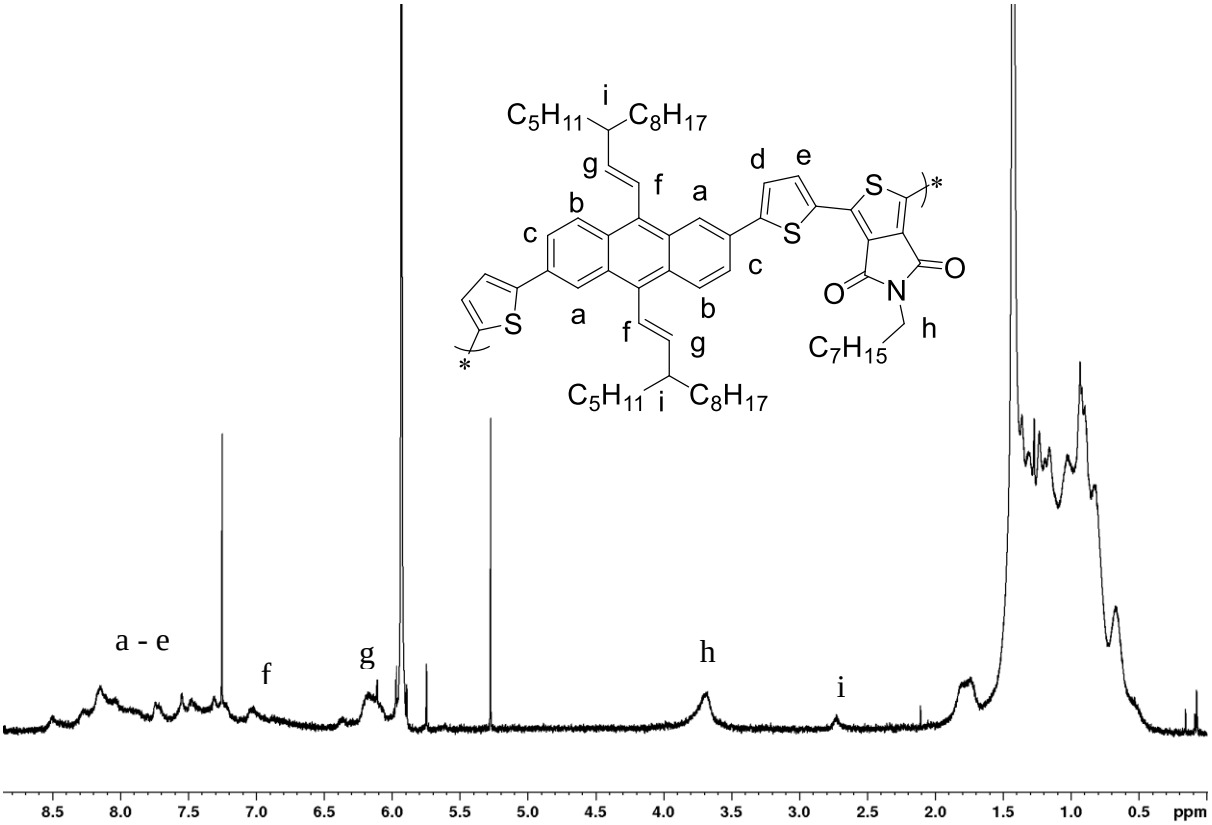


**Figure 7-20:** $^{1}$H-NMR Spectrum of Poly[2,6-di-(thiophen-2-yl)-9,10-bis-(3-pentylundec-1-yne)-anthracene -5-dyil-alt-5-octyl-4H-thieno[3,4-c]pyrrole-4,6(5H)-dione[3,4-c]pyrrole-4,6-dione] **(PVA(PU)TPD-8).**

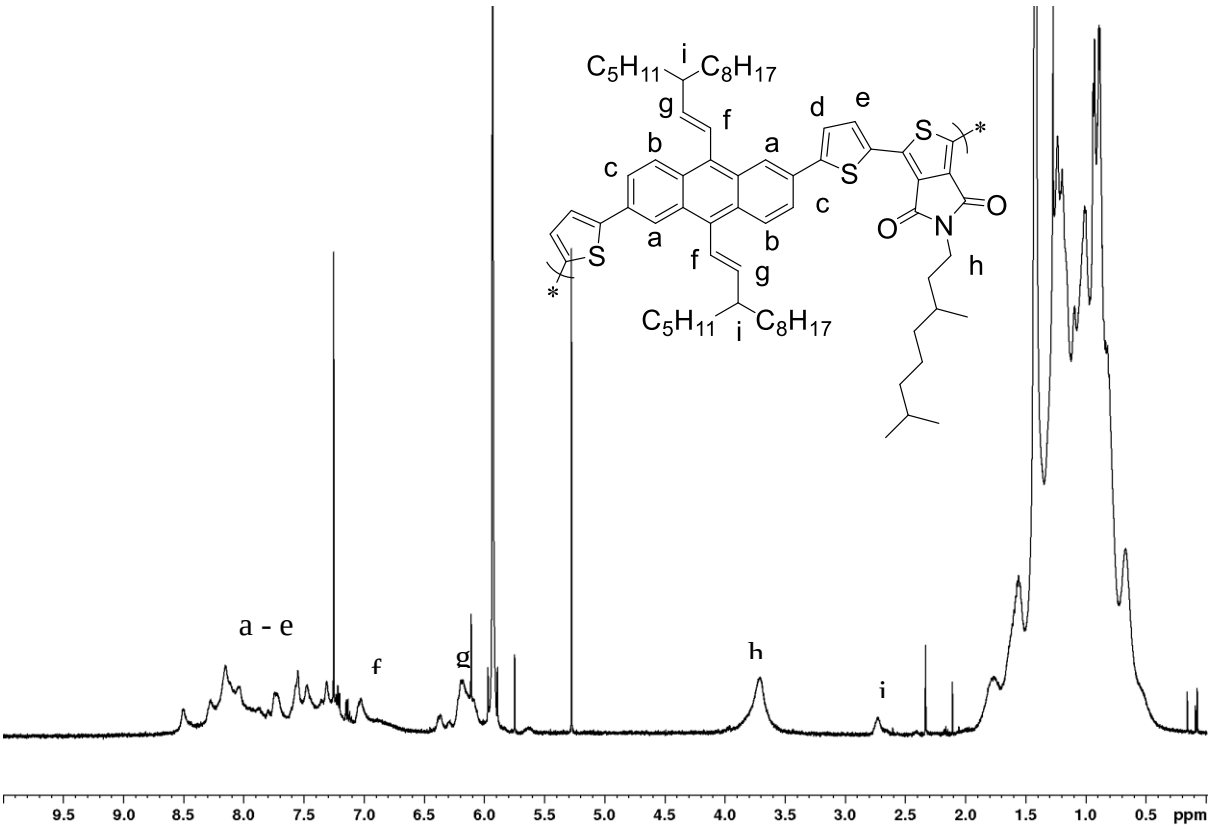


**Figure 7-21:** $^{1}$H-NMR Spectrum of Poly[2,6-di-(thiophen-2-yl)-9,10-bis-(3-pentylundec-1-yne)-anthracene -5-dyil-alt-5-(3,7-dimethyl-octyl)-4H-thieno[3,4-c]pyrrole-4,6(5H)-dione[3,4-c]pyrrole-4,6-dione] **(PVA(PU)TPD-DMO).**